Illinois U Library

ЖУРНАЛ
ЭКСПЕРИМЕНТАЛЬНОЙ И ТЕОРЕТИЧЕСКОЙ
ФИЗИКИ
АКАДЕМИЯ НАУК СССР

SOVIET PHYSICS

JETP

VOLUME 3 NUMBER 2

A Translation
of the
Journal of Experimental and Theoretical Physics
of the
Academy of Sciences of the USSR

SEPTEMBER, 1956

Published by the
AMERICAN INSTITUTE OF PHYSICS
INCORPORATED

SOVIET PHYSICS
JETP

A translation of the Journal of Experimental and Theoretical Physics of the USSR.

A publication of the
AMERICAN INSTITUTE OF PHYSICS

Governing Board

Frederick Seitz, *Chairman*
Allen V. Astin
Robert F. Bacher
W. S. Baird
H. A. Bethe
R. T. Birge
Frank D. Dezter
I. C. Gardner
S. A. Goudsmit
Charles Kittel
Hugh S. Knowles
R. B. Lindsay
William F. Meggers
Harry F. Olson
R. R. Palmer
R. F. Paton
Eric Rodgers
Ralph A. Sawyer
H. D. Smyth
Mark W. Zemansky

Administrative Staff

Henry A. Barton,
Director
Mark W. Zemansky,
Treasurer
Wallace Waterfall,
Executive Secretary
Theodore Vorburger,
Advertising Manager
Ruth F. Bryans,
Publication Manager
Edith I. Neftel,
Circulation Manager
Kathryn Setze,
Assistant Treasurer
Eugene H. Kone,
Director of Public Relations

American Institute of Physics Advisory Board on Russian Translations

Elmer Hutchisson, *Chairman*
Dwight Gray, Morton Hamermesh, Vladimir Rojansky,
Victor Weisskopf

Editor of Soviet Physics
Robert T. Beyer, Department of Physics, Brown University,
Providence, R.I.

Soviet Physics is a monthly journal published by the American Institute of Physics for the purpose of making available in English reports of current Soviet research in physics as contained in the Journal of Experimental and Theoretical Physics of the Academy of Sciences of the USSR. The page size of Soviet Physics will be 7⅞" x 10½", the same as other Institute journals.

Transliteration of the names of Russian authors follows the system employed by the Library of Congress.

This translating and publishing project was undertaken by the Institute in the conviction that dissemination of the results of researches everywhere in the world is invaluable to the advancement of science. The National Science Foundation of the United States encouraged the project initially and is supporting it in large part by a grant.

The American Institute of Physics and its translators propose to translate faithfully all the material in the Journal of EXPERIMENTAL AND THEORETICAL PHYSICS OF THE USSR appearing after January 1, 1955. The views expressed in the translated material, therefore, are intended to be those expressed by the original authors, and not those of the translators nor of the American Institute of Physics.

Two volumes are published annually, each of six issues. Each volume contains the translation of one volume of the Journal of EXPERIMENTAL AND THEORETICAL PHYSICS OF THE USSR. New volumes begin in February and August.

Subscription Prices:

Per year (12 issues)	
United States and Canada	$60.00
Elsewhere	64.00
Back Numbers	
Single copies	$ 6.00

Subscriptions should be addressed to the American Institute of Physics, 57 East 55 Street, New York 22, New York.

Copyright by American Institute of Physics 1956

SOVIET PHYSICS

JETP

SOVIET PHYSICS JETP VOLUME 3, NUMBER 2 SEPTEMBER, 1956

Investigation at Low Gas Pressure of an Intermediate Frequency Discharge Occurring Between High Frequency and Low Audio Frequency Discharges

N. A. Popov and N. A. Kaptsov
Moscow State University

(Submitted to JETP editor November 15, 1954)
J. Exptl. Theoret. Phys. (U.S.S.R.) 30, 68-76 (January, 1956)

An experimental investigation was made of the lower frequency limit at which high-frequency discharge can occur in tubes filled with hydrogen, neon, or krypton at a pressure of several mm. mercury. It was found that high-frequency discharges and discharges at low audio frequencies are separated by an intermediate frequency region within which the discharge exhibited properties commom to both types of discharge; the lower limit of the transition region is several hundred cycles. The time dependence of the drop in emission intensity of the discharge plasma during the de-ionization of hydrogen and krypton was obtained, and it was shown that with increasing frequency the duration of the de-ionization phenomenon is a principal factor in the transformation of the a-c discharge into a high-frequency discharge.

1. INTRODUCTION

THE purpose of our investigation was to determine at what frequencies the discharge typical of low audio frequencies stops and the high-frequency discharge begins, and to explain what elementary processes play a principal role in the transformation from the low-audio-frequency discharge to the high-frequency one.

It is known that the glow of a 50-cycle electric discharge produced in a rarefied gas is seen by the eye as two simultaneous d-c discharges with overlapping cathode and anode portions; in this case the discharge arc is ignited and extinguished within the same half cycle. If the frequency of the voltage applied to the low-pressure gas-discharge tube is 100 kc and above, the discharge glows continuously and there is no overlap of the cathode and anode portions[1-4]. Investigators of high-frequency discharges have noted that the ignition voltage drops sharply at frequencies above 10^5-10^6 cycles, but all indicated that the ignition voltage is independent of frequency below 10^5 cycles[5-6]. No detailed experimental investigation of an a-c discharge at frequencies below 10^5 cycles but above 50 cycles has been made up to now*.

The distribution function of the electrons in high-frequency and commercial-frequency discharges was analyzed theoretically by Margenau and Hartman[7-8]. It follows from their work that the distribution function for electrons in a discharge is continuous over a frequency range from zero (d-c discharge) to several megacycles (high-frequency discharge). If this be so, there should

---

[1] N. A. Kaptsov, *Electric Phenomena in Gases and in Vacuum*, Gostekhizdat, Moscow-Leningrad, 1950.

[2] E. Hiedemann, Ann. Physik. **85**, 649 (1928); **2**, 221 (1929).

[3] E. Hiedemann, Phys. Rev. **37**, 978 (1931).

[4] J. J. Thomson, Phil. Mag. **23**, 1 (1937).

* Note added in proof: With the exception of a recently published article by G. Francis, Proc. Phys. Soc. (London B68, 137 (1955).

[5] L. Rohde, Ann. Physik **12**, 569 (1932).

[6] H. Bocker, Archiv Elektrotech. **31**, H. 3, 1937.

[7] H. Margenau, Phys. Rev. **73**, 297 (1948).

[8] H. Margenau and L. Hartman, Phys. Rev. **73**, 309 (1948).

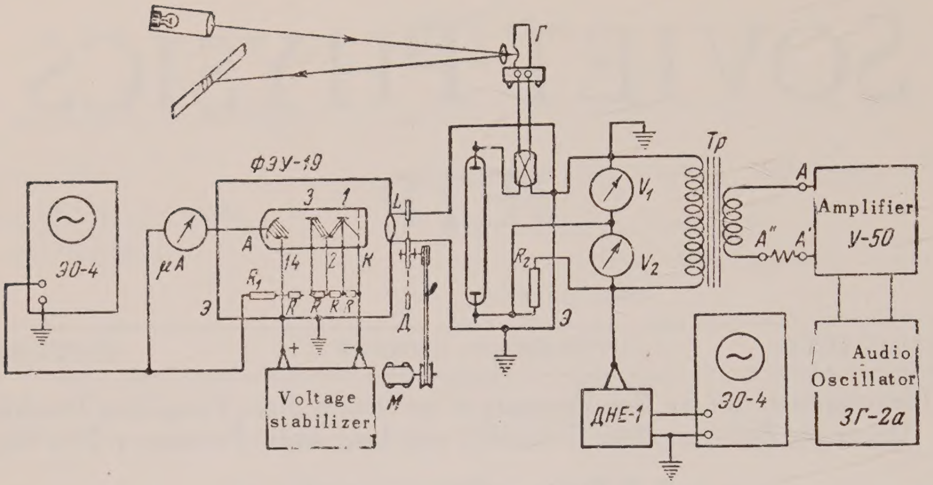

FIG. 1. Diagram of Experimental setup.

be a smooth transition between both types of discharge (commercial- and high-frequency) as the frequency is varied in either direction.

Restricting ourselves to low pressure, we shall from now on call a high-frequency discharge any discharge occurring in a tube operating at any radio frequency, provided first, that the alternation of the applied voltage causes no observable flicker in the intensity of the discharge, and second, that the character of the ignition and glow of the discharge remain the same when either internal or external electrodes are used. We shall call an a-c discharge one occurring in a tube operating at audio frequencies, provided first that the intensity of the discharge changes noticeably with the voltage alternations, and second that the type of electrodes used (external or internal) affects substantially the character of the ignition and glow of the discharge.

The frequency dependence of the ignition and glow of an a-c discharge in tubes with external electrodes was studied by us with the aid of oscillographs of the discharge emission[9]. It was established in that investigation that at low frequencies individual flashes of a nonself-maintaining discharge occur in tubes with external electrodes. Such unstable discharges can be changed into ordinary stable ones by increasing the frequency, or by increasing the voltage across the electrodes. At frequencies of several tens of kilocycles the discharge ignition and glow characteristics become practically the same for internal and external electrodes and thus, in this respect, the discharge behaves like a high-frequency one.

2. EXPERIMENTAL PROCEDURE

In this work, which is a continuation of the earlier investigation[9], we employed a further modification of the older method of oscillographing the discharge emission, adapted from the work by Huxford and Platt[10] and by Beese[11].

The principle diagram of the experimental setup is given in Fig. 1. The audio-frequency source was the same as in Ref. 9, as were the methods of measuring the current and voltage. The light from the central portion of the discharge tube was made to pass through lens *L* and semi-transparent antimony-cesium cathode of electrostatically electron-focussed photomultiplier FEU-19. Voltage was applied to the plates of the photomultiplier through a voltage divider, connected to a stabilized rectifier with a smoothly variable output voltage. The output current of the photomultiplier was monitored with a microammeter and recorded with an EO-4 oscillograph. A DNE-1 capacitative voltage divider and another EO-4 oscillograph were used to monitor the waveform of the voltage across the discharge tube. A systematic check showed the voltage waveform to be sinusoidal in all the experiments. All the set-up elements, including the photomultiplier

---

[9] N. A. Kaptsov and N. A. Popov, J. Exptl. Theoret. Phys. (U.S.S.R.) 27, 97 (1954).

[10] W. Huxford and J. Platt, J. Opt. Soc. Am. 37, 10 (1947).

[11] N. S. Beese, J. Opt. Soc. Am. 36, 555 (1946).

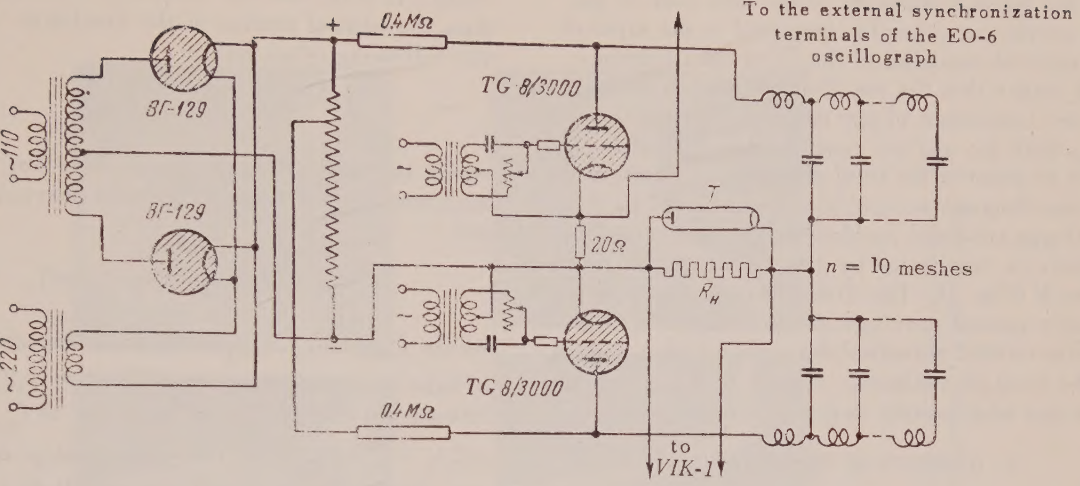

FIG. 2. Diagram of pulse generator.

and the discharge tube, were thoroughly shielded to prevent interference. Shield E was made of tin and the outer braid of the shielded conductors was grounded.

To investigate the emission of a pulsed discharge, we assembled another variant of the experimental setup, in which the source of voltage was a rectangular pulse generator (Fig. 2). The circuit of this generator was adapted by us from one described in an article by Gavrilov [12]. With the aid of two TG-8/3000 thyratrons and two artificial lines, this generator formed two identical rectangular voltage pulses from each positive sinusoidal half-cycle of the voltage fed to the thyratrons from the rectifier, which in turn employed VG-129 gas-filled diodes. The time interval between these two rectangular pulses could be varied with two phase shifters.

The artificial lines were made up of ten meshes each and formed pulses of 20 microsecond duration. A noninductive resistance, equal to the characteristic impedance of the line (600 ohms), was connected in parallel with the discharge tube, The voltage on the discharge tube was measured with a VIK-1 pulse voltmeter. Type EO-6 oscillographs with driven sweep were used. The peak working voltage of the pulse was 800.

According to our preliminary assumptions, the duration of the de-ionization of the gas, occurring in the discharge tube at the instant of voltage polarity reversal. is of great importance in the transformation of the a-c discharge into a high-frequency discharge with increasing frequency. We therefore filled the discharge tubes with hydrogen, neon, and krypton. Hydrogen is the lightest gas and furthermore is a molecular one, and the de-ionization phenomenon in hydrogen was thoroughly studied by Gavrilov [12]. From the work of Ardonova it is known [13] that the de-ionization rate in neon is noticeably different from that of krypton.

The hydrogen was obtained electrolytically, and was then purified of all possible organic impurities water vapor, and oxygen. The mercury vapor was frozen out with liquid nitrogen. A spectral check showed the absence of other gases from the hydrogen-filled tubes. Neon and krypton were obtained in glass flasks from the All- Union Electrotechnical Institute.

The discharge was investigated both in sealed-off discharge tubes as well as in tubes joined to the setup. After degassing, the tube was filled with hydrogen and a glow discharge lasting not less than one hour was started. The hydrogen was then removed, the tube again degassed and refilled with the investigated gas, and the discharge restarted in the fresh gas. This conditioning procedure was carried out again for not less than an hour and only then was the tube sealed off (or the discharge studied with the tube attached). The observations covered the central portion of the discharge in symmetrical tubes with internal nickel electrodes. The spacing between electrodes was 300-400 mm, and the internal diameter of the tube was 25 mm.

---

[12] S. N. Gavrilov, Dokl. Akad. Nauk SSSR **71**, 265 (1950).

[13] S. I. Ardonova, J. Exptl. Theoret. Phys. (U.S.S.R.) **22**, 981 (1952).

A series capacitor is connected in the input of the vertical amplifier of the EO-4 oscillograph. This means that the oscillograph screen shows only the a-c component of any periodic process that contains both d-c and a-c components. Therefore, in order to observe the total photoelectric current on the oscillograph screen, the light emitted by the discharge tube and incident on the photomultiplier cathode is interrupted by disk D, rotated by electric motor M (Fig. 1). The disk has four symmetrical equally-spaced openings of equal size.

This method permitted determining what portion of the total photoelectric current is the a-c component and what portion is the d-c component.

3. RESULTS OF OBSERVATIONS

Figure 3 shows a series of photocell-current oscillograms of an a-c discharge in hydrogen. The first three oscillograms were taken with the disk stationary and with the light passing directly through the lens to the photomultiplier cathode (Figs. 3a-c). The remaining oscillograms were taken with the disk rotating and with the oscillograph sweep synchronized with the frequency at which the light was interrupted by the disk (Figs. 3d-k). In the latter case, the oscillograph shows clearly the zero line corresponding to the absence of photocell current and consequently to the absence of the light in the photomultiplier. We also synchronized the sweep frequency with the frequency of the voltage applied to the discharge-tube electrodes. Both methods of synchronizing the frequencies on the oscillographs are equivalent. and the results obtained are numerically the same. However, in practice it proved more convenient to synchronize the sweep frequency with the light-interruption frequency at low audio frequencies and with the tube-voltage frequency at higher frequencies.

The oscillograms show that starting with 200-300 cycles, a d-c component appears in the photocell current and starts rising rapidly with the frequency. This means that the tube starts glowing continuously at the instant in which the voltage changes polarity. In other words, at these frequencies and above, we deal with a modulated emission at a frequency f' which equals twice the frequency f of the electrode voltage: $f' = 2f$.

In our experiments the waveform of the alternating voltage applied to the discharge tube was strictly sinusoidal. In the first approximation, it is possible to assume that the time variation of the light intensity is also sinusoidal, as can be seen from the accompanying oscillograms (Figs. 3d-k). In this case the intensity of the light coming from the central portion of the discharge tube obeys the following relationship:

$$I(t) = I_0 + I_1 \sin 2\omega t, \qquad (1)$$

where the modulation frequency $2\omega = 4\pi f$. For measurement purposes, it is more convenient to put

$$I(t) = I_{\min} + I_1(1 + \sin 2\omega t), \qquad (2)$$

where $I_{\text{мин}} = I_0 - I_1$ is the minimum intensity of tube emission. If $\omega = \pi n/2$ $(n = 1, 2, 3 \ldots)$, $I(t)$ becomes a constant quantity, equal to $I_{\text{peak}} = I_{\min} + 2I_1 = I_0 + I_1$. This last relationship is valid not only for a sinusoidally-varying light intensity, but also for any other variation. The percentage modulation K is given by the following relationship:

$$K = 100\,(I_{\text{peak}} - I_{\min})/I_{\text{peak}}. \qquad (3)$$

The quantities I_{peak} and $I_{\min}$ entering into this expression were determined by us by counting the number of squares on a transparent grid placed on the oscillograph screen, with the rotating disk interrupting the light from the discharge tube.

The measurement procedure chosen permitted us to investigate the transformation of the low-frequency discharge into a high-frequency one in various gases (hydrogen, neon, and krypton) as a function of the discharge current and of the pressure of the gas filling discharge tube.

The graph showing the transformation from the low- to the high-frequency discharge and its dependence on the type of gas is shown in Fig. 4. The discharge was studied in three identical sealed-off discharge tubes with hydrogen, neon, and krypton at a pressure of 2 mm mercury and at a discharge current of 2 ma. Flat electrodes, 15 mm in diameter and 300 mm apart, were placed inside the tube. The internal diameter of the tube was 25 mm. The abscissa of the graph indicates the frequency in kc and there are two ordinate scales. One indicates the ratio of the fraction T_2 of the period during which no discharge glow is observed in the tube to the total period T. The frequency dependence of this ratio T_2/T is represented graphically by the descending branches in the curves in the frequency range from 50 to 200 cycles. The ascending branches of the curves for the same gases correspond to the second ordinate scale, shifted to the right for convenience, which represents the percentage modulation K of the light from the discharge

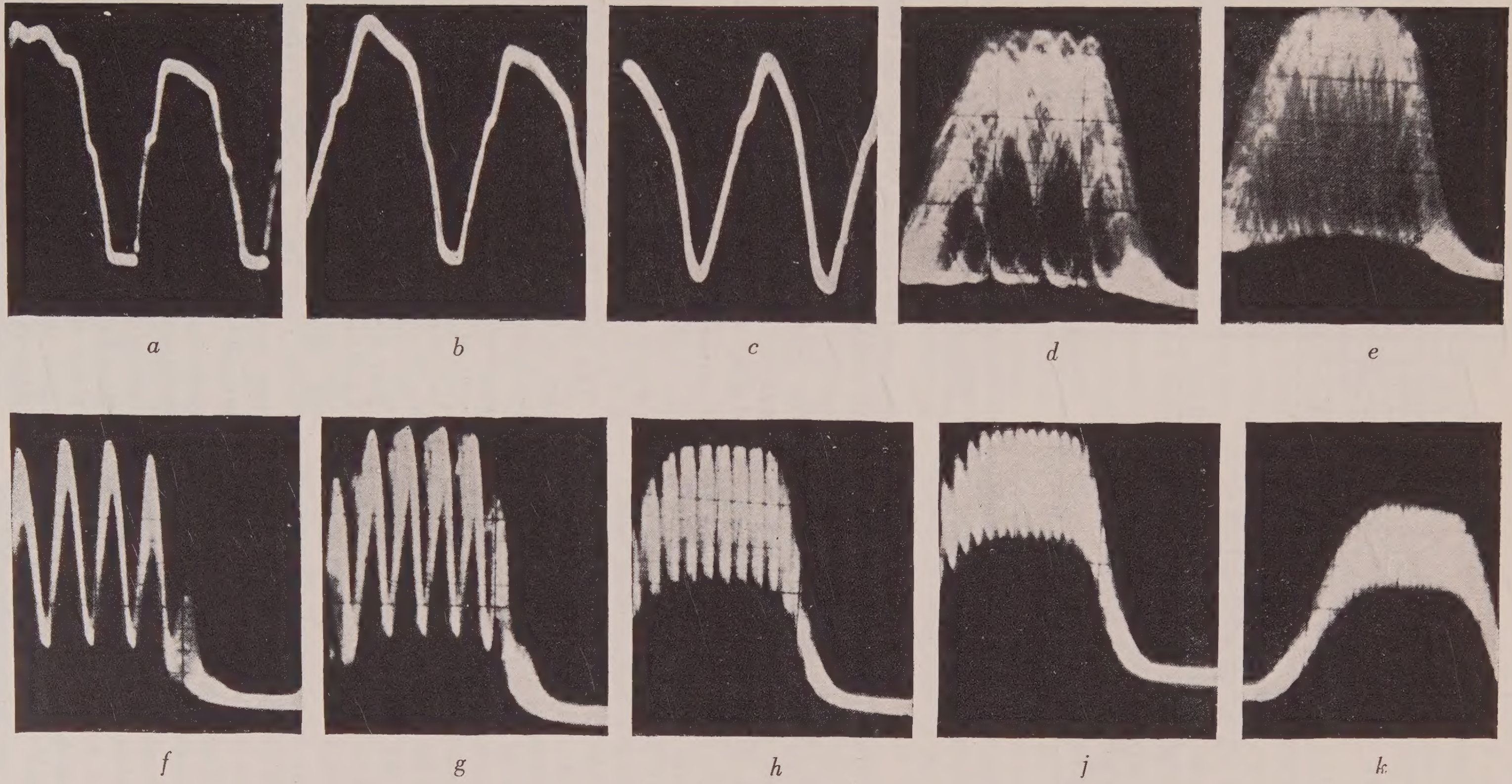

FIG. 3. Oscillographs of photocell current. Discharge in hydrogen at various frequencies of voltage applied to discharge-tube electrodes: *a* – 50 cycles; *b* – 100 cycles; *c*, *d*, – 200 cycles; *e* – 400 cycles; *f* – 800 cycles; *g* – 1 kc; *h* – 2 kc; *j* – 3 kc; *k* – 5 kc.

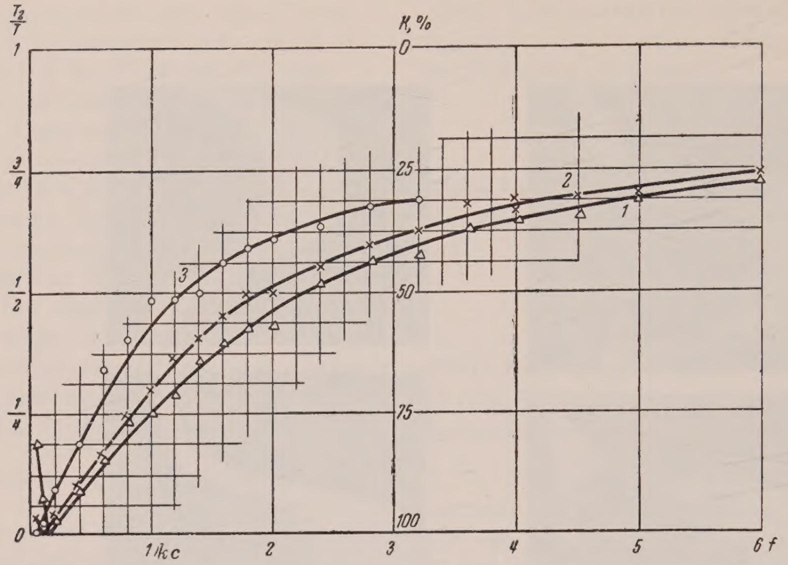

FIG. 4. Graph showing transition between low- and high-frequency discharge for different gases. 1 – hydrogen; 2 – neon; 3 – krypton; $i = 2$ ma; $p = 2$ mm mercury.

tube.

It is evident from this graph that even at frequencies as low as 200 cycles the discharge cannot become completely distinguished within a single cycle in any of these three gases. This means that at these frequencies (50-200 cycles, depending on the type of gas) the ratio T_2/T vanishes and the photocell current starts containing a d-c component proportional to the light intensity. Even at 2.5 kc the modulation factor of the constant light flux from the discharge tube is less than 50% for all three gases. Characteristically, for different gases, the higher the atomic number of the element, i.e., the longer the de-ionization time of a given gas, the higher the position of the right-hand branch of the curve, other conditions being equal.

For all three gases, a detailed study was made of the transformation of the a-c discharge into a high-frequency one, both as a function of the discharge current, as well as a function of the gas pressure, other conditions being equal. The experiments were carried out at gas pressures ranging from 0.8 to 25 mm mercury and at discharge currents from 0.5 to 5 ma. The form of the K vs. f curves is in all cases similar to that of the curves of Fig. 4. The curves in similar graphs run parallel to each other, both when the parameter varied is the pressure and when it is the current.

The sequence in which the curves range themselves on the graphs when the parameter is the discharge current or the gas pressure depends not only on the de-ionization time but also on the ratio between the ignition voltage and the amplitude of the voltage applied to the tube. We increase the latter, thereby increasing the discharge current. The ignition and extinction voltage vary with the pressure. All this leads to a change in the time elapsed from the instant of ignition to the instant of extinction of the discharge within the same voltage half-cycle, and consequently also effects the position of the curves that show the dependence of T_2/T and of K on f.

The form of these curves depends considerably more on the gas pressure in the tube than on the discharge current. The frequency variation of the modulation factor, plotted by us for various pressures of the same gas at a fixed distance between electrodes, has shown that two different relationships hold in this case. On one hand, at lower pressures (region of left branch of ignition characteristic) the K vs. f curves occupy higher and higher positions as the pressure is increased. On the other hand, at higher pressures (region of right branch of the same characteristic), this relationship is reversed; starting with a certain pressure, the curves occupy lower and lower positions as the pressure increases. Investigations of the transformation of the a-c discharge into a high-frequency discharge, made at various values of the discharge current, show that the higher the discharge current in these gases, the higher the position of the K vs. f curves. In our experiments, over the entire range of variation of the current and of the gas pressure, the point on the frequency axis corresponding to $T_2/T = 0$ or $K = 100\%$ never lies beyond 500 cycles.

Measurements were made of the frequency dependence of T_2/T and K in two sealed-off discharge tubes of identical internal diameter and 40 and 30 cm long filled with hydrogen at a pressure of 2 mm mercury. The curves obtained for identical discharge currents are in sufficiently good agreement over their entire length. This experimental fact is well explained by the de-ionization theory developed by Granovskii[14]. In fact, plasma in the de-ionization stage exhibits ambipolar diffusion of electrons and ions from the plasma to the walls of the tube and to the electrodes. On the other hand, in the central portion of the tube there is ambipolar diffusion of electrons and ions only to the walls. Since both tubes had the same internal diameter, the speed of plasma de-ionization and consequently also the intensity of emission from the plasma in the de-ionization stage were the same for both tubes. This evidently also caused the corresponding frequency-dependence curves of T_2/T and K to be the same for tubes of different lengths.

To obtain more details on the mechanism of the transformation of the low-frequency discharge into a high-frequency one with increasing frequency, we investigated the drop in intensity of emission of a pulsed discharge with time in the de-ionization stage in hydrogen and krypton. The presence of two periodically repeating light pulses in the photocell-current oscillograms has led to a sufficiently accurate determination of the time behavior of the drop in the intensity of emission from the plasma in the central portion of the discharge tube with hydrogen and krypton at pressures of 2-3 mm mercury (Fig. 5). The fact that the curves of Fig. 5 differ insignificantly from straight lines is an indication that at these pressures the intensity of emission from the discharge tube in the de-ionization stage drops nearly exponentially. There is therefore every reason for assuming that in our experiments the charged particles become diverted from the plasma principally by diffusion onto the wall[14].

Knowing the discharge ignition and extinction voltages, and knowing also the amplitude of the sinusoidal voltage applied to electrodes, we determined graphically the time interval between the instant when the diminishing sinusoidal voltage becomes equal to the discharge extinction potential in a given half cycle and the time the voltage rises to the value of the ignition potential in the next half cycle. The plasma becomes de-ionized during this time interval, which depends on the frequency. Knowing the drop in emission intensity of the discharge in the de-ionization stage, it was easy to calculate to what minimum value should the emission intensity of the a-c discharge decrease during the polarity reversal.

The K vs. f curves thus computed for hydrogen and krypton agree sufficiently well with similar curves obtained directly by measuring I_{peak}/I_{min} on the oscillogram for the same gases, other conditions being equal. This result confirms the previously-made assumption that the duration of the plasma de-ionization plays a substantial role in the transition between the low- and high-frequency discharges as the frequency is increased.

If the electrode voltage varies sinusoidally, the de-ionization in the post-discharge period takes place first in a diminishing direct field and then in an increasing reverse field. In this case, as shown in references 15 and 16, the plasma breaks up, mostly in the vicinity of the electrodes, owing to the formation of an ever-increasing space charge layer, consisting of positive ions. The space charge is initially formed at the cathode, and after the voltage passes through zero it is formed at the former anode. For the discharge tube and for the gases, voltages, and electrode spacing used in our investigations, the plasma breaks up before the space charge boundary manages to approach it. Consequently, in our case the speed of de-ionization is independent of the electrode-voltage amplitude.

When the drop in intensity of emission from a pulse discharge in the de-ionization stage is used to plot analytically the curves showing the frequency dependence of the modulation factor of an a-c discharge, it turns out that it is possible to compute these curves, to a certain approximation, up to frequencies of 10^5 cycles. The results obtained are plotted in Fig. 6.

4. CONCLUSIONS

The experimental material gathered in this investigation of fluctuations in the emission of a discharge at alternating current, in tubes with internal electrodes, as well as the material on the ignition

---

[14] V. L. Granovskii, *De-ionization of Gas*. From the collection *Electron and Ion Instruments*, edited by P. V. Timofeev, Gosenergoizdat, 1941, p. 93.

[15] B. G. Mendelev and E. A. Sviatoezerskaia, J. Exptl. Theoret. Phys. (U.S.S.R.) 21, 18 (1951).

[16] V. D. Andreev, V. E. Levina and B. G. Mendelev, J. Exptl. Theoret. Phys. (U.S.S.R.) 21, 149 (1951).

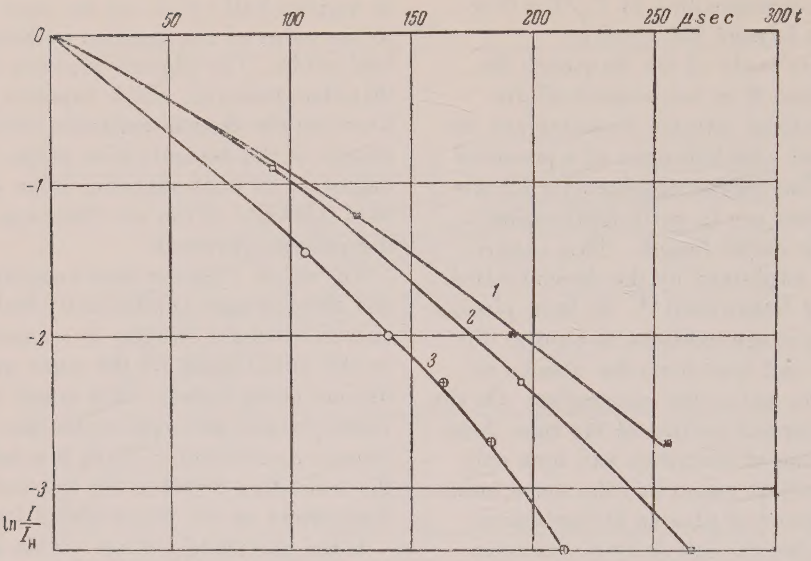

FIG. 5. Semi-logarithmic plot of the drop in emission intensity I of a discharge in the de-ionization stage with time. I_H — initial emission intensity. 1 — krypton, 2.8 mm mercury; 2 — 1.5 mm mercury; 3 — hydrogen, 2.1-3.1 mm mercury.

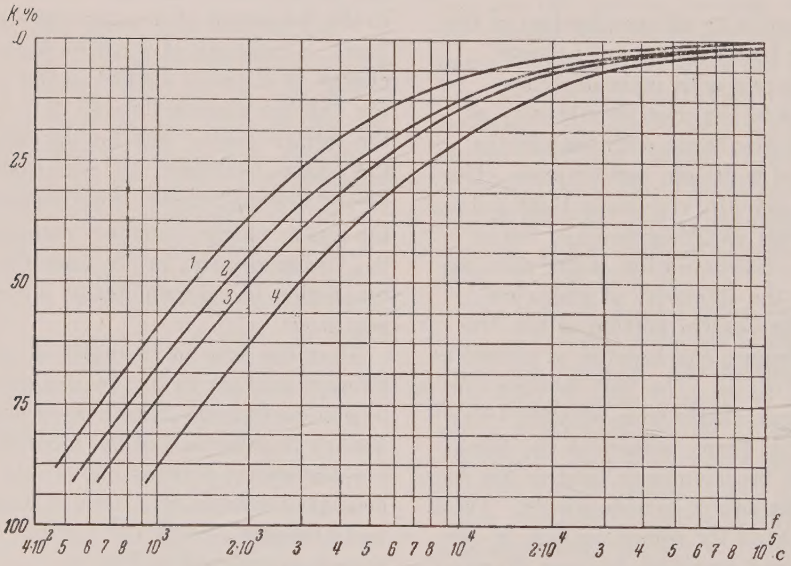

FIG. 6. Graph showing frequency dependence of modulation factor K of the a-c discharge emission intensity. Krypton: 1 — 2mm mercury; 2 — 2.7 mm mercury; Hydrogen: 3 — 2 mm mercury; 4 — 2.5 mm mercury.

of discharge tubes with internal and external electrodes in audio-frequency circuits, obtained by us in Ref. 9, leads to the following deductions:

1. There is no sharp boundary between an a-c discharge and a high-frequency discharge. Between these two types of discharge there is a transition region within which the discharge exhibits properties of both types of discharge.

2. The positions of the boundaries of the transition region depend on the pressure and on the type of gas. The lower limit of the transition region is several hundred cycles. The upper limit cannot be established accurately, for with increasing frequency the discharge in the intermediate frequency region approximates asymptotically in its basic properties the high-frequency discharge.

3. As the a-c discharge changes into a high-frequency one, and as the frequency is increased, a substantial role is played by the finite time of deionization occurring in the plasma of the a-c discharge when the voltage reverses polarity.

Translated by J. G. Adashko
10

SOVIET PHYSICS JETP VOLUME 3, NUMBER 2 SEPTEMBER, 1956

The Structure of Superconductors. IX. Roentgenographic Determination of the Structure of α - Bi_4Rh

V. P. Glagoleva and G. S. Zhdanov
Moscow Physico-engineering Institute

(Submitted to JETP editor December 29, 1954)
J. Exptl. Theoret. Phys. (U.S.S.R.) 30, 248-251 (February, 1956)

We have determined the structure of the low temperature modification of Bi_4Rh, which belongs to the space group $O_h^{10}-Ia3d$, with a lattice period $a = 14.928$ A. The positions of the bismuth and rhodium atoms were determined by a very precise method of constructing the cross sections and projecting the series of interatomic vectors (F^2-series) and the series of electron densities (F-series).

In the work of one of us and Zhuravlev[1] it was shown that the compound Bi_4Rh has three modifications; α, β, and γ. The low temperature modification has a cubic lattice with a period $a = 14.928$ A and belongs to the space group $O_h^{10}-Ia3d$. In the simple lattice there are 120 atoms: 96 atoms of bismuth and 24 rhodium atoms. Alekseevskii[2] has shown that the low temperature modification α - Bi_4Rh does not exhibit superconductivity down to a temperature ~ 0.1 K, whereas the two other modifications - β - Bi_4Rh and γ - Bi_4Rh pass over into the superconducting state. In the same manner as in white and gray tin, the superconductivity in Bi_4Rh is a property of the high temperature modification which is metastable at low temperatures. The compound Bi_4Rh, having a considerable number of modifications and various superconducting properties, appears to be interesting, since a study of the structure of its polymorphic modifications may enable one to explain the connection between polymorphism and superconductivity. The problem in question in this work[3] was to determine the atomic structure of one of these modifications (α-Bi_4Rh), which contains a large number of atoms in the elementary cell. A short report of the results of this work was published previously[4].

An analysis of the regularity of the extinctions and the possible atomic positions shows that the bismuth atoms may occupy just the general position 96 h and the rhodium atoms – the one of the two 24 – fold positions 24 c or 24 d.

For determining the positions of the bismuth atoms, which forms the framework of the structure, we selected the method of constructing the cross sections of the F^2-series. A three dimensional assembly of the reflected intensity received from a series of oscillating-crystal roentgenograms, was taken by the method of irradiating in a RKV camera 86 mm in diameter. We derived the layer lines from zero to an eighth with a total number of independent reflections equal to 235. The reflected intensity was measured by a visual comparison of the spots for quality of blackening. For calculating $F^2(hkl)$ we took only angular factors into account; temperature and absorption factors were not considered.

The sections of the F^2-series were selected so that the number of maxima were as small as possible with a small probability of overlapping, so that the connection between the coördinates of the maxima and the atomic coordinates was of a very simple form. There are three types of maxima: Bi-Bi,

---

[1] N. N. Zhuravlev and G. S. Zhdanov, J. Exptl. Theoret. Phys. (U.S.S.R.) **28**, 228 (1955); Soviet Phys. JETP **1**, 91 (1955).

[2] N. E. Alekseevskii, G. S. Zhdanov and N. N. Zhuravlev, J. Exptl. Theoret. Phys. (U.S.S.R.) **28**, 237 (1955); Soviet Phys. JETP **1**, 99 (1955).

[3] V. P. Glagoleva, Dissertation. MIFI (Moscow Physico-Engineering Institute), 1954.

[4] G. S. Zhdanov, Works (Trudy) of the Crystallograph. Inst. **10**, 243 (1954).

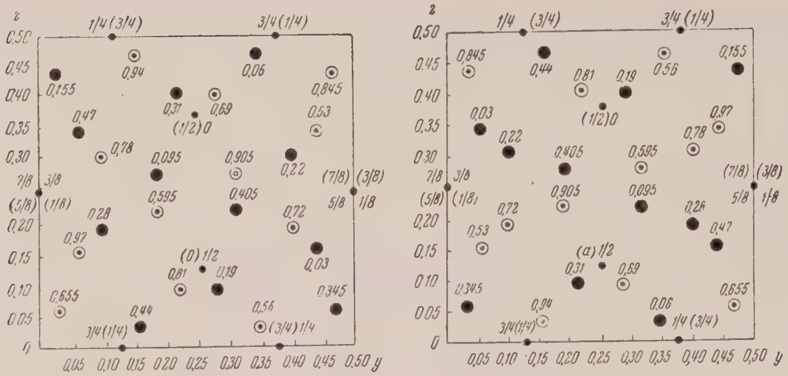

a *b*

FIG. 1. • – Rh; ⊙ — Bi, $x > 0.5$; ● — Bi. $x < 0.5$

Bi-Rh, Rh-Rh; with the same factors and of relative weights: $Z^2_{\mathrm{Bi}} : (Z_{\mathrm{Bi}} \cdot Z_{\mathrm{Rh}}) : Z^2_{\mathrm{Rh}} = 3.4 : 1.8 : 1$. The appearance of maxima is principally characteristic of the spacing Bi-Bi, therefore the cross section can be found by considering only these maxima. We analyzed certain sections for flatness and for direction having simple indices, i.e., that were composed of pairs of the different coordinate positions 96 h, so that the values $u = x_i - x_j$, $v = y_i - y_j$; $w = z_i - z_j$ satisfied the relations for flatness and direction in every case selected. Sections were selected in the directions $[0, {}^1/_2, w]$, from which 12 maxima are possible, corresponding to to the direction Bi-Bi, having a multiplicity of 8 and having coordinates $\pm 2x$; $\pm 2y$; $\pm 2z$; $\pm({}^1/_2 - 2x)$; $\pm({}^1/_2 - 2y)$; $\pm({}^1/_2 - 2z)$; for both positions of the rhodium atoms it is possible to have Rh-Rh maxima with multiplicity 2, from the coordinates 0 and 1/2, and a multiplicity of 4 from the coordinates ¼ and ¾; Bi-Rh maxima are not possible.

As a result of constructing and analyzing the sections of the F^2-series there were derived 32 variations of the coordinates (xyz) of the bismuth atoms. A geometrical analysis eliminated 16 of the variations. From the remainder there were selected two variations of the positions of the bismuth atoms, for which the calculated value of $F(hkl)$ was very large and a single weak reflection with small indices agreed well with the experiments. A comparison of a large number of calculations for these two variations and the experimental value of $F(hkl)$ confirmed the selection, but did not indicate any preference for either of them. In Fig. 1 *a* and *b* are shown the projections of the nuclei of the bismuth and rhodium atoms on the (100) planes for both variations. We adopted that variation which corresponded to a greater uniformity in the distribution of the bismuth atoms over the volume of the cell (Fig. 1*a*). At the same time, the analysis of the interatomic spacing Bi-Rh gave for the rhodium atoms, the positions 24 c without any parameters. The coordinates of the bismuth atoms were: $x = 0.028$; $y = 0.437$; $z = 0.154$.

A direct check on the accuracy of the choice between the alternatives for the coordinates of the bismuth and rhodium atoms may be made by constructing any projection and section of the series of electron densities. The projections of the electron densities from all cells onto the (100) planes are of no interest, since they are alike for both variations. Aside from this, in these projections, the overlapping is a maximum.

We chose for the region of projection of the electron density (the projection of the electron cloud) that which was included between $x = 0$ and $x = {}^1/_2$. In the projection, there appeared four sharp maxima and two very diffuse ones, whose distribution verified the accuracy of the choice of the coordinates of the bismuth atoms. Accordingly, the four greatest and sharpest maxima were used with the parabolic method to make more precise the coordinates of the bismuth atoms, i.e., $x = 0.026$; $y = 0.437$; $z = 0.151$. The rhodium atoms do not appear in this projection. The positions of the latter were determined by constructing the sections of a series of electron densities from the direction $[x, {}^1/_4, {}^1/_8]$. Calculation and construction of these sections confirmed the positions 24 c for the rhodium atoms.

From a second construction of a projected region of a series of electron densities the sign of $F(hkl)$ was calculated from the coordinates of the bismuth and rhodium atoms which were derived from the first construction. In Fig. 2 is shown the results of this second construction of the region of projection of the F-series. From it we derive sharper outlines of the maxima in those spots which were

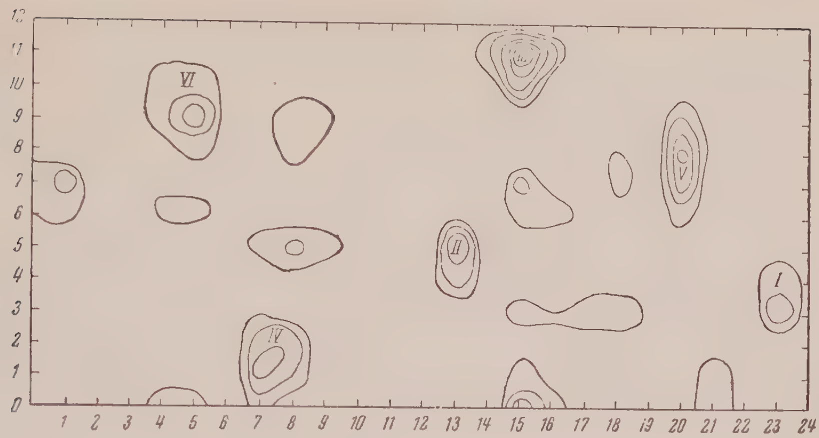

FIG. 2.

TABLE 1.

Calculation of the coordinate maxima-(u, v) and the derivation from them of the coordinates of the bismuth atoms from the second construction of the region of projection of the F-series.

No. of the maxima	u	v	Connection to xyz		x	y	z
			u	v			
I	0.478	0.086	$^{1}/_{2}-x$	$^{1}/_{2}-y$	0.022	0.434	—
II	0.272	0.100	$^{1}/_{4}+x$	$^{1}/_{4}-z$	0.022	—	0.150
III	0.314	0,225	$^{3}/_{4}-y$	$^{1}/_{4}-x$	0,025	0.436	—
IV	0,153	0,029	z	x	0.029	—	0,153
V	0.436	0.160	y	z	—	0.436	0,160
VI	0.100	0.187	$^{1}/_{4}-z$	$^{3}/_{4}+y$	—	0.437	0.150
	Average				0.024	0.436	0 153

found from the first construction. The coordinates u and v of the maxima were determined in this manner by the parabola method and from them were calculated the coordinates x, y, z of the bismuth atoms given in Table 1 .

The coordinates given by the second construction of the projection differed from the coordinates obtained from the first construction by no more than 0.003. The final values of the coordinates of the bismuth atoms were: $x=0.024$; $y=0.436$; $z=0.153$.

In Table 2 are shown the interatomic spacings and the number of neighbor atoms in the structure ∝ - Bi_4Rh.

The Bi-Rh spacing is less than the sum of the atomic radii by 3%. The coordination polyhedron of the rhodium atoms with eight vertices (a twisted cube) is shown in Fig. 3. In ∝ - Bi_4Rh there are two forms of twisted cube, right and left handed, one of which is obtained from the other by a reflection through the center of symmetry. The tetragonal face of the eight-cornered figure which is parallel to the 110 planes appears as an external face of the ∝ - Bi_4Rh crystal. An analogous coordination polyhedron is found in the series of structures of the compounds of the transition metals with elements of the B subgroup of the periodic table ($PtSn_4$, $PdPb_4$, $AuSn_4$, $CuAl_2$, $CoGe_2$).

Each bismuth atom has three neighboring atoms of bismuth arranged on one side of it as in the structure of pure bismuth. One of the Bi-Bi spacings is nearly equal to the shortest spacing in pure bismuth, two are somewhat larger , and the remaining six Bi-Bi spacings are near the largest spacings in pure bismuth.

N. V. Belov pointed out to us the analogy between the structure of ∝ - Bi_4Rh and garnet

TABLE 2.

Interatomic Spacing and Number of Nearest Atoms

Atom	Atom	Spacing in A	Number of Neighbors
Bi	Bi 2Bi 2Bi 4Bi 2Rh	3,10 3,27 3,50 3,85 2,80	11 (9Bi + 2Rh)
Rh	8Bi	2,80	8Bi

($Ca_3Al_2Si_3O_{12}$) . The oxygen atoms in the structure of garnet occupy the same positions as the bismuth atoms in ∝ - Bi_4Rh, and also form an eight-cornered figure — a twisted cube, in which are found octahedrons and tetrahedrons. In the garnet structure, the calcium atoms occupy an eight-cornered figure, the aluminum atoms — octahedrons, the silicon atoms — tetrahedrons formed by the oxygen atoms. In the structure ∝ - Bi_4Rh the coordinates of the bismuth atoms nearly coincide with the coordinates of the atoms of oxygen in the garnet structure . The rhodium atoms occupy eight-cornered figures, octahedrons and tetrahedrons at the remaining vacancies.

RESULTS

1. The crystal ∝ - Bi_4Rh has a cubic lattice with a period $a = 14.928 \pm 0.005$ A; and belongs to the space group $O_h^{10} - Ia3d$. The bismuth atoms occupy the positions 96 h with coordinates $x = 0.024$; $y = 0.436$; $z = 0.153$; the rhodium atoms — the positions 24 c.

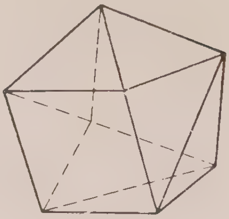

FIG. 3.

2. The coordination polyhedron of the rhodium atoms in ∝ - Bi_4Rh is eight-cornered — a twisted cube , analagous to the coordination polyhedra in the structures
The bismuth atoms have a coordination number of 11 (9 bismuth atoms and two rhodium atoms).

3. The interatomic spacing Bi-Rh in ∝ - Bi_4Rh is less than the sum of the atomic radii by 3%. Three of the Bi-Bi spacings are nearly equal to the shortest spacing, the remaining six near the largest values of the spacing in pure bismuth.

The authors wish to express their thanks to Professors N. E. Alekseevskii and N.N. Zhuravlev for discussions of the results and also to N. S. Semenko for help in conducting the experiments.

Translated by B. Hamermesh
46

SOVIET PHYSICS JETP VOLUME 3, NUMBER 2 SEPTEMBER, 1956

Effect of an Adsorbed Film of Dipole Molecules on the Electronic Work Function

N. D. MORGULIS AND V. M. GAVRILIUK
Institute of Physics, Academy of Sciences, Ukrainian SSSR

(Submitted to JETP editor, October 11, 1954)
J. Exper. Theoret. Phys. USSR 30, 149-159 (January, 1956)

An experimental investigation was performed, under high-vacuum conditions, of the variation of the work function of tungsten when an accurately measured film (of varying thickness) of cesium chloride molecules was deposited on it; these molecules contained an admixture of radioactive isotope Cs^{134} and, as a result, the density of the molecules in the film could be determined fairly accurately by the magnitude of its activity. It was shown that a film of CsCl molecules, having their own dipole moment, causes a decrease in the value of the work function of the tungsten; however, this decrease is considerably less than that produced by a film of cesium atoms. A comparison was made between these systems and data extracted from the literature for BaO--W and Ba--W systems. A discussion of several ways in which the results obtained here may be interpreted theoretically closes the paper.

THE investigation of the electronic properties of the surfaces of metals covered by adsorbed films of various, usually electropositive atoms has been the object of numerous works that have been carried out over a fairly long period of years.[1] Interest in this question lies, first, in the possibility of a broad and convenient study of the given physical problem and the application of electronic methods to the study of adsorption phenomena and, second, in the fact that systems such as these are invariably the base for many modern, efficient electron emitters. In the past the object of these investigations has usually been films of cesium, barium and thorium atoms and of the products of evaporation from an oxide cathode; the method of investigation was the following: variation in the magnitude of the photo- and thermoemissions; variation of contact potential as determined from the displacement of the current-voltage curves; and variation of the work function as determined from the shift of the red end of photoemission and from the change in the slope of the temperature dependency of thermoemission as expressed in the form: $\ln(I/T^2)=f(1/T)$.

As a result of these investigations, which were performed almost entirely with metals under conditions of high vacuum, the limits of the variation of the work function φ were determined; however, the density of the atoms adsorbed in the film N, on which this variation was based, was determined indirectly and this fact would usually introduce a certain element of arbitrariness, hampering a subsequent reliable interpretation of the results obtained. Moreover, there were absolutely no data on the effect of films of atoms deposited on the surface of nonmetals or on the effect of films of molecules, including polar molecules, i. e., those having a permanent dipole moment, deposited on the surface of solids of unlike nature, under high-vacuum conditions. Here we can mention only investigations of the effect of the adsorption of molecules of different vapors (water, alcohol, etc.) on the work function of various semiconductors under ordinary--not high-vacuum--conditions in connection with the problem of surface conditions;[2] these investigations are somewhat removed from the problem in which we are presently interested. Nevertheless, it is understandable that all these problems are of prime importance in the electronics of the surfaces of solids and of modern, efficient electron emitters--the cathodes.

It was not until 1950 that a work[3] appeared in which was posed the problem of studying the separate effect of films of BaO, SrO, and CaO dipole molecules on the variation of the work function of metals by means of a comparatively accurate measurement of the density of the molecules composing the adsorbed film. In this work a number of interesting results were reported; however, the conditions under which the experiments were performed do not give complete assurance of a sufficiently accurate determination of the value of N; furthermore, an unsatisfactory circumstance here was the heating of the substrate together with the adsorbed layer in the determination of the thermoelectric constants; consequently, there was the possibility of an uncontrolled alteration in the layer.* Therefore, with a far-reaching and more reliable study of this entire problem in mind, a series of similar investigations was performed in our laboratory; the first and second parts of these investigations, devoted to the Ba--W and BaO--antimony-cesium photocathode systems, have been completed.[4] Determination of the value of φ was made by means of contact potential and the shift of the red end of the photoeffect; this did not require heating the layer. Conductometric titration was used for determining the value of *N*; the part played by the reflection coefficient in the condensation of atoms and molecules on the surface could then be considered additionally. It is important to mention that here, too, we used the taper method successfully, providing the layer with a constantly and widely varying thickness; this procedure was worked out by us and has been extensively used in the past in the investigation of photo- and secondary-electron emission.[5] Finally, a paper was published quite recently which treated the ThO_2--Mo system;[6] here, a method of thermoemission with heating of the film was likewise used for determining the variation of the value of φ; a radiographic method of counting the α-particles of the natural radioactivity of thorium in the thick part of the layer with extrapolation toward the thin portion was used for measuring the value of *N*. However, the necessity of considerable heating of the Mo substrate led to the reduction of the ThO_2 film at its thin part and to results that were typical for the well-known Th--Mo system, etc. Thus, we see that the problem in which we are interested may be considered as barely begun and that it will require extensive and profound study. In this paper we shall present the results of our latest investigations of the problem; and, what is more important in this problem, these investigations have been conducted using the most perfect procedure.

---

[1] Zh. De-Bur, *Electron emission and adsorption phenomena*, ONTI, 1936. A. Reiman, *Thermionic emission*, GITTL, 1940. C. Hering and M. Nichols, *Thermoelectronic emission.* L. Dobretsov, *Electron and ion emission* GITTL, 1952.

[2] N. Morgulis, J. Exper. Theoret. Phys USSR 16, 959 (1946). V. Lashkarev and V. Liashenko, *Memorial volume of the 70th anniversary of the academician A. F. Ioffe*, Publishing House of Academy of Sciences, USSR, p. 535 (1950). V. Liashenko and I. Stepko, Izv. Akad. Nauk SSSR Ser. Fiz. 16, 211 (1952). B. Il'in, *Nature of adsorption forces*, GITTL, 1952.

[3] G. Moore and H. Allison, Phys. Rev. 77, 246 (1950).

The objects of investigation in the present work were the polar molecules of cesium chloride, having in the free or gaseous state a permanent dipole moment $p = 10 \times 10^{-18}$ cgs units;[7] these molecules were deposited on the surface of tungsten. CsCl, tagged by a radioactive isotope Cs^{134}, having a specific activity of ≈ 350 mCu/g and a half-life of 1.7 years, and providing, in the main, β-radiation with an energy of 0.65 mev and γ-radiation with an energy of 0.09 mev, was used in the work. The tube used for the investigation was somewhat similar to that used previously;[4] it is shown schematically in Fig. 1. Its basic components

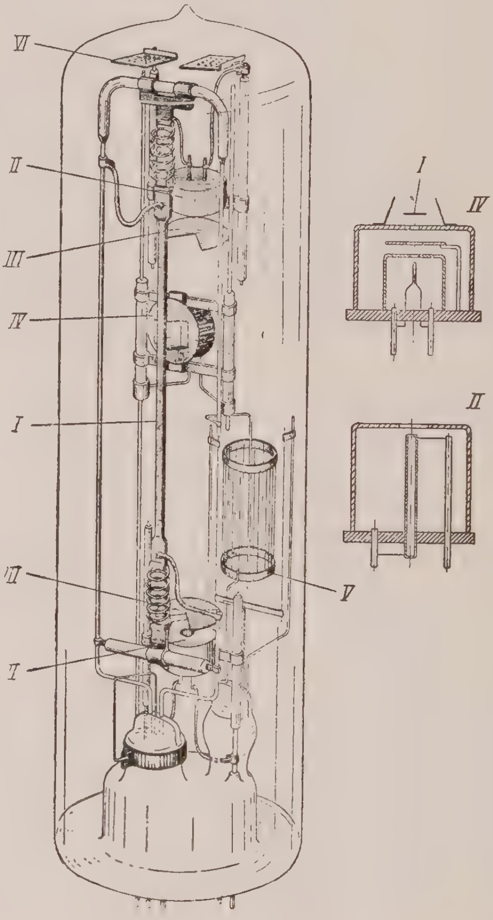

FIG. 1. *1*-Tungsten ribbon; *2*-evaporator; *3*-receiver; *4*-electron gun; *5*-manometer; *6*-getter.

---

* *Correction.* After this work had been sent to prees, there appeared the paper of P. Russell and A. Eisenstein, J. Appl. Phys., 25, 954 (1954), inwhich were given the results of an investigation of thermoelectric emission and electronic diffraction of thin films of barium oxide deposited on nickel. Remarks made by us with respect to work[3] apply fully to this work.

[4] V. M. Gavriliuk, Trudy Inst. Fiz. Akad. Nauk Ukrainian SSR 5, 87 (1954); Zh. Tekhn. Fiz. 25, 14 (1955)

[5] N. D. Morgulis, Trans. Jan. 1942 session, Ukrainian SSR, partII, p. 215. N. Morgulis, P. Borziak, and B. Diatlovitskaia, Izv. Akad. Nauk SSSR Ser. Fiz. 12, 126 (1948). P. Borziak and N. D. Morgulis, Dokl. Akad. Nauk SSSR 61, 625 (1948). B. Diatlovitskaia, Dokl. Akad. Nauk. SSSR 63, 641 (1948). N. Morgulis and N. Nakhodkin, Dokl. Akad. Nauk. SSSR 94, 1029 (1954).

[6] A. Shul'man and A. Rumiantsev, Dokl. Akad. Nauk SSSR 93, 455 (1953).

[7] E. Rittner, J. Chem. Phys. 19, 1030 (1951).

were: 1) a long (≈200 mm), flattened tungsten ribbon *I*, which was coated with a tapering film of CsCl molecules of varying density N; this ribbon was carefully degassed in advance by heating to high-temperature incandescence; 2) a platinum evaporator *II* in the shape of a small tube filled with CsCl and enclosed by a thermal screen of tantalum; an orifice 0.5 mm in diameter was made at the base of the tube; by heating the evaporator to a suitable temperature it was possible to deposit a clump of CsCl molecules on the tungsten surface; 3) a regulating receiver *III*, carefully located, on which a part of the evaporated CsCl molecules were condensed; 4) an electron gun with suitable electrodes *IV*; it was moved along the tungsten ribbon, permitting a determination of the variation of contact potential V_k from the displacement of the current-voltage curves; this gave us the distribution of the average value of the work function φ for a given section of the surface, at various locations along the ribbon; and 5) placed inside the tube envelope, a modified ionization manometer system *V*, having a central ion collector--a thin filament--and an external cathode with deflector;[8] this permitted continuous regulation of the degree of vacuum in the tube down to very low values of the order of $\lesssim 10^{-9}$ mm.

It is quite understandable that particular attention was given to obtaining and maintaining the highest possible vacuum in the experimental tube. With this in mind, the following was done:

1) The process of evacuating and degassing the glass envelope and the entire metal armature of the tube was performed most diligently and lasted for some 25-30 hours; most important, the process was repeated regularly several times. The vacuum plan made it possible to heat the glass enevelope, the last trap, and the ionization manometer and to bake the metal parts of the tube during evacuation. The excessively large barium getter *VI* was degassed and partially dusted before unsoldering the tube and, partially after unsoldering; the getter coating was distributed for maximum gas-absorption capacity; in case of necessity, the tube could still be cooled by immersing the envelope in a Dewar flask filled with liquid nitrogen. In this manner it was possible to obtain and hold a vacuum of $\lesssim 10^{-7}$ mm for a long time in the unsoldered tube.

2) Since this level of pressure of residual gases in the tube is considered absolutely unsatisfactory from the standpoint of the high requirements which must be exhibited at the present time in the methods of investigation for our problem, we resorted to the following procedure. It has long been known that absorption may be increased considerably by ionizing the residual gases in the tube; in this the ionization manometer system was of particular use;[9] in the given case it acted as activator for the absorption of the ionized gas by the carefully degassed surface of the glass envelope and by the getter speculum. Actually, by starting our manometer periodically about every half-hour we were able to obtain and hold a vacuum of the order of $p \approx 1\text{-}3 \times 10^{-9}$ mm; for measuring the value of full pressure p, our manometer was graduated in advance. Moreover, there are at present serious reasons for supposing that the effective partial pressure of that part of the residual gases that can actually be adsorbed on the surface of the tungsten, that is, to distort the results obtained here, is much lower still and may even reach a value of $p_{\text{eff}} \lesssim 10^{-10}$ mm.**

The method of approach for the measurements themselves was as follows. By heating the evaporator filled with CsCl to a temperature of approximately 450°C, where the vapor pressure reaches a value of $\gtrsim 10^{-4}$ mm, evaporation and deposition on the cold tungsten ribbon in the form of a layer having a constantly changing density takes place. At this time neither surface migration nor reevaporation of the CsCl molecules can take place. It is an easy matter to show that, since the evaporator is made of passive material--platinum--and the heat of dissociation of these molecules is fairly high, $Q = 106$ kcal/g mol, they do not dissociate into atoms during the evaporation process, and the layer deposited on the cold tungsten ribbon will consist practically of CsCl dipole molecules alone; incidentally, this is seen from a comparison of the CsCl--W and the Cs--W systems (see Fig.7). Similarly, we assume that there will be no partial reduction of the film of these molecules on the tungsten ribbon during its later temporary heating to a temperature of approximately 600° C[10] (see below), since, for example, the heat of formation of one of the typical chlorides, WCl_6, is equal to

---

[8] R. Bayard and D. Alpert, Rev. Sci. Instr. 21, 571 (1950).

**Correction. After this paper had been sent to press, experiments were completed for an evaluation of the value of p_{eff}; a description and the results of these experiments were presented in a brief report by one of the authors (N. Morgulis, Zh.Tekhn.Fiz. 25,1667 (1955).

[9] H. Schwarz, Z. Physik 122,437 (1944). D. Alpert, J. Appl. Phys. 24, 860 (1953). D. Alpert and R. Buritz, J. Appl. Phys. 25, 202 (1954). H. Hagstram, Rev. Sci. Instr. 24, 1135 (1953).

[10] N. Ionov, J. Exper. Theoret. Phys USSR 12, 58, (1942).

97 kcal/g mol. For other tungsten chlorides there are no data even for this quantity, and the simultaneous absence of other essential parameters prevents us from making a quantitative thermochemical calculation of the degree of reduction of the CsCl by metallic tungsten as was done, for example, for BaO in the problem of the oxide thermocathode.[11] For purposes of comparison, however, let us point out that the film of adsorbed BaO molecules, having Q=126 kcal/g mol, displays no reduction during heating of the tungsten substrate before approximately 600°C, as is seen from the value of the work function.[3] For this reason, the transformation of BaO--W into Ba--O--W, is likewise very improbable.

Having completed all necessary measurements (see below), during which the temporary heating of the tungsten ribbon under investigation to a temperature of approximately 600°C took place, the tube was opened, and the tungsten ribbon *I*, with the CsCl film deposited on it, and the receiver *III* were removed. The use of a cesium compound tagged by the radioactive isotope Cs^{134} had the following very important advantage: it made it possible for us to determine directly, and with great accuracy, the actual final (after heating) density distribution of the molecules along the ribbon at various places $N=f(x)$, as well as the total quantity deposited on the receiver. Knowledge of the latter quantity made it possible for us, analogously to the previous case,[4] to determine also the distribution of the original (before heating) concentration of molecules $N_0 = f(x)$ along the ribbon. This was done by taking into account the shape and location of the evaporator with respect to the tungsten ribbon and the law of density distribution in a molecular clump along the ribbon. Use was also made of the well-known expression for the condensation of vapors leaving an orifice in a tube,[12]

$$N_0 = \frac{n}{\pi h^2} \frac{x/h}{[1+(x/h)^2]^2}(1-R), \qquad (1)$$

where h is the perpendicular distance between the molecules, x is the coordinate of the receiver along the ribbon, n is the total quantity of evaporated molecules, and R is the reflection coefficient of the molecules during incidence on the hard surface. We shall not stop here to discuss the very interesting question of the reflection coefficient;[13] it will be examined in another paper appearing shortly. However, we shall introduce here in Fig. 2 the results of our determinations of the value of R, using a somewhat simplified procedure, for CsCl molecules at various densities of coated film $R=f(N_0)$ for cold substrates of Ni, Mo, and W; these measurements were also made using a procedure of

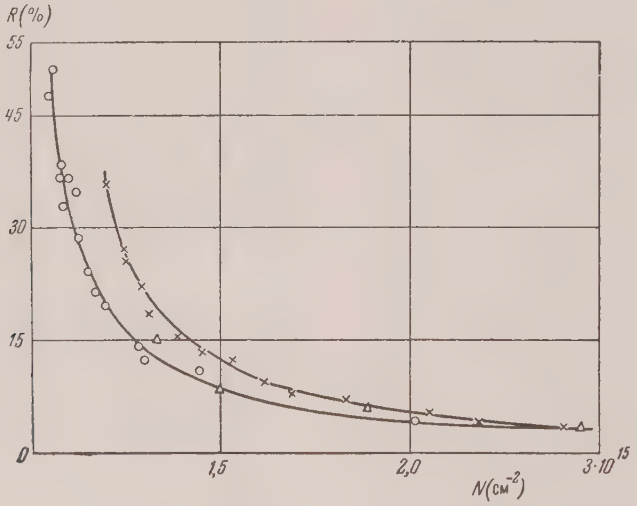

FIG. 2. × — Ni; ○ — Mo, △ — W

---

[11] A. White, J. Appl. Phys. 20, 856 (1949). E. Rittner, Philips Res. Rep. 8, 184 (1953).

[12] S. Vekshinskii, *New method of metallography investigation of alloys*, p. 28, GTTI,, 1944.

[13] Iu. Khariton and Shal'nikov, *Mechanism of condensation and formation of colloids*, GITTI, 1934. M. Devienne, J. phys. radium 13, 53 (1952); 14, 257 (1953). N. Morgulis, V. Gavriliuk, and A. Kulik, Dokl. Akad. Nauk SSSR 101, 479 (1955).

tagged atoms.[13] We observe here a marked decrease in the value of R, from more than 50% at $N=10^{14}$ cm^{-2} (degree of coverage $\theta>1$) to less than 10% at $N=10^{15}$ cm^{-2}, where a second and other layers of molecules begin to form. Therefore, it is clear that a consideration of this factor will be necessary in future studies of adsorption processes.

On the other hand, a direct determination of the final density distribution of the CsCl film on the tungsten ribbon $N=f(x)$ was of particular interest, because it provided the most direct and reliable value of this function with a high degree of accuracy and sensitivity, reaching $\approx 4 \times 10^{13}$ cm^{-2} as a result of the comparitively high specific activity of the original radiocative preparation. In other measurements of the deposition of CsCl molecules at various places on the tungsten ribbon, we either placed a thick lead screen with a narrow slit between computer and ribbon, or divided the ribbon into small parts of the order of three millimeters in length and then determined the activity of the deposit of each division individually, by the usual method. The counting time for obtaining the necessary accuracy[14] varied depending on the background; our accuracy was fairly high. The absolute value of N at various places on the ribbon was determined on the basis of the specific activity of the cesium chloride being used and the efficiency of numeration during a fixed, steady arrangement of the ribbon with respect to the computer; activity was determined on the basis of β-radiation.

Determination of the variation of contact potential V_k, i.e., of the average value of the work function φ at each individual position of the ribbon, resulted from the variation of the displacement of the current-voltage curves from the given position of the tungsten ribbon, which played the role of collector of electrons in the system, and was placed opposite the given position of the electron gun; it was possible to move the latter along the entire ribbon. In order to avoid distortions in the measurements of the current-voltage characteristics (Fig. 3) owing to a varying drop of potential in the leads, the sliding contacts and the tungsten filament of the electron gun, the latter was heated by alternating current obtained from a mercury-vapor rectifier tube having a fixed resistance across the plate circuit. For this reason, the data for the current-voltage curves, that is, the measurement of the electron current, were recorded only during the half-cycle when the heating current circuit was closed by the action of the rectifier tube, i.e., when there was no voltage drop in the cathode circuit of the gun. The example of a similar family of mutually displaced curves is represented in Fig. 3. Their values were recorded, naturally, in the region of initial velocities of very low-density electron emission. This displacement is of an absolutely normal (parallel) character, and the temperature of the electrons of the tungsten filament--cathode of the electron gun, determined from the slope of these curves, has the plausible value of about 1800°K; all this tends to confirm the reliability of our method of approach.

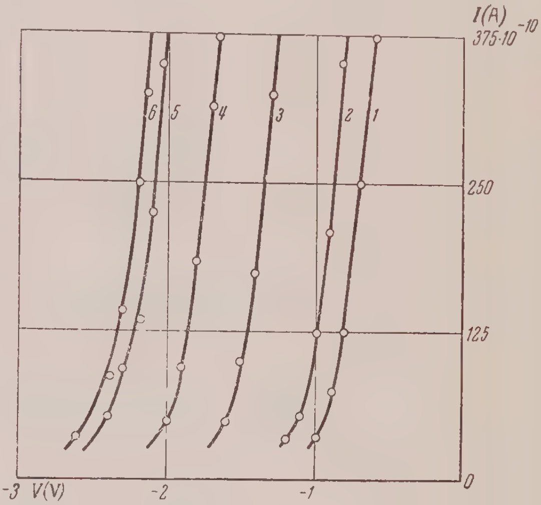

FIG. 3.

The results of measurements performed in this manner are represented in three figures in which the following are given: 1) the distribution of the surface concentration of the CsCl molecules along the tungsten ribbon immediately after dusting $N_0=f(x)$ (Curve I) and, then, after heating at T=600°C for one minute, $N=f(x)$ (Curve II, Fig. 4); 2) the distribution of the variation of the work function along the ribbon $\Delta\varphi=f(x)$ for these two extreme cases (solid lines) and for one intermediate case (broken line, Fig. 5); and 3) the same distribution $\Delta\varphi=f(x)$ for the same three cases but for a different tube (Fig. 6), where, naturally, the distribution $N=f(x)$ along the ribbon was somewhat different. For example, we see in Fig. 4 the variation in the linear distribution of the surface concentration which exists as a result of equal heating; this variation is obviously connected with the evaporation of an excess of CsCl molecules, corresponding somewhat to a nonuniform distribution of the temperature of the ribbon; Fig. 4 also shows the variation of the linear distribution of the work function caused by the above variation.

---

[14] D. Taylor, J. Sci. Instr. 27, 206 (1950).

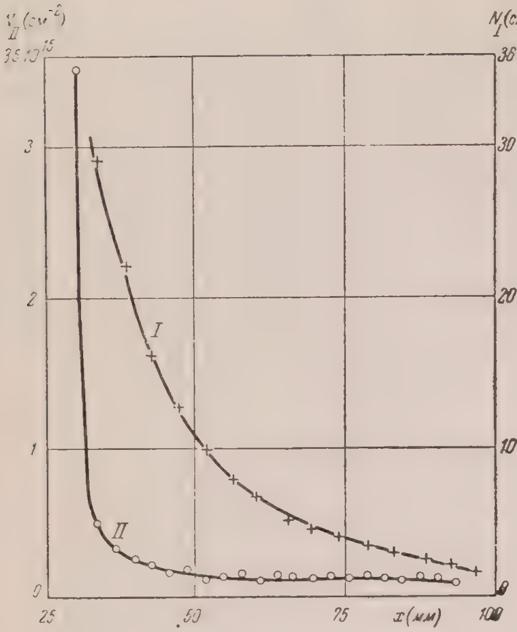

FIG. 4.

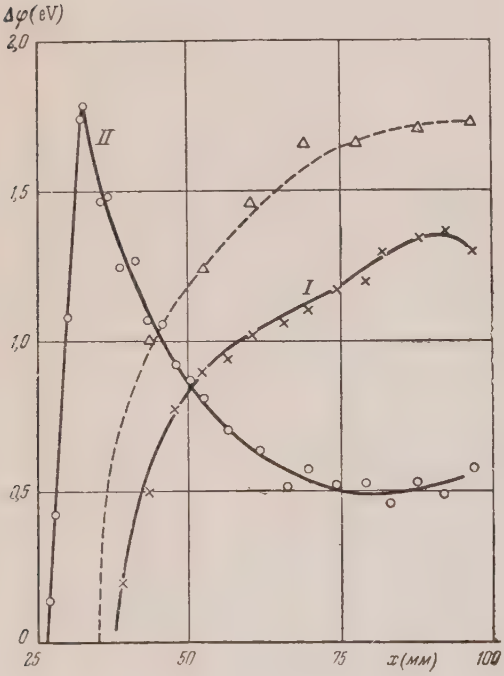

FIG. 5.

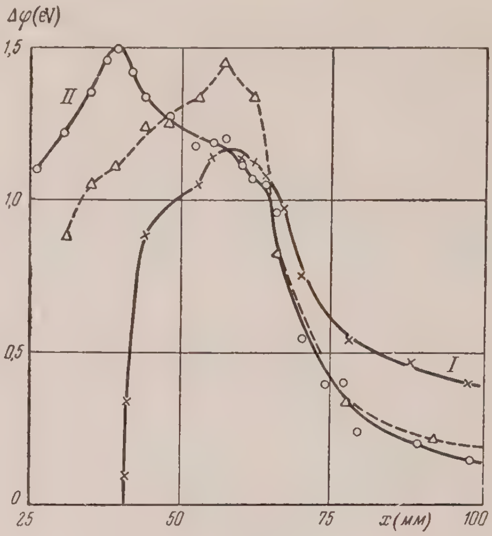

FIG. 6.

The results of the recorded measurements are represented (on two different scales) in Fig. 7, where the fundamental function $\varphi=f(N)$ is plotted for the following cases: a) the film of CsCl molecules on the tungsten immediately after dusting (before heating), represented by triangles; b) two different films (Figs. 5 and 6) after heating as described above, represented by circles and crosses. As seen from Fig. 7, all experimental points, with the exception of the two to the right, are found well within the single function $\varphi=f(N)$, which obviously implies the unchangeableness of the state of the CsCl molecules adsorbed on the surface of the tungsten substrate before and after heating. The error in the statistical determination of the value of N in one cycle of measurements is represented by the horizontal lines ; in other measurement cycles the error was many times smaller, and was too small to show on the graph. For greater clarity, we have plotted in Fig. 7 the function of the variation of the work function of tungsten $\varphi=(\varphi_0-\Delta\varphi)=f(N)$, taking $\varphi=4.5$ ev for pure tungsten.[1] Here, too, we have represented the similar function for a film of cesium atoms on tungsten substrate as derived from the literature (broken line).[15]

Inspection of the composite Fig. 7 shows that the adsorbed film of CsCl dipole molecules, having in the free gaseous state their own dipole moment $p=10 \times 10^{-18}$ cgs units, does reduce the work function of the tungsten substrate, but to a much lesser degree than does a film of cesium atoms. This is demonstrated by the fact that the maximum value of $\Delta\varphi$ is considerably less here, while the surface concentration N needed to obtain this effect is noticeably greater. It is interesting to note that this result, for some reason, is exactly contrary to that derived from a parallel comparison of the similar BaO--W and Ba--W systems. Thus, the film of BaO dipole molecules influences the work function of tungsten to a greater degree--a reducing effect--than does a film of Ba atoms, although the Cs--W and Ba--W systems are fairly similar to each other. All this can be seen from the composite table, where the dipole moment of BaO molecules in the free state, which is still undetermined, can be evaluated as

---

[15] J. Taylor and I. Langmuir, Phys. Rev. 44, 423, (1933). I. Langmuir, cited in Usp. Khim. 10, 570(1941).

$$p = ne(R_1 + R_2) - ne(\alpha_1 + \alpha_2)(R_1 + R_2)^{-2}. \quad (2)$$

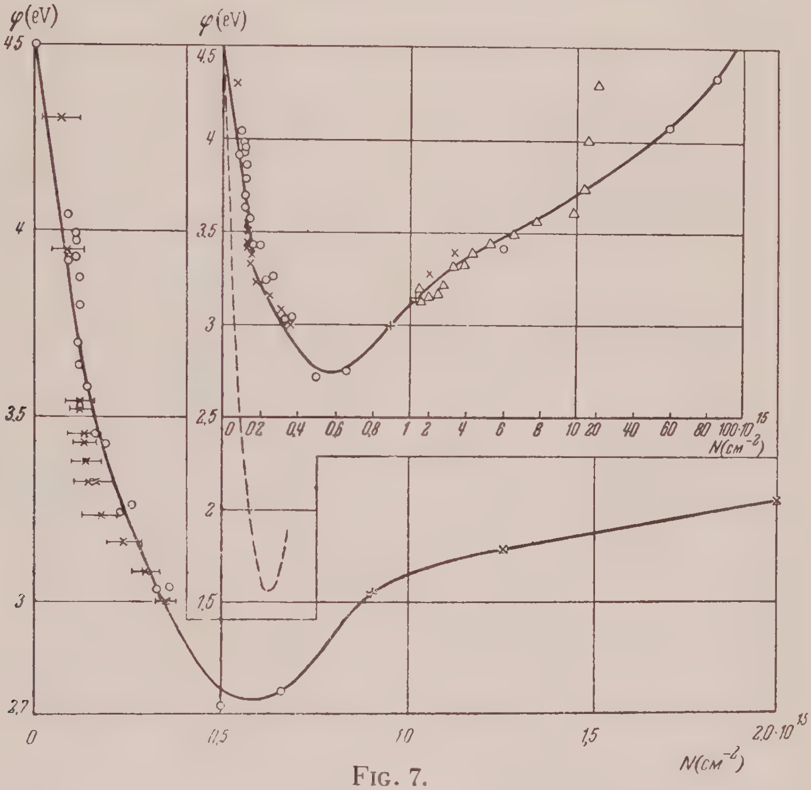

FIG. 7.

Herein R_1 and R_2 are the radii of the cation and the anion, α_1 and α_2 are their polarizabilities,[16] and n is the multiplicity of charges of the ions; for a free BaO molecule the latter must also be equal to unity, since only thus is the criterion satisfied[16] that the difference between the ionization energy of the cation and the affinity energy of the anion must be fairly small. The quantity p_0 in the table given below is the effective dipole moment of the unknown molecules in the adsorbed state in a film of infinitesimal (degree of coverage $\theta \approx 0$) surface concentration, where their interaction can be disregarded; p_0 is defined as $p_0 = (1/4\pi)(d\varphi/dN)_{N=0}$. As regards the interesting (in particluar for CsCl, as well) optimum degree of coverage $\theta_{opt} = N_m/N_1$, there is always some element of arbitrariness in its determination, owing to ignorance of the density of the total number of vacant sites N_1. Here, one should bear in mind[17] that in our case of flattened tungsten ribbon, the exterior surfaces of the microcrystalline particles should display a tendency toward advantageous grain formation with indices (100), for which $N_1 = 1.0 \times 10^{15}\,cm^{-2}$.

The results given in the table include our own for CsCl--W, and those derived and worked out for comparison from other investigations for Cs--W[15], BaO--W[4], and Ba--W[4]; they can be summarized as follows.

---

[16] O. Rice, *Electronic structure and chemical binding*, 1940, pp.178 and 220. F. Seitz, *Modern theory of solids*, 1949. G. Herzberg, *Molecular spectra and molecular structure*, 1939.

[17] I. Langmuir, Phys. Rev. 22, 374 (1923). L. Tonks, Phys. Rev. 38, 1030 (1931). L. Apker, E. Taft and J. Dickey, Phys. Rev. 73, 46 (1948).

System	$(\Delta\varphi)_{\max}$ eV	$N_{\max}$ 10^{-14} cм$^{-2}$	$P_0 \cdot 10^{18}$ **cgs units**	$P \cdot 10^{18}$ **cgs units**
CsCl—W	1,8	5	4	10
Cs—W	3,0	2,4	8	—
BaO—W	3,5	1,1	8	14 ($n=1$)
Ba—W	2,9	$\leqslant 4$	$\geqslant 9$	—

1) The question of Cs--W and Ba--W systems, i.e., of atomic films on the surface of a metal, has already been fairly well examined qualitatively in the literature;[18] here, the value of $\Delta\varphi$ is equal to

$$\Delta\varphi = (\varphi_0 - \varphi) = 4\pi a\sigma = 4\pi N\bar{p}, \qquad (3)$$

where σ is the average density of the positive surface charge produced by the double layer formed by a single system: adsorbed atoms--surface of the metal, with close electron interaction between them; p is the average dipole moment for one adsorbed atom. Unfortunately, however, these ideas have not yet been formulated into a theory that might lead to quantitative relations which would permit their direct experimental verification.

2) In contrast to the preceding case of atomic adsorption on the surface of a metal, the case of adsorption of molecules having a permanent dipole moment is still entirely unexplained, even along general lines, at the present time. In this case, the expression for the variation of the work function can probably be written in the following form:

$$\Delta\varphi = 4\pi(\beta p N + a\sigma) = 4\pi N\bar{p}, \qquad (4)$$

where the factor $\beta > 1$ characterizes the increase in the value of $\Delta\varphi$ due to the permanent dipole moment p; σ is the average density of the surface charge produced by additional electron interaction of the single system: adsorbed molecular film--surface of the metal; in general, β, p, and σ will depend on N. Unfortunately, however, before a theoretical examination of this new question, which we are undertaking at present, it is impossible to state anything conclusive. For the time being, we are limited to the following, purely qualitative remarks concerning the first and second members of Eq. (4) for the simpler case of a film with a very small degree of coverage, where we can disregard the interaction of the adsorbed molecules.

a) In a molecular clump, before deposition on the surface, all directions of the moments of the dipole molecules are equally probable and, therefore, a quite insignificant effect of a film of these molecules on the work function of the substrate was to be expected. However, the fact that not only in former cases of the molecules of BaO, SrO, and CaO[3] but in our case of CsCl molecules as well, we always obtain a noticeable decrease in the work function, clearly indicates that, near the surface of the metal, there is a fairly strong, definitely oriented electric field. This follows, too, from the general nature of the surface field of force of the metal and its electrostatic component. This field E orients the molecules in a definite preferential manner, producing a situation that is somewhat similar to that described by the well-known Langevin theory. Moreover, for the case of infinitesimal surface concentrations, where interaction of the adsorbed dipoles can be neglected, direct application of the data of this theory to the question being examined here is possible; for example, for the ratio p_0/p (see the table), we can write

$$p_0/p = L\,(pE/kT), \qquad (5)$$

where $L(x)$ is the well-known Langevin function. Taking the necessary values for the CsCl--W and BaO--W systems from our Table, we obtain (for $T = 300°K$) the field intensities in the region of these dipoles: $E = 1.7 \times 10^6$ and 2.1×10^6 v/cm, respectively, i.e., approximately the same values characterizing the tungsten surface, etc. The generalization of a similar theory for the case of adsorbed films of dipole molecules of any concentration whatsoever and the basis for it will be presented in near fututre by I. M. Dykman.

---

[18] R. Gurney, Phys. Rev. 47, 479 (1935). A. Ansel'm, Uch. Zap. Leningrad State University 38, 16 (1939). F. Vol'kenshtein, Zh. Fiz. Khim. 21, 1317 (1947). V. Bonch-Bruevich, Zh. Fiz. Khim. 25, 1033 (1951). L. Dobretsov. [e.g., see Ref. 1, L. Dobretsov. *Electron and ion emission*, GITTL, p. 136.].

b) The question of the role played by the second member of Eq. (4), characterizing the additional double layer produced by electron interaction between the molecular film and the metal, must be decided analogously to the preceding case of the presence of an adsorbed atomic film on the metal.[18] However, in our case of the CsCl --W system, we experience additional difficulty in determining the sign of the quantity σ , i.e., the sign of the double layer obtained here. In fact, this sign depends on whether a surplus or an insufficiency of negative electron charge is produced in the adsorbed film; this, in turn, depends on whether the CsCl molecules are in stable states as negative and positive ions and on the electron level in these states with respect to the Fermi level in the metal. Actually, experimental investigation of a gaseous discharge in CsCl vapors[19] has already indicated the formation of the negative ions of these molecules and in the future their positive ions will probably also be discovered; however, the energies of the electron states here are still unknown. Therefore, this second question as to the role of additional surface charge also remains open for the time being.

Finally, let us point out that the small additional (irreversible) increase of $\Delta\varphi$ by ≈ 0.3 ev observed in the experiment during momentary heating of the film can probably be interpreted as an indication of the existence of a certain number of individual places on the surface of the metal where the state of the adsorbed molecules, based on factors a) and b) above, is different from the normal states. Both these states are separated from each other by a potential barrier, and it is possible to examine them within the framework of modern notions on activated adsorption. The possibility of a slight dissociation of the CsCl with the appearance in the film of a certain quantity of Cs atoms is not excluded here.

In this manner, then, using the CsCl--W system as a model, we have examined the details of the variation of the work function of a metal during the presence of an adsorbed layer of dipole molecules. The theoretical interpretation of this phenomenon is a matter for the future.

Translated by G. F. Shultz
19

---

[19] N. Ionov, Dokl. Akad. Nauk SSSR **59**, 467 (1948). V. Dukel'skii, E. Zandberg and N. Ionov, Dokl. Akad. Nauk SSSR **68**, 31 (1949).

SOVIET PHYSICS JETP VOLUME 3, NUMBER 2 SEPTEMBER, 1956

Contact Phenomena in a Plasma

L. A. SENA AND N. S. TAUBE
Scientific Research Institute for Direct Current,
Ministry of Electric Power Plants, USSR

(Submitted to JETP editor November 9, 1954)
J. Exptl. Theoret. Phys.(U.S.S.R.) 30, 287-290 (1956)

Jumps in the potential at a boundary between regions of a plasma with different concentrations and temperatures of electrons are considered from the point of view of the classical theory of contact phenomena in metals. Measurements carried out in a discharge tube with two parts of a positive column differing in their concentrations of electrons confirmed the admissibility of such a procedure.

THE basic properties of the plasma of an ionized gas render it in many respects like a metal as represented in the classical theory of Drude. To such properties belong, in the first place, the quasi-neutrality of the plasma in the presence of a simultaneous high concentration of charged particles, and the maxwellian distribution of electron velocities on which is superposed a directed movement in the electric field, determining almost completely the electrical conductivity of the plasma. The analogy between a metal and a plasma has, of course, definite limitations. Thus, for example, while the increase in current strength in a metal is determined, for a given concentration of electrons, by the increase in the longitudinal gradient, in a plasma, on the other hand, for an almost constant gradient (sometimes even falling with increasing current density), the growth of the current is connected with an increase in the concentration of electrons.

At the same time the analogy between a plasma and the classical model of a metal is not limited to the properties just mentioned, but extends also to several more specialized phenomena, such as, for example, the Hall effect.[1] And here we will take up the phenomena at the boundary between two regions of a plasma with different electron concentrations or temperatures.

If the first region is characterized by an electron concentration n_1 and an electron temperature T_1, and the second by n_2 and T_2, then between these two regions there arises a potential difference ΔU, which in the absence of a directed current between the regions is determined, as in the classical theory of metals, by the expression[2]

$$\Delta U = \frac{k}{e}\int_{n_1}^{n_2} \frac{1}{n}\frac{d(Tn)}{dn}\,dn. \qquad (1)$$

Here the integration is carried out over the entire region of change of concentration and temperature.

As is well known, the difference in potential calculated for a metal under actual conditions according to formula (1) amounts to only some thousandths or hundredths of a volt. Actually the observed potential jumps at the boundary between two metals do not depend on the cause we have just mentioned, but on the difference in the work functions, which amounts to something between tenths of a volt and 1-2 volt.

In the electron plasma the picture is the reverse. If we try to evaluate the "work function" for taking an electron from the plasma as the work done by a mirror image force extending from infinity to an intermediate position between the electrons, then even for very high concentrations of electrons -- of the order of $10^{12} - 10^{14}$ cm^{-3} -- this work turns out to be equal to a few thousandths of an electron volt. At the same time the difference in potential between regions of a plasma with an electron temperature of the order of 10^4°K and a ratio of concentrations of the order of a few times unity may reach several volts.

When the electron temperatures of the contiguous regions of the plasma are different, the exact calculation by means of formula (1) is made more difficult, since ordinarily the temperature and concentration distributions of the electrons, which one needs in order to substitute for the $T(n)$ occurring under the integral sign, are not previously known. For a monotonic change in temperature formula (1) may be written in the form

$$\Delta U = \frac{k}{e}\left(T_2 - T_1 + \bar{T}\ln\frac{n_2}{n_1}\right), \qquad (2)$$

where $\bar{T}$ is a value of the electron temperature intermediate between T_1 and T_2. As a rough approximation we may take $T = 1/2(T_1 + T_2)$. The problem is notably simplified if the contiguous regions differ only in concentration, so that $T_1 = T_2$. In this case

---

[1] M. I. Rodin and G. V. Spivak, Compt. rend. Acad. Sci. USSR, Nouv. Ser. 24, 247 (1939). (In English.).

[2] P. I. Lukirskii, *Foundations of Electronic Theory*, Moscow-Leningrad, 1929, Ch. 5.

$$\Delta U = (k/e)\, T \ln (n_2/n_1). \tag{3}$$

For an experimental demonstration of the proposed representation of the "contact" potential difference in a plasma, we took just this latter case, as being the more simply analyzable. The representation was realized in practical form in the discharge tube drawn schematically in Fig. 1.

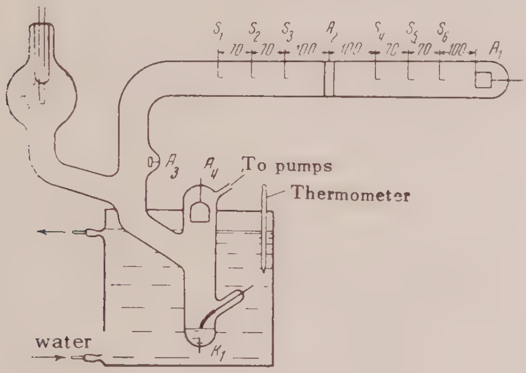

FIG. 1. Tube used in the experiments.

A mercury vapor discharge was maintained between one of the cathodes -- K_1, of mercury, or K_2, of wolfram -- and the auxiliary anodes A_3 and A_4. Two anodes were located in the main tube, the hollow cylinder A_1 at the end of the tube and A_2 in the form of a ring of width 12 mm in flat contact with the wall. Six cylindrical wolfram probes S, of length 7 mm and diameter 0.215 mm, were spaced along the axis of the tube. The distances between the probes are indicated in the drawing. In order to establish a definite vapor density the entire lower part of the tube was immersed in a vessel of water.

By using suitable resistances in order to set up various values of the currents I_1 and I_2 in the circuits of the anodes A_1 and A_2, we could create different concentrations of electrons in the parts of the discharge tube: n_2 to the left of anode A_2 and n_1 between anodes A_2 and A_1. For practical purposes the ratio of the concentrations n_2 and n_1 with this arrangement could be estimated as

$$n_2/n_1 = (I_1 + I_2)/I_1. \tag{4}$$

Due to the fact that the cross section of the tube was uniform along its entire length and the applied current density and vapor pressure of mercury were sufficiently small, cascade processes should not have played any important role, and we may suppose that the electron temperatures in the two parts of the tube were the same. This should be correct, at any event, at a sufficiently great distance from the transition region. A few remarks concerning the phenomena in this region will be made below. We merely note here that the electron temperature measurements which were carried out in each experiment at all probes gave results coinciding within the limits of the accuracy of the measurements.

The analysis of the results of the probe measurements was carried out in the following manner. On the one hand the jump in potential ΔU was calculated from formula (3), using the values of the electron temperatures and the ratios of the electron concentrations [determined both from the probe characteristics and from formula (4)]. On the other hand, the potential distribution along the tube was plotted from the measured values (Fig.2). From the graph given in Fig. 2, the jump in poten-

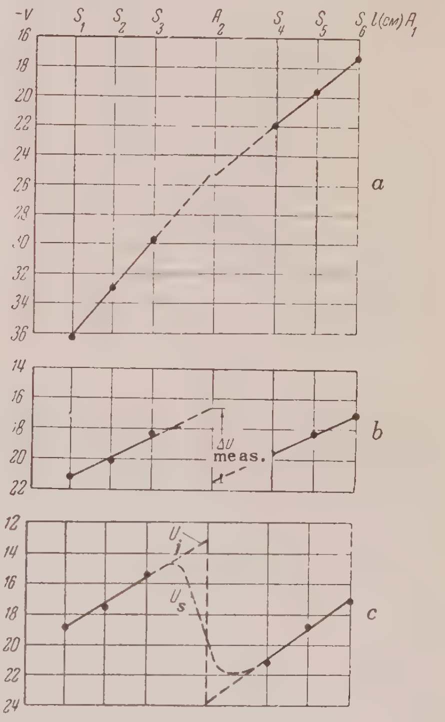

FIG. 2. Potential distribution in the tube, as measured by the probes; a: $I_1 = 1{,}2$ amp. $I_2 = 0$ amp. $T = 22000°$ K; b: $I_1 = 0{,}2$ amp. $I_2 = 1$ a:, $T = 28000°$K c: $I_1 = 0{,}4$ amp. $I_2 = 0{,}8$ amp. $T = 26000°$ K

tial is determined by extrapolating the potential curves from the left and right parts of the tube back to the "surface of contact", which is taken as the surface at which the anode was located.

With respect to the two means of determining ΔU, we may make the following remarks. The application of formula (3), which is correct in the absence of a directed current, does not seem completely legitimate under the present experimental conditions. We must also take account of the fact that for a distribution of concentrations such as occurs in the experiment, the directed current of electrons moving toward anode A_1, when in the region between the two sections of the plasma, is moving in a retarding field. In this region the energy balance is upset, the average energy of the electrons decreases, and the very form of the electron velocity distribution function may change. All this, in its turn, has an effect on the potential distribution. Taking into account, however, that the directed electron current is small in comparison with the disordered, we may expect that these circumstances will not have a great effect on the magnitude of the jump in potential.

With respect to the determination of ΔU from the graph of the potential distribution, it should be pointed out here that the true plot of the potential in the transition region is given, of course, not by the broken line U_j, with an infinitely sharp jump, but by some smoothed curve U_s drawn schematically in Fig. 2b. Consequently the jump ΔU determined by extrapolation of the linear parts of the potential distributions will be somewhat larger than that which actually occurs.

The remarks just made should be kept in mind when estimating the extent of coincidence of the calculated and measured results for the potential jump. The results of all the measurements are given in the table. The currents I_1 and I_2 are given in the first two columns, the ratio of the concentrations n_1/n_2 in the next, the electron temperature in the fourth, and finally, in the last two, the calculated and measured potential jumps.

TABLE

I_1, amps	I_2, amps	$\frac{n_2}{n_1}$	$T\cdot 10^{-3}$°K	$\Delta U_{\text{calc.}}$	$\Delta U_{\text{meas.}}$
1,2	0	1	22	0	0
1,0	0,5	1,5	25	0,87	1
0,3	1,5	6	28	3,53	4
0,2	1,0	6	28	4,3	5,5
0,1	1,0	11	29	6	5
0,1	1,0	11	26	5,4	6
0,1	1,4	15	27	6,3	7
0,04	0,8	21	18	4,7	5
0,04	0,8	21	26	6,85	11
0,04	1,3	32,5	27	8,2	10,5
0,04	0,4	11	27	5,6	5
0,04	0,6	16	27	6,45	7
0,2	2	11	28	5,8	8
0,2	2	11	30	6,3	8

In order to represent graphically the degree of separation between the calculated and measured values of ΔU, $\Delta U_{\text{calc.}}$ was plotted as abscissa and $\Delta U_{\text{meas.}}$ as ordinate in Fig. 3. We see that as a rule $\Delta U_{\text{meas.}}$ is somewhat larger than $\Delta U_{\text{calc.}}$ This agrees with the remarks made above concerning the exaggerated evaluation of the jump which results from our method of measuring it.

The case which we have considered of "contact" potential difference between contiguous regions of

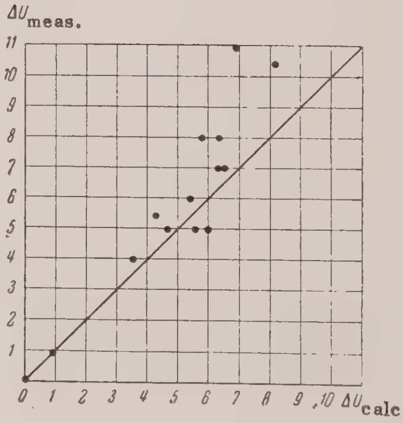

FIG. 3. Comparison of the calculated and measured values of the potential jump.

a plasma is, as we have said, an extremely simple one. However, in principle it is possible to extend our proposed approach to the consideration of phenomena in an inhomogeneous plasma and to more complicated cases, in which there occur differences in the electron temperatures as well as in their concentrations.

Translated by M. G. Gibbons
53

SOVIET PHYSICS JETP VOLUME 3, NUMBER 2 SEPTEMBER, 1956

Paramagnetic Resonance in Synthetic Ruby

M. M. ZARIPOV AND IU. IA. SHAMONIN*
Kazan State University

(Submitted to JETP editor November 19, 1954)
J. Exptl. Theoret. Phys. (U.S.S.R.) **30**, 291-295 (February, 1956)

The paramagnetic resonance absorption spectrum in monocrystals of synthetic ruby containing from 0.1 to 0.01% Cr is investigated at a frequency of 9.58×10^9 cycles. A theoretical explanation of the observed spectrum is given. By comparison of the results of theory and experiment there are found: the splitting of the basic level of energy in the electrical field of the crystal ($\delta = 0.38$ cm^{-1}) and the factors of spectroscopic splitting: $g_{\|} \approx g_{\perp} = 1.98$.

IN the majority of investigations on the paramagnetic resonance of elements of the iron group, the hydrated salts of these elemests were studied. In compounds of this type the internal electrical field causing splitting of the basic condition of the magnetic ion is created mainly by the molecules of water surrounding the ion in the form of an octahedron. For this reason the electrical field acting on the ion is divided into a strong cubic field created by the molecules of water and a weak field of much lesser symmetry caused by the remaining atoms of the lattice.

The paramagnetic properties of the investigated specimens of synthetic ruby are due to Cr^{+++}, which at low concentrations isomorphically displaces Al^{+++} in the lattice of corundum.[1] Closely surrounding the Cr^{+++} ion in the ruby is the octahedron of oxygen; here the chromium ion is not located at the center of the octahedron, but is displaced from the center along its trigonal axis, which is the optical axis of the crystal. On the whole, the individual cell of the ruby possesses a trigonal symmetry with respect to this self-same axis of the oxygen octahedron. Consequently, the internal electrical field within the ruby, created basically by the ions of oxygen, must be a powerful trigonal field.

1. RESULTS OF MEASUREMENT

The fine structure of paramagnetic resonance absorption in monocrystals of synthetic ruby containing from 0.1 to 0.01% Cr was investigated at room temperature at a frequency of 9.58×10^9 cycles.

The investigated specimens were placed in a cavity resonator which was excited by a magnetic H_{112} wave. The power through the resonator served as the magnitude being measured. The external constant magnetic field which varied from 0 to 5500 oersteds was modulated by a frequency of 50 cycles with an amplitude of modulation of $A_{\max} \approx \pm 350$ oersteds. Due to such broad modulation, the resonance curves were traced out completely on the screen of the oscilloscope.

The optical axis of the monocrystals had been determined previously at the Institute of Crystallography of the Academy of Sciences, U.S.S.R. However, for our purposes, the accuracy of this determination was inadequate. For more precise establishment of the optical axis, the great position sensitivity of several lines of the magnetic spectrum of ruby with respect to the magnitude of the angle between the directions of the optical axis and the constant field was employed. Coincidence of the optical axis with the axis of rotation of the crystal, perpendicular to the constant field, was established by the constancy of position of all lines of the spectrum on the oscilloscope screen.

---

* Experimental portion of the work carried out by Iu. Ia. Shamonin.

[1] E. S. Rudnitskaia, Works (Trudy) of the Institute of Crystallography, Academy of Sciences, USSR 8, 1953, p. 13.

The paramagnetic resonance of the spectrum of a monocrystal of ruby was studied with the orientation of the optical axis a) parallel and b) perpendicular to the constant magnetic field. Photographs of the spectra for both instances are reproduced in Fig. 1.

Given below are the resonance values of the magnetic field (in oersteds) which were determined with the aid of an instrument, which had been graduated by proton resonance, with an accuracy of 0.5%:

	Case a)			Case b)			
Experiment	650	3465	not observed	1178	1562	1967	5425
Theory	650	3465	7580	1174	1555	1952	5451

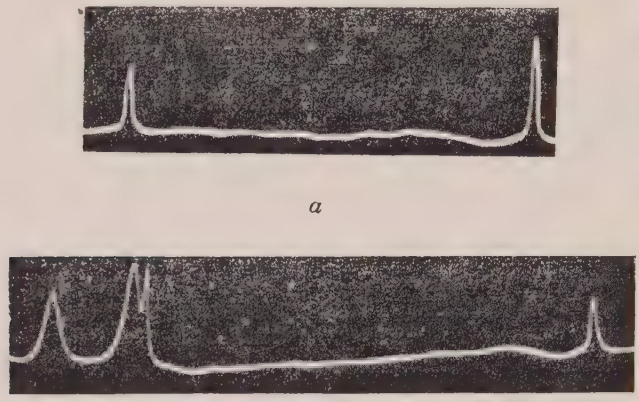

a

b

FIG. 1. Paramagnetic resonance spectrum of ruby at a frequency of 9.86×10^9 cycles: a) constant magnetic field parallel to the optical axis of the crystal; b) constant magnetic field perpendicular to the optical axis of the crystal.

2. THEORETICAL INTERPRETATION OF THE SPECTRUM

Having formulated the task of a theoretical explanation of the magnetic spectrum of ruby, it is necessary to examine the following Hamiltonian:

$$\mathcal{H} = \mathcal{H}_0 + V + \lambda (\mathbf{LS}) + (\mathbf{L} + 2\mathbf{S})\,\mathbf{H}, \qquad (1)$$

where $\mathcal{H}_0$ is the Hamiltonian of the free ion of chromium, V is the energy of the electrons of this ion in the electrical field created by all the remaining atoms in the crystal lattice. The third member of the Hamiltonian represents the operator of spin-orbital interreaction, and the fourth is the energy of the electrons in an external magnetic field of intensity **H**.

It is well known that the splitting caused by the internal electrical field of the crystal in elements of the iron group is of at least two orders higher multiplicity. For this reason, applying the method of perturbation, we will at first examine the influence of the electrical field, and then the remaining members of the Hamiltonian (1).

The potential of the electrical field of trigonal symmetry with the aid of equivalent operators[2] can be represented in the following form:

$$\begin{aligned} V = {} & B_0^0 + B_2^0 \overline{r^2}\, \alpha \{3L_z^2 - L(L+1)\} \\ & + B_4^0 \beta \overline{r^4} \{35L_z^4 - 30L(L+1)L_z^2 \\ & + 25L_z^2 - 6L(L+1) + 3L^2(L+1)^2\} \\ & + {}^1/_4 B_4^3 \overline{r^4} \beta \{L_z(L_+^3 - L_-^3) \\ & + (L_+^3 - L_-^3) L_z\}. \end{aligned} \qquad (2)$$

---

[2] K. W. H. Stevens, Proc. Phys. Soc. (London) **A65**, 209 (1952).

The basic condition of Cr^{+++} is ^4F. From theoretico-group considerations it is known[3] that in a field of trigonal symmetry the F-level splits into 3 simple and 2 double-degenerate levels. And it is a fact that after computation of the matrix elements of perturbation (2) we obtain a series equation of the seventh order, which breaks down into one cubic equation:

$$\begin{array}{c|ccc|l} L_z & 3 & 0 & -3 & \\ 3 & A-W & B & 0 & \\ 0 & B & -W & -B & =0 \\ -3 & 0 & -B & A-W & \end{array} \qquad (3)$$

and two quadratic equations:

$$\begin{array}{c|cc|l} L_z & 2 & -1 & \\ 2 & C-W & D & =0; \\ -1 & D & E-W & \end{array} \qquad (4)$$

$$\begin{array}{c|cc|l} L_z & 1 & -2 & \\ 1 & E-W & -D & =0. \\ -2 & -D & C-W & \end{array}$$

where

$$A=\frac{18}{35}\overline{r^2}B_2^0-\frac{8}{7}\overline{r^4}B_4^0, \quad B=-\frac{8\sqrt{7}}{7}\overline{r^4}B_4^3,$$

$$C=-\frac{8}{35}\overline{r^2}B_2^0-\frac{8}{21}\overline{r^4}B_4^0, \quad D=-\frac{8\sqrt{14}}{21}\overline{r^4}B_4^3.$$

The solution of Eq. (3) results in three simple equations of energy

$$W_1=A, \quad W_{2,3}={}^1/_2(A\pm\sqrt{A^2+8B^2}),$$

having their own corresponding functions:

$$\Psi_1=2^{-1/2}(\Phi_3+\Phi_{-3}), \qquad (5)$$

$$\Psi_i=[2(1+2\alpha_i^2)]^{-1/2}(\Phi_3+2\alpha_i\Phi_0-\Phi_{-3}),$$

where

$$i=2,3, \text{and } \alpha_i=B/W_i.$$

Equations (4) result in two doubly degenerate equations of energy:

$$W_{4,5}={}^1/_2(C+E\pm\sqrt{(C+E)^2+4D^2})$$

with their own functions:

$$\Psi_i^{(1)}=\alpha_i\Phi_2+\beta_i\Phi_{-1}, \quad \Psi_i^{(2)}=-\alpha_i\Phi_{-2}+\beta_i\Phi_1,$$

where $i=4.5$; $\alpha_i=-D/\sqrt{(C-W_i)^2+D^2}$ and $\beta_i=\sqrt{1-\alpha^2{}_i}$. Analysis of the experimentally obtained spectrum of magnetic resonance demonstrates that the basic level must be simple; consequently, no matter what the sign of A is, the lowest level will be W_3.

In ref. 4 it is shown that, if the basic level is simple and non-magnetic, then (with an accuracy up to magnitudes of the second order) the energy levels are determined as the intrinsic values of the following matrix, depending only on the spin variables:

$$W_0+2\beta(\delta_{ij}-\lambda\Lambda_{ij})S_iH_i \qquad (6)$$

$$-\lambda^2\Lambda_{ij}S_iS_j-\beta^2\Lambda_{ij}H_iH_j,$$

$$\Lambda_{ij}=\sum_{n\neq 0}\frac{\langle 0|L_i|n\rangle\langle n|L_j|0\rangle}{W_n-W_0}.$$

The subscripts i, j refer to the cartesian coordinates, and 0,..., n to the orbital levels of energy. Note that in our problem $\Lambda_{ij}=0$ when $i\neq j$. The last member in matrix (6) is not taken into consideration, because the correction to the energy introduced by this member with the magnetic fields employed at present is less than 0.001 cm^{-1}.

In conjunction with the completed experiment, we will examine the following two cases: 1) constant magnetic field parallel to the optical axis of the crystal, 2) magnetic field perpendicular to this axis.

In the first case, formula (6) results in the matrix:

$$C+g_{\parallel}\beta HS_z+{}^1/_2\,\delta S_z^2, \qquad (7)$$

---

[3] H. A. Bethe, Ann. Physik 3, 133 (1929).

[4] A. Abragam and M. H. L. Pryce, Proc. Roy. Soc. (London) A205, 135 (1951).

where

$$g_{\parallel} = 2(1 - \lambda\Lambda_{zz}), \quad C = W_3 - \lambda^2\Lambda_{xx}\, S(S+1), \quad \delta = 2\lambda^2(\Lambda_{xx} - \Lambda_{zz}),$$

$$\Lambda_{xx} = \frac{3}{4}\,\frac{1}{1+2\alpha_3^2}\left[\frac{(\alpha_4\sqrt{3} + 4\alpha_3\beta_1)^2}{W_4 - W_3} + \frac{(\alpha_5\sqrt{5} + 4\alpha_3\beta_5)^2}{W_5 - W_3}\right],$$

$$\Lambda_{zz} = \frac{9}{1+2\alpha_3^2}\,\frac{1}{W_1 - W_3}.$$

Rejecting the inapplicable constant, we obtain the following equations of energy from (7):

$$g_{\parallel}\beta H_m + {}^1/_2\,\delta m^2 = E_m \; (m = {}^3/_2,\ {}^1/_2,\ -{}^1/_2,\ -{}^3/_2),$$

where m is the projection of the spin moment. Designating $2E_m/\delta = \varepsilon_m$, $g_{\parallel}\beta H/\delta = x$, we obtain the final expression in the form:

$$\varepsilon_{\pm 3/2} = 2 \pm 3x, \quad \delta_{\pm 1/2} = \pm x. \tag{8}$$

A graphic representation of (8) is given in Fig. 2.

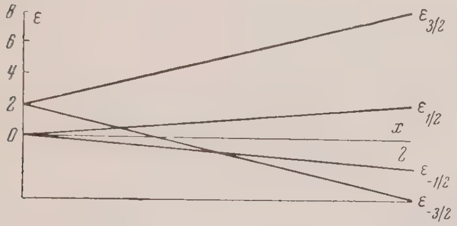

FIG. 2. Schematic of the splitting of the basic level of the Cr^{+++} ion in ruby when the magnetic field is directed along the axis of the crystal.

The number and position of the line of paramagnetic resonance are easily determined with the aid of (8) if it is remembered that the probability of magnetic dipolar transitions is noticeably large only for those pairs of equations whose spin-magnetic quantum numbers differ by unity. These probabilities for the transitions $^1/_2 \leftrightarrow {}^3/_2$, $^1/_2 \leftrightarrow -{}^1/_2$, $-{}^3/_2 \leftrightarrow -{}^1/_2$ as a first approximation are related in the ratio 3:4:3. Identification of the experimental and theoretical spectra with the aid of (8) results in $g_{||} = 1.98$ and $\delta = 0.38$ cm^{-1}. One should note, however, that at the frequency of the variable field employed, a third resonance absorption line at $H \simeq 7580$ oersteds was to be expected.

In the case in which the constant magnetic field is perpendicular to the optical axis of the crystal, formula (6) results in the matrix:

$$C + g_{\perp}\beta H S_x + {}^1/_2\,\delta S_z^2, \tag{9}$$

where $g_{\perp} = 2(1 - \lambda\Lambda_{xx})$. The series equation of matrix (9) has the roots

$$\varepsilon_{1,2} = 1 + x \pm \sqrt{(1-x)^2 + 3x^2}, \tag{10}$$

$$\varepsilon_{3,4} = 1 - x \pm \sqrt{(1+x)^2 + 3x^2},$$

where $\varepsilon_i = 2E_i/\delta$ and $x = g_{\perp}\beta H/\delta$. The graphic representation of (10) is given in Fig. 3.

In order to compare the spectra obtained experimentally and theoretically, the probabilities of transitions between the various levels were calculated. The theoretical values of the resonance

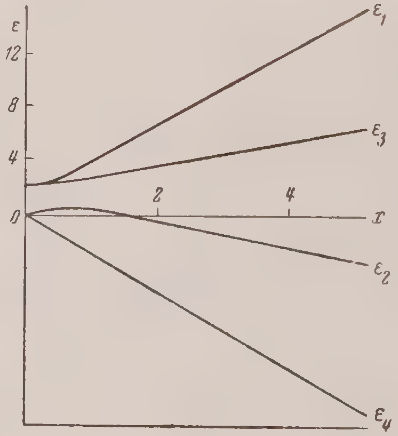

FIG. 3. Schematic of the splitting of the basic level of the Cr^{+++} ion in ruby when the magnetic field is directed perpendicular to the axis of the crystal.

fields, noted above, were computed according to formulas (10) using the values of $g_{||}$ and δ obtained previously.

The authors express their gratitude to S. V. Grum-Grzhimailo and B. N. Grechushnikov for making the specimens of synthetic ruby available and for determining their major axes by the optical method.

Translated by A. Certner
54

SOVIET PHYSICS JETP VOLUME 3, NUMBER 2 SEPTEMBER, 1956

The Inelastic Scattering of Electrons from a Copper Oxide Surface

N. B. GORNYI
Leningrad Institute for Electrotechnical Communication

(Submitted to JETP editor, November 15, 1954)
J. Exptl. Theoret. Phys.(U.S.S.R.) 30, 160-170 (January, 1956)

An electrical differentiation method in a spherical condenser is used to study the inelastic scattering of electrons from a copper oxide surface. Inelastically scattered electrons with discrete energy losses were observed from both monocrystalline and polycrystalline surfaces. The discrete energy losses are equal to the energies required to transfer an electron of the crystal lattice from a filled band to an allowed one. It is shown that the inelastically scattered electrons, with discrete energy losses, are produced by the same mechanism as accounts for the group of genuinely secondary electrons, of discrete energies, which we had discovered previously.

INTRODUCTION

WHEN a group of electrons enters matter, individual electrons undergo changes in their direction of motion, and also lose energy. Little is known about the mechanism by which electrons of low and medium energies (tens and hundreds of ev) lose energy as they pass through a solid body. A study of this mechanism is both interesting for its own sake, and relevant to the understanding of many phenomena, in particular the emission of secondary electrons.

In the course of investigations on the distribution of secondary electrons emitted from metal and metal oxide surfaces, several authors[1-4] have observed inelastically scattered primary electrons with small, discrete energy losses. The primary electrons had energies of approximately 100 volts in these investigations and the inelastically scattered groups were observed at energies close to the primary energy. The fundamental method used in the study of spontaneous energy losses was that of magnetic analysis. This method has high resolving power, but suffers from the disadvantage that only a small fraction of the electrons can be analyzed: namely those traveling in a small solid angle determined by the slit of the analyzer. The retarding field and spherical condenser method proposed by Lukirskii[5] avoids this drawback, but does not have high enough resolving power to investigate the fine structure in the energy distribution of the electrons. As our experiments on the energy distribution of genuinely secondary electrons[7] have shown, the use of electric differentiation in the spherical condenser method[6] increases the resolution considerably and allows one to study the fine structure.

In the present work we examine the fine structure in the energy distribution of secondary electrons at energies close to the primary electron energy. As samples to be investigated, we used copper

---

[1] R. Whiddington, Proc. Leeds Phil. Lit. Soc. 1, 162 (1927).

[2] L. J. Hawort, Phys. Rev. 48, 88 (1935); 50 216 (1936)

[3] E. Rudberg, Phys. Rev. 50, 138 (1936); Proc. Roy. Soc. (London) A 127, 111 (1930).

[4] A. R. Shulman and E. I. Miakinin, Dokl. Akad. Nauk SSSR 91, 1075 (1953).

[5] P. I. Lukirskii, Zh. Rus. Fiz-Khim Ob., Ch. Fiz. 57, 463 (1925).

[6] N. B. Gornyi and L. M. Rakhovich, J. Exptl. Theoret. Phys. U.S.S.R. 26, 454 (1954).

[7] N. B. Gornyi, J. Exptl. Theoret. Phys. U.S.S.R. 27, 171 (1954).

covered with copper oxide. In previous work with these samples, the distribution curve had been observed to have fine structure in the neighborhood of the genuinely secondary electrons.

APPARATUS

The principles of the electrical differentiation method for investigating the energy distribution of secondary electrons are described in references 6,7. The circuits described in reference 6 were set up in our laboratory by Rakhovich and are described in detail in his dissertation[8]. Fig. 1 shows a block schematic of the electrical circuit used. The generator frequency was chosen to be 29 cps. The effective value of the alternating component of the potential applied to the collector by the generator was $\Delta V_k = 0.42$ volts. With the preamlifier we could observe currents as low as 10^{-13} amp. In order to measure currents of this size, it was necessary to choose a very narrow band width for the amplifier--no larger than 0.5 cps. This was attained by using a phase sensitive detector.* The phase sensitive detector consists of a synchronous detector and a low frequency filter. As a synchronous detector we used a mechanical relay, which works well at low frequencies. The synchronous detector scheme worked quite satisfactorily . A microammeter at the output gave not only the magnitude of the derivative, but also its sign.

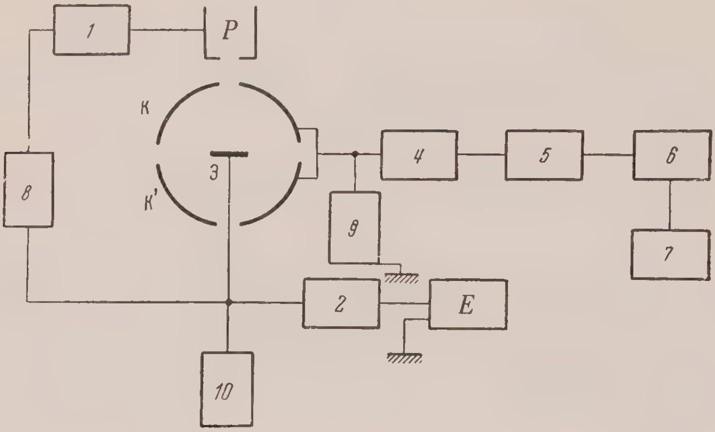

FIG. 1. Block-schematic of the apparatus: *E*-emitter, *P*-electron gun, *K* and *K'*-collectors, *1*-electron gun power supply; *2*-source for D.C. component of the collector potential; *3*-generator of the alternating, sinusoidal potential, *4*-preamplifier, *5*-band pass amplifier, *6*-synchronous filter, *7*-measuring apparatus *8* and *9*-galvanometers, *10*-apparatus for outgassing the emitter.

Our investigations led us to the conclusion that the experimental energy distributions of the secondary electrons, as obtained by the retarding field method, can be distorted in the spherical condenser.[9] This distortion is due to the fact that the number of tertiary electrons knocked out of the collector by secondary ones, subsequently reaching the emitter, depended on the retarding potential. The distortion of the experimental distributions is significant for small values of V_k, and for the values of interest to us--those near the potential V_a accelerating the primary electrons. In order to correct for this distortion, we used the vacuum apparatus shown schematically in Fig. 2. In the present investigations we used the same mono- and polycrystalline samples of copper oxide on copper as used earlier.[7,9] The electrode with the emitter *E* was cylindrical, and contained a bifilar heating filament inside it. The diameter of the cylindrical electrode was 20 mm, while its length was 17 mm. The construction of the electrode and emitter was similar to that in reference 9. The preparation and outgassing of the apparatus was as in reference 7. Before the getter was unsoldered and fired, the pressure in the apparatus was less than 10^{-6} mm of mercury at 450°C.

---

* We are grateful to A. M. Bonch-Bruevich for pointing out to us the advantages of using a synchronous filter in our apparatus.

[8] L. M. Rakhovich. Thesis, Leningrad Institute for Electrotechnical Communications, 1953.

[9] N. B. Gornyi, J. Exptl. Theoret. Phys. U.S.S.R. **26**, 327 (1954).

The spherical part of the apparatus was 120 mm. in diameter, covered inside with aquadag, and served as the collector. The collector was divided into two hemispheres K and K', insulated from each other and such that the secondary electrons could reach only the upper hemisphere K. The secondary electrons 2 (Fig. 2) incident on the collector K knock out tertiary electrons 3, which can go back to the collector K, to the electrode with emitter E, or to the collector K'.

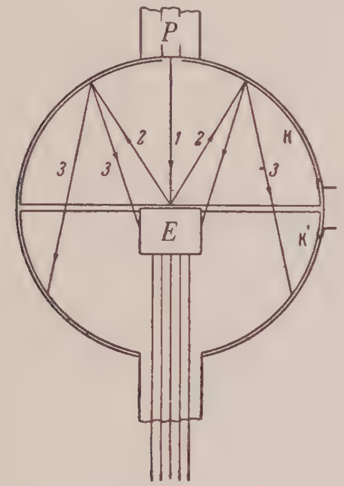

FIG. 2. The vacuum apparatus. E-electrode with the emitter, P-electron gun; K and K'-collectors.

Our data were taken with both collectors K and K' in the measuring circuit, (arrangement 1), with only one collector K (arrangement 2) and with only the collector K' (arrangement 3). In all runs the collectors K and K' were at the same potential. In order to avoid distortion of the electron trajectories by the earth's magnetic field, the latter was compensated for by two coils of 1 m diameter.

RESULTS OF THE MEASUREMENTS, AND APPLICATION OF CORRECTIONS FOR THE TERTIARY ELECTRONS

Figure 3 shows the curves obtained using a monocrystalline copper oxide surface (111) with V_a=128.5 volts and emitter temperature 420°C. The bias curves 1,2,3 and the distribution curves 4,5,6 were obtained using the first, second and third measuring arrangements respectively. Curves 1--6 are shown on an enlarged scale in the voltage region $V_k \approx V_a$.

We note that curves 1 and 2 fall off for $V_k \approx V_a$; the fall off is due to a decrease in the number of elastically scattered electrons, and occurs over a voltage range of about one volt. Corresponding to this, the width of the elastically scattered peak is also about one volt. This indicates that there is a spread in the energy of the primary electrons, the spread being due to the thermal energy distribution of electrons leaving the cathode filament, or to the non-uniformity of the filament potential. In the following, "primary electron energy" shall mean the energy at the maximum of the peak due to the elastically scattered electrons.

Curve 3 in Fig. 3 shows how the current from the collector K' varied. Since secondary electrons from the emitter cannot reach K' , curve 3 evidently gives the tertiary electron current between K and K' as a function of V_k, while curve 6 gives the "speed" relative to changes in V_k with which this current varied. Curve 1 (Fig.3) becomes negative for values of V_k between 16 and 80 volts. It follows that in this voltage range the number of secondary electrons from the collector (tertiaries) which fall on the emitter is larger than the number of secondary electrons (from the initial scattering of the primaries) falling on the collector K. This is quite possible, since the secondary emission coefficient δ of aquadag depends strongly on the conditions of preparation, as well as on the temperature of the initial heating, and can be larger than unity. Thus, according to the measurements of Titkov [10], aquadag which has been warmed for 6 hours at a temperature of 500°C at a pressure of 2 x 10^{-6} mm mercury has $\delta > 1$ for V_a about 100 to 500 volts. As the (negative) values of V_k are increased above 70-80 volts, curves 1 and 2 (Fig. 3) become positive. This corresponds to a decrease in the number of tertiary electons emitted, the decrease being due to the lower energy of the scattered primary electrons which reach the collector.**

When V_k reaches ~ 126 volts, i. e., when the

** The bias curve 2 (Fig. 3) becomes negative at a smaller V_k (13 volts) than does curve 1 (16 volts), and becomes positive again at a larger V_k (90 volts) than curve 1 (80 volts). This can be explained by the fact that the bias curve 2 is distorted by the large tertiary electron current to the emitter and collector K' , while curve 1 is distorted only by the tertiary electron current reaching the emitter.

[10] A.S. Titkov, Zh. Tekhn. Fiz. 23, 1361 (1953).

energy of the elastically scattered primary electrons reaching the collector has decreased to V_a-V_k~2-3 volts, then curves 1 and 2 increase sharply. Correspondingly, the distribution curves (4 and 5) become negative in the same region of V_k, while the "rate-of-change" curve 6 for the current of tertiary electrons reaching the collector K' exhibits a small peak. These data indicate that the tertiary electron current decreases the current of secondary electrons when V_k is less than about 126 volts. When the energy V_a-V_k of the electrons falling on the collector decreases to 2-3 volts, the efflux of tertiary electrons either ceases or becomes negligibly small.

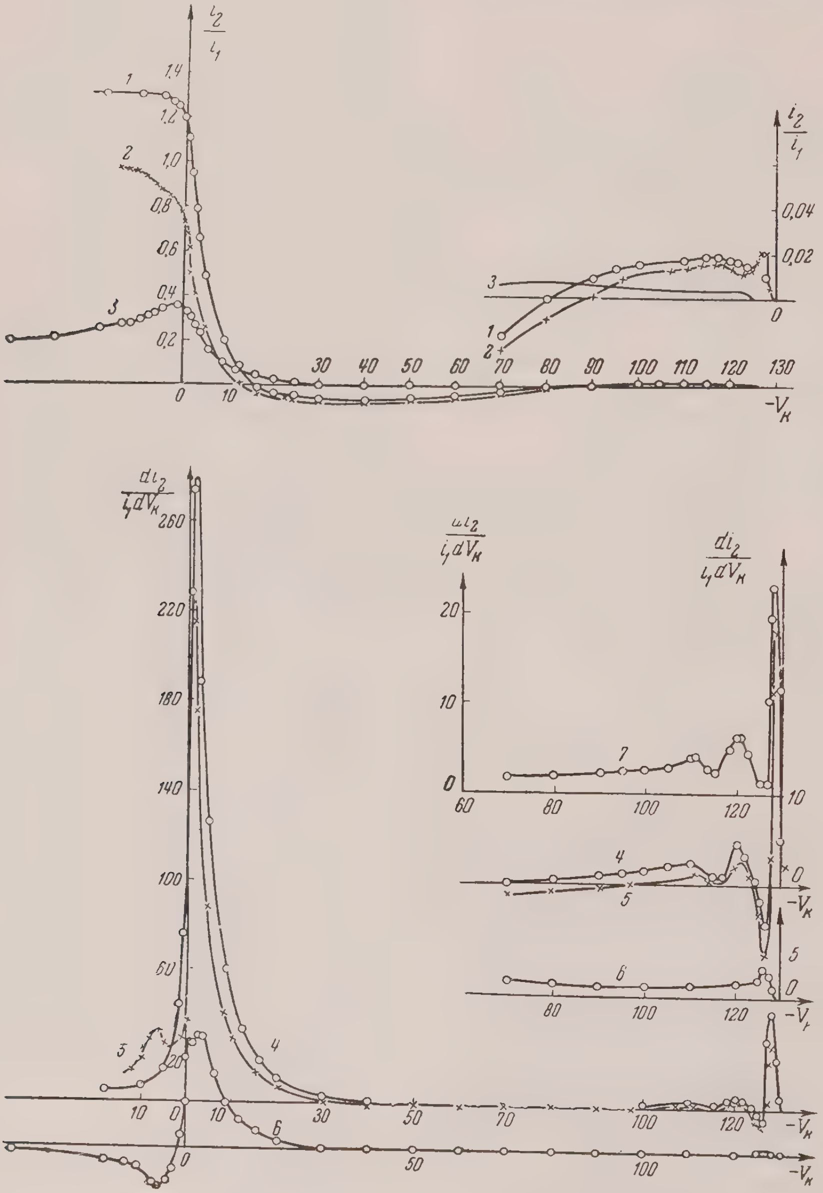

FIG. 3. Curves obtained for a monocrystalline copper oxide surface (111) with V_a=128.5 volts and t=420°C.; *1,2* and *3*-bias curves; *4,5*, and *6*-distribution curves, obtained by electrical differentiation, *7*-corrected distribution curve.

Let us consider how to find the ratio of the tertiary electron currents $I_{k'}$, reaching the collector K', and I_E reaching the emitter E (Fig. 2). Since $I_{k'}$ is measured directly, knowledge of this ratio would allow us to correct for the distortion due to the current I_E. When the space between emitter and collector is field free, i.e., when $V_k=0$, then both the tertiary and secondary electrons move in straight lines. If we assume that the angular distributions of the secondary electrons leaving the emitter, and of the tertiary electrons leaving the collector K, are given by the cosine law, then from the geometry and a direct measurement of $I_{k'}$ one can calculate the tertiary electron current I_E falling on the electrode E. Calculations showed that in our experimental set up, the current I_E was about $(1/2)\ I_{k'}$.

In the present work, we are particularly interested in the possibility of corrections at large negative values of V_k, close to V_a. Under these conditions, the electric field could bend the trajectory of the tertiary electrons in such a way as to deflect some tertiary electrons from the collector K' to the electrode E, thus increasing I_E. We could try to calculate the increase in I_E by finding the trajectories of tertiary electrons moving in a radial electric field. However, such calculations would be difficult because of the large, but unknown, spread in tertiary electron energy at a definite V_k. In addition, since the electrode with the emitter is cylindrical, the field is not strictly radial and hence the calculations would not be exact. Hence, we looked for another method of correcting the experimental data. It turned out that it was possible to make this correction by obtaining the values of $I_{k'}$ and I_E, for V_k in the region of interest (close to V_a), directly from the experimental data.

The bias curves 1 and 2 (Fig.3) rise sharply as V_k approaches V_a ($V_k \sim 126$ volts); as mentioned above, this is explained by the decrease(to zero or a negligible value) in tertiary electron emission as the energy of the primary electrons scattered from the emitter and reaching the collector K decreases to 2-3 volts. In making the corrections for tertiary electron current, we assume that the emission of tertiary electrons under the above described conditions ceases completely. The rise in curve 1 is due to the tertiary electrons reaching only the electrode with the emitter E, while the rise in curve 2 is due to the tertiary electrons reaching the electrode E and the collector K'. Clearly, the difference between the maximum ordinate in curve 1 for $V_k \sim V_a$, and the minimal ordinate for $V_k \sim 125$ volts gives I_E, while the corresponding difference in curve 2 gives $I_E + I_{k'}$. Since the ordinates of curves 1 and 2 in this region are small, the value of I_E and $I_{k'}$ found by this method will be quite inaccurate. I_E and $I_{k'}$ can be determined more accurately from curves 4--6 (Fig. 3).

The distortion of the bias curves by the tertiary electron currents corresponds to a distortion in the distribution curves (curves 4 and 5, Fig. 3) caused by changes in the tertiary electron current with changes in V_k. Curve 4 is lowered by the changes in the number of tertiary electrons reaching only the electrode E, while curve 5 is lowered by the changes in the number of tertiary electrons reaching the electrode E and the collector K'. Since curve 6 (Fig. 3) gives the "speed", relative to changes in V_k, of the changes in the number of tertiary electrons reaching only the collector K', then clearly the differences of the ordinates in curves 4 and 5 should equal the value of the ordinate in curve 6 at the corresponding V_k. This is indeed the case. The negative peaks in curves 4 and 5 at $V_k \sim 126$ volts, and the peak in curve 6 at the same voltage, correspond to the above mentioned abrupt decrease in the tertiary electron current as the energy of the primary electrons falling on the collector K decreases to 2--3 volts. Clearly, the area of the negative peak in curve 4 corresponds to the tertiary electron current I_E, the area of the negative peak in curve 5 to the sum of the tertiary electron currents I_E and $I_{k'}$, and the area of the peak in curve 6 corresponds to the current $I_{k'}$, all at the same value of V_k.

From this we can find the ratio of the tertiary electron currents I_E and $I_{k''}$. The distortion introduced by changes in the tertiary electron current I_E for given values of V_k can be found by changing the ordinates in curve 6 in the ratio of the currents I_E and $I_{k'}$. Correcting curve 4 for the "speed" of changes in tertiary electron current reaching the electrode E, and curve 5 for the "speed" of changes in the tertiary electron current reaching the electrode E and collector K', we obtain curve 7, shown in Fig. 3. Curves similar to those shown in Fig. 3 were obtained for other values of V_a and on other samples of copper oxide. Only for low energy electrons ($V_a = 21.5$ volts) did the results differ from those given above.

Figure 4 shows the curves obtained with the same monocrystalline copper oxide surface (111) for $V_a = 21.5$ volts and emitter temperature $t=400$°C. The bias curves 1, 2 and 3, and the distribution curves 4, 5 and 6 were obtained with the first, second, and third measuring arrangements respectively. Curves 1 and 2, Fig. 4, differ from the curves 1 and 2, Fig.

3, in the absence of a sharp rise in i_2/i_1, as V_k increases to V_a. Correspondingly, the distribution curves 4 and 5 in this range of V_k do not become negative. One might conclude from these data that in this case (V_a=21.5 volts) there is no decrease in the tertiary electron emission as the energy of the electrons falling on the collector decreases to ~2 volts, and the distribution curves for the secondary electrons are not distorted by changes in the tertiary current. However, the presence of a rather distinct peak at V_k=20 volts in curve 6, which gives the "speed", relative to changes in V_k, of changes in the tertiary current falling on the collector K', indicates an abrupt decrease in the tertiary electron emission in this case. This contradiction can be explained if one supposes that when electrons of energy 21.5 volts are scattered there appears a group of inelastically scattered electrons with energy loss ~2 volts, which compensate for the decrease in the tertiary electron emission. The existence of this group of inelastically scattered electrons is supported by the small peaks in curves 4 and 5 (Fig. 4) at V_k=19 volts.

In Fig. 5 there are shown several corrected curves giving the relative number of electrons falling on the collector as a function of the energy loss in the emitter, obtained at various values of V_a and on various samples of copper oxide.

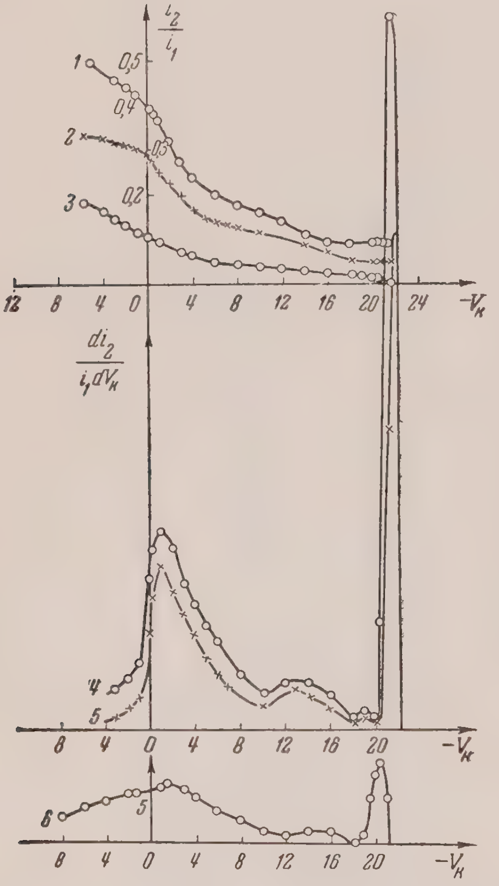

FIG. 4. Curves obtained for a monocrystalline copper oxide surface (111) with V_a=21.5 volts and t=400°C.; *1,2,* and *3*-bias curves; *4,5,* and *6*-distribution curves, obtained by electrical differentiation.

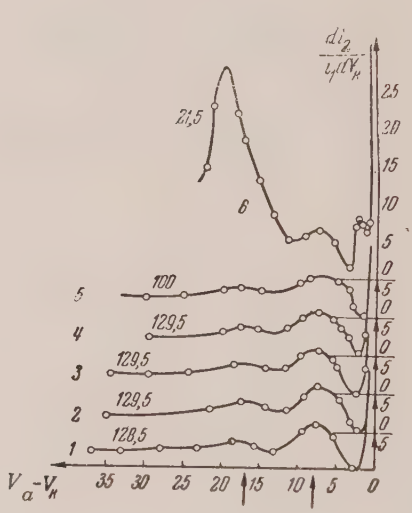

FIG.5. Curves obtained at 400°C. for the relative number of electrons as a function of their energy loss at various values of V_a, which are shown next to the appropriate curve. *1,2* and *6*-for a monocrystalline (111) surface, *3* and *5*-for a monocrystalline (110) surface, *4*-for a polycrystalline surface. Curve 6 has been magnified by a factor 3.34 relative to other curves. The peak in curve 6 at V_a-V_k=20 volts corresponds to a maximum in the genuinely-secondary electrons .

DISCUSSION OF THE RESULTS

In our study of the energy distribution of genuinely-secondary electrons from a monocrystalline surface of copper oxide[7], we demonstrated the existence of fine structure--i.e., supplementary maxima. These supplementary maxima are due to transitions which the electrons of the crystal lattice can make from the filled energy band to other allowed bands lying above the Fermi level. Each transition is associated with the absorption of a definite amount of energy from the primary electrons; the possible energy transfers are given by the formula [11,12]

$$W = (h^2/8m\pi^2)(2\pi n/d)^2, \qquad (1)$$

where h is Planck's constant, m the electron mass, d the lattice constant, and $n^2 = h^2 + k^2 + l^2$ (h, k, l, being the Miller indices of the appropriate lattice planes).

It is natural to assume that some of the primary electrons can be scattered after losing the energies given above. Then in addition to the elastically scattered primary electrons, there must appear inelastically scattered primary electrons in the distribution curve. In both the corrected curve (Fig. 3, curve 7) and the uncorrected ones (curves 4 and 5), there are 2 distinct peaks, corresponding to primary electrons which have lost energy $V_a - V_k = 8.5$ and 17.5 volts. These values agree well with formula (1), which for $n^2 = 1$ and 2 gives 8.3 and 16.5 volts, respectively. There are also well defined peaks in all the curves giving the relative numbers of electrons as a function of energy loss (Fig. 5). The arrows under the curves give the energy losses computed from formula (1) for $n^2 = 1$ and 2 (8.3 and 16.6 volts).

The energy loss of the primary electrons, as obtained from the peaks, agrees well with the calculated energy loss in all cases except one, namely for $V_k \sim 2$ volts in the distribution curve corresponding to $V_a = 21.5$ volts. An energy of 2 ev is apparently insufficient to take an electron from the full band of copper oxide to the outside. The investigations of Zhuze and Ryvkin on the photoconductivity of copper oxide[13] showed that the maximum in the photoconductivity is at $\lambda = 0.63\,\mu$, which corresponds to a quantum energy of 1.96 ev. It is natural to suppose that the discrete energy loss of 2 ev which we obtained, and which agrees well with the 1.96 ev mentioned above, is the energy required to transfer an electron from the full band to the conduction band.

It should be noted that, while in the investigation of the energy distribution of genuinely-secondary electrons there were supplementary maxima only for monocrystalline surfaces of copper oxide[7], peaks due to the inelastically scattered electrons exist in the distribution curves obtained both with monocrystalline and polycrystalline surfaces. It should also be noted that as the energy V_a of the primary electrons is decreased, then the second peak, corresponding to inelastically scattered primary electrons with energy loss 16.6 volts, decreases also. In the distribution curve obtained with $V_a = 100$ volts this peak is weaker than in the distribution curve at $V_a \sim 130$ volts, while in the distribution curve at $V_a = 21.5$ volts, the peak has disappeared.

The vacuum apparatus used in our earlier work[7] on the distribution of genuinely-secondary electrons from the monocrystalline surface (111) of copper oxide differed from the present one in having the collector covered with powdered platinum; data were there taken on the distribution of secondary electrons over the whole energy range right up to $V_k = V_a$. Figure 6 shows these data. Curves 1 and 2 give the distributions obtained with the electrical differentiation method at $V_a = 75$ and 76 volts respectively, while curve 3 gives the bias curve at $V_a = 75$ volts. The electrical differentiation circuit used in obtaining these curves did not have a synchronous filter, and used a vacuum tube AC voltmeter on the output. As a consequence of this, the negative peaks do not differ from the positive ones. However, the slope of the bias curve (Fig. 6, curve 3) for values of V_k corresponding to the first peak (near the elastically scattered maximum in curves 1 and 2) clearly shows that the first peak must be negative. The second peak must be positive for similar reasons.

The reason for the increase in the bias curve as V_k approaches V_a, and the subsequent negative peak, is the same as applies to the curves considered above (Fig. 3)--the decrease in the tertiary electron emission associated with a decrease in the energy of the elastically scattered primary electrons reaching the collector to 2-3 volts. Thus in the distribution curves for $V_a = 75$ volts, we have only one peak, corresponding to inelastically scattered primary electrons with an energy loss of 8 volts, which agrees well with calculations from formula (1) (8.3 volts).

Reference 4 gives several distribution curves for nickel which were obtained at various values of V_a in the range 20--50 volts by differentiating the bias curves. These distribution curves also exhibit one peak, corresponding to inelastically scattered electrons. The energy at which this peak occurs

---

[11] A. Ia. Viatskin , J. Exptl. Theoret. Phys. U.S.S.R. **20**, 547 (1950); **20**, 557 (1950); **21**, 851 (1951).

[12] D. E. Woolridge, Phys. Rev. **56**, 562 (1939).

[13] V. P. Zhuze and S. M. Ryvkin, J. Exptl. Theoret. Phys. U.S.S.R. **20**, 152 (1950).

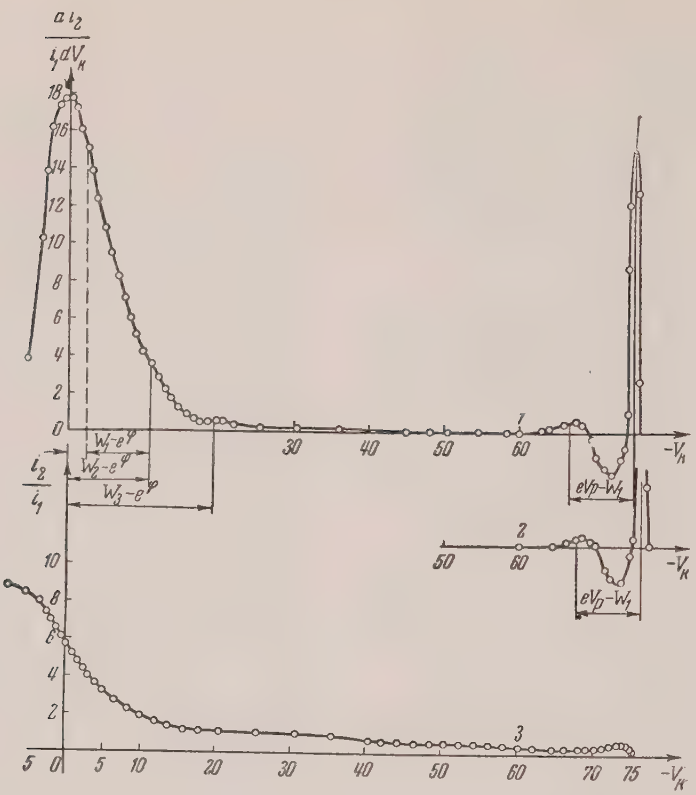

FIG. 6. Curves obtained for a monocrystalline copper oxide (111) surface at t=450 °C. *1* and *2*-distribution curves, obtained at V_a=75 and 76 volts respectively; *3*-bias curve at V_a=75 volts.

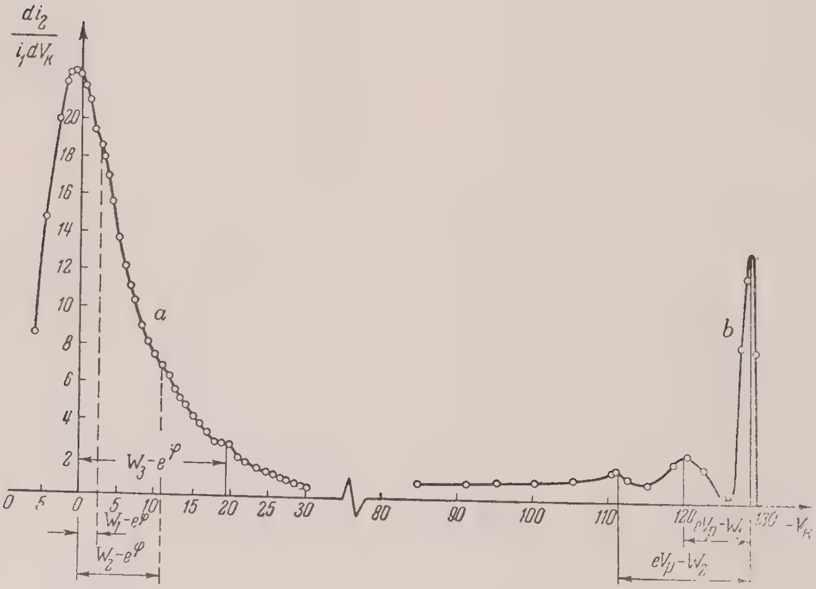

FIG. 7. Distribution curves obtained for a monocrystalline copper oxide (111) surface. Curve *a* obtained with V_a=140 volts and *t*=450 °C.[7], curve *b* obtained with V_a=128.5 volts and *t*=420 °C.

agrees well with the energy calculated from formula (1) for nickel, using $n^2 = 1$ (12.2 volts).

These investigations on inelastically scattered electrons confirm Viatskin's theory of discrete energy losses associated with band transitions[11]. The mechanism by which these energy losses occur consists in the transfer of definite energies from primary electrons moving in the solid body to the electronsof the crystal lattice in this body; these definite energies correspond to transitions from one energy band to another lying above the Fermi level. The electrons from the crystal lattice form, upon emerging from the solid body, the discrete energy groups which we observed when investigating the energy distribution of genuinely --secondary electrons[7].

Under the distribution curves of Figs. 6 and 7, we show the calculated energy losses $ev_a - W_1$ and $ev_a - W_2$ (the latter only on Fig. 7) of inelastically scattered electrons, where W is calculated from formula (1), and also the calculated energies $W_1 - e\varphi$, $W_2 - e\varphi$, and $W_3 - e\varphi$ which electrons of the crystal lattice must have on leaving the emitter as secondary electrons. On curve 1, of Fig. 6, we see that the peak due to inelastically scattered electrons with energy loss $ev_a - W_1$ corresponds to the fine structure maximum in the energy distribution of genuinely-secondary electrons at an energy $W_1 - e\varphi$, while in Fig. 7, in addition, the second inelastically scattered peak, with energy loss $ev_a - W_2$, corresponds to the second maximum in the fine structure with energy $W_2 - e\varphi$.

Thus we see that the inelastically scattered electrons of discrete energy loss which we have discovered in this work, and the groups of discrete energy genuinely-secondary electrons discovered previously,[7] are due to the same mechanism .

CONCLUSIONS

1. The bias curves obtained with the spherical condenser method, and the energy distribution curves obtained by electrical differentiation, are distorted by tertiary electron currents in the voltage region $V_k \sim V_a$.

2. Electrons are scattered both elastically and inelastically, the latter undergoing discrete energy losses.

3. The appearance of inelastically scattered electrons with discrete energy losses is due to electron transitions between the full and allowed bands of the crystal lattice, the necessary energy coming from the primary electrons.

4. The inelastically scattered electrons with discrete energy losses are produced by the same mechanism as accounts for the genuinely-secondary electrons of discrete energies.

In conclusion, I should like to express my gratitude to L. M. Rakhovich for his help in setting up the apparatus and carrying out the experiments. I am also thankful to V. Bolotin, R. Breslav and A. Reitsakas for their help in taking data.

Translated by R. Krotkov
20

SOVIET PHYSICS JETP VOLUME 3, NUMBER 2 SEPTEMBER 1956

The Reaction $p + p \to \pi^0 + p + p$ in the Range 400-660 mev

L. M. SOROKO

(Submitted to JETP editor October 25, 1955)
J. Exptl. Theoret. Phys. (U.S.S.R.) 30, 296-303 (February, 1956)

The energy-dependence of the differential cross section for emission of γ-rays, coming from the decays of π^0-mesons produced in the process $p + p \to \pi^0 + p + p$ is measured at 90° in the center of mass system. An analysis is made of the way in which a resonance in the $T = 3/2$, $I = 3/2$, $l = 1$ state might appear in the energy range in this reaction.

THE first measurements of the cross section of the process

$$p + p \to \pi^0 + p + p, \tag{1}$$

carried out at proton energies of 340 mev[1,2] indicated a certain forbiddenness in the reaction (1). This fact is in agreement with the assumption that the neutral meson is produced in a p-state in nucleon-nucleon collisions. The study of this reaction for protons in the energy range 450-500 mev would provide a valuable link in our knowledge of the mechanism of neutral meson production, because, as the energy available for the π^0-meson and nucleons increases, the degree of forbiddenness should decrease. The experiments carried out in the Institute of Nuclear Problems[3,4,5] and also those carried out at the University of Chicago[6] completely confirm this explanation of the forbiddenness.

In accordance with the phenomenological analysis carried out in Refs. 7,8, the experimental data of (1) are consistant with an energy dependence of the type

$$\sigma = 0{,}2\eta_{\max}^8 \cdot 10^{-27}\ \text{см}^2, \tag{2}$$

where $\eta_{\max}$ is the maximum momentum of the π^0-meson in the center of mass system, in units of $m_{\pi^0}c$. This growth of the cross section with energy corresponds to a mechanism of emission of the π^0-meson in p-states, leaving the nucleons in a state of $l = 1$.

The processes of π-meson production in nucleon-nucleon collisions,

$$N + N \to \pi + N + N' \tag{3}$$

in terms of the hypothesis of charge-independence, can be split into three groups of transitions, the total cross sections of which are denoted by σ_{10}, σ_{11} and σ_{01}. For the characteristics of these cross sections it is necessary and sufficient to study only three processes, for example, $p + p \to \pi^+ + n + p$ $(\sigma_{10} + \sigma_{11})$; $p + p \to \pi^0 + p + p$ (σ_{11}) and $n + p \to \pi^+ + n + n$ $[1/2(\sigma_{11} + \sigma_{01})]$. The process $p + p \to \pi^0 + p + p$ occupies a special position, since it corresponds to only one group of transitions, while all of the remaining processes include two groups of transitions.

For the considerations of (3) it is convenient to separate off the sub-system of two nucleons, characterizing it by the relative motion of the nucleons and by the motion of the sub-system as a whole. In the energy-region near to threshold, the angular momentum of the two-nucleon sub-system has an upper limit of one or two. It is useful to take into account the interaction between nucleons phenomenologically.

Besides the interaction between nucleons, it is necessary also to note the interaction of the π-meson with the nucleon, which appears to have a resonance character in the state with $T = 3/2$, $I = 3/2$ and $l = 1$. This is indicated by three groups of experiments: the process of scattering of π-mesons on protons, the process of photoproduction of π-mesons, and also the process of production of π^+-mesons in p–p collisions with formation of deuterons, $p + p \to \pi^+ + d$. In the first two cases the interaction in the state with $T = 3/2$, $I = 3/2$ $l = 1$ appears directly; in the case of the reaction $p + p \to \pi^+ + d$ the resonance leads to an in-

---

[1] R. W. Hales, R. H. Hildebrand, N. Knable and B. J. Moyer, Phys. Rev. 85, 373 (1952).

[2] J. W. Mather and E. A. Martinelli, Phys. Rev. 92, 780 (1953).

[3] B. M. Pontecorvo, G. I. Selivanov and V. A. Zhukov, Reports (Otchet) Inst. Nucl. Prob., Acad. Sci. (U.S.S.R.), 1952.

[4] M. S. Kozodaev, A. A. Tiapkin and R. Vanetsian, Reports (Otchet) Inst. Nucl. Prob., Acad. Sci. (U.S.S.R.) 1952.

[5] L. M. Soroko, Reports (Otchet) Inst. Nucl. Prob., Acad. Sci. (U.S.S.R.), 1952.

[6] J. Marshall, L. Marshall, V. A. Nedzel and S. D. Warshaw, Phys. Rev. 88, 632 (1952).

[7] A. H. Rosenfeld, Phys. Rev. 96, 139 (1954).

[8] M. Gell-Mann and K. M. Watson, Annual Review of Nuclear Science 4, 245 (1954).

crease in the cross section by a factor[7] 3-5, and the non-monotonic character of the energy dependence of the transition matrix element of this reaction, established in Ref. 9, appears clearly.

An analogous appearance of the resonance interaction in the state with $T = 3/2$, $I = 3/2$, $l = 1$ can be expected in all remaining processes of meson production, in particular in the processes $p + p \rightarrow \pi^+ + n + p$ and $p + p \rightarrow \pi^0 + p + p$. However, there is an essential difference between these last processes and the reaction $p + p \rightarrow \pi^+ + d$.

In the first place, one must take into account the fact that the process (3) is connected with a considerably larger number of transitions than the reaction $p + p \rightarrow \pi^+ + d$. In order to trace which of the possible transitions can be connected with a resonance in the state $T = 3/2$, $I = 3/2$, $l = 1$ we divide the system of three particles $\pi + N + N$ into two sub-systems: $(\pi + N)$ and (N). The total angular momentum of the sub-system $(\pi + N)$ in the case of resonance should be $I = 3/2$ (and the orbital momentum $l = 1$, i.e., the sub-system is in a $^2P_{3/2}$ state). To this sub-system we add the second nucleon, having various orbital momenta relative to the sub-system. As a result we obtain the possible states of the three particles shown in Table 1.

TABLE 1

Total angular momentum I	0		1		2		3		4
Total parity	+	−	+	−	+	−	+	−	+
Possible states	$^2P_{3/2}d_0$	$^2P_{3/2}p_0$	$^2P_{3/2}s_1$ $^2P_{3/2}d_1$	$^2P_{3/2}p_1$ $^2P_{3/2}f_1$	$^2P_{3/2}s_2$ $^2P_{3/2}d_2$	$^2P_{3/2}p_2$ $^2P_{3/2}f_2$	$^2P_{3/2}d_3$ $^2P_{3/2}g_3$	$^2P_{3/2}p_3$ $^2P_{3/2}f_3$	$^2P_{3/2}d_4$ $^2P_{3/2}g_4$

It would seem that the sharpest appearance of the resonance in the state with $T = 3/2$, $I = 3/2$, $l = 1$ can be expected in those cases where the second nucleon is in an s-state relative to the $(\pi + N)$ sub-system. If this is so, then the states $^2P_{3/2}s_1$ and $^2P_{3/2}s_2$ turn out to be most essential. To the first of these, $^2P_{3/2}s_1$, corresponds an initial nucleon with even l and total angular momentum $I = 1$, which can occur only in case $T_{\text{initial}} = 0$. This means that the $^2P_{3/2}s_1$ state is not connected with the resonance since $T_{\pi N} = 3/2$ and $T_N = 1/2$ cannot be combined to give $T = 0$.

Therefore, we will consider only the $^2P_{3/2}s_2$ state, to which only one of the initial nucleon states can lead, namely $^1D_2$. In terms of the first type of classification of states, the transitions arising in this case are

$$^1D_2 \rightarrow {}^3S_1p_2, \quad {}^1D_2 \rightarrow {}^3P_2s_2, \quad {}^1D_2 \rightarrow {}^3P_{1,0}d_2.$$

The first of these is essential only in the reaction $p + p \rightarrow \pi^+ + n + p$, wheras the remaining two relate to the process $p + p \rightarrow \pi^+ + n + p$, and to the process $p + p \rightarrow \pi^0 + p + p$. The latter transitions should, it would appear, occur with less probability than the first, since the nucleons are in p-states. Besides the smaller cross section in these transitions, the emission of a proton in a p-state leads to a distortion of the energy dependence of the cross-section, for example, to a displacement of the maximum to higher energies.

Thus the resonance character of interaction in the $T = 3/2$, $I = 3/2$, $l = 1$ state, which occurs in the 'purest' aspect only in case of the transition $^1D_2 \rightarrow {}^3S_1p_2$ in the reaction $p + p \rightarrow \pi^+ + n + p$, can be covered up by other non-resonance transitions. In case of the reaction $p + p \rightarrow \pi^0 + p + p$ there is no basis to expect a sharp appearance of the resonance which could lead to a non-monotonic dependence of the cross section $p + p \rightarrow \pi^0 + p + p$ in the region of π-meson energies ~ 160 mev.

In the second place, the reactions $p + p \rightarrow \pi^+ + d$ and $N + N \rightarrow \pi + N + N'$ differ because of the statistical factor. Namely, the statistical factor of the cross section of the reaction $N + N \rightarrow \pi + N + N'$ depends, in the non-relativistic region, on the maximum meson momentum as η^4_{max}, whereas for the reaction $p + p \rightarrow \pi^+ + d$ the statistical factor is proportional to the

---

[9] M. G. Meshcheriakov and B. S. Neganov, Dokl. Akad. Nauk. SSSR 100, 677 (1955).

first power of the momentum.

In the third place, the reaction $N + N \to \pi + N + N'$ gives rise to a wide spectrum of π-mesons, so that an integral effect enters into the total cross section, leading to a smoothing out of the resonance effect even in those transitions where it occurs.

In this work the energy-dependence of the cross section, reaction (1), was studied at proton energies of 400 to 660 mev. Measurements were carried out at an angle of ~ 90° of the differential cross section for γ-rays from the decay of π^0-mesons produced in the process $p + p \to \pi^0 + p + p$. If it is assumed that there is not a sudden variation in the π^0-meson emission with respect to angle or energy, then the observed cross section reflects the energy dependence of the total cross-section $\sigma_{pp}^{\pi^0}$.

1. EXPERIMENTAL ARRANGEMENT

The experiment was carried out with the 657 mev proton beam of the synchro-cyclotron of the Institute of Nuclear Problems of the Academy of Science of the U.S.S.R. The experimental arrangement is shown in Fig. 1. The proton beam emerged from a concrete shielding wall through a 4 m collimator, traversed the ionization chamber and hit the target which was liquid hydrogen contained in a glass Dewar. The ionization chamber served as a monitor, and also as instrument for measuring the intensity of the proton beam. Calibration of this chamber was carried out in a separate experiment[10]. The working part of the target was defined within the volume of liquid hydrogen by lead collimators, which shielded the γ-ray counter from radiation arising from interactions of the protons in the glass walls of the Dewar. The mean path of protons in this working part of the target, taking into account the penumbra formed by the collimators, was about 8 cm. The measurement of the background was carried out with the glass Dewar full of hydrogen gas at atmospheric pressure.

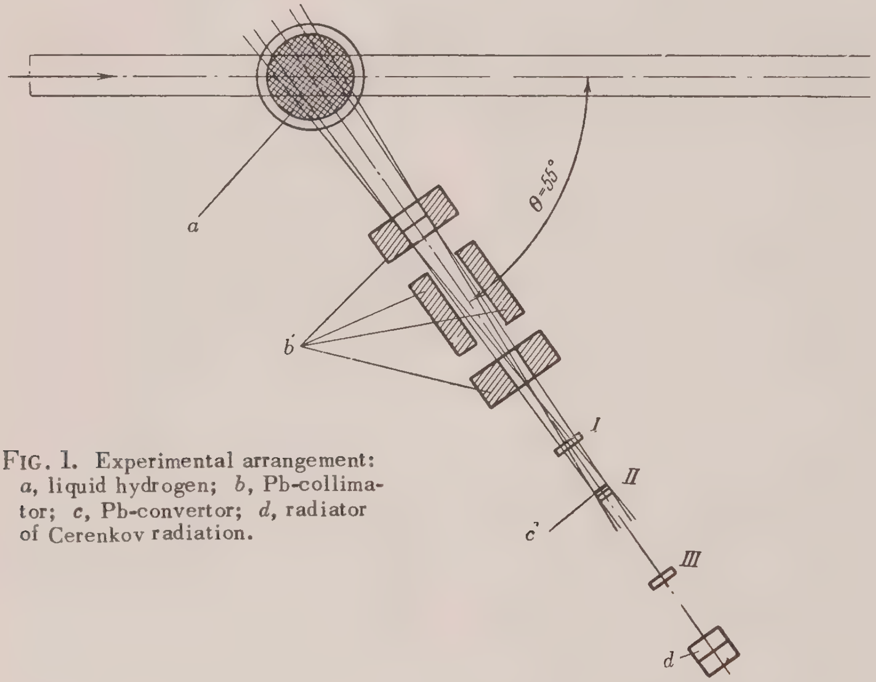

FIG. 1. Experimental arrangement: *a*, liquid hydrogen; *b*, Pb-collimator; *c*, Pb-convertor; *d*, radiator of Cerenkov radiation.

Proton beams of energy less than 657 mev were obtained by inserting blocks of polythene in the path of the beam in the collimator to slow them down. At energies of 400-500 mev the energy spread of the beam of protons was ±12 mev.

The passage of the protons through the retarding blocks was accompanied by various processes in the blocks which made the experimental conditions worse. Thus, for example, the slow charged particles emerging from the blocks created misleading ionization in the ionization chamber. The necessity which was found experimentally, of introducing corrections on account of this effect arose in all experiments with proton beams of diminished energy. In the study of process (1), there occurred the additional hindrance of charge-exchange neutrons produced in the retarding blocks from the exchange interaction of protons in collisions with carbon atoms. Such neutrons impinging on the liquid hydrogen target initiate the process $n + p \to \pi^0 + n + p$, the relative yield of which exceeds the yield of process (1), especially in the region of reduced proton energy. In the worst conditions this background did not exceed 15%.

---

[10] B. S. Neganov, O. V. Savchenok and L. M. Soroko, Reports (Otchet) Inst. Nucl. Prob., Acad. Sci. (U.S.S.R.) 1954.

In this experiment γ-rays from π^0-meson decays were registered by a system consisting of a telescope and a Cerenkov counter. In the experiments determining the absolute cross-section only the telescope was employed. The telescope consisted of three scintillation counters (tolane). Counters II and III were in coincidence and counter I in anti-coincidence with II and III. A lead converter of dimensions 2×2 cm^2 and thickness 0.5 cm was inserted or left out before counter II.

The Cerenkov counter had two photo-multipliers arranged vertically, between which was placed a plexiglass radiator in the form of a cube cut into two sections. Each section of the cube was joined optically with only one of the photo-multipliers. Pulses from each photo-multiplier were fed into amplifying channels. After shaping the amplitudes and lengths of the pulses, they acted in a system of two-fold coincidence, so that the major part of the noise in each photo-multiplier was suppressed. An analogous arrangement was also used in the telescope described above.

Measurements of the intensity of Cerenkov radiation[11] for fast electrons in the plexiglass showed that the number of photo-electrons was about 8 for a 2.5 cm thickness of plexiglass. For such a small number of photo-electrons it was necessary for the system to be triggered by the emission of a single electron. For this, with an amplification coefficient of the photo-multiplier of 5×10^5 and an output capacity of the photo-multiplier ~ 5 pF it was necessary to have a further amplification of approximately 200. The stages of the wide-band amplifier employed had a complicated correction, the parameters of which were found using the nomogram and table given in Ref. 12.

2. EFFICIENCY OF COUNTING CHARGED PARTICLES OF VARIOUS VELOCITIES BY CERENKOV RADIATION

The experiment to define the efficiency of counting charged particles by Cerenkov radiation was carried out in the following fashion. Two telescopes I and II in coincidence were placed at angles relative to the proton beam so as to register p–p elastic scattering events. The targets in this experiment were of paraffin and carbon. Immediately behind the telescope registering high energy protons a Cerenkov counter was placed so as to be traversed by all protons which were registered in the telescope in front. Pulses from the counter and telescopes acted in coincidence. In this experiment the number of coincidences between telescopes was compared with the number of times there was also a coincidence with the Cerenkov counter. The following values were obtained for the dependence of the efficiency of counting the Cerenkov radiation on the energy of the proton counted by the telescope:

330 mev	380 mev	440 mev	600 mev
(3 ± 4) %	(22 ± 5) %	(37 ± 3) %	(55 ± 7) %

In addition to this experiment a measurement in the direct beam of 450 mev protons of decreased intensity was carried out. In this the efficiency found was (36 ±4)%. The results of these measurements show that the Cerenkov counter is to the extent given really a threshold counter.

Together with this even at high proton velocities a counting efficiency less than 100% was observed. It is possible to explain the incomplete efficiency in the region of the plateau in counter characteristics if considerable fluctuations in the number of photo-electrons are assumed. As a consequence of this, the process in which no electron is emitted in the photo-cascade or in which the electron disappears before it starts a shower, has a high probability. The efficiency of the Cerenkov counter can increase, it would appear, if the sensitivity of the photo-cascade is made greater and if the loss of electrons at the initial stages of development of the shower is decreased.

---

[11] J. Marshall, Phys. Rev. 86, 685 (1952).

[12] G. V. Braude, K. V. Epaneshnikov and B. Ia. Klumushev, Radiotekhnika 4, 24 (1949); 5, 16 (1950).

3. DEPENDENCE OF THE CROSS SECTION $(d\sigma/dw)^{\gamma}_{90^\circ}$ ON THE ENERGY OF THE INCIDENT PROTON

In the relative measurements of the cross section $(d\sigma/d\omega)^{\gamma}_{90^\circ}$, the system of telescope and Cerenkov counter was employed. The efficiency of this system of counting γ-rays at different proton energies was calculated in the following way. The following were taken in succession into the calculation: The 'vanishing' of the electron and positron in traversing the lead converter on account of bremsstrahlung, multiple scattering of electrons in the lead converter, and also the experimental value for the cross section of pair production in lead. The character of the γ-spectra arising at different proton energies was calculated under the assumption that the energy spectrum of the π°-mesons was determined by only the statistical factors, and that the π°-mesons were distributed isotropically in the center of mass of the two protons.

In addition, a rough evaluation of the absolute cross section was carried out in experiments where only the telescope was employed. In this case $(d\sigma/d\omega)^{\gamma}_{0^\circ} = (4,5 \pm 1,8) \times 10^{-28}$ cm^2/sterad, and the total cross section $\sigma^{\pi^\circ}_{pp} = (2,8 + 1) \times 10^{-27}$ cm^2, if the π°-mesons are distributed isotropically in the center of mass system.

4. DISCUSSION OF RESULTS

The results obtained in this work are given in Fig. 2. The most detailed measurements were

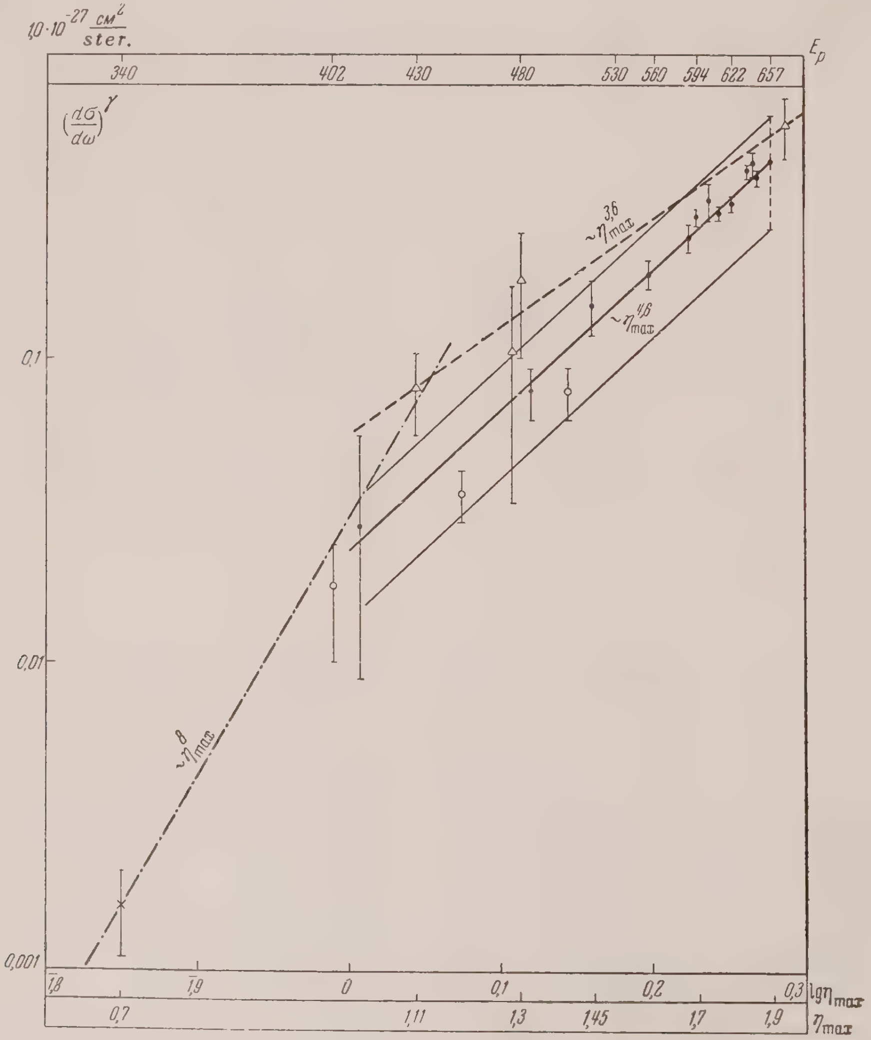

FIG. 2. ● and ○ — $(d\sigma/d\omega)^{\gamma}_{\sim 90^\circ}$, in this experiment, × — $(d\sigma/d\omega)^{\gamma}$ according to Ref. 2, Δ — $(d\sigma/d\omega)^{\gamma}_{0^\circ}$ according to Ref. 4-6, 13.

carried out at the maximum energy of the π^0-mesons in the region 120-150 mev (proton energy of 580-660 mev), at which energies non-monotonic variations with energy of the total cross sections are observed in the reaction $p + p \rightarrow \pi^+ + d$ and in the processes of scattering and photo production of mesons in hydrogen. In the present experiment a non-monotonic change of the cross section $(d\sigma/d\omega)^{\gamma}_{90^\circ}$ in the range of proton energies 580-660 mev was not observed. If we assume that in the given region no sharp change occurs in the dependance on energy or angle of the cross section for emission of a π^0-meson, then this conclusion relates also to the total cross-section $\sigma^{\pi^0}_{pp}$. This result is in accordance with the conclusions arrived at at the beginning of this article. Results of others are also shown on Fig. 2. A list of these is given in Table 2.

TABLE 2

Proton energy in mev	Maximum momentum of the π^0-meson in c. m. system	$(d\sigma/d\omega)^{\gamma}_{0^\circ}$ in the lab system in units of 10^{-28} cm^2 / sterad	$(d\sigma/d\omega)^{\gamma}_{0^\circ}$ in c. m. system (10^{-28} cm^2/sterad)	total cross-section σ^{π^0} (10^{-28}/cm^2)	assumed angular distribution of the π^0-meson.	References
340	0,70	—	$(1,6\pm0,5)\cdot10^{-2}$	$(1,0\pm0,3)\cdot10^{-1}$	—	[2]
430	1,11	2	0,8	$4.5\pm1,5$	$a+\cos^2\theta$	[6]
460	1,23	—	—	4 ± 2	$\cos^2\theta$	[3]
—	—	—	—	$5\pm2,5$	isotropic	—
480	1,30	$2,6\pm1,7$	$1.04\pm0,7$	$4,4\pm3$	$\cos^2\theta$	[4]
480	1,30	4.5 ± 2	$1,8\pm0,8$	$(1.05\pm0,45)\cdot10$	isotropic	[5]
—	—	—	—	$(0,62\pm0,28)\cdot10$	$\cos^2\theta$	—
650	1,88	—	—	$(3,6\pm0,7)\cdot10$	$\cos^2\theta$	[15]
—	—	—	—	$(3,0\pm0,6)\cdot10$	isotropic	—
670	1,94	—	$5,9\pm1,3$	$(3,7\pm0,8)\cdot10$	isotropic	[13]

The solid line shows the dependence according to the power law

$$(d\sigma/d\omega)^{\gamma}_{90^\circ} = C_1 \eta_{\max}^{4,6\pm0,5}$$

which approximates to the experimental results obtained in this experiment for $1 < \eta_{\max} < 1.9$. The magnitude of the absolute error for $E_p = 657$ mev is shown on Fig. 2 by dashes. Other results[4-6,13] for $\theta = 0°$ are represented by the dashed line which corresponds to the power law

$$(d\sigma/d\omega)^{\gamma}_{0^\circ} = C_2 \eta_{\max}^{3,6}$$

for $1 < \eta_{\max} < 1.9$.

All of these results can be reconciled with a dependence of the total cross section for production of π^0-mesons in process (1) in the region $1 < \eta_{\max} < 1.9$ according to the power law

$$\sigma^{\pi^0}_{pp} \sim \eta_{\max}^{\alpha}, \quad \text{where } \alpha \approx 4.$$

It is of interest to compare these results with the energy dependence of the total cross section $\sigma^{\pi^0}_{pp}$ which would be expected if the transition matrix element is constant. Calculation[16] leads to the expression

$$\times \quad \sigma^{\pi^0}_{pp} = \text{const}\,\frac{1}{v} \tag{5}$$

$$\int\limits_0^{p_{\max}} [M(W - \sqrt{p^2 + m^2}) - {}^1\!/_4\, p^2]^{1/2} p^2 dp,$$

---

[13] A. A. Tiapkin, M. S. Kozodaev and Iu. D. Prokoshkin, Dokl. Akad. Nauk SSSR **100**, 689 (1955).

[14] W. E. Crandall and B. J. Moyer, Phys. Rev. **92**, 749 (1953).

[15] B. D. Balashov, V. A. Zhukov, B. M. Pontecorvo and G. I. Selivanov, Report (Otchet) Inst. Nucl. Prob., Acad. Sci. (U.S.S.R.), 1954.

[16] E. Fermi, *Elementary Particles*, Yale University Press, 1951.

where v is the velocity of the incident proton, p is the momentum of the π-meson, M and m are the masses of nucleon and π-meson respectively, W is the kinetic energy of two nucleons in the center of mass system. To derive this formula the relation between energy and momentum for the π-meson was taken as $\mathcal{E}_\pi = \sqrt{p^2 + m^2}$, and for the nucleon as $\mathcal{E}_N - M = p_n^2/2M$. The choice of the last relation is justified by the fact that the maximum nucleon energy in the region considered does not exceed 75 mev.

In the energy region studied in this experiment the dependence shown in (5) can be approximated by a power law of the form: $\sigma^{\pi^\circ}_{pp} = \text{const}\ \eta^{3.6}_{\max}$. As is known, in the region $\eta \ll 1$, the statistical factor is proportional to $\eta^4_{\max}$.

Through comparison of this calculated dependence (power equal to 3.6) with the given experiments (power of approximately 4) it can be concluded that the energy dependence of the transition matrix element for (1) is small.

In conclusion the author expresses his gratitude to M. G. Meshcheriakov, L. I. Lapidus and S. M. Bilen'kii for discussion of experimental results, and also to A. S. Kuznetsov who took part in the construction of the electronic apparatus.

Translated by G. E. Brown
55

SOVIET PHYSICS JETP VOLUME 3, NUMBER 2 SEPTEMBER, 1956

The Possibility of a Two-Step Excitation Mechanism in Sulfide Phosphors

N. A. TOLSTOI

(Submitted to JETP editor, July 26, 1954)

J. Exptl. Theoret. Phys. (U.S.S.R.) 30, 171-179 (January, 1956)

Experimental data on the kinetics of luminescence in strongly quenched phosphors indicate that in spite of widely held ideas to the contrary, the bimolecular theory is not applicable. An interpretation of the experiments in terms of a two-step phosphorescence excitation mechanism is presented. It is shown that a two-step excitation process is responsible for photoconductivity in CdS (Cu) having high copper concentrations. Moreover luminescence in this material exhibits properties typical of strong quenching.

1. The kinetics of "fast" luminescence in sulfide phosphors (for example, ZnS, CdS, etc.) has been studied in a number of investigations[1] in which the tau-meter method[2] was employed. At temperatures far below the temperature at which quenching occurs, the growth and decay curves are approximated by functions which do not satisfy any simple kinetic equations. The possibility of interpreting these relaxation curves or of drawing even qualitative conclusions concerning processes in these phosphors is very remote. The expression which approximates the decay curve

$$I \sim (1 + at)^{-\alpha}. \qquad (1)$$

(where, for ZnS-Cu at room temperature, α has a value of the order of 0.7) cannot be correct *a priori* if the time is allowed to increase without limit because of the infinity which appears in the stored light-sum. Moreover, Eq. (1) is not valid at the very beginning of the decay curve (for example in the region of 100-90 per cent of the steady-state luminescence); using a method developed by the author[3] in which the relaxation curves are electrically differentiated, it has been shown that the curve in (1) is affected by the intensity of excitation E in a manner which is given by the expression[1] $a \sim E^p$ (where for ZnS-Cu at $t=20°$C, d is 0.6-0.7) and that the dependence on E is very much weaker in the initial relaxation stages. In the limit (of increasing E) the initial slope of the decay curve, in general, tends toward a constant value. Hence, a single approximation cannot be used to describe the entire decay curve. From the point of view of methodology, the matter is further complicated by the fact that in the phosphors in question there occur slow processes which do not have time to reach completion when undergoing excitation by rectangular light pulses. This situation introduces additional difficulties in the interpretation of the relaxation curves.

---

[1] V. A. Arkhangel'skaia, A. M. Bonch-Bruevich, N. A. Tolstoi and P. P. Feofilov, Dokl. Akad. Nauk SSSR 64, 187, (1949); J. Exptl. Theoret. Phys. U.S.S.R. 21, 290 (1951). D. B. Gurevich, N. A. Tolstoi and P. P. Feofilov, Dokl. Akad. Nauk SSSR 71, 29 (1950). V. A. Arkhangel'skaia, A. M. Bonch-Bruevich and N. A. Tolstoi, Izv. Akad. Nauk SSSR Ser. Fiz. 15, 695 (1951).

[2] N. A. Tolstoi and P. P. Feofilov, Usp. Fiz. Nauk 41, 44, (1950).

[3] N. A. Tolstoi, Izv. Akad. Nauk SSSR Ser. Fiz. 15, 712 (1951).

2. We shall use an approach which offers the possibility of great simplification in the interpretation of the relaxation curves[4]. Consider the general symbolic kinetic equation

$$dn/dt = -I - T + \gamma E, \tag{2}$$

where n is the number of excited centers, I is the number of electrons which return to the initial state per second with radiation, and T is the same quantity without radiation, and γE is the number of electrons excited per second by light with an intensity E. For brevity we will call I the luminescence, T the quenching, and E the excitation.

Suppose the phosphor to be in a state of strong concentration or temperature quenching. Then, obviously, $I \ll T$ and we can write as a first approximation

$$dn/dt = -T + \gamma E, \tag{3}$$

i.e., the net number of electrons depends only on the quenching and the excitation. In general it will be assumed that

$$T = \beta n \tag{4}$$

(physically, Eq. (4) is connected with the fact that the interaction between a finite number of excited electrons or centers and the virtually infinite number of thermal fluctuations is a process of the first type or "pseudo-monomolecular" process). Then

$$dn/dt = -\beta n + \gamma E, \tag{5}$$

whence

$$n_\infty = \gamma E/\beta \qquad \text{(steady-state)}; \tag{6}$$

$$n = n_\infty e^{-\beta t} \qquad \text{(decay)}; \tag{7}$$

$$n = n_\infty (1 - e^{-\beta t}) \qquad \text{(growth)}. \tag{8}$$

Thus the number of excited electrons n is given by the simplest kind of exponential kinetics. The form of the relaxation curves does not depend on E and $n_\infty \sim E$. Formulas (6)-(8) are called the "quenching kinetics" formulas.

We now consider the second approximation and will assume that $I \neq 0$ although $I \ll T$. Then, whatever the algebraic dependence of $I(n)$, the kinetics of luminescence will be algebraically connected with the exponential quenching kinetics which are already known. For example, if the luminescence is monomolecular or pseudo-monomolecular (recombination) in character, i.e., $I = \alpha n$, then

$$I_\infty = \alpha\gamma E/\beta, \tag{9}$$

$$I = I_\infty e^{-\beta t} \qquad \text{(decay)}; \tag{10}$$

$$I = I_\infty (1 - e^{-\beta t}) \qquad \text{(growth)}; \tag{11}$$

while if the luminescence is bimolecular, i.e., $I = \alpha n^2$, then

$$I_\infty = \alpha\gamma^2 E^2/\beta^2, \tag{12}$$

$$I = I_\infty e^{-2\beta t} \qquad \text{(decay)}; \tag{13}$$

$$I = I_\infty (1 - e^{-\beta t})^2 \qquad \text{(growth)}. \tag{14}$$

Hence, under conditions of strong quenching, the luminescence mechanism emerges, so to speak, in "bare" form. It has been assumed that I is a function only of the number n and does not depend, for example, on the distribution of excited electrons over trap levels at different depths (in such a case I, in general, would not be determined uniquely by the quantity n). Generally speaking, I is not a unique function of n, but this assumption is justified under conditions of strong quenching, especially when the quenching is due to high temperatures. The exponential behavior of the decay of luminescence or the falling-off of photoconductivity appears, in this case, as a criterion of the validity of an assumed dependence of the type $I = \alpha n^m$ (m= const).

Finally we may note that when there is strong quenching the methodological difficulties connected with the existence of slow relaxation processes are avoided.

3. We now recapitulate certain experimental data relating to relaxation in strongly quenched phosphors.

a) The steady-state luminescence shows superlinearity as a function of the intensity of the exciting light E. In a number of cases the function

---

[4] N. A. Tolstoi, Dokl. Akad. Nauk SSSR 95, 249 (1954).

$I_\infty(E)$ tends toward $I_\infty \sim E^2$.

b) The decay curve is found to be exponential or very close to exponential; τ is independent of E but falls off with increasing temperature.

c) The growth curve starts with a parabolic dependence ($I \sim t^2$) and then after inflection goes considerably slower than the decay curve. The form of the curve depends markedly on E. Schematic curves of growth and decay are shown in Fig. 1.

d) The area above the growth curve L_g (Fig. 1) is much greater than the area under the decay curve L_d. The ratio L_g/L_d, which we call s below, decreases with an increase in E; this however may be seen from b and c. A typical ratio $s=10$*.

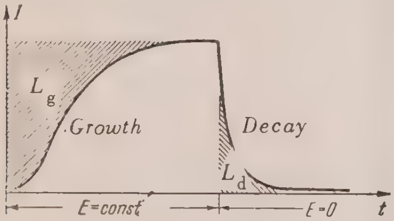

FIG. 1.

e) The maximum slope of the growth curve (at the inflection point) $I'_{\max}$ is much smaller than the maximum slope of the decay curve (at the beginning of the latter).**

4. We now examine the extent to which the considerations developed in Sec. 2 are useful in explaining the experimental data given in Sec. 3. At first glance it would seem that the formulas given in (12)-(14) (bimolecular luminescence) are in agreement with the experimental data (the quadratic dependence of $I_\infty(E)$, the exponential behavior of decay and the parabolic nature and the inflection of the growth curve). However, the experimental results contradict the theory in one essential point: according to (14) the form of the growth curve is independent of E; actually, however, such a dependence exists. The only approach which reconciles theory and experiment lies in assuming a strong dependence of the quenching probability β on E [since the form of the growth curve depends only on the time coefficient in (14)]. Physically this means taking cognizance of the strong quenching property of the exciting light (QPEL). When this is taken into account the quenching probability appears in the form

$$\beta = \beta_T + \beta_0 E, \tag{15}$$

where β_T is the probability for purely thermal quenching, and $\beta_0 E$ is the optical quenching probability. Then we should write in place of (12)-(14)

$$I_\infty = \alpha\gamma^2 E^2 (\beta_T + \beta_0 E)^{-2}, \tag{16}$$

$$I = I_\infty \exp\{-2\beta_T t\} \qquad \text{(decay)}; \tag{17}$$

$$I = I_\infty (1 - \exp\{(\beta_T + \beta_0 E)t\})^2 \quad \text{(growth)}, \tag{18}$$

The assumption of (QPEL) appears to be unavoidable if one starts from the considerations developed in Sec. 2 and the experimental dependence of the growth on E. We shall find, however, that even the modified equations are found to be in quantitative disagreement with the experiments.

Having calculated L_g and L_d (Fig. 1) starting from formulas (13) and (14), we obtain $L_d = I_\infty/2\beta$ and $L_g = 3I_\infty/2B$ so that*** $s=3$. If, however, we use the modified formulas (17) and (18), i.e., if (QPEL) is taken into account, then

$$s = 3\beta_T/(\beta_T + \beta_0 E) < 3. \tag{19}$$

The ratio s falls off with an increase in E and for $\beta_0 E > 2\beta_T$ it becomes less than unity. Thus the ratio s can never have a value greater than 3; with sufficient intensity of the exciting light, moreover, (QPEL) can bring about a situation in which the area above the growth curve becomes smaller than the area under the decay curve.+ The experiments, as we have seen, yield $s > 3$; for large E, $s \approx 10$ is observed and with a reduction in E this ratio grows still larger. The disagreement between experiment and Eq. (19) indicates that the growth curve (18) cannot be brought into quantitative agreement with experiment for any value of the exponent $\beta = \beta_T + \beta_0 E$ in the exponential term. Actually $\beta > \beta_T$, but for agreement with experiment we require at least that $\beta < \beta_T$, i.e., that $\beta_0 E > 0$. If one allows the possibility, even formally, that $\beta_0 E<0$ (negative QPEL) then one is quickly brought into another contradiction with experiment: with an increase of the exciting light intensity a slower growth curve is obtained and not a faster one as is actually observed. Furthermore, the dependence of the steady-state luminescence on the intensity of excitation is found to be greater than quadratic [cf Eq. (16)]. Although such a dependence has been mentioned in the literature, it is not appropriate for those phosphors and those experimental conditions which are under discussion here.

---

* This ratio can be determined by an objective method for measuring L_g and L_d, (the "L-meter") developed by the author in conjunction with I. A. Litvinenko.[5]

** This can be determined by electrical differentiation.[3]

[5] N. A. Tolstoi and I. A. Litvenenko, J. Exptl. Theoret. Phys. (U.S.S.R.) 29, 507 (1955).

*** For a nonquenched "pure bimolecular" phosphor ($dn/dt = -\alpha n^2 + \gamma E$) s may be taken equal to unity.

+It has been shown in a paper by Tolstoi and Shatilov[6] that the limit on the values of s, $s \leq 3$, is valid under more general assumptions as to the recombination mechanism.

[6] N. A. Tolstoi and A. V. Shatilov, J. Exptl. Theoret. Phys. U.S.S.R. 30, 109 (1956).

Thus we are confronted by a serious difficulty: not making any assumptions of an arbitrary nature as to the mechanism of luminescence and quenching we obtain theoretical curves which are found to be in strong disagreement with experiment. We may point out the fact that the growth curve is the "corner stone" of our analysis. It is obvious that in general the growth kinetics will be more sensitive to the luminescence mechanism, but strangely enough only a small amount of work in the literature is devoted to a study of growth phenomena.

To show the necessity for the assumptions $T=\beta n$ and $I=\alpha n^2$ which were made in Sec. 2 we point out that violating the first of these would lead to a nonexponential decay, i.e., to a stronger disagreement with experiment (for example $T=\beta n^2$ would indicate a hyperbolic decay). Violation of the requirement $I=\alpha n^2$ would mean a nonparabolic dependence at the beginning of growth, i.e., it would also contradict experiment (for example $I=\alpha n$ would indicate a linear dependence at the beginning of the growth curve). Departure from the idea of a single-valued dependence of $I(n)$ would also lead to a non-exponential decay and could lead to a dependence of the form of the decay curve on E. The notion that the indicated assumptions are in fact violated but are "compensated" in such a way as to lead to the required results is so artificial as not to warrant discussion.

The only alternative which remains is to investigate the admissibility of one tacitly made assumption which has not been mentioned up to this point and which is usually considered indisputable: the number of electrons excited by the light is proportional to its intensity (γE). This relation can be violated in two ways.

1) Absorption of light causes an impoverishment of the phosphor due to electrons which are not yet excited, i.e., γ depends on E, becoming smaller with an increase in the latter. Obviously this effect would be of most importance in non-quenched phosphors, which store large light-sums, where it should tend to make the functional dependence of $I(n)$ less than linear. Aside from the fact that this is not found in our case, (thus strengthening the idea that it does not occur in quenched phosphors), such an assumption would only worsen the difficulty since, as is easily shown, it can lead only to a lower value for s.

2) The excitation of electrons in the phosphor is not a one-step process. In the first stage the excited electrons are trapped and form the "first light-sum". A second excitation of these electrons forces them into other states in which they constitute the "second light-sum" which can be dissipated both by radiative and nonradiative transitions. Although this picture of the phosphor mechanism may seem strange, as we shall show below, it favors many experimental facts associated with photoconductivity.[8] The theory based on these ideas is found to be in good agreement with the experimental material we have presented above.

5. We begin with a consideration of a simple formal scheme for a two-step phosphor mechanism (Fig. 2). Let n_0 be the number of electrons in the unexcited state, n_1 the number at an "intermediate" trapping level from which (in the particular case under consideration) radiative transitions cannot be performed (n_1 is the "first light-sum"), and n_2 the number of electrons in the "excited" levels from which radiative transitions to the "ground" states are possible (n_2 is the "second light-sum"). We shall take n_0 to be infinite. Then the kinetic equations, under the assumption that *all transitions in the scheme are of pseudo-momomolecular nature*, take on the form

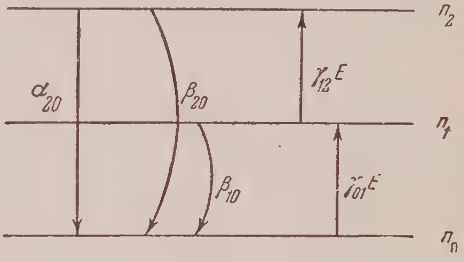

FIG. 2.

$$dn_2/dt = -(\alpha_{20}+\beta_{20})n_2+\gamma_{12}En_1, \qquad (20)$$

$$dn_1/dt = -(\beta_{10}+\gamma_{12}E)n_1+\gamma_{01}En_0.$$

The quantities β_{20}, β_{10} express the probabilities for the respective nonradiative transitions,

---

[8] V. E. Lashkarev and G. A. Fedorus, Izv. Akad. Nauk SSSR Ser. Fiz. 16, 81 (1952).

α_{20} is the probability for a radiative transition, $\gamma_{12}E$ is the probability for secondary excitation, and $\gamma_{01}En_0$ is the probability for primary excitation. Then in the simplified theory, the solution of equations (20) will have for the first light-sum the form

$$n_{1\infty} = \gamma_{01}En_0 / (\beta_{10} + \gamma_{12}E) \quad (21)$$

(stationary light sum)

$$n_1 = n_{1\infty}e^{-\beta_{10}t} \text{ (decay)} \quad (22)$$

$$n_1 = n_{1\infty}(1 - e^{-(\beta_{10}+\gamma_{12}E)t}) \text{ (growth)} \quad (23)$$

and for the second light-sum

$$n_{2\infty} = \gamma_{01}\gamma_{12}E^2n_0 / AB \quad (24)$$

(stationary light sum)

$$n_2 = n_{2\infty}e^{-At} \text{ (decay)} \quad (25)$$

$$n_2 = n_{2\infty}\left(1 - \frac{A}{A-B}e^{-Bt} + \frac{B}{A-B}e^{-At}\right) \text{ (growth)} \quad (26)$$

where A and B indicate:

$$A = \alpha_{20} + \beta_{20}, \; B = \beta_{10} + \gamma_{12}E. \quad (27)$$

If, in place of the quantities A and B, we introduce the quantities τ_A=1/A and τ_B=1/B and make use of Eq. (24), then the expressions for decay and growth of luminescence take on the following forms:

$$n_2 = n_{2\infty}e^{-t/\tau_A}, \quad (25')$$

$$n_2 = \frac{n_{2\infty}}{\tau_B - \tau_A}[\tau_B(1 - e^{-t/\tau_B}) - \tau_A(1 - e^{-t/\tau_A})]. \quad (26')$$

We now consider the extent to which the expressions (24)-(27) are capable of describing the kinetics of luminescence in the quenched phosphors which are of interest here. From (24)-(27) it is apparent that the second light-sum n_{200} increases more rapidly than linear with respect to E if β_{10} is comparable with $\gamma_{12}E$. Inasmuch as we are considering the luminescence to be pseudo-monomolecular, the intensity of luminescence I=$\alpha_{20}n_2$ depends on E in exactly the same fashion. The decay (25) is exponential and its rate does not depend on E. On the other hand, the form of the growth curve (26) depends on E through the quantity B. As is shown by (26′), the growth is given by the sum of two increasing exponential terms of different sign and with time constants proportional to their amplitudes. It is not difficult to show that the growth curve behaves parabolically at the beginning. Expressing (26) as a series with respect to t and limiting ourselves to terms up to t^2, we have

$$I = \alpha_{20}n_2 = {}^1/_2\,\alpha_{20}\gamma_{01}\gamma_{12}E^2t^2.$$

It is apparent that the growth behavior in the parabolic region is independent of A and B.

We now form the ratio s. From Eqs. (25) and (26) we obtain (after integration)

$$L_P = \frac{\alpha_{20}n_{2\infty}}{A}\left(1 + \frac{A}{B}\right); \quad L_3 = \frac{\alpha_{20}n_{2\infty}}{A}; \quad (28)$$

$$s = 1 + A/B.$$

It is obvious that the quantity s can assume values greater than unity. The increase in the magnitude of s with increasing temperature, which is observed experimentally, can be interpreted, for example, by assuming that the quenching probability for the second light-sum $n_{2\infty}$ increases faster than the quenching probability for the first light-sum $n_{1\infty}$. Thus the notion of a two-step excitattion process yields a possible explanation of all the characteristics of the kinetics of quenched phosphors which were indicated earlier: the more-than-linearity of the steady-state luminescence, the dependence of the form of the growth curve on E, the parabolic behavior at the beginning of the growth curve, the exponential decay, and the large value of the ratio s. We emphasize once again that these results are obtained on the basis of a pseudo-monomolecular recombination mechanism.

6. The hypothesis of a two-step excitation mechanism in phosphors, which brings the theory into agreement with experiment for strongly quenched phosphors (high temperatures) cannot be disregarded when considering unquenched phosphors (the same materials at ordinary temperatures). In fact, the number of electrons in the 1-levels (Fig.2) must be larger for unquenched phosphors and their trapping "stability" (in the thermal sense) greater. Direct optical excitation 0→2, which is considered virtually impossible at high temperatures (this is one of the fundamental hypotheses of the proposed theory), should be still less probable at low temperatures (since the thermally introduced energy, which, in general, might "free" excited electrons from the initial fast trapping at the 1-level will be smaller at low temperatures). Thus,

in any case, we must show that the two-step excitation does not contradict the experimental data on the properties of the phosphors at low temperatures.

We now give a more exact system of equations for the two-step mechanism which takes into account an effect which we have neglected in forming system (20). We have in mind the fact that the additional absorption at the 1-level reduces the absorption at the ground 0-level so that E, the total number of light quanta incident in one second on the phosphor, can be divided into two parts:

$$\frac{\gamma_{01}n_0}{\gamma_{01}n_0+\gamma_{12}n_1}E \quad \text{and} \quad \frac{\gamma_{12}n_1}{\gamma_{01}n_0+\gamma_{12}n_1}E, \tag{29}$$

which are absorbed respectively at the 0-level and the 1-level. In this connection we assume that the number of electrons in the 0-level is virtually infinite so that a reduction of their absorption is to be associated not with a smaller number, but rather with the fact that electrons in the 1-levels, as though shielding the electrons in the 0-levels, tend to intercept the exciting-light quanta. Hence our more exact equations assume the form

$$\frac{dn_2}{dt}=\frac{E\gamma_{12}}{\gamma_{01}n_0+\gamma_{12}n_1}n_1-(\alpha_{20}+\beta_{20})\,n_2; \tag{30}$$

$$(31)$$

$$+\frac{E\gamma_{01}n_0}{\gamma_{01}n_0+\gamma_{12}n_1}.$$

We solve these for the case in which there is no quenching: $\beta_{20}=\beta_{10}=0$. Calling $\gamma_{12}/\gamma_{01}n_0=\gamma$ and $\gamma n_1=\varphi$ we have, in place of (31),

$$(1/E\gamma)\,d\varphi/dt=(1-\varphi)/(1+\varphi). \tag{32}$$

the solution of which is

$$(1-\varphi)^2e^{\varphi}=Ce^{-E\gamma t}. \tag{33}$$

The constant C is determined from the condition $n_1=0$, whence $\varphi=0$ at $t=0$. Then from (33) we have $C=1$. The steady-state value of φ (for $t\to\infty$) is obviously equal to unity. Thus the steady state value for n_1 will be

$$n_{1\infty}=1/\gamma=\gamma_{01}n_0/\gamma_{12}. \tag{34}$$

Whence, taking (29) into account, we obtain the following results: in the steady state (no quenching!) half of the quanta are absorbed in the 0-level and the other half at the 1-level. It will be seen that the result does not contradict our assumption of no "impoverishment" of the 0-levels if it is assumed that $\gamma_{12}\gg\gamma_{01}$, i.e., if it is assumed that the absorption probability in the 1-levels is much greater than the absorption probability in the 0-levels. We call attention to the fact that the expression for $n_{1\infty}$ (34) coincides with formula (21), which is obtained by the quenching case, if we set $\beta_{10}=0$ in the latter. As is apparent, $n_{1\infty}=\text{const}$ and is also independent of E. Physically, this result is similar to the well known discovery due to Antonov-Romanovskii concerning the light-sum storage limit as a function of the stimulation properties of the exciting light (cf. reference 7).

We now consider the quantity n_2. Formula (31) can be rewritten in the form

$$dn_2/dt=E\varphi/(1+\varphi)=-\alpha_{20}n_2, \tag{35}$$

whence, by (33) we have for the steady-state luminescence

$$I_\infty=\alpha_{20}n_{2\infty}=E\left.\frac{1-e^{-(\varphi+E\gamma t)/2}}{2-e^{-(\varphi+E\gamma t)/2}}\right|_{t\to\infty}=\frac{E}{2}. \tag{36}$$

Thus the steady-state luminescence is proportional to the intensity of the exciting light and has a quantum yield equal to 0.5.

We now show that the quantity $n_2(t)$ increases initially according to a quadratic law. Considering (33) at small t we have $\varphi=E\gamma t$, whence, to the same accuracy, Eq. (35) yields

$$I=\alpha_{20}n_2=\frac{\alpha_{20}\gamma E^2t^2}{2}=\frac{\alpha_{20}\gamma_{12}}{2\gamma_{01}n_0}E^2t^2. \tag{37}$$

Thus our scheme predicts two well known properties of the nonquenching case: the linearity of the steady-state luminescence and the quadratic dependence of the luminescence intensity of the phosphor for "pulse excitation" (Antonov-Romanovskii, Levshin). It is worthy of note that the latter result has been obtained under the assumption that recombination takes place not according to a bimolecular law, but rather according to a pseudo-monomolecular relation ($I\sim\propto n$ and not $I\sim\propto n^2$). As in the strong quenching case the decay exhibits an exponential dependence on the time

$$I=I_\infty e^{-\alpha_{20}t}. \tag{38}$$

This result does not agree with experiment[1] but may perhaps be explained by the crude nature of the scheme under consideration here (in particular the

---

[7] V. V. Antonov-Romanovskii, Izv. Akad. Nauk SSSR Ser. Fiz. 15, 637 (1951).

existence of levels at only one depth).

7. We have considered the possibility of a two-step luminescence excitation mechanism inasmuch as we are convinced of the impossibility of satisfying the experimental data on quenched phosphors through the use of a one-step theory. There are, however, other facts which give much more direct evidence for the validity of a two-step mechanism. Lashkarev and Fedorus[8] have observed photoconductivity in certain single-crystals of CdS in which the steady-state value $\Delta\sigma_0$ as a function of the intensity of the exciting light is given by the relation $\Delta\sigma_0 \sim E^{3/2}$ (over a particular intensity range). The existence of such a "more-than-linear" dependence for $\Delta\sigma_0$ can be explained only by a two-step excitation mechanism, although the possibility exists that a one-step mechanism may also be playing a role. A two-step mechanism for the excitation of photoconductivity was also postulated by Lashkarev. We have also observed[++] a marked "more-than-linear" dependence for $\Delta\sigma_0$ in copper-activated polycrystalline cadmium-sulfide. In certain cases this dependence is found to be purely quadratic $\Delta\sigma_0 \sim E^2$ (see Fig. 3a and 3b). This semiconductor exhibits phosphorescence in the red-infrared region of the spectrum; the dependence of the steady-state luminescence I_∞ on the intensity of excitation E is found, in certain cases, to be close to quadratic. The growth curve has an inflection at its beginning and goes much slower than the decay curve ($L_g \gg L_d$). In other words the luminescence in this material displays all the characteristic properties mentioned above in connection with quenched sulfide phosphors. Consequently, if one assumes that the photoconduction and luminescence mechanisms in CdS-Cu are not separate and independent, it is reasonable to assume that the two-step excitation which is responsible for the "quadratic" photoconductivity in this material is also responsible for the "quadratic" luminescence. If this is so, it would seem that the origin of the "quadratic" behavior of luminescence in quenched ZnS-Cu and similar phosphors (exhibiting the same characteristics as CdS-Cu) lies in a two-step mechanism and that it is unnecessary to look for any other explanation; this reasoning is even more compelling when one considers that the alternative bimolecular scheme, as we have shown, is in disagreement with a large number of experimental criteria. For these reasons it deems desirable to analyze in detail the results which can be obtained from a more complete theory of phosphorescence and photoconductivity based on a two-step excitation mechanism and to compare these results with experiment. This project will be the subject of a forthcoming paper.

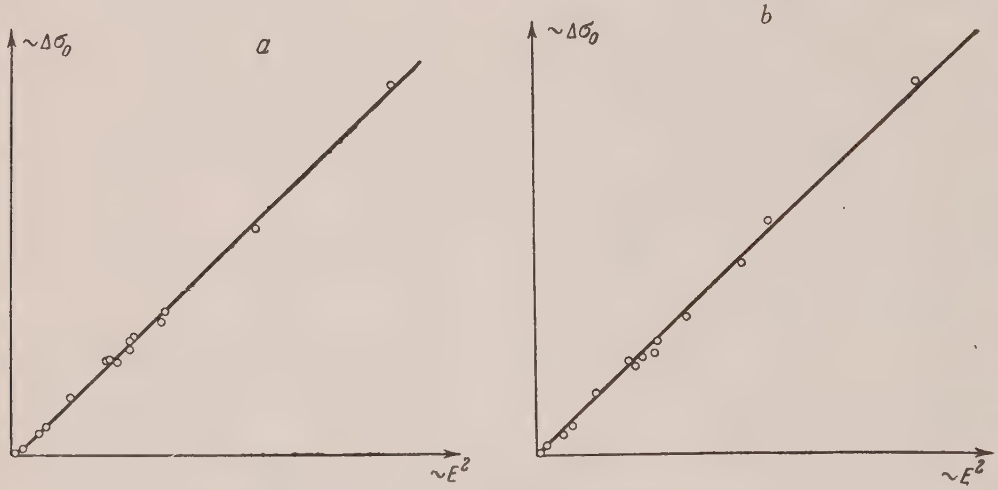

FIG. 3. CdS—Cu, crystal; *a*-γ=546 mμ, *b*-γ=578 mμ

[++] This work was carried out in conjunction with B. T. Kolomiits.

Translated by H. Lashinsky
21

SOVIET PHYSICS JETP VOLUME 3, NUMBER 2 SEPTEMBER, 1956

General Theory of Relativity or a Theory of Gravitation?

M. F. SHIROKOV

(Submitted to JETP editor, September 14, 1954)
J. Exptl. Theoret. Phys. (U.S.S.R.) 30, 180-184 (January, 1956)

IN a series of articles, V. A. Fock[1-5] gives a new interpretation of the general theory of relativity, according to which its physical content consists entirely of the familiar law of universal gravitation of A. Einstein

$$R^{\mu\nu} - {}^1\!/_2 g^{\mu\nu} R = -kT^{\mu\nu}, \tag{1}$$

which determines the deviation of the metric of space-time from the Galilean metric. In contradiction to the general principle of relativity, it is assumed that a preferred reference system exists with coordinates which satisfy the "harmonic" condition:

$$\partial(\sqrt{g}\, g^{\mu\nu})/\partial x^{\nu} = 0. \tag{2}$$

Hence in the articles of Fock cited above it is proposed to replace the designation "general theory of relativity" by another: "theory of gravitation".* This proposal involves not merely a change of terminology, as has been assumed by some physicists, but a fundamentally different interpretation of the general theory of relativity, as is seen from the following quotations:

"From what has been said it is clear that the use of the terms "general relativity", "general theory of relativity" or "the general principle of relativity" is inadmissible. It not only leads to misunderstandings, but reflects an incorrect understanding of the theory itself. Paradoxically, such a lack of understanding has been shown by the very author of the Einstein theory..." (p. 135 in reference 5.) "As for accelerated motion, the principle of relativity is inapplicable to it, to say nothing of the fact that the very concept of the "accelerated reference system" is not clearly defined" (p. 25 in reference 4). "The principle of equivalence has a strictly local character (in space and time) and is applicable only to weak and homogeneous fields and slow motions: only under these conditions can one replace, in an approximate manner, a field of acceleration by a gravitational field, and vice versa. As a general principle, it is, in general, incorrect" (p. 25 in reference 4) "Thus, in itself, the covariance of equations is by no means the expression of any physical law" (p. 133 in reference 5).

What has been said above prompts us to make certain observations concerning the problem formulated in the title of the present article.

1. DOES THE GENERAL PRINCIPLE OF RELATIVITY HOLD IN NATURE?

Mathematically this principle is expressed in the covariance of the fundamental equations of physics with respect to a rather extensive class of coordinate transformations, including also changes of all kinds from one inertial or non-inertial reference system to another. The physical essence of the general principle of relativity reduces to the fact that the curvilinear nature of space-time coordinates is manifested in the existence of two fields: gravitational and inertial, which underlie various physical effects existing in nature and possessing objective reality.

In the absence of gravitational fields the Riemann-Christoffel curvature tensor vanishes:

$$R^{\varepsilon}_{\mu\nu\sigma} = 0. \tag{3}$$

This equality is the necessary and sufficient condition for space-time to be Galilean. In such a space, a coordinate system can always be constructed, which satisfies, upon introduction of the imaginary time coordinate $x_4 = ict$, the requirement:

$$g_{\mu\nu} \begin{cases} = 1, & \mu = \nu; \\ = 0 & \mu \neq \nu. \end{cases} \tag{4}$$

In the presence of gravitational fields, on the other hand, Eq. (3) is no longer satisfied, space-time is no longer Galilean, and its metric is determined by the equation of gravitation (1).

The opinion is expressed[4] that the difference between the "special" and "general" theories of relativity reduces only to whether Eq. (3) is satisfied or not; it is also asserted that in the "special" theory, while Eq. (3) is valid for the coordinates, the general covariance of the equations is trivial and has no physical content. If this were so, the general theory of relativity would in fact reduce fully and completely to the theory of gravitation formulated in the form of Eq. (1), which determines the properties of spaces which do not satisfy Eq. (3). Actually, however, the situation is different. The region of application of the special theory of relativity is considerably narrower than the region defined by Eq. (3), and is limited to the reference systems which satisfy Eq. (4).

---

*Unfortunately, this point of view of Fock, at best controversial, has been reflected in the new edition of the "Great Soviet Encyclopedia", in which, in the article "Relativity, Theory of" only the special theory of relativity is treated, and instead of an article on the general theory of relativity an article "Gravitation, Theory of" is planned.

[1] V. A. Fock, J. Exptl. Theoret. Phys. (U.S.S.R.) 9, 375 (1939).

[2] V. A. Fock, *Nicholas Copernicus*, Acad. Sci. USSR (1947).

[3] *Some Applications of the Ideas of N. I. Lobachevsky in Mechanics and Physics*, GTTI, 1950.

[4] V. A. Fock, *Modern Theory of Space and Time*, Priroda, 12, 1953.

[5] V. A. Fock, Vopосy filosofii (Problems of Philosophy) 4, 1955.

There is an essential difference between requirements (3) and (4). Eq. (4) is satisfied by all inertial reference systems, without gravitational field, and with coordinate meshes (nets) which are connected with each other by linear Lorentz transformations. But Eq. (3) is satisfied also by all non-inertial reference systems which do not contain gravitational fields. In these latter, however, there appear the effects of the fields of inertial forces on the course of mechanical, electromagnetic (optical) and other processes which can in no way be explained on the basis of Lorentz transformations, i.e., within the framework of the special theory of relativity.

It is also very essential that in non-inertial systems, when Eq. (3) for space to be Galilean is satisfied, the metric of space-time does not satisfy the conditions (4). In particular, Einstein himself has pointed out the possibility of deviations from the Euclidean properties of space in non-inertial reference systems (e.g., rotating systems). It is well-known, however, that in the special theory of relativity the axioms of Euclidean geometry are valid for space.

Thus, the extension of the principle of special relativity to phenomena satisfying Eq. (3), combined with a denial of physical content to the generally covariant formulation of the laws of nature, reduces, in fact, to a denial of the objective reality of the fields of inertial forces and of specific effects produced by them in non-inertial reference systems, many of which have been experimentally demonstrated a long time ago. This makes it necessary to generalize the principle of relativity to inertial* reference systems also, i.e., to formulate the general principle of relativity as a physical assertion, which reflects the objective reality of nature.

2. DO PREFERRED REFERENCE SYSTEMS EXIST?

In the references 1-5 the existence of privileged, or, in our terminology, preferred, coordinate systems, defined by these solutions, is inferred from the fact of uniqueness of the solutions of the equation of gravitation (1) with the harmonic condition (2) for coordinates and boundary conditions (4) at infinity for isolated aggregates of matter. The existence of such solutions is therefore regarded as a weighty argument against the general principle of relativity. They are, indeed, determined by equations (1) and (2), the second of which is obviously not covariant with respect to general coordinate transformations.

Without doubt the solution quoted, whose discovery was to a considerable degree facilitated by a fortunate choice of condition (2), has considerable value and scientific interest. However, its uniqueness would be an argument against the general theory of relativity only if Eq. (2) were the expression of some physical law. Then the law of universal gravitation would be formulated by Eqs. (1) and (2). However, Eq. (2) is simply an arbitrary condition which defines the system of coordinates in which it is most advantageous to seek the solution of the proposed problem. The choice of the harmonic coordinates (2) is, in a sense, equivalent to the choice of cylindrical, spherical, and other coordinates convenient for the solution of the given problem.

It is, however, necessary to make completely clear the concept of a preferred reference system. Actually, in Newtonian mechanics, such a system was taken to be one in which the center of inertia of a given collection of matter is at rest or moves uniformly and rectilinearly. The existence of the center of inertia was guaranteed by the laws of conservation of mass, energy, momentum and angular momentum. Such a concept of a preferred reference system for an isolated collection of matter can be formulated also in the general theory of relativity, since in this theory also it has been shown that the theorem concerning the center of inertia holds in generally covariant form, i.e., for arbitrary coordinate systems, but with the Galilean conditions (4) at infinity.[6]

In accordance with this theorem, and without any contradiction with the general theory of relativity, the heliocentric system of coordinates of Copernicus will be a preferred system for our planetary system even in the general theory of relativity.

---

*Translator's note: It would appear that this word should be "non-inertial."

[6] Iu. M. Shirokov, J. Exptl. Theoret. Phys. (U.S.S.R.) 21, 748 (1951). M. F. Shirokov, J. Exptl. Theoret.Phys. (U.S.S.R.)27, 251 (1954).

For this reason, a negative solution is given to the problem of equivalence of the Copernican and Ptolemaic systems, which is thought to follow from the general theory of relativity by some physicists and philosophers abroad. To this it must be added that a rotating reference system can exist in reality only in limited regions of space[7], as a result of which the geocentric system of Ptolemy for the world as a whole does not exist in nature.

3. IS THE PRINCIPLE OF EQUIVALENCE OF INERTIAL FORCES AND GRAVITATION CORRECT?

The general principle of relativity contains inherently the principle of equivalence of gravitational and inertial forces, without which the generally covariant formulation of the equations of physics is altogether impossible. This is the reason why Einstein's efforts to create a general theory of relativity have led him to formulate a new law of universal gravitation. The physical essence of the principle of equivalence consists in the identity of the physical actions of fields of inertial and gravitational forces in spite of their different origin.. For instance, the equation of a geodesic is a differential equation of the trajectory of a small test body in gravitational as well as inertial fields, and it is impossible to separate them at a given point of space. The equations of electrodynamics, mechanics of continuous media, etc., also have the same form in the fields of both inertial and gravitational forces.

The principle of equivalence holds exactly only locally, i.e., only at a given point of space-time. This is quite sufficient for the formulation of physical laws in a generally covariant form. The fact that the principle of equivalence does not hold for the entire gravitational field as a whole means that it is impossible to interpret gravitational fields purely kinematically, and cannot be regarded as an objection against the principle of equivalence in its present form.

4. REMARKS CONCERNING PROSPECTS OF APPLICATION OF THE GENERAL THEORY OF RELATIVITY TO PHENOMENA OF THE MICROWORLD

The general theory of relativity is usually regarded to be applicable only to macroscopic phenomena, for instance the motion of celestial bodies in astronomy. Does it have any prospects of application to processes taking place in the microworld? We should like to point out here certain circumstances which are of significance for a correct answer to this question.

It is well known that in recent years a consistent covariant formulation of quantum electrodynamics (Schwinger, Feynman, Tomonaga and others), with respect to Lorentz transformations has led to marked successes in achieving a clearer formulation of the theory and in interpreting certain new experimental data. This makes it possible to hope that a still more complete generally covariant formulation of the quantum theory of fields and particles may turn out to be fruitful in view of its undoubtedly greater physical content (due to account being taken of gravitational and inertial fields). Even if it should turn out that these fields do not play an essential role in the processes of the microworld, the very proof of the correctness of this supposition could be regarded as an important result, since at present it is usually assumed without any serious attempt at justification. It should be pointed out, however, that certain calculations of a methodological character in the classical theory of fields and particles suggest doubts as to its correctness. It turns out that even in the well-known linear and non-linear generalizations of electrodynamics due to Born-Infeld and Bopp-Podolsky, in which point charges do not lead to divergences and possess a finite electromagnetic mass, the hypothesis of weak (Newtonian) gravitational field, assumed in these theories, is not fulfilled, and this results in a substantial contribution to the mass of particles[8,9].

CONCLUSIONS

The general theory of relativity is a physical theory concerning the dependence of the properties of space and time on matter and its motion. This theory is based on the assumptions of identity (covariance) of the laws of nature in all inertial and non-inertial reference systems which exist or can objectively exist in nature (general principle of relativity), and on the law of universal gravitation (1). The theory contains two universal constants: c-the velocity of light in inertial reference systems without gravitational fields, and k-the constant of gravitation, which occurs in Eq. (1) of the law of universal gravitation. The first expresses the mutual connection between space and time, and the second the dependence of the properties of space-time on matter and its motion.

---

[7] L. Landau and E. Lifshitz, *Classical Theory of Fields*.

[8] M. F. Shirokov, Vestnik Moscow State Univ. 4, 67, (1947).

[9] Ia. Pugachev and M. Shirokov, J. Exptl. Theoret. Phys.(U.S.S.R.)24, 375, 1953.

The interpretation of the general theory of relativity as only a theory of gravitation, while rejecting the general principle of relativity as a law of nature, is unacceptable because it leads to a denial of the objective reality of the fields of inertial forces and all physical effects (mechanical, electrodynamic, etc.) caused by them.

The division of the theory of relativity into special and general has no fundamental significance, and results from practical considerations in using the theory in various degrees of approximation.

Translated by A. V. Bushkovitch
22

SOVIET PHYSICS JETP VOLUME 3, NUMBER 2 SEPTEMBER, 1956

The Electron Spectrum of U^{237}

S. A. Baranov and K. N. Shliagin

(Submitted to JETP editor, April 19, 1955)
J. Exptl. Theoret. Phys. (U.S.S.R.) 30, 225-230 (February, 1956)

The electron spectrum of U^{237} was investigated on a $\pi\sqrt{2}$ focussing angle magnetic β spectrometer, beginning with electron energies of 1 kev. Two components of the spectrum were determined, with energy limits E_{0A}=84 kev (26%) and E_{0B}=249 kev (74%). The following γ transitions for Np^{237} were computed from the conversion electron lines; 26; 33; 43; 60; 69 (?); 101 (?) 124 (?); 165; 193 (?); 208; 267; 331; 370 and 436 kev. A tentative decay scheme of U^{237} is given.

The study of the decay of U^{237} has been clarified by several researches.[1-4] However, these investigations, with the exception of the last,[4] were not carried out with sufficient accuracy, and do not give the complete picture of the decay of U^{237}. We have undertaken to carry out more carefully the study of the electron spectrum of U^{237}, including the low energy region, on a spectrometer with increased resolving power and light sum.

APPARATUS

A magnetic β spectrometer with double focussing of the electrons at an angle of $\pi\sqrt{2}$ was employed for the study of the electron spectrum of U^{237}.[5] The radius of the central trajectory of the electrons was r_0=22.5 cm. The resolving power of the spectrometer, determined by the relative half width of the conversion line of Ba^{137} (Cs^{137}, $h\nu$= 661.6 kev) for a source width of 1.5 mm, coincided with the calculated value and equaled 0.3%.

The U^{237} source has the dimensions 1.5 x 25 mm^2; for it, the relative halfwidth of the conversion lines had a value > 0.3%. The deviation from the computed value (0.3%) is explained by the effect of the thickness of the source. The relative solid angle of the spectrometer amounted to about 0.43 % of 4π.

A vacuum of $\sim 10^{-5}$ mm was maintained in the spectrometer chamber. The intensity of the magnetic field at the central orbit was measured by the ballistic galvanometer method. The magnetic field of the spectrometer was calibrated by the conversion line of Ba^{137}.

The electrons were recorded by a single cylindrical Geiger-Muller counter. A window (dimensions 1.5 x 25 mm^2) was located on the lateral wall of the counter to admit electrons. The window was covered by a celluloid film of thickness $\sim 10^{-5}$ cm. The film was supported by a tungsten wire grid (φ= 0.04 mm, spacing $\sim$ 0.3 mm). The counter was filled with a gas mixture of argon and ethyl alcohol (10% alcohol, 90% argon). The pressure of the mixture was $\sim$ 50 mm mercury. The voltage level of the counter was 100-150 v. Pulses from the counter were recorded by the usual counting apparatus of the type PS-64.

PREPARATION OF THE RADIOACTIVE SOURCE

For the investigations, the preparation of U^{237},

---

[1] Y. Nishina, T. Yasaki, H. Ezoe, K. Kimura and M. Ikawa, Phys. Rev. 57, 1182 (1940).

[2] E. McMillan, Phys. Rev. 58, 178 (1940).

[3] L. Melander and H. Slatis, Arkiv. Mat. Astr. Fys. A36, No. 15 (1948).

[4] F. Wagner, Jr., M. S. Freedman, D. W. Engelkemeir and J. R. Huizenga, Phys. Rev. 89, 502 (1953).

[5] S. A. Baranov, A. F. Malov and K. N. Shliagin, *Apparatus and Techniques of Experiment* 1, 1, 1956).

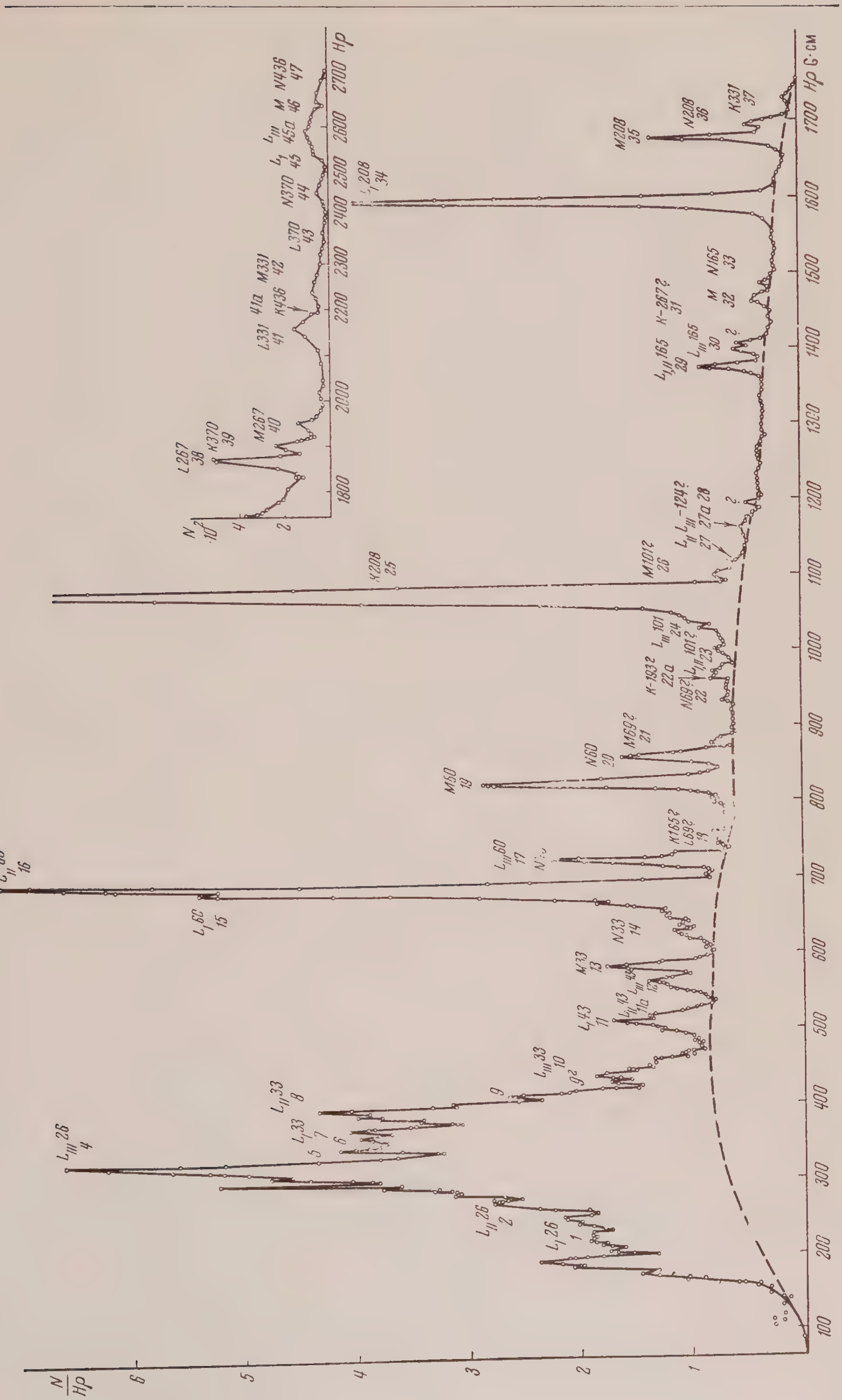

FIG. 1. Electron spectrum of U^{237}

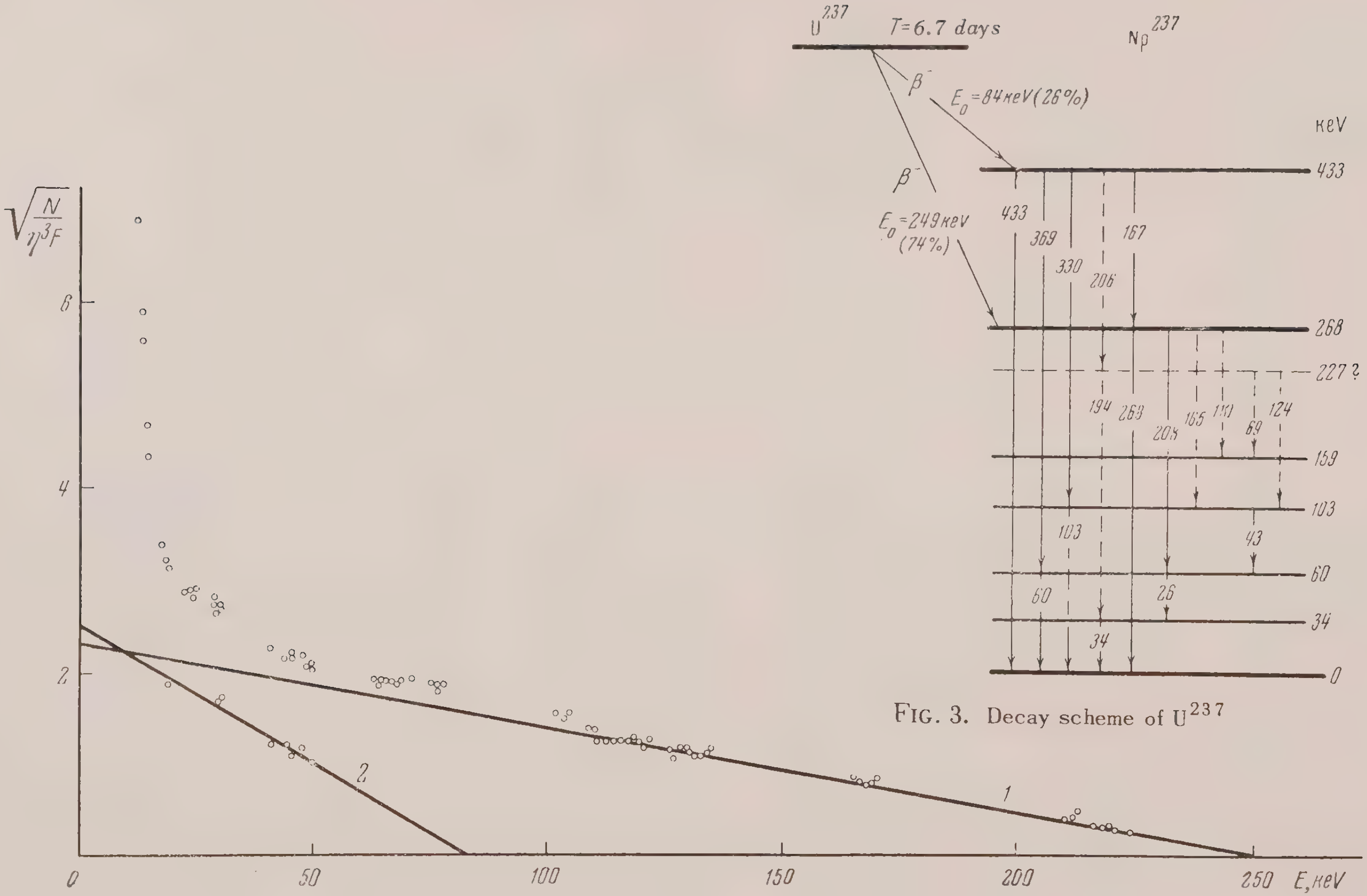

FIG. 3. Decay scheme of U^{237}

FIG. 2. Kurie graph of the spectrum of U^{237}. *1* — $E_{OA} = 249 \pm 5$ **kev**, *2* — $E_{OB} = 84 \pm 5$ **kev**

which decays with a halflife of $T = 6.7$ days, was obtained as the result of exposure of the isotope U^{236} to neutrons, the reaction being U^{236} (n, γ) U^{237}. Isotopic analysis of the product showed that it contained ~91% U^{236} (by weight). The amount of U^{238} was negligible.

The irradiated specimen was "seasoned" for some time before chemical purification, in order that any U^{239} (formed as a result of the presence of a small amount of U^{238}) might decay (halflife= 23.5 min). After this the specimen was carefully purified chemically, to remove Np^{239} and other foreign radioactive isotopes not belonging to uranium.

The radioactive source U^{237} was prepared from the nitrate salt of uranium, by precipitating it from a water solution on a thin organic film (thickness 10^{-5} cm). A narrow (1.5 x25mm^2) semi-transparent strip of aquadag was first placed on the latter. The aquadag guaranteed a good wetting of the film and the necessary conductivity of the source. This source had a surface density in the active layer of ~20 gm/cm^2.

RESULTS OF MEASUREMENT

The electron spectrum of U^{237} is shown in Fig. 1. As is seen from the drawing, a number of lines of Auger electrons are observed in the soft part of the spectrum. A series of conversion lines, not previously observed, were also discovered.

Analysis of the β spectrum with the aid of a Kurie graph (Fig. 2) permitted us to separate two partial spectra with bounding energies and intensities, respectively equal to 249 ±5 kev (74%) and 84 ±5 kev (26%). For the given β transitions, $\lg ft \approx 6$. The transitions under consideration are evidently related to transitions of first order of forbiddenness (tensor variant, $\Delta I = 0; \pm 1$), having spectra which coincide in form with resolved spectra. A small number of experimental points in the intervals between the conversion peaks do not permit us to draw any conclusion as to the actual form of the partial spectra.

Beta transitions with $E_0 > 260$ kev were not discovered. The number of observed electron lines amounted to more than 50, whereas the number given in the work by Wagner et al[4], was about 20.

Multiple recording of the electron spectrum showed that all the conversion lines coincide with the halflife of U^{237} ($T = 6.7$ days). This once again verifies the purity of the preparation used. The results of claculation of the kinetic energy of the conversion electrons, and also the value of the energy of the β transitions are given in the table. Here there are also given the relative intensities of the conversion lines and the multiplicities of some transitions. The interpretation of the lines

Interpretation of electron lines

No. of electron line	Energy of electrons in kev	Conversion shell	Transition energy in kev and multiplicity		Intensity relative to β spectrum $E_0 = 249$ keV	Intensity in arbitrary units
1	4,1	L_I	26,5	26.4	Lines appear to be Auger electrons	
2	4,8	L_{II}	26,4			
4	8,8	L_{III}	26,4			
7	10,8	L_I	33,2	33.3	lines appear to be Auger electrons	
8	11,7	L_{II}	33,3			
10	15,8	L_{III}	33,4			
13	27,7	M_I	33,4		$1{,}9 \cdot 10^{-2}$	0,68
14	32	N	33,5			
11	21,1	L_I	43,5	43.5 $E2 + M1$	$2{,}7 \cdot 10^{-2}$	0,97
11a	22	L_{II}	43,6		$1{,}6 \cdot 10^{-2}$	0,57
12	25,8	L_{III}	43,4			

No. of electron line	Energy of electrons in kev	Conversion shell	Transition energy in kev	and multiplicity	Intensity relative to β spectrum E_0=249 keV	Intensity in arbitrary units
15	37	L_{I}	59,6	59,7 $E1 + M2$	0,17	6,1
16	38,1	L_{II}	59,7		$2{,}8\cdot10^{-2}$	1,0
17	42,2	L_{III}	59,8		$5{,}2\cdot10^{-2}$	2,85
19	54	M_{I}	59,7		$2{,}2\cdot10^{-2}$	0,79
20	58,3	N	59,8			
18	46,8	L_{I}	69,2	69 (?)	very weak lines	
21	∼62,0	M_{I}	∼68,0			
22	∼69,0	N	∼69,0			
23	∼79,0	L_{I}	∼101	∼101 (?)	very weak lines, possibly Auger electrons	
24	∼83,0	L_{III}	∼101			
26	∼96,2	M	∼101			
27	∼100	L_{II}	∼123	∼124 (?)	very weak lines, possibly Auger electrons	
27a	∼107	L_{III}	∼125			
18	46,8	K	165,0	165,4 $E2 + M1$	$1{,}1\cdot10^{-2}$	0,39
29	143,8	L_{II}	165,4		$6{,}6\cdot10^{-3}$	0,24
30	148,2	L_{III}	165,8			
32	159,7	M_{I}	165,4		$3{,}5\cdot10^{-3}$	0,12
33	163,9	N_{I}	165,4			
22a	∼75	K	∼193	∼193 (?)	Possible Auger electrons	
25	90,0	K	208,2	208,2 $M1$	0,35	12,3
34	185,6	L_{I}	208,0		$9{,}0\cdot10^{-2}$	3,2
35	202,7	M_{I}	208,4		$2\cdot10^{-2}$	0,72
36	206,2	N_{I}	207,7		$7{,}6\cdot10^{-3}$	0,27
31	149,3	K	267,5	267,5	very weak lines	
38	244,6	L_{I}	267,0			
40	262,5	M_{I}	268,1			
37	213,3	K	331,5	331,5	very weak lines	
41	308,8	L_{I}	331,2			
42	326,3	M	332			
39	251,4	K	369,6	369,5	very weak lines	
43	346,7	L_{I}	369,1			
44	370	N	371			
41a	317,8	K	436	∼436	very weak lines	
45	413,2	L_{I}	436,6			
45a	418,7	L_{III}	436,3			
46	428,3	M	∼434			
47	433,8	N	∼435,3			

of the Auger electrons (soft) was not carried out.

The tables show that the observed lines are determined by the following transitions of the Np^{237} nucleus: 26.4; 33.3; 43.5; 59.7; 69 (?); 101 (?); 124 (?); 165; 193 (?); 208, 268; 331; 370 and 436 kev.

On the basis of the experimental results here, and of data on the investigation of the electron and α spectra of Am^{241}, a tentative scheme of the levels of the nucleus Np^{237} was constructed, and is shown in Fig. 3.

The problem of the spins and even energy levels are discussed in another work.*

We consider it our duty to thank G. N. Iakovlev for carrying out the chemical part of this research and also P.S. Samoilov who furnished assistance in the taking of the β spectrum of U^{237}

---

*Note added in proof. The work was published in 1955[6]. The results of the cited and present researches permit us to determine the spin of the ground state of U^{237}. It is equal to ±1/2.

[6] S. A. Baranov and K. N. Shliagin, Sessions of the Academy of Sciences, U.S.S.R., on the peaceful application of atomic energy, June 21-5, 1955, sitting OFMN, p. 251.

Translated by R. T. Beyer
43

SOVIET PHYSICS JETP VOLUME 3, NUMBER 2 SEPTEMBER, 1956

Nucleomesodynamics in Strong Coupling. I. Approximate Method. Spin-Charge Motion

S. I. PEKAR
Physics Institute, Academy of Sciences, Ukrainian SSR

(Submitted to JETP editor July 28, 1954)
J. Exptl. Theoret. Phys. (U.S.S.R.) 30, 304 (1956)

In the approximation of infinitely heavy nucleons and strong interaction with the meson field, we develop an approximate method and the associated mathematical apparatus which makes possible explicit determination of the wave functions and energy eigenvalues of the system. The mesons are assumed to be pseudoscalar, the coupling to be symmetric pseudovector (gradient) coupling, and the nucleon is assumed to be an extended source. Using the approximation method, the Hamiltonian of the system is simplified, and the spin-charge part of the system wave function is separated off and determined along with the corresponding energy.

1. INTRODUCTION

In previous papers on this same subject[1,2], it was assumed that the spin-charge and translational motion of the nucleon follow the relatively slow oscillations of the meson field adiabatically. To solve the problem, mathematical methods were used which are similar to those in the theory of polarons. Further investigations showed that in the most important case of nucleons and π-mesons the interaction is actually not as strong as is necessary to make the translational motion follow the meson field oscillations adiabatically. Quite the contrary, the vibrations of the meson field are adiabatic relative to the translational motion of the nucleon. Therefore, in zeroth approximation, we should consider the spin-charge motion and the oscillations of the meson field for the case of a fixed (infinitely heavy) nucleon. This is done in this and the succeeding paper.

Thus, in contrast to the above-mentioned earlier papers, we shall assume that only the spin-charge motion follows the meson field adiabatically, and shall, as before, use the methods of the theory of polarons[3] in treating this motion. In an earlier paper[4] it was shown, without the use of any ap-

---

[1] S. I. Pekar, J. Exptl. Theoret. Phys. (U.S.S.R.) 27, 398 (1954).

[2] S. I. Pekar, J. Exptl. Theoret. Phys. (U.S.S.R.) 27, 411 (1954).

[3] S. I. Pekar, *Studies in Electron Theory of Crystals*, GTI, 1951. (also available as *Untersuchungen uber die Elektronentheorie der Kristalle*, Akademische Verlag, Berlin, 1954).

[4] S. I. Pekar, J. Exptl. Theoret. Phys. (U.S.S.R.) 29, 599 (1955).

proximation methods (strong or weak coupling, quasistationary approximation, etc.), that, at least in the case where we treat the translational motion of the nucleon non-relativistically, no stationary solution of the wave equation of the system exists in the case of pseudovector coupling. We shall therefore assume the nucleon to be an extended source.

The problem treated here was first investigated by Pauli and Dancoff in 1942.[5] These authors, by cleverly introducing a new system of canonical field variables, separated off the terms in the energy operator which are proportional to the square of the total momentum of the system. The eigenvalues of the momentum are known from general arguments for any system. Thus it turns out that one knows, from general considerations, the eigenvalues of one of the terms in the Hamiltonian, the energy levels of the isobar states of the system. Unfortunately, in the paper of Pauli and Dancoff[5], the complete set of quantum numbers of the system was not given explicitely, and no systematic method for calculating matrix elements of all canonical variables was presented. Apparently it was just this point which made difficult the calculation of higher approximations of the theory and the consideration of various specific phenomena (scattering of mesons by nucleons, magnetic moment of the nucleon, nuclear forces, photoproduction of mesons, etc.). In their paper, when they considered, for example, the scattering of mesons, the isobars were not taken into account and they were unable to separate the proton and neutron states of the nucleon. Consequently, the scattering was considered only for the case of a nucleon state which is a superposition of all charge and spin states of the nucleon.

In later papers on the application of strong coupling theory with symmetric pseudovector coupling, for example in the work of Pauli[6] or Wada[7], the spin and isotopic spin of the nucleon were introduced as classical unit vectors, which is not a consistent application of the strong coupling theory developed in Ref. 5. Thus, because of the above-mentioned incompleteness of the solution of the problem in Ref. 5 and the complexity of the mathematics, the theory of strong coupling with symmetric pseudovector interaction did not achieve the necessary development during the next twelve years. Since newer data speak in favor of intermediate or strong coupling and a symmetric pseudovector interaction, further attempts at a more complete solution of the problem are of interest. We here present a method for somewhat more complete solution of the problem which makes possible explicit determination of the wave function of the system, the introduction of a complete set of quantum numbers, and systematic calculation of the matrix elements of all the canonical variables, which is needed for applications of the theory.

2. INITIAL EQUATIONS AND ASSUMPTIONS

By expanding the meson field φ_α ($\alpha = 1,2,3$) and the canonically conjugate field π_α in Fourier series of the form

$$\varphi_\alpha(\mathbf{r}) = \sum_{\vec{\varkappa}} \frac{1}{\sqrt{\omega_{\vec{\varkappa}}}}\, q_{\alpha\vec{\varkappa}}\,\chi_{\vec{\varkappa}}(\mathbf{r}); \qquad (1)$$

$$\pi_\alpha(\mathbf{r}) = \sum_{\vec{\varkappa}} \sqrt{\omega_{\vec{\varkappa}}}\, g_{\alpha\vec{\varkappa}}\,\chi_{\vec{\varkappa}}(\mathbf{r}),$$

where

$$\chi_{\vec{\varkappa}}(\mathbf{r}) = \sqrt{\frac{2}{L^3}} \begin{cases} \cos \vec{\varkappa}\mathbf{r}; & \varkappa_x \leqslant 0 \\ \sin \vec{\varkappa}\mathbf{r}; & \varkappa_x > 0 \end{cases} \qquad (2)$$

(the $\chi_{\varkappa}(r)$ are orthonormalized in a volume L^3), we can put the Hamiltonian of the meson field in the form

$$\hat{H}_0 = \frac{1}{2}\sum_{\alpha=1}^{3} \int [\pi_\alpha^2 + (\nabla\varphi_\alpha)^2 + \mu^2\varphi_\alpha^2]\, dV \qquad (3)$$

$$= \frac{1}{2}\sum_{\alpha\vec{\varkappa}} \omega_{\vec{\varkappa}} [g^2_{\alpha\vec{\varkappa}} + q^2_{\alpha\vec{\varkappa}}].$$

We shall use the natural system of units ($\hbar = c = 1$); μ is the meson mass in cm^{-1},

$$\omega_{\vec{\varkappa}} = \sqrt{\mu^2 + \vec{\varkappa}^2} \quad (\omega_{\vec{\varkappa}} > 0). \qquad (4)$$

The dimensionless generalized coordinates $q_{\alpha\vec{\varkappa}}$ and momenta $g_{\alpha\vec{\varkappa}}$ of the field satisfy the following commutation relations:

$$[q_{\alpha\vec{\varkappa}}, q_{\alpha'\vec{\varkappa}'}] = [g_{\alpha\vec{\varkappa}}, g_{\alpha'\vec{\varkappa}'}] = 0; \qquad (5)$$

$$[q_{\alpha\vec{\varkappa}}, g_{\alpha'\vec{\varkappa}'}] = i\delta_{\alpha\alpha'}\delta_{\vec{\varkappa}\vec{\varkappa}'}.$$

---

[5] W. Pauli and S. M. Dancoff, Phys. Rev. **62**, 85 (1942).

[6] W. Pauli, *Meson Theory of Nuclear Forces*, Interscience (1946).

[7] W. W. Wada, Phys. Rev. **88**, 1032 (1952).

We choose a representation in which the $q_{\alpha\vec{\varkappa}}$ are ordinary numbers; then the $g_{\alpha\varkappa}$ can be represented as differential operators $g_{\alpha\vec{\varkappa}} = -i\partial/\partial q_{\alpha\vec{\varkappa}}$. The operator for the interaction of the nucleon with the meson field is taken to be of the symmetric gradient (pseudovector) type:

$$\hat{H}' = -\frac{g}{\mu}\sqrt{4\pi}\sum_{\alpha=1}^{3}\tau_\alpha\int(\nabla\varphi_\alpha,\ \vec{\sigma})\ u(\mathrm{r})\,dV \qquad (6)$$

$$= \frac{g}{\mu}\sqrt{4\pi}\sum_{\alpha=1}^{3}\tau_\alpha\int\varphi_\alpha(\vec{\sigma},\nabla u)\,dV,$$

where g is the dimensionless coupling constant, $\vec{\sigma}$ and τ_α are the familiar spin and isotopic spin matrices for the nucleon, $u(\mathbf{r})$ is the spherically symmetric form factor for the extended nucleon, normalized to unity. We shall try to find the eigenfunctions of the operator $\hat{H} = \hat{H}_0 + \hat{H}'$. Without loss of generality, we can expand these functions in terms of eigenfunctions of the operators σ_3 and τ_3, and shall denote the latter by S_1, S_2, and Q_1, Q_2, respectively. The expansion has the form:

$$\Psi = \overline{C}_1(q)\,S_1Q_1 + \overline{C}_2(q)\,S_2Q_1 + \overline{C}_3(q)\,S_1Q_2 + \overline{C}_4(q)\,S_2Q_2 \qquad (7)$$

where q stands for the collection of variables $q_{\alpha\vec{\varkappa}}$. The four basis functions $S_i \cdot Q_j$ form a complete set. Applying the operators $\vec{\sigma}$ and τ_α to the wave function (7) is equivalent to transformation of the components $\overline{C}_\nu$ by the following four-by-four matrices:

$$\sigma_1 = \begin{vmatrix} 0 & 1 & 0 & 0 \\ 1 & 0 & 0 & 0 \\ 0 & 0 & 0 & 1 \\ 0 & 0 & 1 & 0 \end{vmatrix},\quad \sigma_2 = \begin{vmatrix} 0 & -i & 0 & 0 \\ i & 0 & 0 & 0 \\ 0 & 0 & 0 & -i \\ 0 & 0 & i & 0 \end{vmatrix},\quad \sigma_3 = \begin{vmatrix} 1 & 0 & 0 & 0 \\ 0 & -1 & 0 & 0 \\ 0 & 0 & 1 & 0 \\ 0 & 0 & 0 & -1 \end{vmatrix},$$

$$\tau_1 = \begin{vmatrix} 0 & 0 & 1 & 0 \\ 0 & 0 & 0 & 1 \\ 1 & 0 & 0 & 0 \\ 0 & 1 & 0 & 0 \end{vmatrix},\quad \tau_2 = \begin{vmatrix} 0 & 0 & -i & 0 \\ 0 & 0 & 0 & -i \\ i & 0 & 0 & 0 \\ 0 & i & 0 & 0 \end{vmatrix},\quad \tau_3 = \begin{vmatrix} 1 & 0 & 0 & 0 \\ 0 & 1 & 0 & 0 \\ 0 & 0 & -1 & 0 \\ 0 & 0 & 0 & -1 \end{vmatrix}. \qquad (8)$$

3. THE APPROXIMATION METHOD

The basis of our approximation is the assumption that the motion in the spin-charge degree of freedom follows the relatively slow oscillations of the meson field adiabatically. In zeroth approximation, it is assumed that for each instantaneous configuration of the meson field q, a stationary state of the system with respect to the spin-charge degree of freedom of the nucleon can be established. The mathematical formulation of this approximation consists of the following: we assume that the eigenfunction (7) can be split into two factors

$$\overline{C}_\nu(q) = C_\nu(q)\,\Phi(q);\quad \Psi = \psi(q)\,\Phi(q);$$

$$\psi(q) = C_1(q)\,S_1Q_1 + C_2(q)\,S_2Q_1 + C_3(q)\,S_1Q_2 + C_4(q)\,S_2Q_2 \equiv \begin{vmatrix} C_1 \\ C_2 \\ C_3 \\ C_4 \end{vmatrix}, \qquad (9)$$

chosen so that $\Phi(q)$ changes much more rapidly with $q_{\alpha\vec{\varkappa}}$ than does $\psi(q)$. This means that the second term in the expression

$$\frac{\partial\Psi}{\partial q_{\alpha\vec{\varkappa}}} = \psi \frac{\partial\Phi}{\partial q_{\alpha\vec{\varkappa}}} + \frac{\partial\psi}{\partial q_{\alpha\vec{\varkappa}}}\Phi \tag{10}$$

is much smaller than the first and can be dropped in zeroth approximation

$$\hat{H}_0\psi\Phi = \frac{1}{2}\sum_{\alpha\vec{\varkappa}} \omega_{\vec{\varkappa}}\left(q^2_{\alpha\vec{\varkappa}} - \partial^2/\partial q^2_{\alpha\vec{\varkappa}}\right)\psi\Phi \approx \psi\hat{H}_0\Phi + \dots \tag{11}$$

Then the omitted terms will later be included as a small perturbation (perturbation due to non-adiabaticity).

By substituting Eq. (9) in the wave equation of the system, $\hat{H}\Psi = H\Psi$, $\hat{H} = \hat{H}_0 + \hat{H}'$, and using the approximation (11), we get two equations

$$\hat{H}'(q)\psi = H'(q)\psi, \tag{12}$$

$$[\hat{H}_0 + H'(q)]\Phi = H\Phi, \tag{13}$$

which determine $\psi(q)$ and $\Phi(q)$. In Eq. (12) the $q_{\alpha\vec{\varkappa}}$ act as parameters; the equation determines a state ψ which is stationary with respect to the spin-charge degree of freedom, for a fixed configuration q of the meson field. Equation (13) is the wave equation of oscillation of the meson field in the presence of the nucleon. Equation (13) is conveniently interpreted, using (3), as the equation of motion of a system of harmonic oscillators in the presence of a given auxiliary field $H'(q)$, which shifts the equilibrium positions of the oscillators. The potential energy of these oscillators is

$$V(q) = H'(q) + \frac{1}{2}\sum_{\alpha\vec{\varkappa}} \omega_{\vec{\varkappa}} q^2_{\alpha\vec{\varkappa}} \equiv H'[\varphi_1\varphi_2\varphi_3] + \frac{1}{2}\sum_{\alpha=1}^{3}\int[(\nabla\varphi_\alpha)^2 + \mu^2\varphi_\alpha^2]\,dV. \tag{14}$$

If the functional

$$F[\psi\varphi_\alpha] \equiv \{\psi^*, \hat{H}'\psi\} + \frac{1}{2}\sum_{\alpha=1}^{3}\int[(\nabla\varphi_\alpha)^2 + \mu^2\varphi_\alpha^2]\,dV \tag{15}$$

is made an extremal relative to ψ, subject to the supplementary condition that ψ be normalized, it becomes the potential energy (14) of the oscillators, since its first term, according to the variational principle of quantum mechanics, becomes $H'(q)$.

In order to determine the equilibrium positions of the oscillators $q^v_{\alpha\vec{\varkappa}}$ or the corresponding equilibrium self-consistent form of the field $\varphi^v_\alpha(\mathbf{r})$, we must find the minimum of (14) with respect to $q_{\alpha\vec{\varkappa}}$, i.e., with respect to $\varphi_\alpha(\mathbf{r})$. Thus the equilibrium self-consistent form of the field corresponds to the extremum of $F[\psi, \varphi_\alpha]$ with respect to both ψ and φ_α. This extremum is to be found by first making F an extremal relative to φ_α for fixed ψ, and then making the resultant functional an extremum relative to ψ.

If we set the variation of $F[\psi, \varphi_\alpha]$ with respect to φ_α equal to zero, we get

$$\Delta\bar{\varphi}_\alpha - \mu^2\bar{\varphi}_\alpha = -4\pi\eta_\alpha \tag{16}$$

($\bar{\varphi}_\alpha$ is the extremal value of φ_α), where the function $\eta_\alpha(\mathbf{r})$ acts as a source density for the meson field $\bar{\varphi}_\alpha$; it is equal to

$$\eta_\alpha[\mathbf{r}, \psi] = -\frac{g}{\mu}(4\pi)^{-1/2}\sum_{\beta=1}^{3}\overline{\tau_\alpha\sigma_\beta}\frac{\partial u}{\partial x_\beta}, \tag{17}$$

$$\overline{\tau_\alpha\sigma_\beta} \equiv \{\psi^*, \tau_\alpha\sigma_\beta\psi\}.$$

The solution of equation (16) has the form

$$\bar{\varphi}_\alpha(\mathbf{r}) = \int \frac{\eta_\alpha[\mathbf{r}'\psi]\exp\{-\mu|\mathbf{r}-\mathbf{r}'|\}}{|\mathbf{r}-\mathbf{r}'|}\,dV'. \tag{18}$$

Upon substituting $\bar{\varphi}_\alpha(\mathbf{r})$ in the functional (15), we get a new functional which depends only on ψ:

$$J[\psi] \equiv F[\psi, \bar{\varphi}_\alpha] = -2\pi\sum_{\alpha=1}^{3}\int\bar{\varphi}_\alpha\eta_\alpha\,dV. \tag{19}$$

We must now make this functional an extremum by varying ψ, subject to the supplementary condition $\{\psi^*, \psi\} = 1$. We shall denote the extremal of the functional $J[\psi]$ by ψ^v. When this ψ^v is substituted in formula (18), we get a meson field which we denote by φ^v (r) It is self-consistent in the following sense: the Euler equation determining the extremum of $J[\psi]$ is Eq. (12) with the q's replaced by the equilibrium q^v's. Thus the ψ^v which makes $J[\psi]$ an extremum is a solution of the equation

$$\hat{H}'(q^v)\psi^v \equiv \hat{H}'[\varphi^v_\alpha]\psi^v = H'(q^v)\psi^v, \tag{20}$$

in which the parameters of the Hamiltonian, $q^v_{\alpha\vec{\varkappa}}$ themselves depend on ψ^v, since the φ^v_α are expressed in terms of ψ^v by formula (18):

$$\varphi_\alpha^v(\mathbf{r}) = \int \frac{\eta_\alpha[\mathbf{r}', \psi^v] \exp\{-\mu|\mathbf{r}-\mathbf{r}'|\}}{|\mathbf{r}-\mathbf{r}'|} dV'; \tag{21}$$

φ_α^v and ψ^v mutually determine one another through formulas (20) and (21). Such problems are customarily called self-consistent.

By expressing $J[\psi^v]$ and $H'(q^v)$ in terms of ψ^v, it is easy to get

$$J[\psi^v] = \frac{1}{2} H'(q^v) = -\frac{1}{3} G \sum_{\alpha\beta} (\overline{\tau_\alpha \sigma_\beta}^{\psi^v})^2, \tag{22}$$

where

$$\overline{\tau_\alpha \sigma_\beta}^{\psi^v} = \{\psi^{v*}, \tau_\alpha \sigma_\beta \psi^v\};$$
$$G = \frac{g^2}{2\mu^2} \iint (\nabla u(\mathbf{r}), \nabla' u(\mathbf{r}')) \frac{\exp\{-\mu|\mathbf{r}-\mathbf{r}'|\}}{|\mathbf{r}-\mathbf{r}'|} dV dV'. \tag{23}$$

In a semiclassical treatment of the system, where the spin-charge motion is treated quantum-mechanically while the meson field oscillations are treated classically, the functions φ_α^v, ψ^v would be an exact solution of the problem, and would describe a state in which the static meson field φ_α^v corresponds to the minimum of the potential energy (14), the oscillators are at rest in their equilibrium positions, and the spin-charge state ψ^v is determined by the exact quantum equation (20).

However, in the investigation of most phenomena, the meson field must be treated quantum-mechanically. In this case, the oscillators of the meson field cannot be at rest, but will go through zero-point vibrations in the neighborhood of the equilibrium positions $q^v_{\alpha\varkappa}$. These oscillations are described by Eqs. (12) and (13). We shall solve them approximately, under the assumption that the oscillators stay for the most part in the neighborhood of their equilibrium positions. In other words, it is assumed that the meson field $\varphi_\alpha(\mathbf{r})$ varies only slightly around $\varphi_\alpha^v(\mathbf{r})$ during the course of its oscillation.

4. DETERMINATION OF THE SPIN-CHARGE PART OF THE WAVE FUNCTION

We find ψ^v as the extremal of the functional (19). The latter is expressed explicitly in terms of ψ as follows:

$$J[\psi] \equiv -\frac{1}{3} G \sum_{\alpha,\,\beta=1}^{3} (\overline{\tau_\alpha \sigma_\beta})^2, \tag{24}$$

where

$$\begin{aligned}
&\overline{\tau_1\sigma_1} = C_1^*C_4 + C_2^*C_3 + C_3^*C_2 + C_4^*C_1, \quad \overline{\tau_2\sigma_3} = -iC_1^*C_3 + iC_2^*C_4 + iC_3^*C_1 - iC_4^*C_2,\\
&\overline{\tau_1\sigma_2} = -iC_1^*C_4 + iC_2^*C_3 - iC_3^*C_2 + iC_4^*C_1, \quad \overline{\tau_3\sigma_1} = C_1^*C_2 + C_2^*C_1 - C_3^*C_4 - C_4^*C_3,\\
&\overline{\tau_1\sigma_3} = C_1^*C_3 - C_2^*C_4 + C_3^*C_1 - C_4^*C_2, \quad \overline{\tau_3\sigma_2} = -iC_1^*C_2 + iC_2^*C_1 + iC_3^*C_4 - iC_4^*C_3,\\
&\overline{\tau_2\sigma_1} = -iC_1^*C_4 - iC_2^*C_3 + iC_3^*C_2 + iC_4^*C_1, \quad \overline{\tau_3\sigma_3} = C_1^*C_1 - C_2^*C_2 - C_3^*C_3 + C_4^*C_4,\\
&\overline{\tau_2\sigma_2} = -C_1^*C_1 + C_2^*C_3 + C_3^*C_2 - C_4^*C_1.
\end{aligned} \tag{24'}$$

We set $C_k = \sqrt{u_k} e^{i\varepsilon_k}$ ($k = 1, 2, 3, 4$; $u_k \geqslant 0$, ε_k is real), and get

$$Z \equiv \sum_{\alpha\beta} (\overline{\tau_\alpha \sigma_\beta})^2 = 8 \left| \sqrt{u_1 u_4}\, e^{i\varepsilon} - \sqrt{u_2 u_3} \right|^2 + (u_1 + u_2 + u_3 + u_4)^2, \tag{25}$$

where $\varepsilon = \varepsilon_1 - \varepsilon_2 - \varepsilon_3 + \varepsilon_4$. When we set the derivatives of $Z - \lambda(u_1 + u_2 + u_3 + u_4)$, with respect to ϵ and u_k equal to zero (λ is a Lagrange multiplier), we arrive at the following system of equations:

$$(u_1 u_2 u_3 u_4)^{1/2} \sin\varepsilon = 0; \tag{26}$$
$$u_1 = u_4; \quad u_2 = u_3; \quad (u_1 - u_2)(1 + \cos\varepsilon) = 0;$$
$$u_1 + u_2 = 1/2.$$

This system can be satisfied only if $\sin\epsilon = 0$, i.e., $\epsilon = \pi\nu$ where ν is an integer. For odd ν, the solution is any set of numbers u_k satisfying the conditions

$$u_1 = u_4, \quad u_2 = u_3, \quad u_1 + u_2 = {}^1\!/_2. \qquad (27)$$

This gives $Z = 3$, For even ν, the solution of Eq. (26) has the form

$$u_1 = u_2 = u_3 = u_4 = {}^1\!/_4; \quad Z = 1. \qquad (28)$$

Clearly, the stable state of the nucleon is the state with the lowest energy, i.e., the case of (27). In this state [cf. Eq. (24), $J[\psi^\nu] = -G$. From now on we shall treat only this state.

Without loss of generality, we can multiply all the components C_k of any solution by a constant of modulus unity. This means that all the phases ϵ_k can be increased simultaneously by an arbitraty real number. We shall choose this number so that $\epsilon_1 + \epsilon_4 = 0$, whereupon $\epsilon_2 + \epsilon_3 = -\pi\nu$, with ν odd. Then the solution (27) takes the form:

$$C_4 = C_1^*, \quad C_3 = -C_2^*, \qquad (29)$$

$$|C_1|^2 + |C_2|^2 = {}^1\!/_2.$$

Rotation of the coordinate system, first through angle φ about the Oz axis, and then through angle θ about the Oy axis results in the following coordinate transformation:

$$r' = \|a\| r, \quad \|a\| = \left| \begin{array}{ccc} \cos\vartheta\cos\varphi & \cos\vartheta\sin\varphi & -\sin\vartheta \\ -\sin\varphi & \cos\varphi & 0 \\ \sin\vartheta\cos\varphi & \sin\vartheta\sin\varphi & \cos\vartheta \end{array} \right| . \qquad (30)$$

The spinor ψ is transformed in the following way as a result of such a rotation:

$$\psi' = \|S\|\psi, \quad \|S\| = \left| \begin{array}{cccc} \cos\frac{\vartheta}{2}e^{i\varphi/2} & \sin\frac{\vartheta}{2}e^{-i\varphi/2} & 0 & 0 \\ -\sin\frac{\vartheta}{2}e^{i\varphi/2} & \cos\frac{\vartheta}{2}e^{-i\varphi/2} & 0 & 0 \\ 0 & 0 & \cos\frac{\vartheta}{2}e^{i\varphi/2} & \sin\frac{\vartheta}{2}e^{-i\varphi/2} \\ 0 & 0 & -\sin\frac{\vartheta}{2}e^{i\varphi/2} & \cos\frac{\vartheta}{2}e^{-i\varphi/2} \end{array} \right| . \quad (31) \qquad (31)$$

The quantities $\overline{\tau_\alpha\sigma_1}, \overline{\tau_\alpha\sigma_2}, \overline{\tau_\alpha\sigma_3}$ transform like the components of a three-dimensional vector. Therefore the functional (24) is invariant under the transformation (31). Consequently, if ψ° is an extremal of $J[\psi]$, then $\|S\|\psi^0$ will also be an extremal. We can similarly rotate the coordinate system in the isotopic spin space. The matrix $\|b\|$ of the rotation will have a form similar to (30) except that we introduce in place of ϑ and φ the corresponding angles β and γ. Under such a rotation, ψ again transforms like a spinor:

$$\psi'' = \|T\|\psi', \quad \|T\| = \left| \begin{array}{cccc} \cos\frac{\beta}{2}e^{i\gamma/2} & 0 & \sin\frac{\beta}{2}e^{-i\gamma/2} & 0 \\ 0 & \cos\frac{\beta}{2}e^{i\gamma/2} & 0 & \sin\frac{\beta}{2}e^{-i\gamma/2} \\ -\sin\frac{\beta}{2}e^{i\gamma/2} & 0 & \cos\frac{\beta}{2}e^{-i\gamma/2} & 0 \\ 0 & -\sin\frac{\beta}{2}e^{i\gamma/2} & 0 & \cos\frac{\beta}{2}e^{-i\gamma/2} \end{array} \right| . \qquad (32)$$

Under such a rotation, the quantities $\overline{\tau_1\sigma_\beta}\ \overline{\tau_2\sigma_\beta}\overline{\tau_3\sigma_\beta}$ transform like the components of a three-dimensional vector in the isotopic spin space, while the functioanl (24) remains invariant. Consequently,

$$\psi^v = \|T\|\cdot\|S\|\psi^0 \qquad (33)$$

is also an extremal of $J[\psi]$. If we choose as our "initial" solution ψ° the special case of (29):

$$C_1^0 = C_4^0 = 2^{-1/2}, \quad C_2^0 = C_3^0 = 0, \tag{34}$$

then we can express the "rotated" solution (33) in the following form:

$$\begin{aligned}
C_1^v &= \frac{1}{\sqrt{2}}\left(\cos\frac{\vartheta}{2}\cos\frac{\beta}{2}e^{i\delta/2} + \sin\frac{\vartheta}{2}\sin\frac{\beta}{2}e^{-i\delta/2}\right);\\
C_2^v &= \frac{1}{\sqrt{2}}\left(-\sin\frac{\vartheta}{2}\cos\frac{\beta}{2}e^{i\delta/2} + \cos\frac{\vartheta}{2}\sin\frac{\beta}{2}e^{-i\delta/2}\right);\\
C_3^v &= \frac{1}{\sqrt{2}}\left(-\cos\frac{\vartheta}{2}\sin\frac{\beta}{2}e^{i\delta/2} + \sin\frac{\vartheta}{2}\cos\frac{\beta}{2}e^{-i\delta/2}\right);\\
C_4^v &= \frac{1}{\sqrt{2}}\left(\sin\frac{\vartheta}{2}\sin\frac{\beta}{2}e^{i\delta/2} + \cos\frac{\vartheta}{2}\cos\frac{\beta}{2}e^{-i\delta/2}\right),
\end{aligned} \tag{35}$$

where $\delta = \varphi + \gamma$. It can be shown that every extremal $J[\psi]$ of the form (29) is given by the expression (35) with the appropriate choice of angles ϑ, β and δ. If the angles are limited to the intervals $0 \leqslant \delta \leqslant \pi$, $0 \leqslant \vartheta \leqslant 2\pi$, $0 \leqslant \beta \leqslant 2\pi$, then only one set of angles will correspond to each ψ^v.

Even though four independent angles ϑ, φ β, γ appear in the rotation matrices $||S||$ and $||T||$, the "rotated" solution (35) is determined by only three independent angles ϑ, β and $\delta = \varphi + \gamma$.

Corresponding to the initial ψ° and the "rotated" ψ^v we should introduce densities $\eta^\circ_\alpha(\mathbf{r})$ and $\eta^v_\alpha(\mathbf{r})$ as well as the self-consistent meson fields $\varphi^\circ_\alpha(\mathbf{r})$ and $\varphi^v_\alpha(\mathbf{r})$. The relation between them is given by formulas (17) and (21). The quantities η_α and φ_α are three-dimensional vectors in the isotopic spin space. Therefore

$$\begin{aligned}
\eta_\alpha^v(\mathbf{r}) &= \sum_{\alpha_1=1}^{3} b_{\alpha\alpha_1}\eta^0_{\alpha_1}(\|a^{-1}\|\mathbf{r})\\
&= -\frac{g}{\sqrt{4\pi}\,\mu}\sum_{\alpha_1=1}^{3} b_{\alpha\alpha_1}(\|a\|\overline{\tau_{\alpha_1}\sigma}^{\psi^\circ}, \mathbf{r})\frac{1}{r}\frac{\partial u}{\partial r}\\
&= -\frac{g}{\sqrt{4\pi}\,\mu}\sum_{\alpha_1\beta_1\beta} b_{\alpha\alpha_1}a_{\beta\beta_1}\overline{\tau_{\alpha_1}\sigma_{\beta_1}}^{\psi^\circ}\frac{x_\beta}{r}\frac{\partial u}{\partial r}\\
&= -\frac{g}{\sqrt{4\pi}\,\mu}\sum_{\beta=1}^{3}\overline{\tau_\alpha\sigma_\beta}^{\psi^v}\frac{\partial u}{\partial x_\beta},
\end{aligned} \tag{36}$$

where

$$\overline{\tau_\alpha\sigma_\beta}^{\psi^v} = \sum_{\alpha_1,\ \beta_1=1}^{3} b_{\alpha\alpha_1}a_{\beta\beta_1}\overline{\tau_{\alpha_1}\sigma_{\beta_1}}^{\psi^\circ}. \tag{37}$$

Using formulas (34), (24 '), and (37), we get

$$\begin{aligned}
&\overline{\tau_1\sigma_1}^{\psi^v} = \cos\vartheta\cos\beta\cos\delta + \sin\vartheta\sin\beta, \quad \overline{\tau_2\sigma_3}^{\psi^v} = -\sin\vartheta\sin\delta,\\
&\overline{\tau_1\sigma_2}^{\psi^v} = -\cos\beta\sin\delta, \quad \overline{\tau_3\sigma_1}^{\psi^v} = \cos\vartheta\sin\beta\cos\delta - \sin\vartheta\cos\beta,\\
&\overline{\tau_1\sigma_3}^{\psi^v} = \sin\vartheta\cos\beta\cos\delta - \cos\vartheta\sin\beta,\\
&\overline{\tau_2\sigma_1}^{\psi^v} = -\cos\vartheta\sin\delta, \ \overline{\tau_3\sigma_2}^{\psi^v} = -\sin\beta\sin\delta,\\
&\overline{\tau_2\sigma_2}^{\psi^v} = -\cos\delta, \overline{\tau_3\sigma_3}^{\psi^v} = \sin\vartheta\sin\beta\cos\delta + \cos\vartheta\cos\beta.
\end{aligned} \tag{38}$$

5. CONSIDERATION OF SMALL OSCILLATIONS OF THE MESON FIELD IN THE NEIGHBORHOOD OF THE EQUILIBRIUM FORM

The self consistent solutions $\varphi^v_\alpha(\mathbf{r})$ which we found in the preceding section correspond to the equilibrium positions of the meson field oscillators. We now go on to consider the small vibrations of $\varphi_\alpha(\mathbf{r})$ in the neighborhood of the equilibrium form $\varphi^v_\alpha(\mathbf{r})$. We shall assume that the oscillators of the meson field vibrate mainly close to the configuration in which their potential energy is a minimum. This means $\varphi_\alpha(\mathbf{r})$ is almost always close to one of the functions $\varphi^v_\alpha(\mathbf{r})$. Thus if we set

$$\varphi_\alpha(\mathbf{r}) = \varphi^v_\alpha(\mathbf{r}) + \varphi'_\alpha(\mathbf{r}), \tag{39}$$

and select the appropriate angles ϑ, β, and δ for each $\varphi_\alpha(\mathbf{r})$, we can regard $\varphi'_\alpha(\mathbf{r})$ as a small perturbation in that portion of the space in which $\varphi^v_\alpha(\mathbf{r})$

is essentially different from zero. The term $\varphi'_\alpha(\mathbf{r})$ drops out in zeroth approximation, so that equation (12) becomes (cf. Eqs. 6, 21, 17, 23):

$$\hat{H}'(q^v)\psi_s^v \equiv -\frac{2}{3}G\sum_{\alpha\beta}\overline{\tau_\alpha\sigma_\beta}^{\psi^v}\tau_\alpha\sigma_\beta\psi_s^v = H'_s(q^v)\psi_s^v. \tag{40}$$

This solution simplifies considerably if we go over to the wave function ψ_s^0 by means of the substitution (33). Then Eq. (40) becomes:

$$-\frac{2}{3}G\sum_{\alpha\beta}\overline{\tau_\alpha\sigma_\beta}^{\psi^0}\tau_\alpha\sigma_\beta\psi_s^0 \equiv -\frac{2}{3}G\begin{vmatrix} 1 & 0 & 0 & 2 \\ 0 & -1 & 0 & 0 \\ 0 & 0 & -1 & 0 \\ 2 & 0 & 0 & 1 \end{vmatrix}\begin{vmatrix} C_{1s}^0 \\ C_{2s}^0 \\ C_{3s}^0 \\ C_{4s}^0 \end{vmatrix} = H'_s(q^v)\psi_s^0. \tag{41}$$

The four eigenfunctions and eigenvalues of this equation have the form:

$$1)\ H'_1 = -2G,\quad 2)\ H'_2 = {}^2/_3G,\quad 3)\ H'_3 = {}^2/_3G.\quad 4)\ H'_4 = {}^2/_3G;$$

$$\psi^0 \equiv \psi_1^0 = \begin{vmatrix} \frac{1}{\sqrt{2}} \\ 0 \\ 0 \\ \frac{1}{\sqrt{2}} \end{vmatrix},\quad \psi_2^0 = \begin{vmatrix} 0 \\ 1 \\ 0 \\ 0 \end{vmatrix},\quad \psi_3^0 = \begin{vmatrix} 0 \\ 0 \\ 1 \\ 0 \end{vmatrix},\quad \varphi_4^0 = \begin{vmatrix} \frac{1}{\sqrt{2}} \\ 0 \\ 0 \\ -\frac{1}{\sqrt{2}} \end{vmatrix}. \tag{42}$$

From this equation we see that the ground state of the unperturbed problem is non-degenerate, so that the energy of the spin-charge motion in first approximation can, as usual, be expressed in terms of the exact energy operator (6) and the zeroth order wave function:

$$H'(q) = \{\psi^{v*}, \hat{H}'\psi^v\} \tag{43}$$

$$= \frac{g\sqrt{4\pi}}{\mu}\sum_{\alpha\beta}\overline{\tau_\alpha\sigma_\beta}^{\psi^v}\int\varphi_\alpha\frac{\partial u}{\partial x_\beta}\,dV =$$

$$= -4\pi\sum_\alpha\int\varphi_\alpha(\mathbf{r})\,\eta_\alpha^v(\mathbf{r})\,dV.$$

We now proceed to Eq. (13) which describes the oscillations of the meson field. Upon substituting $H'(q)$ in the form (43) in the operator on the left side of the equation and using Eqs. (3), (39), (16), and (17), we get

$$\hat{H}_0 + H'(q) = H'(q^v) \tag{44}$$

$$+\frac{1}{2}\sum_\alpha\int[(\nabla\varphi_\alpha^v)^2 + \mu^2\varphi_\alpha^{v^2}]\,dV$$

$$+\frac{1}{2}\sum_\alpha\int[\pi_\alpha^2 + (\nabla\varphi'_\alpha)^2 + \mu^2\varphi'^2_\alpha]\,dV$$

$$= J[\psi^v] + \frac{1}{2}\sum_{\alpha\vec{\varkappa}}\omega_{\vec{\varkappa}}\left[(q_{\alpha\vec{\varkappa}} - q^v_{\alpha\vec{\varkappa}})^2 - \frac{\partial^2}{\partial q^2_{\alpha\vec{\varkappa}}}\right].$$

A question arises as to how the parameters

$$\vartheta \equiv v_1,\quad \beta \equiv v_2,\quad \delta \equiv v_3, \tag{45}$$

should be chosen so that the functions $\varphi_\alpha^v(\mathbf{r})$ give the best approximation to $\varphi_\alpha(\mathbf{r})$. Obviously the values of v_i must depend on $\varphi_\alpha(\mathbf{r})$, since the parameters of an approximation always depend on the function to be approximated. We should regard as the best choice of the v_i that set for which the energy $H(q)$ is most accurately given by formula (43). According to the variational principle of quantum mechanics, the highest accuracy in calculating $H(q)$ is achieved for that choice of the v_i which makes the energy (43) a minimum. The minimum condition has the following form:

$$\sum_{\alpha=1}^{3}\int \varphi_\alpha \frac{\partial \eta_\alpha^v}{\partial v_i}\, dV = 0, \quad i = 1, 2, 3. \tag{46}$$

The v_i are determined from these three equations; they are functionals of $\varphi_\alpha(\mathbf{r})$, i.e., functions of $q_{\alpha\vec{\varkappa}}$. If we introduce the operator $\hat{\omega} = \sqrt{\mu^2 - \Delta}$ and use Eq. (16), Eq. (46) can be rewritten as

$$\sum_{\alpha}\int \varphi_\alpha \frac{\partial \hat{\omega}^2 \varphi_\alpha^v}{\partial v_i}\, dV = 0, \quad i = 1, 2, 3. \tag{47}$$

There are also other methods for determining the parameters v_i. For example, we can approximate φ_α by functions φ_α^v using the method of least squares, and choose the v_i so that the integral

$$\sum_{\alpha}\int [\varphi_\alpha - \varphi_\alpha^v]^2\, dV \tag{48}$$

is a minimum. Upon expanding the square of the difference and noting that the square of the first term and the integral of the square of the second term do not depend on v_i, we can express the minimum condition in the form

$$\sum_{\alpha}\int \varphi_\alpha \frac{\partial \varphi_\alpha^v}{\partial v_i}\, dV = 0, \quad i = 1, 2, 3. \tag{49}$$

These equations can be used in place of (47) for determining the v_i; the results thus obtained are very close to those from (47) so long as the φ_α actually differ little from the φ_α^v. We could also use a system of equations intermediate in type between (47) and (49):

$$\sum_{\alpha}\int \varphi_\alpha \frac{\partial \hat{\omega} \varphi_\alpha^v}{\partial v_i}\, dV = 0, \quad i = 1, 2, 3. \tag{50}$$

The operator (44) is the required Hamiltonian, determining the motion of the meson field in the presence of the nucleon. Its eigenvalues give the energy H of the total system, as shown by Eq. (13). The eigenfunctions of this operator, $\Phi(q)$, when multiplied by ψ^v give the wave functions of the system (cf. Eq. 9). The operator (44) is essentially different from the energy operator of a system of independent harmonic oscillators, since the quantities v_i, and consequently also the $q^v_{\alpha\vec{\varkappa}}$, are complicated functions of the $q_{\alpha\vec{\varkappa}}$.

It is appropriate here to compare our method with that of Geilikman[8], who represents the meson field in the form

$$\varphi_\alpha(\mathbf{r}) = f_\alpha(\mathbf{r}) + \varphi'_\alpha(\mathbf{r}), \quad \varphi'_\alpha \ll f_\alpha \tag{51}$$

and treats $f_\alpha(\mathbf{r})$ as a classical quantity, commuting with π_α. He determines the quantity $f_\alpha(\mathbf{r})$ as the minimum of our expression (14), i.e., as the equilibrium form of the meson field when it is treated classically.

As we pointed out earlier, there are an infinity of mimima of Eq. (14), determined by the parameters ϑ, β, δ, $\varphi_\alpha^v(\mathbf{r})$, so that f_α depends essentially on ϑ, β, δ. In formula (51), $\varphi'_\alpha(\mathbf{r})$ can be treated as a small quantity only if, for each $\varphi_\alpha(\mathbf{r})$, the parameters v_i are determined in an appropriate way [for example, as done above, through Eq. (47), (49), or (50).] Consequently the v_i are functions of the $q_{\alpha\vec{\varkappa}}$ and therefore $f_\alpha(\mathbf{r}, v_i)$ does not commute with π_α, in contradiction to the assumption of Ref. 8.

No explicit form of the wave function for the spin-charge motion was found in Ref. 8, so that the author did not discover the presence of parameters v_i (or an equivalent set). As a result, the quantities $q^v_{\alpha\vec{\varkappa}}$, in the operator analogous to (44), were treated as constants, and the operator itself was regarded to be the energy operator of a system of independent harmonic oscillators. As a result Geilikman's results[8,9] differ essentially from ours.

6. SOME PROPERTIES OF THE FUNCTION $v_i(\ldots q_{\alpha\vec{\varkappa}}\ldots)$, AND SOME RELATIONS WHICH ARE NEEDED LATER

We shall obtain various results without determining the explicit form of the function $v_i(\ldots q_{\alpha\vec{\varkappa}}\ldots)$, by using some of the properties of these functions which are already apparent from the implicit definition of v_i given by formulas (47), (49) or (50). We write these formulas in the form

$$\sum_{\alpha}\int \varphi_\alpha \frac{\partial \hat{\omega}^n \varphi_\alpha^v}{\partial v_i}\, dV = 0, \tag{52}$$

$$i = 1, 2, 3, \quad n = 0, \text{ or } 1, \text{ or } 2.$$

If we expand φ_α and φ_α^v in Fourier series of the form (1), Eq. (52) is replaced by

$$\sum_{\alpha\vec{\varkappa}} q_{\alpha\vec{\varkappa}}\, \omega_{\vec{\varkappa}}^{n-1} \frac{\partial q^v_{\alpha\vec{\varkappa}}}{\partial v_i} = 0. \tag{53}$$

---

[8] B. T. Geilikman, Dokl. Akad. Nauk SSSR **90**, 359 (1953).

[9] B. T. Geilikman, Dokl. Akad. Nauk SSSR **90**, 991 (1953); **91**, 39, 225 (1953).

It is obvious that if we multiply all the $q_{\alpha\vec{\varkappa}}$ by an arbitrary common factor t, the roots v_i of equation (53) remain unchanged. Consequently,

$$v_i(\cdots tq_{\alpha\vec{\varkappa}}\cdots) = v_i(\cdots q_{\alpha\vec{\varkappa}}\cdots), \tag{54}$$

i.e., the v_i are homogeneous functions of degree zero in the $q_{\alpha\vec{\varkappa}}$, so that

$$\sum_{\alpha\vec{\varkappa}} \frac{\partial v_i}{\partial q_{\alpha\vec{\varkappa}}} q_{\alpha\vec{\varkappa}} = 0. \tag{55}$$

We can also show that

$$\int \sum_{\alpha} [\hat{\omega}^{n_1}\varphi^v_{\alpha}(\mathbf{r})]\,[\hat{\omega}^{n_2}\varphi^v_{\alpha}(\mathbf{r})]\,dV \tag{56}$$

$$= \int \sum_{\alpha} \varphi^0_{\alpha}(\mathbf{r})\,\hat{\omega}^{n_1+n_2}\varphi^0_{\alpha}(\mathbf{r})\,dV$$

does not depend on v_i. The proof can be given by making use of the invariance of the function in the integrand with respect to rotations in both ordinary and isotopic space, and by changing variables in the integral. If we set $n_1 = n_2 = n/2$ in (56) and differentiate with respect to v_i and v_j, we get

$$\sum_{\alpha}\int \frac{\partial\varphi^v_{\alpha}}{\partial v_i}\hat{\omega}^n\varphi^v_{\alpha}\,dV = 0, \tag{57}$$

$$\sum_{\alpha}\int \frac{\partial\varphi^v_{\alpha}}{\partial v_i}\frac{\partial\hat{\omega}^n\varphi^v_{\alpha}}{\partial v_j}\,dV = -\sum_{\alpha}\int \frac{\partial^2\varphi^v_{\alpha}}{\partial v_i\,\partial v_j}\hat{\omega}^n\varphi^v_{\alpha}\,dV. \tag{58}$$

Later on we shall repeatedly deal with the quantities

$$R^{(n)}_{i} = -\sum_{\alpha}\int \frac{\partial^2\varphi^v_{\alpha}}{\partial v_i\,\partial v_j}\hat{\omega}^n\varphi^v_{\alpha}\,dV \tag{59}$$

$$= \sum_{\alpha\vec{\varkappa}} \omega^{n-1}_{\vec{\varkappa}} \frac{\partial q^v_{\alpha\vec{\varkappa}}}{\partial v_i}\frac{\partial q^v_{\alpha\vec{\varkappa}}}{\partial v_j},$$

which we now calculate. The field φ^v_{α}, defined by formula (21), can be expressed, using formula (36), as

$$\varphi^v_{\alpha}(r) = -\frac{g}{\sqrt{4\pi}\,\mu}\sum_{\beta-1}^{3}\overline{\tau_{\alpha}\sigma_{\beta}}^{\psi^v}\int\frac{\partial u(\mathbf{r}')}{\partial x'_{\beta}}\frac{\exp\{-\mu\,|\mathbf{r}-\mathbf{r}'|\}}{|\mathbf{r}-\mathbf{r}'|}\,dV' = -(\overline{\tau_{\alpha}\sigma}^{\psi^v}, \nabla W) \tag{60}$$

$$= -\frac{1}{r}\frac{dW}{dr}(\overline{\tau_{\alpha}\sigma}^{\psi^v}, \boldsymbol{r}),$$

where

$$W(r) = \frac{g}{\mu}\frac{1}{\sqrt{4\pi}}\int u(\mathbf{r}')\frac{\exp\{-\mu\,|\mathbf{r}-\mathbf{r}'|\}}{|\mathbf{r}-\mathbf{r}'|}\,dV'. \tag{61}$$

If we substitute (60) in (59), we get

$$R^{(n)}_{ij} = -\frac{1}{2}I^{(n)}\sum_{\alpha\beta}\overline{\tau_{\alpha}\sigma_{\beta}}^{\psi^v}\frac{\partial^2\overline{\tau_{\alpha}\sigma_{\beta}}^{\psi^v}}{\partial v_i\,\partial v_j}. \tag{62}$$

Here we have introduced the notation

$$2\int\frac{\partial W}{\partial x_{\beta}}\hat{\omega}^n\frac{\partial W}{\partial x_{\beta'}}\,dV = \delta_{\beta\beta'}I^{(n)}. \tag{63}$$

From formulas (62) and (38) we get

$$R^{(n)}_{11} = R^{(n)}_{22} = R^{(n)}_{33} = I^{(n)}, \tag{64}$$

$$R^{(n)}_{12} = R^{(n)}_{21} = -I^{(n)}\cos\delta,$$

$$R_{13} = R^{(n)}_{31} = R^{(n)}_{23} = R^{(n)}_{32} = 0.$$

Now we calculate $\partial v_i/\partial q_{\alpha\vec{\varkappa}}$. For this purpose we differentiate (52) or (53) with respect to $q_{\alpha\vec{\varkappa}}$:

$$\sum_{\alpha_1, j}\int\varphi_{\alpha_1}\frac{\partial^2\hat{\omega}^n\varphi^v_{\alpha_1}}{\partial v_i\,\partial v_j}\frac{\partial v_j}{\partial q_{\alpha\vec{\varkappa}}} + \frac{\partial q^v_{\alpha\vec{\varkappa}}}{\partial v_i}\omega^{n-1}_{\vec{\varkappa}} = 0. \tag{65}$$

Since, according to our assumption, φ_{α_1} is close to $\varphi^v_{\alpha_1}$, we replace φ_{α_1} in the integrand by the approximation $\varphi^v_{\alpha_1}$. Then by using (59), we can write equation (65) in the form

$$\sum_{j=1}^{3}R^{(n)}_{ij}\frac{\partial v_j}{\partial q_{\alpha\vec{\varkappa}}} = \frac{\partial q^v_{\alpha\vec{\varkappa}}}{\partial v_i}\omega^{n-1}_{\vec{\varkappa}}, \quad i = 1, 2, 3. \tag{66}$$

The quantities $\partial v_j/\partial q_{\alpha\vec{\varkappa}}$ are determined from these three linear equations as follows:

$$\frac{\partial\vartheta}{\partial q_{\alpha\vec{\varkappa}}} = \frac{\omega^{n-1}_{\vec{\varkappa}}}{I^{(n)}\sin^2\delta}\left(\frac{\partial q^v_{\alpha\vec{\varkappa}}}{\partial\vartheta} + \cos\delta\,\frac{\partial q^v_{\alpha\vec{\varkappa}}}{\partial\beta}\right), \tag{67}$$

$$\frac{\partial\beta}{\partial q_{\alpha\vec{\varkappa}}} = \frac{\omega^{n-1}_{\vec{\varkappa}}}{I^{(n)}\sin^2\delta}\left(\frac{\partial q^v_{\alpha\vec{\varkappa}}}{\partial\beta} + \cos\delta\,\frac{\partial q^v_{\alpha\vec{\varkappa}}}{\partial\vartheta}\right), \tag{68}$$

$$\frac{\partial\delta}{\partial q_{\alpha\vec{\varkappa}}} = \frac{\omega_{\vec{\varkappa}}^{n-1}}{I^{(n)}}\,\frac{\partial q^{v'}_{\alpha\vec{\varkappa}}}{\partial\delta}. \qquad (69)$$

The approximate method which we have developed enabled us to reduce the initial problem of finding the eigenvalues and eigenfunctions of the operator $\hat{H}_0 + \hat{H}'$ (cf. Eqs. 3 and 6) to the solution of Eq. (13) with the operator (44). The latter describes the oscillations of the meson field in the presence of the nucleon; the spin-charge degrees of freedom of the system no longer appear in it. The solution of this equation is given in a succeeding paper, which appears in this same issue.

The following approximations have been made in this paper:

1) The approximation of "infinitely heavy nucleons"; the nucleon was assumed to be fixed.

2) The adiabatic approximation: we dropped the second term on the right hand side of (10), which led to the approximate formula (11). 3) It

3) It was assumed that the meson field $\varphi_\alpha(\mathbf{r})$ deviates only slightly from the self-consistent field $\varphi^{v}_{\alpha}(\mathbf{r})$, if the parameters ϑ, β, δ are suitably chosen. This assumption (39) is used for the calculation of the energy $H'(q)$. by the method of small perturbations [formula (43)] and for the transition from formula (65) to formula (66).

The omitted small quantities which are enumerated above will be taken into account as small perturbations in one of the later papers. Including these terms will enable us to estimate the accuracy of the theory and to derive criteria for its applicability. It will be shown that assumptions 2 and 3 are based on one and the same inequality: $g/\mu a \gg 1$. Here a is the effective radius of the nucleon, which is defined to be

$$a^{-1} = \iint u(\mathbf{r})\,\frac{1}{|\mathbf{r}-\mathbf{r}'|}\,u(\mathbf{r}')\,dV\,dV'.$$

The inequality we have given defines the case of strong coupling.

Translated by M. Hamermesh
56

SOVIET PHYSICS JETP VOLUME 3, NUMBER 2 SEPTEMBER, 1956

Investigation of Radioactive Decay Chains

V. S. SHPINEL' AND G. A. KUZNETSOVA
Moscow State University

J. Exptl. Theoret. Phys.(U.S.S.R.)**30**, 231-242 (February, 1956)
(Submitted to JETP editor October 11, 1954)

Using a β-spectrometer with two magnetic lenses and a γ-spectrometer with NaI (Tl) scintillator, an investigation of the following transitions has been carried out: $Zr^{97} \to Nb^{97} \to Mo^{97}$; $Ru^{97} \to Tc^{97}$; $Ru^{105} \to Rh^{105} \to Pd^{105}$; and $Ru^{103} \to Rh^{103}$. The results obtained are generally in agreement with published decay schemes with the exceptions that a sample of $Zr^{97} + Nb^{97}$ emits a β spectrum with $E_\beta \sim 0.48$ mev (intensity 15%) and low intensity hard γ-rays of 2.2 and 1.6 mev. The decay of Rh^{105} is accompanied by the emission of 0.08 mev γ-rays. The occurrence of corresponding β and γ transitions in odd nuclei differing by two neutrons is noted.

INTRODUCTION

IN a previous paper of one of the authors[1] certain regularities were noted in corresponding levels of selected nuclei with odd number of nucleons. To obtain further and more precise data on the excited states of these nuclei, we undertook a spectroscopic investigation of radioactive transitions in nuclei of mass number A=97, A=103 and A=105.

1. Zr^{97} AND Nb^{97}

PUBLISHED DATA

Investigation of the 17 hour Zr^{97} and 75 minute Nb^{97} activities has previously been carried out by absorption methods with the aid of a lens spectrometer, and by the method of β-γ coincidences.[2-4] Zr^{97}-Nb^{97} sources were obtained by slow neutron bombardment of either a natural isotopic mixture, or one enriched in Zr^{96}, or alternatively by chemical separation from the fission fragments of uranium. Measurements were made with a mixture of zirconium and niobium in radioactive equilibrium as well as with separated niobium. Spectrometer measurements[2] showed that Zr^{97} makes a β-transition to an isomeric level of Nb^{97m} with excitation energy E=0.747 ±0.005 mev, and subsequently decays to the ground state of Nb^{97} with a period of 60 seconds. The β-spectrum of Zr^{97} is simple, with an upper energy E_β =1.91 ±0.02 mev. Subsequently Nb^{97} decays by β emission, accompanied by γ-rays of energy E_γ = 0.665 ±0.02 mev. The maximum energy of the niobium β-spectrum is E_β= 1.267 ±0.02 mev.

Measurements of γ-energy by the absorption method (Ref. 3) show the existence of quanta with energy E_γ = 1.42 mev which the authors ascribe to Zr^{97}.

β AND γ SPECTRA OF Zr^{97} AND Nb^{97}

Powdered ZrO_2 was bombarded by slow neutrons; investigation of the induced radioactivity with the two lens β-spectrometer[5] began 9 hours after the end of bombardment. The first spectrum was taken with a disk shaped source, diameter 10mm and thickness 5 mg/cm^2. The source was mounted on a mica sheet of 6.3 mg / cm^2, and the counter window was celluloid of 0.5-0.7 mg / cm^2. Measurements were repeated three times in the course of four days. Intensity reduction of the spectrum has a characteristic half period of 17 hours, which is in good agreement with the known value for Zr^{97}. The observed β-spectrum is shown in Fig. 1. The two K-electron conversion lines give γ-ray energies $E_{\gamma 1}$ = 0.666 ±0.006 mev and $E_{\gamma 2}$ = 0.750 ±0.005 mev. The straightened β-spectrum (Kurie plot) in Fig. 2, shows the superposition of two spectra with limit energies $E_{\beta 1}$=1.90 ±0.025 mev and $E_{\beta 2}$=1.18 ±0.050 mev. These values are in satisfactory agreement with known values for the limit energies of Zr^{97} and Nb^{97} respectively. The experimental points on the Kurie plot show the presence of another soft β spectrum with limit energy $E_{\beta 3}$=0.48 mev. This value is close to the spectrum limit energy for Zr^{95} which could have been formed during the bombardment. Our measurements show that the intensity of this spectrum, obtained by subtraction of the harder spectra, diminishes with a period of the order of 20 hours. This shows

---

[1] V. S. Shpinel, J. Exptl. Theoret. Phys.(U.S.S.R.)224, 90 (1953).

[2] W. H. Burgus. Phys. Rev. **79**, 104 (1950).

[3] C. E. Mandeville et al., J. Frankl. Inst., **254**, 381 (1952).

[4] C. E. Mandeville et al., Phys. Rev. **86**, 813 (1952).

[5] V. S. Shpinel, J. Exptl. Theoret. Phys.(U.S.S.R.)**22**. 225 (1952).

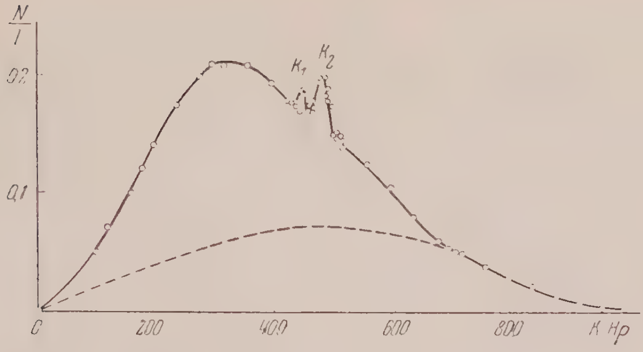

FIG. 1. Primary spectrum of Zr^{97} and Nb^{97} in radioactive equilibrium. K_1 --0.666 ±0.006 mev, K_2--0.750 ± 0.005 mev.

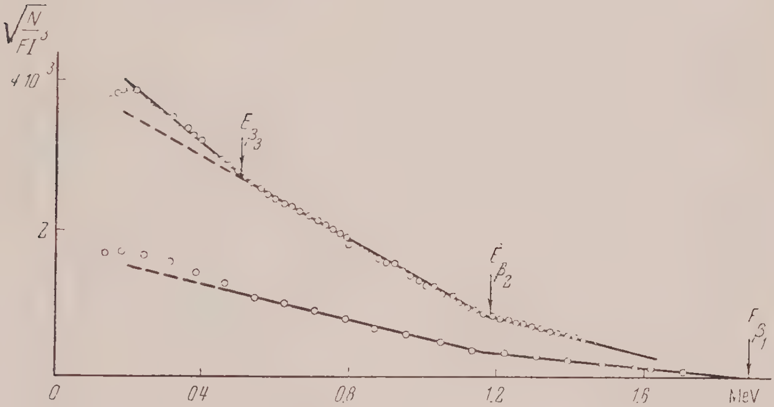

FIG. 2. Kurie plot for Zr^{97} and Nb^{97}. E_{β_1} —1.9±0.025 mev, E_{β_2} —1.18±±0.025 mev, E_{β_3} — 0.48 ± 0.05 mev

that it can not depend on Zr^{95}, and we have assigned it to Zr^{97} +Nb^{97}. The areas of the Zr^{97} and Nb^{97} β spectra are equal, within our accuracy, as would be expected for sources in radioactive equilibrium. The area of the $E_{\beta 3}$= 0.48 mev. β spectrum comprises 15% of the area of each of the above β spectra. From the ratios of the conversion peak areas from 0.666 and 0.75 mev γ-rays to the β-spectrum area, we have obtained the conversion coefficients (2.5 ±0.3) x 10^{-3} and (1.43 ± 0.17) x 10^{-2} respectively.

Control measurements of the initial Zr^{97} +Nb^{97} spectra were made with a source obtained by neutron irradiation of an enriched target, with 48% Zr^{96}. In this case also, a Kurie plot shows a soft β- spectrum, with an upper limit ≈ 0.5 mev. The source thickness in these measurements was 0.6 mg/cm^2.

To obtain the spectrum of secondary electrons (Fig. 3), active ZrO$_2$ powder was put into a brass container, inside diameter 10mm and height 8mm. The thickness of the front wall of the container, in which the initial β-spectrum was absorbed, was 1.3 mm. The lead converter had a thickness of 49.3 mg/cm^2 and a diameter of 10 mm. The observed photoelectron lines give the following γ-ray energies (with correction for absorption in the converter) : 0.662 ± 0.006 mev and 0.742 ± 0.007 mev, which are in good agreement with the conversion data.

The γ-spectrum of this source taken with a NaI (Tl) scintillation spectrometer is shown in Fig. 4. Besides the photoelectron peak associated with the 0.664 ± 0.746 mev γ-ray lines, a hard γ-spectrum ending at about 2.2 mev was observed. Detailed examination of the hard γ-spectrum, carried out by N. N. Deliagin, showed two rays of energies 2.2 and 1.6 mev, if the observed maxima on the spectrum are assumed to be caused by photoelectrons.

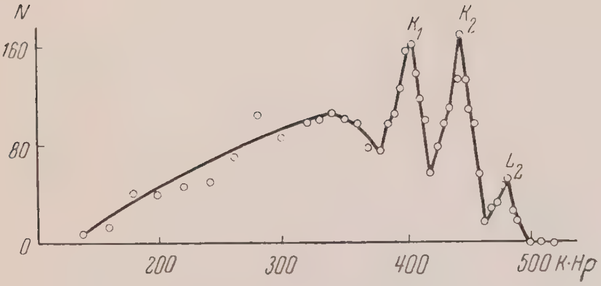

FIG. 3. Photoelectron spectrum Zr^{97} and Nb^{97} K_1 — 0.662, K_2 and L_2 — 0.742 mev

2. Ru^{97}, Ru^{103}, AND Ru^{105}

When a natural isotopic mixture of ruthenium isotopes is irradiated by slow neutrons, the radioactive isotopes Ru^{97}, Ru^{103} and Ru^{105} are produced, In this section we give results of measurements performed with these isotopes.

PUBLISHED DATA

Ru^{97}. The radiation of Ru^{97} was first investigated by the absorption technique in Ref. 6. It was determined that Ru^{97}, obtained by slow neutron bombardment, decays by K-capture with a period of 2.8 days. This decay is accompanied by a γ-ray of energy 0.23 mev. The observed weak electron emission with energy 0.097 mev was assigned to the daughter isotope Tc^{97} with period of 90 days[7]. In Ref. 8 Ru^{97} was obtained by ∝-bombardment of Mo^{94}, and subsequent electromagnetic enrichment to 75%. In Ref. 9 a Ru^{97} ∝-ray energy $E_\gamma = 0.217$ mev was found. Photoelectrons were observed in a lens spectrometer, using a slow neutron irradiated ruthenium source. The observed photoelectron line was quite weak compared to the background of γ-radiation due to Ru^{103}.

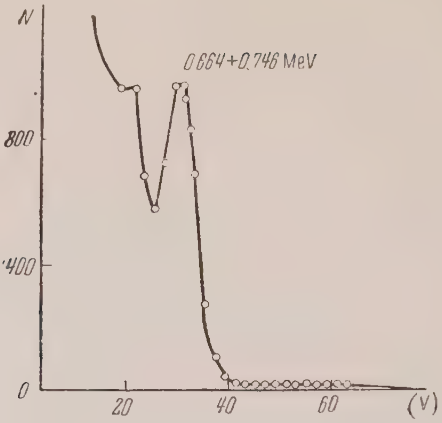

FIG. 4. γ-spectrum of $Zr^{97} + Nb^{97}$ observed with the scintillation spectrometer.

Ru^{103}. The radiations of 42 day Ru^{103} [10,11] have been investigated by several authors. In a number of cases the results are in poor agreement with each other. The first measurements were made with the absorption technique[12]. Ref. 13 made use of a magnetic lens spectrometer with 4% resolution. The decay scheme of Ru^{103} was first given in Ref. 14, in which absorption and coincidence methods were used. More accurate spectroscopic measurements were carried out in Refs. 15, 16. The most accurate measurements of conversion electron energies were made with a 180° focussing β-spectrometer and photographic detection[17].

The above named papers determine the existence of two β-transitions and two γ-transitions; the energies found by various authors are given in Table 1. Besides these radiations, reference 17 observed γ-rays of 0.0529, 0.295, and 0.610 mev. The discovery of the 0.610 mev γ-ray allowed the authors to assume the existence of a third β-transition with limit energy $E_\beta = 0.137$ mev.

---

[6] W. H. Sullivan, N. R. Slight and E. M. Gladrow, Phys. Rev. **70**, 778 (1946).

[7] B. N. Cacciopuoti and E. Segre, Phys. Rev. **52**, 1252 (1937).

[8] D. T. Eggen and M. L. Pool, Phys. Rev. **74**, 57 (1948).

[9] T. Y. Mei, C. M. Huddleston and A.C. G. Mitchell, Phys. Rev. **79**, 429 (1950).

[10] T. J. Livingood, Phys. Rev. **50**, 425 (1936).

[11] W. H. Sullivan, N. R. Slight and E. M. Gladrow, Phys. Rev. **70**,778 (1946).

[12] E. Bohr and N. Hole, Arkiv. f. Mat. Astr. o. Fysik. **32A**, No. 15 (1945).

[13] N. Hole, Arkiv f. Mat. Astr. o. Fysik. **36A**, No. 2, (1948).

[14] C. Mandeville and E. Shapiro, Phys. Rev. **77**, 439 (1950).

[15] F. Kondiah, Arkiv f. Fysik **4**, 81 (1952).

[16] T.Y. Mei, C. M. Huddleston and A. C. G. Mitchell, Phys. Rev. **79**, 429 (1950).

[17] J. M. Cork, T. Le Blanc, E. Stumpf and W. Nester, Phys. Rev. **86**, 575 (1952).

TABLE 1.

Reference	[10]	[11]	[12]	[13]	[14]	[15]	[16]
Half life (days)	42	41	—	—	39,8	43	—
Energy (mev)							
β_1	0.200	—	0,350	0,150	0,217	0.204	—
β_2	0.800	0.750	0,665	0,680	0,698	0.648	—
γ_1	—	—	—	—	0,040	0,0404	0,0396
γ_2	0,530	0.400	0,312	0,520	0,498	0,494	0,4985

Two conversion lines at 0.215 and 0. 290 mev were observed in reference 13. According to the decay schemes proposed in Refs. 15, 16, the soft β-spectrum is accompanied by a cascade of γ-transitions of 0.495 and 0.040 mev, while the hard γ-spectrum corresponds to a transition to the 0.040 mev level. The decay scheme assumed in Ref. 17 differs from the above in that the hard β-spectrum is connected with a transition to a third level at 0. 0529 mev.

Ru^{105}. Early investigations of the chain $Ru^{105} \rightarrow Rh^{105} \rightarrow Pd^{105}$ were carried out by the absorption method [12, 18]. More exact data on the β and γ radiation were obtained by using a lens spectrometer with resolution of 3 and 6%.[19] This work showed that the β-spectrum of Ru^{105} was simple, with a limit energy 1.15 mev. The excited state of Rh^{105} arising from the β-decay of ruthenium decays to a metastable level of energy ~0.1 mev (45 sec) through the emission of a 0.726 mev γ-ray of low multipolarity.

Rh^{105}(36 hour.) in its ground state emits electrons with maximum energy 0.570 mev, and goes to the ground state of Pd^{105}. In Ref. 20 Rh^{105} was found to emit a β-spectrum with intensity of 10% and upper limit of energy of 0.26 mev, a 0.322 mev γ-ray, and weak γ-rays of 0.157 and 0.080 mev.

β AND γ SPECTRA

Measurements on ruthenium were made with a lens spectrometer under conditions analogous to those in Sec. 2. The initial measurements were made with neutron irradiated metallic ruthenium powder and showed background radiation originating in an admixture of iridium. Subsequently, chemical separation of the ruthenium was used*. The metallic ruthenium was melted with alkali, became rutanate ($H_2RuO_4 + K_2RuO_3$), and subsequently was made into the salt ($RuCl_3 + RuCl_4$). The mixture obtained was volatilized in the form RuO_4 and absorbed by a weak solution of hydrochloric acid saturated with hydrogen sulfide gas. As a result we obtained a pure powder of $RuCl_3$, which was again irradiated by slow neutrons. The spectroscopic investigation of this sample was repeated several times in the course of more than a month.

The photoelectron spectrum, from a source of the same geometry as in the zirconium measurements, is shown in Fig. 5 (thickness of the lead converter 28 mg/ cm^2). Curves 1, 2, and 3 correspond respectively to measurements made 6 hours, 26 hours, and 8 days after irradiation. A further three measurements, made after 3 days and 40 days, are not shown on Fig. 5.

The energy of γ-lines and their periods, obtained from changes in intensity, are shown in Table 2. From this data it is possible to assign each line to the isotope listed in the 6th column.

This γ-radiation was also investigated with the scintillation spectrometer. Two series of measurements were taken using two ruthenium sources that differed by the length of neutron bombardment. The first series of measurements was made with a source that had been bombarded 4 hours; the second series, with the aim of increasing the 36 hour Rh^{105} intensity, was made with a 10 hour bombarded source. The first measurements were taken 4 hours after the end of bombardment, and in the next 70 hours, the spectrum was taken 8 times. In the second series measurements were begun 5

---

[18] H. T. Born and W. Sulmann-Eggebert, Naturwissen. 31, 420 (1943).

[19] R. B. Duffield and L. M. Langer, Phys. Rev., 81, 203 (1951).

[20] G. E. Boyd, Phys. Rev. 86 , 578 (1952).

---

* We would like to take the opportunity to express our thanks to H. P. Rudenko, in whose laboratory the necessary chemical separations were carried out.

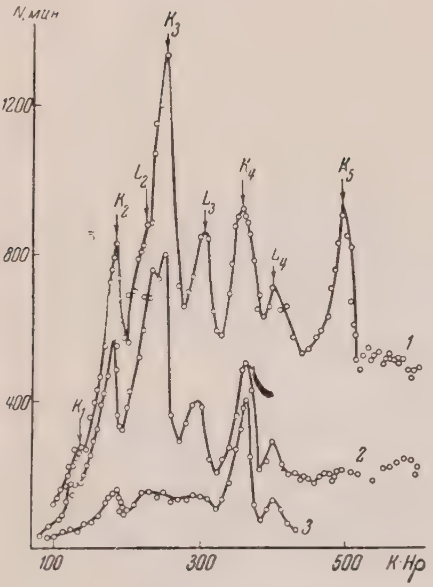

FIG. 5. Photoelectron spectrum taken with a source produced by slow neutron bombardment of ruthenium. Curves *1*, *2*, and *3* correspond to measurements taken 6 hrs., 26 hrs., and 9 days respectively after the end of bombardment. K_2 and L_2 --0.219 mev (Ru^{97}, 68 hrs.); K_3 and L_3 --0.320 mev (Ru^{105}, 36 hrs.); K_4 and L_4 --0. 497 mev (Ru^{103}, 42 days); K_5 --0.728 mev (Ru^{105}, 4.2 hrs.).

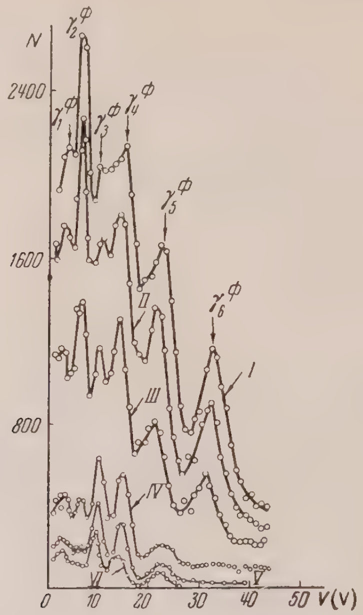

FIG. 6. Spectrum for a ruthenium source bombarded by slow neutrons. Curves *I*, *II*, *III*, *IV*, *V*, and *VI* were taken 4, 7, 9, 27, 36, and 56 hours after the bombardment respectively. γ_1^Φ — 0.08; γ_2^Φ — 0.133; γ_3^Φ — 0.22; γ_4^Φ — 0.33; γ_5^Φ — 0.5; γ_6^Φ — 0.74 mev

TABLE 2.

Line	Photo-electron energy (mev)	Absorption corrections in converter (kev)	γ-ray energy (mev)	Half life	Isotope
K_1	0.067	9	0,164 ?	—	Rh^{105}
K_2	0.124	7	0,219±0,004	68 hrs.	Ru^{97}
L_2	0.187	7	0.220±0,004	68 „	—
K_3	0.226	6	0,320±0,006	36 „	Rh^{105}
L_3	0.298	6	0,320±0,006	36 „	—
K_4	0,403	6	0.497±0,004	—	—
L_4	0,478	6	0,500±0,004	42 days	Ru^{103}
K_5	0,636	6	0.728±0,004	4,2 hrs.	Ru^{105}

hours after bombardment, and the spectrum was taken 8 more times in the course of 140 hours.

The spectra obtained in the first series of measurements are shown in Fig. 6. The γ-ray energies on Fig. 6 as well as the decay period obtained from a decay curve for each line are in good agreement with the results obtained from the magnetic spectrometer measurements. Furthermore, on this spectrum we clearly observe a γ-line at 0.133 mev, as well as a weak line at 0.08 mev; these lines did not appear on the spectrum of Fig. 5. The 0.5 mev γ-line decays with two periods, of ~ 4 hours and of the order of tens of days, which allows us to consider the line as complex. One of these lines must be dependent on photoelectrons from the known 0.496 mev γ-line of 42 day Ru^{103}, while the short period line must be due to Ru^{105}. Since the γ-spectrum of Ru^{105} taken with the magnetic spectrometer does not show a line near 0.5 mev, we may associate the short period component with

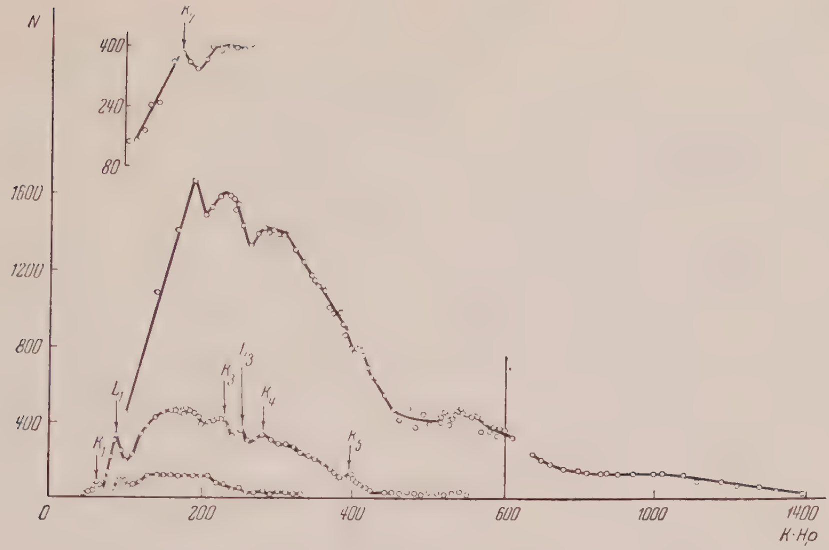

FIG. 7. Primary spectrum of a source obtained by slow neutron bombardment of ruthenium. Each curve was taken at a different time. K_1 and L_1 --0.04 mev (Ru^{103}); K_2--0.133 mev (Ru^{105*}); K_3 and L_3 --0.216 mev (Ru^{97}); K_4--0.311 mev (Ru^{105}); K_5--0.492 mev (Ru^{103}).

TABLE 3.

Line	electron energy (mev)	γ-ray energy (mev)	Isotope
K_1	0.019	0.041	—
L_1	0.035	0.038±0.002	Ru^{103}
K_2	0.110	0.133±0.010	$Rh^{105}m$
K_3	0.194	0.216±0.011	Ru^{97}
L_3	0.217	0.220	—
K_4	0 288	0 311±0.010	Rh^{105}
K_5	0.470	0.492±0.009	Ru^{103}

Compton electrons from the 0.74 mev Ru^{105} line, which must give a maximum superimposed on the position of the 0.5 mev photoelectron line. Figures 5 and 6 show spectra taken with a source which emitted an additional hard γ-radiation. Repetition after chemical purification showed no hard γ-radiation, which had presumably been caused by an admixture of Na^{24}.

The β-spectrum source was made from activated $RuCl_2$ powder mixed in a weak zapon lacquer solution, and deposited on a cellophane backing (6.3 mg/cm^2). Source thickness was 2 mg/cm^2 with an 8 mm diameter. Figure 7 shows the results of several series of measurements of the primary spectrum carried out at various times. Energies of the observed conversion lines and corresponding γ-rays are given in Table 3. These results agree, within the experimental errors, with those obtained from photoelectrons.

Figure 8 gives a Kurie plot of this data; the upper limit energies and decay periods are shown in Table 4. The third column of this table shows the isotopes to which the observed β-spectra are assigned.

We have assigned the hard β-spectrum E_β= 2.72 mev to a contamination of our source by manganese during the chemical purification. Repetition of purification reduced the intensity of this

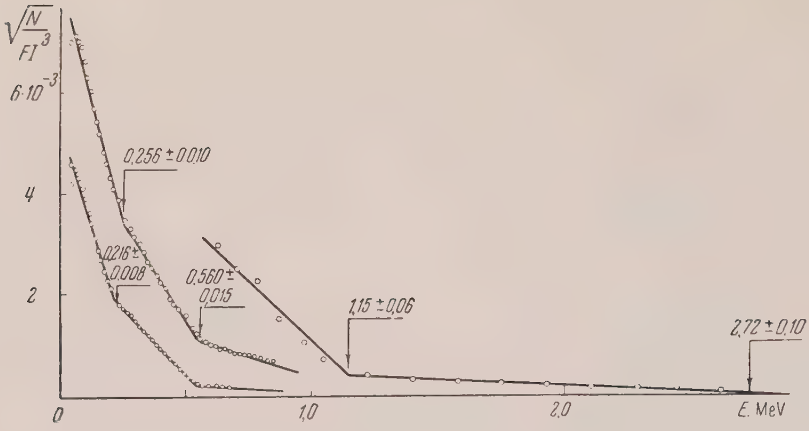

FIG. 8. Kurie plot for the curves shown in Fig. 7.

TABLE 4.

Upper spectrum limit (mev)	Observed period	Isotope
0.216±0.008	—	Ru^{103}
0.256±0.010	—	Rh^{105}
0.560±0.015	33 hrs.	Rh^{105}
1.150±0.020	4.5 hrs.	Ru^{105}

spectrum from a value of 15% to 6% (of the β-spectrum with E_β= 1.15 mev). The decay period of the hard β-spectrum in the vicinity of E > mev is ~ 2.5 hours, which corresponds to the known period of Mn^{56}--2.57 hours. The period of the hard spectrum in the region E < 2 mev is ~ 3.5 hours, and may be caused by a Ru^{105} β-spectrum with upper limit E_β ~ 2 mev, and an intensity not exceeding a few percent. It was, however, impossible to make this assignment definite because of the remaining admixture of manganese.

For the γ-transition at 0.496 mev assigned to Ru^{103}, the conversion coefficient was obtained from the ratio of the conversion peak area to that of the continuous β-spectrum. We obtained N_e/N_β ~ 0. 6%. Comparison of this result to theory shows that the transition is $E\,2$, although the possibility of $M1$ cannot definitely be excluded.

3. DECAY SCHEMES

A) THE SELECTED A =97 FAMILY

The data we have obtained on the radioactive transitions Zr^{97}→Nb^{97}→Mo^{97} are in agreement with the decay scheme shown in Fig. 9. The data from the Ru^{97}→Tc^{97} transition shows that Tc^{97} has a level 0.219 mev above the known 0.097 isomeric level. The isomeric transitions 0.750 mev in Nb^{97} and 0.097 in Tc^{97} are usually considered as $M4$ transitions between $p_{1/2}$ and $g_{9/2}$ states.[21] Such a γ-transition follows in particular from our measured value for the conversion coefficient for 0.75 mev γ-rays. Our value of the conversion coefficient for the 0.666 mev γ-transitions implies an electric quadrupole transition $E\,2$.

The value of lg τf for the β-transition Nb^{97}→ Mo^{97} with E_β = 1.18 mev is 5.51; consequently this may be considered a first order forbidden transition. For the β-transition (E_β=1.9 mev) the value of lg τf is 7.4, and apparently this is a 2nd or 3rd order forbidden transition.[22] If we assume that the ground state of Mo^{97} is $d_{5/2}$[22], then the above data on β and γ transitions allows the probable assignment of quantum states as shown in Fig. 9.

Ru^{103}. The results of the present investigation, as well as the observations of H. V. Forafontov on β-γ coincidences, can be arranged in the decay scheme (Fig. 10) proposed in [9,15] and improved in [17]. Reference 15 makes the ground state assignment 7/2 + and a $p_{1/2}$ isomeric state for Rh^{103}. However measurements of the spin and magnetic moment show that the ground state of stable Rh^{103} is $p_{1/2}$. It follows that the isomeric state should be assigned 7/2 + . Since the 0.496 γ-transition is $E\,2$, the upper excited state of Rh^{103} may be assigned 3/2 +.

---

[21] M. Goldhaber and A. W. Sunyar, Phys. Rev. 83, 906 (1951).

[22] B. S. Dzhelepov and A.V. Kurdiavtseva, J. Exptl. Theoret. Phys.(U.S.S.R.)19, 761 (1949).

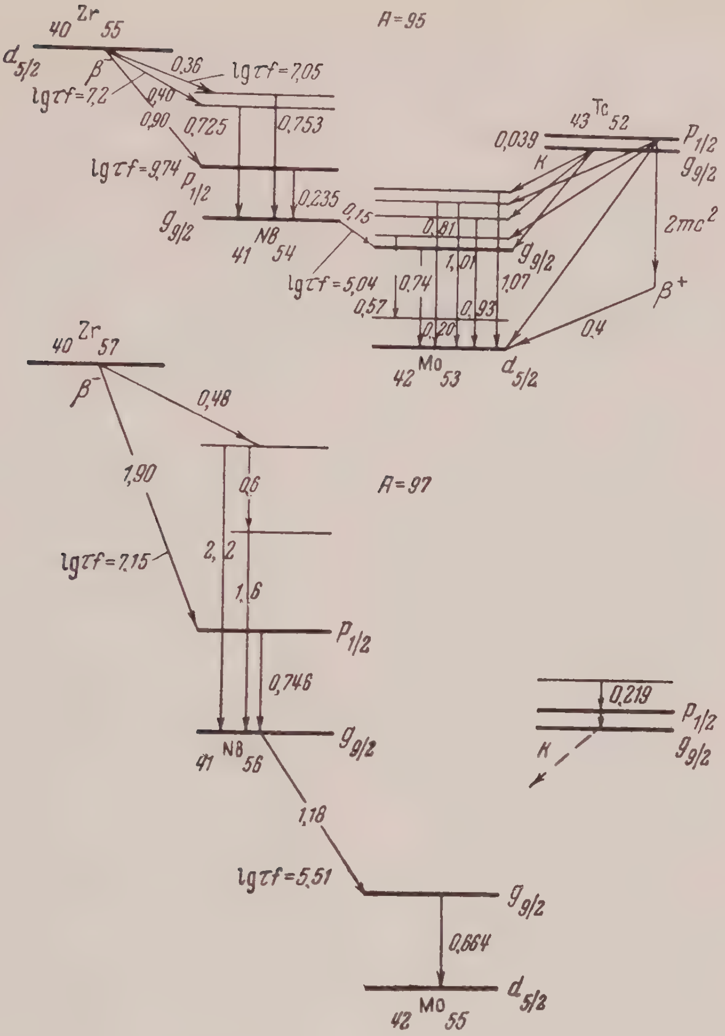

FIG. 9. Decay schemes for the selected families with A=95 and A=97. Corresponding levels for isotopes differing by two neutrons are indicated as thick lines.**

B) THE SELECTED A= 105 FAMILY

Our data on the decay chain $Ru^{105} \to Rh^{105} \to Pd^{105}$ show that the decay scheme (Fig. 10) proposed in Ref. 23 is essentially correct. However this scheme does not contain the low intensity γ transitions of 0.08 and ~ 0.160 mev, which were observed both in Ref. 20 and by us. The isomeric 0.133 mev transition in Rh^{105} has been identified as $E\,3$[21].

**Note added in proof.* After the submission of this article, A. A. Sorokin and N. V. Forafontov carried out measurements on β--γ and γ--γ coincidences for $Zr^{97}+Nb^{97}$. The measurements of β--γ coincidences were made with out β-spectrometer and scintillation γ-spectrometer connected to a coincidence circuit. This allowed the identification of the partial β-spectrum with E_β=0.45 mev and correlated with hard γ-rays. For this β-transition lg τf=5.4. Measurements of γ--γ coincidences were made with two NaI (Tl) γ-spectrometers connected to a coincidence circuit. These showed the existence of a γ-cascade with energies 1.5 mev. and 0.6-0.8 mev, with intensity 7-10% of the total number of Zr^{97} decays. With a Nb^{97} source, chemically separated from Zr^{97} γ--γ coincidences were not observed. The data obtained is in agreement with the decay scheme shown in Fig. 9.

[23] M. Goldhaber and R. D. Hill, Revs. Mod. Phys. **24**, 179 (1952).

4. DISCUSSION

It is interesting to compare the β and γ transitions observed in the selected A=97 family with the corresponding transitions for the family with A=95.[24-26] The scheme of these transitions is shown in Fig. 9.

We first note that the excited states of 0.664 mev in Mo^{97} and 0.740 mev in Mo^{95} differ little in energy, and that in both cases the corresponding γ-transition is $E2$. The β transitions Nb^{97} → Mo^{97} and Nb^{95} → Mo^{95} have similar values of lg τf, 5.41 and 5.04 respectively. The isomeric transitions in Nb^{97} (0.746 mev) and in Nb^{95} (0.235 mev), although differing in energy, are both $M4$. Similarly the isomeric transitions for Tc^{97} and Tc^{95} are $M4$. The transition from the ground state of Zr^{97} to the isomeric level of Nb^{97} with an upper energy limit 1.90 mev and lg τf = 7.4, can be compared to the partial β transition from the ground state of Zr^{95} to the isomeric state of Nb^{95}. The value of lg τf for this β transition with upper energy limit ~ 1 mev is 9.74. This differs significantly from the value given for Zr^{97}.

The above comparison indicates that the addition of two neutrons to a nucleus, in the examined odd nuclei, makes only small changes in some nuclear states and in the correeponding radioactive transitions. This situation is quite natural in the case of single particle states of the same shell. From this point of view it seems probable that the soft β spectrum which we observed with a Zr^{97}+Nb^{97} source is caused by one or two additional β transitions in Zr^{97}, corresponding to the β transitions of Zr^{95}. The existence of a soft β spectrum for Zr^{97} is in agreement with the observation of hard γ-radiation.

Let us note that the energies of the analogous transitions are not identical for the two selected families. Furthermore certain energy levels found in Mo^{95} have not yet been seen in Mo^{97}. This may possibly be explained by assuming that in the latter nucleus certain states may not be excited because the energy levels have been shifted, and consequently certain transitions have become impossible. The displacement of energy levels between two isotopes differing by two neutrons must depend, at least partly, on the change of coulomb energy due to the increase of average distance between protons

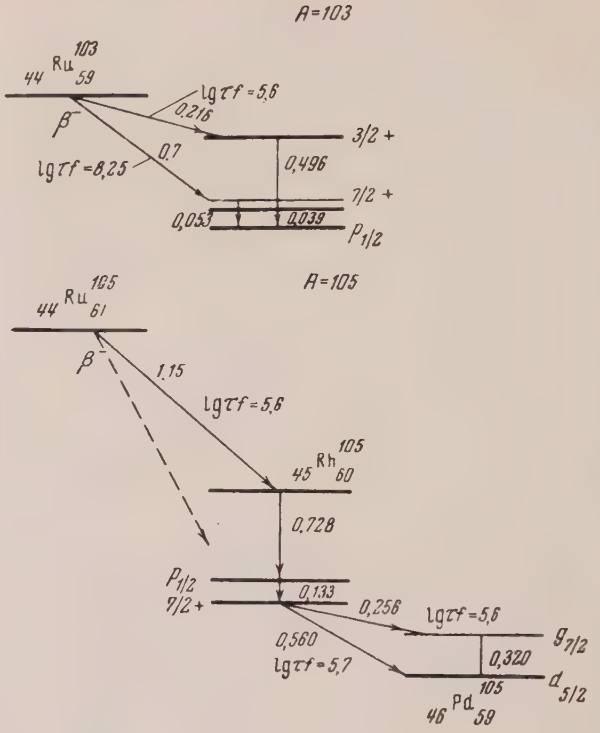

FIG. 10. Decay schemes of Ru^{103} and Ru^{105}; corresponding levels are indicated by thick lines.

From the above considerations, the decay schemes of Ru^{103} and Ru^{105}, shown in Fig. 10, must also be similar. Indeed both cases show transitions with the same lg τf = 5.6.

The isomeric transitions of both nuclei (0.039 and 0.133 mev) are $E3$. However, the assumption that the ground and isomeric states of these nuclei have respectively the same configuration does not agree with the nature of the β transition Rh^{105} → Pd^{105}.

We must therefore assume that the configurations of the isomeric and ground states of Rh^{105} are reversed. i.e., a $p_{1/2}$ isomeric state and a 7/2 + ground state. The existence of a low intensity hard β-spectrum for lg τf = 8.25 in Ru^{103} allows the prediction of a hard β-spectrum for Ru^{105}.

Analogous regularities are observed if two neutrons in a nucleus are replaced by two protons.[1]

In conclusion we would like to thank H. V. Forafontov and Ia. I. Gaziev who carried out a series of control measurements.

---

[24] V. S. Shpinel, J. Exptl. Theoret. Phys.(U.S.S.R.)21, 1370, (1951).

[25] H. Slätis and L. Zappa, Arkiv f. Fysik 6, 81 (1953).

[26] J. M. Cork, T. Le Blanc et al, Phys. Rev. 90, 579 (1953).

Translated by G. L. Gerstein
44

SOVIET PHYSICS JETP VOLUME 3, NUMBER 2 SEPTEMBER, 1956

Dependence of the Dielectric Strength of Some Alkali Halide Monocrystals on the Duration of the Applied Voltage

G. A. VOROB'EV

Polytechnic Institute of Tomsk

(Submitted to JETP editor January 12, 1955)
J. Exptl. Theoret. Phys. (U.S.S.R.) 30, 256-261, (February, 1956)

Dependence of the dielectric strength of monocrystals of NaCl, KCl, KBr and KI on the duration of the applied voltage was studied experimentally. The effects of the formation and rate of growth of the discharge in the dielectric are studied. The assumption is made that the increase in the breakdown potential when the duration of the applied voltage is of the order of 10^{-5} sec relative to the breakdown potentials for voltages of shorter duration is caused by the ionic volume charge. When pulses are used, a proportionality is observed between the dielectric strength and the energy of the crystal lattice. Experimental data and oscillograms point to the existence of two stages in the breakdown process of the investigated dielectrics.

The dependence of the dielectric strength of solid dielectrics on the duration of the applied voltage has not been investigated very much. There are indications[1] that a time interval of 3×10^{-8} sec is sufficient for the development of the breakdown in solid dielectrics.

Valter and Inge[2] found in connection with the study of breakdown of glass in a uniform field that the dielectric strength is independent of the duration of the applied voltage within the limits of 10^{-7} sec and 1 sec.

Dittert,[3] using uniform fields for the breakdown, found an independence of the dielectric strength of paper base bakelite and ebonite on the duration of applied voltage in the interval from 10^{-8} to 10^{-1} sec.

Vorob'ev and Valter[4] observed an increase in the dielectric strength of porcelain in the field of a hemisphere against a plane surface with the decrease of the duration of applied voltage. With a pulse duration of 4 μ sec, the coefficient of the impulse was 1.33, and with a pulse duration of 3500 μ sec, 1.02 Such a dependence is apparently due to the influence of the porosity of porcelain.

Hippel and Alger[5] investigated the dependence of the dielectric strength of monocrystals of KBr on the duration of the applied voltage. For breakdowns with constant voltages or with pulses which persist up to the time of breakdown and are not less than 10^{-4} sec in duration, the dielectric strength was constant. With the decrease of the prebreakdown time, beginning with 10^{-4} sec, the dielectric strength decreases. At a duration of 5×10^{-5} sec the dielectric strength reaches a minimum (the decrease constitutes 12%), then increases and reaches the initial value at 10^{-6} sec. For the prebreakdown time of 1.7×10^{-8} sec, the dielectric strength is higher than for the constant field by 33%.

The dependence of dielectric strength on the duration of the applied voltage is important for the development of the theory of the breakdown. The information permits the evaluation of the rate of the processes involved in the breakdown and of the role of the various factors in the breakdown process. The insufficient and indefinite nature of existing data on the time dependence of the dielectric strength of solid dielectrics and the importance of this question prompted a systematic study in this field.

We have conducted an investigation of the time dependence of the electric strength of monocrystals of NaCl, KCl, KBr and KI. The monocrystals KCl, KBr and KI were grown from melts; rock salt was used in its natural state. Samples used in the experiments included machined spherical surfaces 8 mm in diameter. The thickness of the samples at the thinnest place, where the breakdown occurred, was $150 \pm 10 \mu$. The spherically shaped portion and the opposite side were covered with tin by evaporation in a vacuum.

The breakdown of the samples was carried out in transformer oil. The amplitude of the applied voltage pulse was selected to be greater than the dielectric strength of the samples in order to produce the breakdown on the first rise of the applied pulse. To obtain a change in the order of magnitude of the time before the breakdown, the length of the wave front was changed. In parallel with the sample under test, there was included a voltage divider, a portion of which supplied voltage to the plates of the cathode ray oscillograph. The displacement of the electron beam along the vertical and horizontal axes was calibrated. The accuracy of measuring the breakdown voltage was 5%.

---

[1] A. P. Aleksandrov et al., *Physics of Dielectrics*, GTTI, 1932.

[2] A. F. Valter and L. D. Inge, J. Tech. Phys. USSR 6, 3 (1929).

[3] Dittert, Dissertation, Dresden, 1930.

[4] A. A. Vorob'ev and A. F. Valter, Transactions (Trudy) of Soviet Conference on Electrical Insulating Materials 3, 1934.

[5] A. Von Hippel and R. S. Alger, Phys. Rev. 76, 127 (1949).

In Fig. 1 is shown a photograph of the oscillogram of a breakdown of NaCl for a time interval before the breakdown of 13 x 10^{-8} sec. For every time interval before the breakdown, and for each of the investigated dielectrics, we have obtained from 12 to 39 points. Figure 2 represents the dependence of the dielectric strength of KBr on the application time of the voltage. Figure 3 shows the statistically treated dependence of the dielectric strength of KI on the duration of applied voltage and Fig.4, curves of dependence of the dielectric strength of all the crystals investigated by us on the duration of the applied voltage for a probability of breakdown ψ=90%.

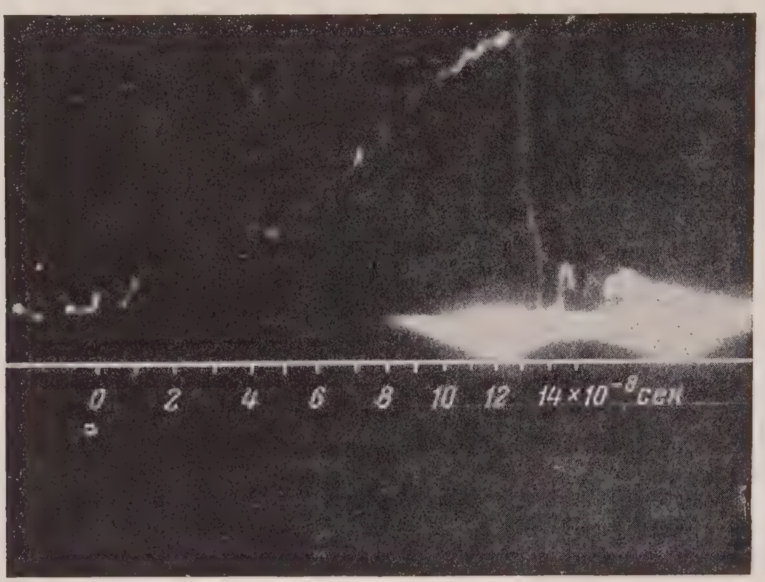

FIG. 1. Oscillogram of a Breakdown of NaCl

For all the investigated dielectrics, there was observed a considerable increase of dielectric strength at voltage duration of 6 to 9 x 10^{-8} sec, compared to the dielectric strength for longer duration of the applied voltage. For all the four salts, we have also obtained a somewhat greater dielectric strength for application times of the order of 10^{-5} sec, compared to that for application time of the order of 10^{-7} to 10^{-6} sec.

The increase in the dielectric strength of the investigated monocrystals for application time of 6 to 9 x 10^{-8} sec, is probably due to the delay in the discharge. The discharge time in solid dielectrics is practically equal to the time of discharge formation, since in a solid dielectric there always exists a certain number of free electrons. Experimental results are shown in Fig. 4 and the oscillograms permit the evaluation of the time of discharge formation. The times of discharge formation were determined from the oscillograms as shown in Fig. 5; E_t is the breakdown voltage for an application time of 6 to 9 x 10^{-8} sec; E_0 is the breakdown voltage for an application time for which no delay in the discharge is yet observed (in this case E_0 was taken as the breakdown voltage for an application time of the order of 10^{-7} to 10^{-6} sec); t_f is the time of charge formation which is to be determined. The curve of variation in the electric field strength with time was obtained from the oscillogram. Thereby it was considered that the formation of the discharge begins when the field strength in the dielectric reaches the breakdown value for the application time of the order of $10^{-7}$to 10^{-6} sec.

The values of t_f obtained and also the values of E_t/E_0 and the mean velocity of the propagation of the discharge v for all the investigated dielectrics are given in the table. The data refer to a probability of breakdown $\psi = 90\%$.

Investigated dielectrics	NaCl	KCl	KBr	KI
E_t / E_0	1.27	1.3	1.55	1.57
t_f, 10^{-8} sec	1.7	1.6	2.2	2.1
V, 10^6 cm/sec	0.88	0.94	0.68	0.72

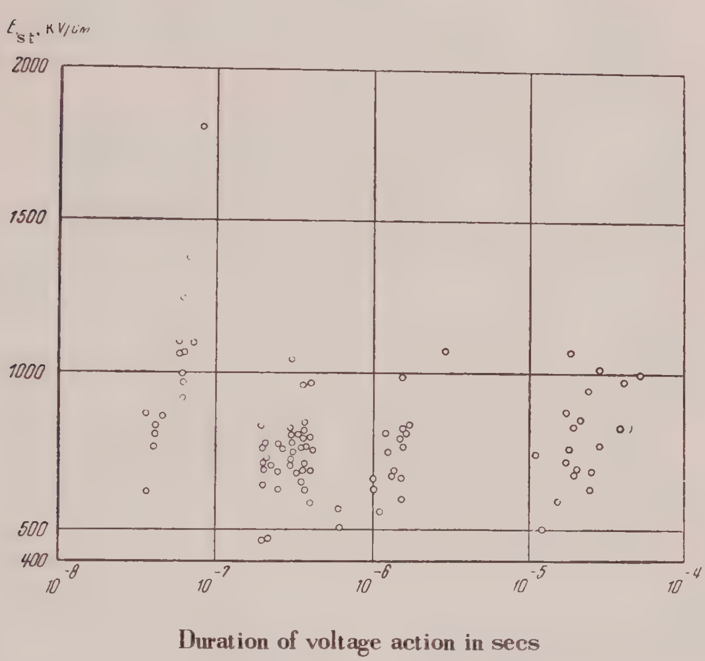

FIG. 2. Dependence of the dielectric strength of monocrystals KBr on the duration of voltage action for the case of uniform field.

For the voltage application time of 6 to 9 x 10^{-8} sec, 30 points were obtained for NaCl, 33 points for KCl, 16 points for KBr, and 12 points for KI.

The mean value of velocity of propagation of the discharge was computed according to the formula $V = d/t_f$ where $d = 0.15$ mm (the mean thickness of the samples at the breakdown point). The values of velocities obtained for the investigated solid dielectrics are a whole order of magnitude smaller than the velocities of propagation of electrons in air, while the field strength in the latter case is of the order of 10 times smaller. This can be explained by the fact that motion of electrons in a solid dielectric is considerably retarded by the high concentration of ions and their strong electrostatic influence upon the electrons.

As shown in Fig. 1, the time of the voltage drop at breakdown does not exceed 10^{-8} sec. We can refer to two stages of the breakdown in the investigated dielectrics. During the first stage of duration t the discharge is being formed. Conductivity during this stage is not high as indicated by the nonvarying form of the pulse. During the second stage, the conductivity rises very rapidly and the voltage across the sample drops.

Below are given values of the ratios E_t'/E_0 for the investigated monocrystals, where E_t' is the breakdown voltage for the duration of the order of 10^{-5} sec., and E_0 is the breakdown voltage for the duration of application of the order of 10^{-7}sec ($\psi = 90\%$)

	NaCl	KCl	KBr	KI
E_t' / E_0	1.13	1.18	1.11	1.01

We have also conducted experiments to determine the dielectric strength of rock salt for voltage pulses of duration of the order of 10^{-4} and 10^{-1} sec, and for constant voltages. The value of the dielectric strength for rock salt obtained in these experiments, within the limits of experimental error, turned out to be the same as for voltage durations of the order of 10^{-5} sec.

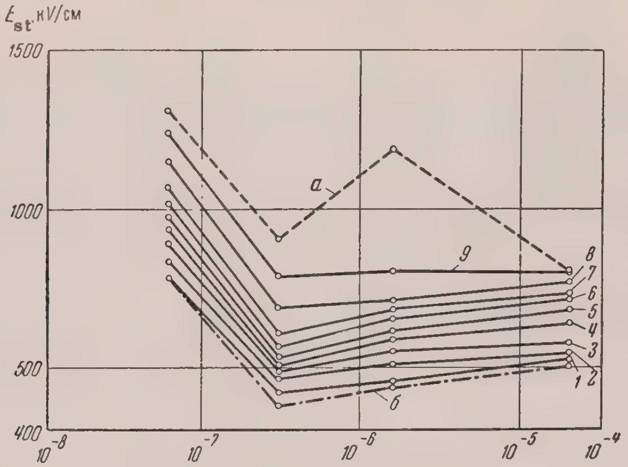

Duration of voltage action in secs

FIG. 3. Statistically treated dependence of the dielectric strength of monocrystals KI on the duration of voltage action for the case of uniform field: *a*-the boundary of maximum values; *б*-the boundary of minumum values; ψ is equal: *1*-10, *2*-20, *3*-30, *4*-40, *5*-50, *6*-60, *7*-70, *8*-80, *9*-90%.

Many investigators have obtained values for dielectric strength of solid dielectrics with constant voltages higher than with short pulses. The authors explain this fact by the action of volume charges. Thus Hippel and Alger[5] explain the increase in the dielectric strength of KBr for voltage duration of the order of 10^{-4} sec compared with shorter periods by the compensating effect of the negative volume charge formed by capture of electrons by the "knots" of the crystal lattice on the positive volume charge formed by

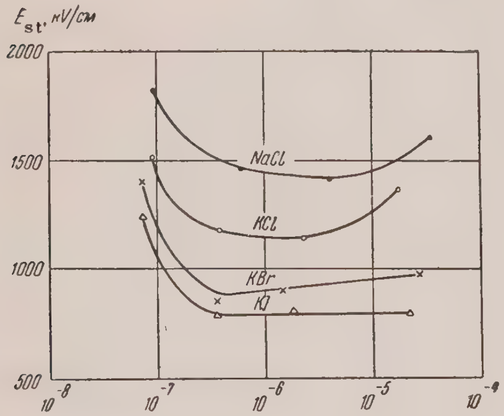

Duration of voltage action in secs

FIG. 4. Dependence of dielectric strength of monocrystals NaCl, KCl, KBr and KI on the duration of voltage action for the case of uniform field and for the probability of breakdown ψ = 90%.

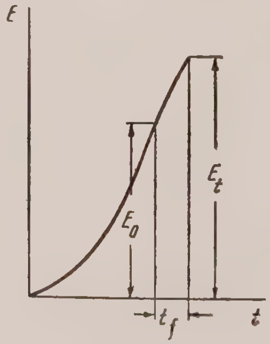

FIG. 5. A graph for the determination of the time of discharge formation.

the movement of positive ions. The negative volume charge by itself, according to these authors, lowers the breakdown voltage. Gochberg and Ioffe[6,7] consider that the volume charge produces in the dielectric a field opposite to the applied field. The mean voltage in the dielectric must thereby decrease and this, according to the authors, should lead to a rise in the dielectric strength of the dielectric. Fauler[8] supposes that the volume charge facilitates the removal of electrons from the cathode which should, according to Fauler's theory, lead to a lowering of the breakdown voltage. However, a lowering of the breakdown voltage with the increase of the duration of the applied voltage was observed only for calcite[9,10], where the volume charge is concentrated in the layers close to the electrodes.

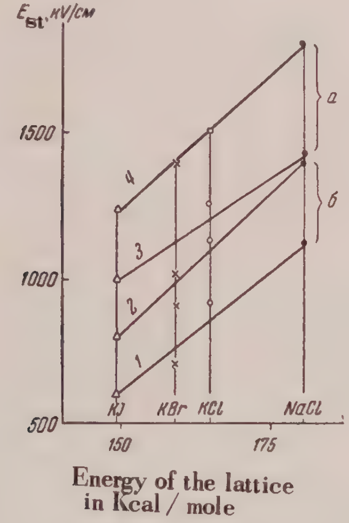

FIG. 6. Dependence of the dielectric strength on the energy of the lattice for NaCl, KCl, KBr and KI for breakdown with pulses. Duration of voltage application: *a*-order of 10^{-8} sec; *b*-order of 10^{-6} sec; ψ is equal: *1* and *3*-50%; *2* and *4*-90%.

The influence of volume charges is confirmed by the fact that the dielectric strength of solid dielectrics, in the case of simultaneous action of a steady and pulsed voltages of the same polarity, is greater than for the case of pulsed voltages alone.[11] The question arises: Is the time interval (of the order of 10^{-5} sec) sufficient for the formation of the volume charge? Is the rise in the breakdown voltage for application time of the order of 10^{-5} sec actually due to the influence of the volume charge? It is known that in air the mobility of ions is about a thousand times smaller than the mobility of electrons. If this relation is preserved in the investigated dielectrics, then, for an electron charge formation time of the order of 10^{-8} sec, the corresponding time required for the ions to move across the thickness of the dielectric is of the order of 10^{-5} sec, which is in agreement with our experiments.

In Fig. 6 there is shown the dependence of the dielectric strength of indicated crystals on the energy of the lattice for two different durations of applied voltage and for two values of probability of breakdown. The general type of this dependence agrees with what has been previously observed by Vorob'ev[12] for breakdown of crystals under constant voltage.

---

[6] V. M. Gochberg and A. F. Ioffe, J. Exptl. Theoret. Phys. (U.S.S.R.) 1, 264 (1931).

[7] A. F. Ioffe, *Physics of Crystals*, Gosizdat, 1929.

[8] K. Fauler, Proc. Roy. Soc., (London) 141 A, 56 (1933).

[9] A. M. Venderovich and A. A. Vorob'ev, Tr. Sib. FTI, 4, 15 (1936).

[10] E. K. Zavadovskaia, Izv. TPI 63, 136 (1944).

[11] E. K. Zavadovskaia, Izv. TPI 63, 127 (1944)

[12] A. A. Vorob'ev, J. Tech. Phys. USSR 12, 10, 183 (1940).

Translated by J. L. Herson
48

SOVIET PHYSICS JETP VOLUME 3, NUMBER 2 SEPTEMBER, 1956

Investigation of the Close-Pair Effect in Cosmic-Ray Stars by Means of Moving Photographic Plates

I. M. GRAMENITSKII, M. I. PODGORETSKII AND
IU. F. SHARAPOVA
P. N. Lebedev Physical Institute, Academy of Sciences, U.S.S.R.

(Submitted to JETP editor, February 7, 1955.)
J. Exptl. Theoret. Phys. (U.S.S.R.) 30, 277-281 (February, 1956)

The problem of simultaneity in the creation of close-pair stars has been studied by means of moving photographic plates. It is shown that the so-called "associated" stars are produced at different moments of time.

IT has been observed in a number of papers[1-11] that emulsions which have been exposed to cosmic rays contain a larger number of close-lying pairs ($r \ll 1$ mm) of nuclear disintegrations (stars) than is to be expected on the basis of a random spatial distribution. The excess of "close pairs" suggests a clue as to the origin of this effect. It is true, however, that this same effect can arise as a result of a number of experimental factors (cf. Refs. 3, 6, 9, 12) which cannot be evaluated quantitatively without a great deal of difficulty.

The question of whether a close-pair effect does, in fact, exist is therefore of great interest. An approach which would seem capable of resolving this question and which is free from the difficulties referred to above has been indicated in Ref. 10. It is assumed that the close-pair stars differ from stars which are accidently produced in close proximity in that the former are created simultaneously while the latter are created at different moments of time. Hence an investigation of simultaneity would appear to be crucial in the identification of true close-pair stars. In the present work this objective has been realized through the use of moving emulsions as proposed in Refs. 13 and 14.

1. Description of the Method

The work was performed with type *P* emulsions 100 μ in thickness mounted on glass plates with dimensions 58 x 86 (± 0.05) mm.

Two plates were superposed with the emulsions lying between them. A clockwork mechanism was used to move the lower plate with respect to the upper one with a velocity of 1 cm in 4 hours. The transverse displacement in this motion did not exceed 100 μ. After a total travel of $\sim$ 1 cm the clockwork mechanism was shut off automatically.

Consider a star produced while the instrument is in operation : if the star has prongs which extend to the surface of the plate, these prongs should have extensions in the other plate. If the distances between the points of egress of the prongs in one plate and the points of entry in the other plate are the same for two close-lying stars, then these stars have been created simultaneously. If this condition is not fulfilled, then the stars have been created at different times and consequently are not related.

The search for prong extensions in the second plate was performed in the following manner. The plates were placed together on the stage of the microscope in exactly the same position they occupied in the holder of the clockwork mechanism before it was set in operation. Both emulsions were scanned together; this is possible at small magnifications (7 x 10 x 1.5 or 7 x 20 x 1.5). When a star of interest was located one of the

---

[1] L. Leprince-Ringuet and J. Heidmann, Nature 161, 844 (1948).

[2] T. T. Li and D. H. Perkins, Nature 161, 844 (1948).

[3] T. T. Li, Phil. Mag. 41, 1152 (1950).

[4] M. M. Addario and S. Tamburino, Phys. Rev. 80, 749 (1950).

[5] Salant, Hornbostel and Dollman, Phys. Rev. 74, 649 (1948).

[6] Davis, Marion, Delord and King, Phys. Rev. 88, 368 (1952).

[7] F. B. Brown and A. V. Masket, Phys. Rev. 88, 1204 (1952).

[8] Barbanti Silva, Bonicini, Depietri, Lovera, Perelli and Fedeli, Nuovo cimento 9, 630 (1952).

[9] F. B. Brown and A. V. Masket, Phys. Rev. 91, 210 (1953) .

[10] I. M. Gramenitskii, G. S. Emel'ianov and M. I. Podgoretskii, J. Exptl. Theoret. Phys. (U.S.S.R.) 27, 654 (1954).

[11] DiCorato, LeviSetti, Panetti, Pinto and Milone, Nuovo cimento 12, 548 (1954).

[12] G. Davis, Phil. Mag. 43, 472 (1952).

[13] J. J. Lord and M. Schein, Phys. Rev. 80, 304 (1950).

[14] Zh. S. Takibaev, J. Exptl. Theoret. Phys. (U.S.S.R.) 24, 363 (1953).

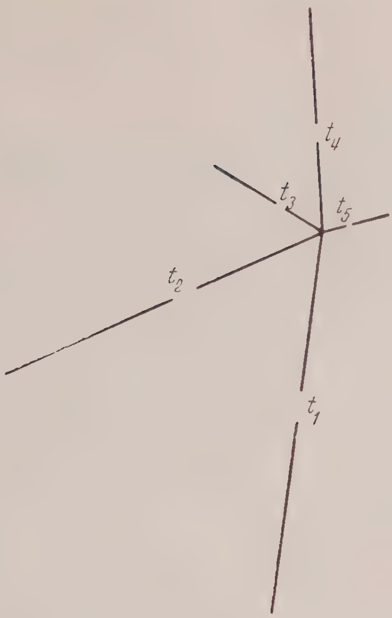

prongs which extended to the surface of the plate was moved to the center of the field in view. Then a strip 500 μ in width and 1 cm in length (in the direction of relative motion of the plates) in the other plate was scanned to find a track running in the same direction as the prong.

For the single-particle density which was observed (690 cm^{-2}) the probability of an accidental coincidence is small. If tracks which are true extensions are neglected, the scanned strip should contain $\sim$ 0.05 tracks running in the appropriate directions (in the plane of the emulsions and depthwise). The possibility of a false coincidence is reduced further if the ionization of the prong is compared with the ionization due to the extension in question. In the case of stars with several (2 or more) prongs which extend to the surface, chance coincidences are virtually impossible.

We now consider the resolving power (with respect to time) of this scheme. When a star has been selected and the extensions of its prongs located, then upon aligning the prongs with the extensions, a picture similar to that shown in the figure is observed. There is a gap t between each prong and its extension caused by the space d between the emulsions; the magnitude of d can be easily determined from the dip angles of the tracks and the gaps t.

We now consider two neighboring stars which might be considered simultaneous on the basis of a preliminary inspection. Having determined the magnitude of d at the site of the first star, it should be possible to predict the points of incidence of the tracks of the second star in the other plate if both stars have been produced simultaneously. The accuracy of this prediction is determined by the length of the track and possible variations in d in going from the site of one star to the other.* Under the conditions of the present experiment this prediction could be made with an accuracy of several (<10) microns corresponding to a resolving power of (10/10,000) x 240 ≈ 0.25 min.

2. Experimental Results

In 34 plates exposed at a height of 9 km, 2126 stars ** with prong-number $n \gtrsim 2$ were found. A strip 6 mm wide at the edge of the plates was not scanned since large distortions are possible in this region. The remaining area of the plate was divided into sections 1 x 1 cm in size in which the number of stars was counted. Then all stars lying closer together than $r = 1$ mm were counted. The number of such stars was found to be 113.

For a random spatial distribution the expected number of pairs of stars is

$$p_{\text{stat}} = \sum_{i=1}^{n} \frac{N_i(N_i-1)}{2} \frac{\pi r^2}{a_i b_i} \left[1 - \frac{4(a_i+b_i)r}{3\pi a_i b_i} + \frac{2r^2}{2\pi a_i b_i} \right]. \qquad (1)$$

where n is the number of sections, N_i is the number of stars in the ith section and a_i and b_i are the sides of the ith section.[3] Expression (1) is valid only if the edge effect can be neglected, i.e., for $r \ll a_i$, b_i ; this requirement is easily met in the present case. Substituting in (1) the values of the appropriate quantities, we obtain $p_{\text{stat}} = 69$ for $r = 1$ mm. Thus there is an excess of close pairs for distances less than or equal to 1 mm. The size of this effect can be judged from

$$(p_{\text{exp}} - p_{\text{stat}}) / \sqrt{p_{\text{stat}}} = 5\,3.$$

The quantity $p_{\text{exp}} - p_{\text{stat}}$ is 44 for $r = 1$ mm; i.e., statistical analysis of our data exhibits a close pair effect approximately the same as that found in Refs. 3 and 6. The existence of this effect has been shown still more conclusively in Ref. 10 in which not only ''doublets'' but also ''triplets'' of close-lying stars were examined. In this work it was shown that two stars separated by a distance less than 300-400 μ were accompanied, as a rule, by a third star located significantly closer than would be expected for a random distribution. Statistical analysis indicates that the probability of obtaining these results on the basis of a random distribution is less than 0.001.

---

*This applies only when the stars are produced simultaneously since the magnitude of the space between the plates and the amount of transverse displacement can change during the movement of the plates.

**So-called radioactive stars were not considered.

The formation of close pairs may be due to one of the neutrons emitted from the primary star which interacts with a nucleus of the emulsion at a distance $r \leqq 1$ mm, thus creating a secondary star. In order to evaluate this effect quantitatively, a count was made of the total number of double stars connected by an ionizing particle (excluding stars which were connected by π^- mesons which had come to rest). In the plates exposed in this work two double stars were observed out of 2126. In other plates 200, 400, and 600 μ in thickness, which had been scanned for other purposes, there were 5 double stars out of 3828 stars. Converting these figures to hundred-micron plates *** 3.25 double stars were found for 5954 stars, i.e., approximately one double star for every 2000. Thus it follows that one pair of neutron-produced stars is found for approximately 1800 single stars. In this connection it has been assumed that the proton is the connecting particle for all the double stars and that the ratio of the number of neutrons to the number of protons in the elements of the emulsions is 1.2.

The test for the close-pair effect was carried out in 14 pairs of plates containing 2078 stars with prong-number $n \geqq 2$. Determination of the time of creation of the stars requires that at least one of the prongs extend to the surface of the emulsion, i.e., that there be an extension in the other plate. 1600 such stars were observed. Not all of these could be used, however, since a fraction of them (51 %) had been created prior to the exposure of the plates in the apparatus and therefore had no extensions. In addition, some of the stars were produced while the apparatus was being elevated, before the clockwork mechanism was set in operation, and so were not useful in this work (38% of the stars with extensions). The final number of useful stars, i.e., those having extensions and formed while the machine was in operation was found to be ~ 480.

Using the method described in Sec. 2, a search was made for extensions of all stars lying within a distance of 1 mm of each other. Not one pair of simultaneously created stars was found.[+]

3. Discussion of the Results

As has been indicated earlier, statistical analysis shows that the quantity $p_{\text{exp}} - p_{\text{stat}}$ is equal to 44 for $r = 1000\ \mu$ and 18 for $r = 500\ \mu$. These data converted to 1000 stars are compared below with the results of other authors (the last column refers to the present work):

$$(r \leqslant 0.5\ \text{MM}) \quad 10^3 \cdot \frac{(p_{\text{exp}} - p_{\text{stat}})}{\Sigma N_i}$$

8.4 [2] 2.9 [3] 18.1 [6] 7.4

$$(r \leqslant 1.0\ \text{MM}) \quad 10^3 \cdot \frac{(p_{\text{exp}} - p_{\text{stat}})}{\Sigma N_i}$$

— 8.2 [3] 2.4 [6] 20

The number of stars (produced while the instrument was in operation) which have extensions is 480; hence if the close-pair effect does, in fact, exist, the number of simultaneous pairs should be ~ 9 if our data are used and ~ 7.2 if the data of Refs. 3 and 6 are used.

In this experiment not one simultaneous pair of stars was observed. The probability of such a result if an effect of the size given above does really exist is $\sim 10^{-3}$ and $\sim 10^{-4}$ depending on which data are used.

The number of close pairs to be expected from trivial causes (cf. Sec. 2) is 0.27, which does not contradict the results of the experiment.

It should be noted that in calculating the number of stars under our experimental conditions we have not taken account of the change in the prong-number with height. It is known, for instance, that the average number of prongs in a star will increase with height (cf. Ref. 15). If this effect is taken into account the original number of single stars (~ 480) should be increased to some extent.

These results show that if the close-pair effect does exist its magnitude is much smaller than is to be expected on the basis of a statistical analysis. This finding agrees with the results of an investigation of the effect carried out with scin-

---

***This calculation was performed under the assumption that the probability of creation of a secondary star is proportional to the thickness of the emulsion.

[+] The large number of stars produced before the machine was set in operation and the possibility of a transverse displacement of the plates can lead to the appearance of false close-pair stars. In the present case this is of no concern since no simultaneous pairs were found.

[15] Powell, Cameron, et al. Usp. Fiz. Nauk 40, 76 (1950) (Russian translation)

tillation counters,[16] although a detailed comparison of the present results with those would be difficult.

In the above we have proceeded from the entirely reasonable requirement that close-pair stars should be created simultaneously. To be perfectly logical, however, we have not ruled out the possibility that the close pairs are formed with a delay time which is beyond the resolution capabilities of this method. This question can be resolved when a considerably greater amount of experimental data is accumulated. In the event of a negative result, there would seem to be a fundamental contradiction between the statistical analysis and the results of the present work; this would seem to indicate the presence of some methodological error in the statistical analysis. In this connection factors such as nonuniformity of exposure, inhomogeneities in the amount of AgBr, differences in the thickness of the emulsion in different parts of the plates, and the higher counting efficiency in the vicinity of neighboring stars as compared with single stars should be considered. A detailed analysis of these and similar effects should be the subject of a special report.

The authors are indebted to their colleagues at MFTI for assistance in performing this work and to A. A. Mizel'kovskii and R. M. Gryzunov who scanned the plates. The authors also wish to thank Prof. N. A. Dobritin for taking part in the discussion of the results.

Translated by H. Lashinsky
51

---

[16] J. B. Harding. Nature 169, 747 (1952).

SOVIET PHYSICS JETP VOLUME 3, NUMBER 2 SEPTEMBER, 1956

On the Theory of Stochastic Processes in Cosmic Radiation

L. Pal
Budapest

(Submitted to JETP editor December 23, 1954)
J. Exptl. Theoret. Phys. (U.S S.R.) 30, 362-366 (February, 1956)

We study a generalization of the kinetic equation of L. Janossy for the case where the physical quantity $\xi(t)$ does not remain constant between two consecutive jumps, but changes in accordance with some causal law. The equation that is introduced can be successfully applied to various problems concerning stochastic processes in cosmic radiation.

In the present paper we consider some problems of the theory of stochastic processes, which play a very important role in nuclear physics and in the theory of cosmic radiation[1]. We shall not touch upon concrete problems, since there are a large number of papers in this direction in the literature[2]; however, a unified treatment of these problems is lacking.

For the stochastic description of an arbitrary physical process (energy loss, scattering, etc.) we must first of all determine the distribution function of the physical quantities which play a decisive role in the given process. If it is known that the value of some physical quantity $\xi(t)$ at the instant of time t is equal to x, then in certain kinds of stochastic processes (processes without after-effect*) it is easy to determine the probability that the value of the random variable $\xi(\tau)$ is greater than y at any instant of time $\tau \geq t$. Let us designate this probability [the distribution function of the random process $\xi(t)$] by $F(t, x; \tau, y)$. As is well known, the function $F(t, x; \tau, y)$ is determined by two integro-differential equations, introduced by Kolmogoroff[3] and Feller[4].

Let us denote by $P(t, x; y)$ the probability that the random process $\xi(t)$ discontinuously changes its value to $\xi(t+0) \leqslant y$ under the condition that a jump occurred at the instant of time t, and that immediately before the jump $\xi(t-0)$ was equal to x. Let $Q(t, x)\Delta t + o(\Delta t)$ be the probability that in the time interval $(t, t + \Delta t)$ there occurs at least one jump of the random process $\xi(t)$ [$o(\Delta t)$ is the probability that in this interval there occurs more than jump of the quantity $\xi(t)$] under the condition that immediately before the jump $\xi(t - 0)$ was equal to x. In physical applications $Q(t, x)$ is called the "total cross section" and the expression $w(t, x; y)\,dy = Q(t, x)\,dP_y(t, x; y)$ is called the "differential cross section".

---

[1] L. Janossy, J. Exptl. Theoret. Phys. (U.S.S.R.) 26, 386, 518 (1954).

[2] A. Bekessy, L. Janossy and L. Pal, Magyar. Fizikai Folyoirat (in press).

* Processes without after-effect are often called Markoff processes.

[3] A. Kolmogoroff ,Math. Ann. 104, 415 (1931).

[4] W. Feller, Math. Ann. 113, 113 (1936).

The Kolmogoroff-Feller equations, which determine the distribution function $F(t,x; \tau, y)$, have the following form:

$$\frac{\partial F(t, x;\tau, y)}{\partial t} = Q(t, x)\{F(t, x; \tau, y) - \int F(t, z; \tau, y)\,dP_z(t, x; z)\}; \tag{1}$$

$$\frac{\partial F(t, x; \tau, y)}{\partial \tau} = \int_{(y)} Q(\tau, z)\,dF_z(t, x; \tau, z) - \int Q(\tau, z)\,P(\tau, z; y)\,dF_z(t, x; \tau, z). \tag{2}$$

The equation (1) is especially suitable for solving a whole series of problems of cascade theory[1]. Janossy[1], using the method of the "first collision", worked out a very graphic method of obtaining a kinetic equation of the type (1) in the case of processes that are homogeneous in time.

1. In connection with certain problems in the statistical theory of the penetration of elementary particles through matter, one needs a generalization of the Kolmogoroff-Feller equation for the case where the physical quantity $\xi(t)$ does not remain constant between two consecutive jumps, but changes in accordance with some causal law, i.e., if it is known that $\xi(t) = x$ at the instant of time t, then after a time u the random variable $\xi(t + u)$ takes the value $f(x, u)$, under the condition that the interval $(t, t + u)$ lies between two consecutive jumps of the random process. It is evident that without the introduction of new random quantities the Markoff character of the process can be preserved if and only if the function which describes the causal character of the random process $\xi(t)$ satisfies the functional equation

$$f(x, u_1 + u_2) = f\{f(x, u_1), u_2\}. \tag{3}$$

The equation (3) was studied in detail by Aczel[5]. As the basis for his study it is easily shown that a function which satisfies equation (3) has the following form:

$$f(x, u) = H\{H^{-1}(x) + u\}. \tag{4}$$

Here it is assumed that the function $H(x)$ has an inverse function $H^{-1}(x)$. Indeed, one can easily convince oneself that

$$f\{f(x, u_1) + u_2\} = H\{H^{-1}[f(x, u_1)] + u_2\}$$

$$= H\{H^{-1}(x) + u_1 + u_2\},$$

i.e., that

$$H\{H^{-1}(x) + u_1 + u_2\} = f(x, u_1 + u_2). \tag{5}$$

It is evident that the functions $xe^{\pm\lambda u}$, $x/(1 \pm \lambda xu)$, $x \pm \lambda u$ etc. satisfy Eq. (3).

In connection with statistical problems concerning recording of nuclear fission using an ionization chamber[6] we studied the solution of the kinetic equation for the case where the physical quantity $\xi(t)$ changes in accordance with an exponential law between consecutive jumps, i.e, $f(x, u) = xe^{-\lambda u}$. The generalized equation is also easily written for the case where all that is required of the function $f(x, u)$ is that it satisfy the condition (3).

First of all we determine the distribution function $I(t, x; t + \Delta t, z)$. It is easily expressed in terms of the functions $Q(t, x)$, $P(t, x; y)$ and $f(x, u)$; i.e.,

$$\begin{aligned} &F(t, x; t + \Delta t, z) \\ &= \{1 - Q(t, x)\Delta t\}\,E\{z - f(x, \Delta t)\} \\ &\quad + Q(t, x)\,P(t, x; z)\,\Delta t + o(\Delta t), \end{aligned} \tag{6}$$

where

$$E(z - z') = \begin{cases} 0, & \text{if} \quad z \leqslant z', \\ 1, & \text{if} \quad z > z'. \end{cases}$$

From the Markoff equations (see Ref. 7, p. 245), we obtain the following equations, using (6):

---

[5] J. Aczel, Publ. Math. 1, 243 (1950).

[6] L. Pal, Magyar. Fizikai Folyoirat 3, 31 (1955).

[7] V. V. Gnedenko, *A Course in Probability Theory*, Moscow-Leningrad, 1951.

$$\left\{\frac{\partial}{\partial t} - Q(t, x) - g(x)\frac{\partial}{\partial x}\right\} F(t, x; \tau, y) \tag{7}$$

$$+ Q(t, x)\int F(t, z; \tau, y)\, dP_z(t, x; z) = 0,$$

$$\left\{\frac{\partial}{\partial \tau} - g(y)\frac{\partial}{\partial y}\right\} F(t, x; \tau, y) - \int Q(\tau, z) P(\tau, z; y)\, dF_z(t, x; \tau, z) \tag{8}$$

$$= \int_{(y)} Q(\tau, z)\, dF_z(t, x; \tau, z),$$

where $g(x) = (\partial f(x, u)/\partial u)_{u=0}$.

If $Q(t, x) = N$, $P(t, x; y) = H(y - x)$ and $F(t, x; \tau, y) = R(\tau - t, y)$, then, introducing the notation $\tau - t = v$, we obtain from (7) for the case $f(x, u) = xe^{-\alpha u}$ the equation

$$\frac{\partial R}{\partial v} - \alpha y \frac{\partial R}{\partial y} = -N\{R(v, y) \tag{9}$$

$$- \int R(v, z)\, dH(y - z)\},$$

which coincides with Eq. (2), studied in Ref. 6. An analogous equation is obtained from (8) in the homogeneous case.

2. In the preceding section we showed that for the class of random processes without after-effect the causal changes of the quantity $\xi(t)$ between consecutive jumps (discontinuities) cannot be arbitrary, but that the functions which describe these changes must satisfy Eq. (3). In the theory of stochastic processes in cosmic radiation, one often encounters such random processes which cannot be described within the framework of Markoff processes by using the distribution function of one random quantity. In these cases a description within the class of processes without after-effect can be achieved in principle with the aid of the distribution function of several mutually dependent random variables.

Thus for the stochastic description of the given physical system, we introduce the random quantities $\xi_1(t), \xi_2(t), \ldots, \xi_n(t)$. The study of such processes is of special interest in the case where, in addition to purely discontinuous changes, the random quantities $\xi_1(t), \ldots, \xi_n(t)$ can change in accordance with certain causal laws, i.e., if it is known that $\xi_k(t) = x_k$ $(k = 1, 2, \ldots, n)$, at the time t, then after the time u the random quantity takes the value $\xi_k(t + u)$ under the condition that the interval $(t, t + u)$ lies between two consecutive jumps of the random vector $\{\xi_1(t), \xi_2(t), \ldots, \xi_n(t)\}$.

Let $Q(t, x_1; \ldots, x_n)\Delta t + o(\Delta t)$ be the probability that in the interval $(t, t + t)$ the state of the system, determined by the equations $\xi_k(t) = x_k$, changes discontinuously, and $P(t, x_1, \ldots, x_n; y_1, \ldots, y_n)$ the probability that $\xi_k(t + 0) = y_k$, $(k = 1, 2, \ldots, n)$ under the condition that a jump occurred at the instant of time t and that immediately before the jump the equations $\xi_k(t - 0 = x_k$ were valid. Let us designate by $F(t, x_1, \ldots, x_n; \tau, y_1, \ldots, y_n)$ the probability that $\xi_k(\tau) \leqslant y_k$, if it is known that at the instant of time t the equalities $\xi_k(t) = x_k$ $(k = 1, 2, \ldots, n)$ were valid.

In an analogous way it is easy to determine the generalized Kolmogoroff-Feller equations

$$\left\{\frac{\partial}{\partial t} - Q(t, x_1, \ldots, x_n) - \sum_k g_k(x_1, \ldots, x_n)\frac{\partial}{\partial x_k}\right\} \times$$

$$\times F(t, x_1, \ldots, x_n; \tau, y_1, \ldots, y_n) + Q(t, x_1, \ldots, x_n) \times$$

$$\times \int \cdots \int F(t, z_1, \ldots, z_n; \tau, y_1, \ldots, y_n)\, dP(t, x_1, \ldots, x_n; z_1, \ldots, z_n), \tag{10}$$

$$\left\{\frac{\partial}{\partial \tau} + \sum_k g_k(y_1, \ldots, y_n)\frac{\partial}{\partial y_k}\right\} F(t, x_1, \ldots, x_n; \tau, y_1, \ldots, y_n) -$$

$$- \underset{(y_1, \ldots, y_n)}{\int \cdots \int} Q(\tau, z_1, \ldots, z_n)\, dF(t, x_1, \ldots, x_n; \tau, z_1, \ldots, z_n) =$$

$$= \int \cdots \int Q(\tau, z_1, \ldots, z_n) P(\tau, z_1, \ldots, z_n; y_1, \ldots, y_n) \times$$

$$\times dF(t, x_1, \ldots, x_n; \tau, z_1, \ldots, z_n). \tag{11}$$

In what follows we shall be concerned only with the first equation. If the process is homogeneous in time, i.e.,

$$F(t, x_1, \ldots, x_n; \tau, y_1, \ldots, y_n)$$

$$= \Phi(v, x_1, \ldots, x_n; y_1, \ldots y_n),$$

then we obtain from Eq. (10)

$$\left\{\frac{\partial}{\partial v} + Q(x_1, \ldots, x_n) - \sum_k g_k(x_1, \ldots, x_n)\frac{\partial}{\partial x_k}\right\} \tag{12}$$

$$\times \Phi(v, x_1, \ldots, x_n; y_1, \ldots, y_n) = \int \cdots \int w(x_1, \ldots, x_n; z_1, \ldots, z_n)$$

$$\times \Phi(v, z_1, \ldots, z_n; y_1, \ldots, y_n)\, dz_1, \ldots, dz_n,$$

$$g_k(x_1, \ldots, x_n) = \left(\partial f_k(x_1, \ldots, x_n; u)/\partial u\right)_{u=0}.$$

where

$$w(x_1, \ldots, x_n; z_1, \ldots, z_n)\, dz_1, \ldots, dz_n$$

$$= Q(t_1, x_1, \ldots, x_n)\, dP(t, x_1, \ldots, x_n; z_1, \ldots, z_n),$$

$$Q(x_1, \ldots, x_n) = \int \cdots \int w(x_1, \ldots, x_n; z_1, \ldots, z_n)\, dz_1 \ldots dz_n.$$

Equation (10) or (12) is a generalization of Janossy's equation[8] and has the advantage that it avoids difficulties connected with the appearance of one and the same quantity several times in the equation. In the next section, we shall show that the kinetic equation, studied in detail by Janossy[8], is easily obtained from our equation.

3. Elementary particles in traversing matter lose their energy and deviate from their original direction. For the stochastic description of the motion of a particle we introduce the following random quantities: $\xi_1(t)$, the energy of the particle, $\xi_2(t)$, the angle between the tangent to the projection of the trajectory of the particle on the (x, z) plane and the x axis, $\xi_3(t)$, the distance of the particle from the x axis in the (x, z) plane, and $\xi_4(t)$, the area determined by the projection of the trajectory of the particle on the (x, z) plane and the x axis. The quantities $\xi_3(t)$ and $\xi_4(t)$ change continuously. From elementary considerations it follows that

$$f_3(x_1, \ldots, x_4; u) \tag{13}$$

$$= x_3 + u \operatorname{tg} x_2 \sim x_3 + u x_2;$$

$$f_4(x_1, \ldots, x_4; u) = x_4 + x_3 u$$

$$+ {}^1/_2 u^2 \operatorname{tg} x_2 \sim x_4 + x_3 u + {}^1/_2 u^2 x_2.$$

Using Eqs. (12) and (13), we can write

$$\left\{\frac{\partial}{\partial v} + Q(x_1) - x_2\frac{\partial}{\partial x_3} - x_3\frac{\partial}{\partial x_4}\right\}\Phi(v, \mathbf{x}, \mathbf{y})$$

$$= \int w(\mathbf{x}, \mathbf{z})\,\Phi(v, \mathbf{z}, \mathbf{y})\, dz, \tag{14}$$

where $\mathbf{x} = \{x_1, \ldots, x_4\}$ is a four-dimensional vector. The cross section $w(\mathbf{x}, \mathbf{z})$ has the form

$$w(\mathbf{x}, \mathbf{z}) = q(x_1, x_2; z_1, z_2) \tag{15}$$

$$\times\, \delta(z_3 - x_3)\,\delta(z_4 - x_4).$$

Since $q(x_1, x_2; z_1, z_2)$ has a sharp maximum at the points $x_1 = z_1$ and $x_2 = z_2$ and its values are very small at other points, we can expand $\Phi(v, \mathbf{x}, \mathbf{y})$ in powers of $(z_1 - x_1)$ and $(z_2 - x_2)$. In this way we get the following equation:

$$\left\{\frac{\partial}{\partial v} - x_2\frac{\partial}{\partial x_3} - x_3\frac{\partial}{\partial x_4} + a(x_1)\frac{\partial}{\partial x_1}\right. \tag{16}$$

$$\left. - {}^1/_2\, b(x_1)\frac{\partial^2}{\partial x_1^2} - {}^1/_2\, \sigma(x_1)\frac{\partial^2}{\partial x_2^2}\right\}\Phi(v, \mathbf{x}, \mathbf{y}) = 0,$$

where $a(x_1)$, $b(x_1)$ and $\sigma(x_1)$ are determined by the following relations:

$$a(x_1) = \iint (x_1 - z_1)\, q(x_1, x_2, z_1, z_2)\, dz_1\, dz_2,$$

$$b(x_1) = \iint (x_1 - z_1)^2\, q(x_1, x_2; z_1, z_2)\, dz_1\, dz_2,$$

$$\sigma(x_1) = \iint (x_2 - z_2)^2\, q(x_1, x_2; z_1, z_2)\, dz_1\, dz_2.$$

Equation (16) was studied in detail in the work of Janossy for the case $b(x_1) = 0$. If we take into consideration the variance of the energy loss, then it is more difficult to obtain a solution of (16). However, in the neighborhood of the mean value of the random quantity $\xi_1(t)$, the solution of equation (16) can be easily found. Indeed, if in the expressions $a(x_1)$, $b(x_1)$, $\sigma(x_1)$ we replace x_1 by the mean value of the random quantity $\xi_1(t)$, then going from the distribution function $\Phi(v, \mathbf{x}, \mathbf{y})$ to the probability density $\varphi(v, \mathrm{x}, \mathrm{y})$, and assuming that $\varphi(v, \mathrm{x}, \mathrm{y}) = \psi(v, x_2, x_3, x_4; y_2, y_3, y_4)$ $\times \chi(v, x_1; y_1)$, we obtain the following equation

---

[8] L. Janossy, J. Exptl. Theoret. Phys. (U.S.S.R.) **30**, 351 (1956).

$$\frac{\partial \chi(v, x_1; y_1)}{\partial v} = \frac{1}{2} b[\bar{x}_1(v)] \frac{\partial^2 \chi(v, x_1; y_1)}{\partial x_1^2} \tag{17}$$

$$- a[\bar{x}_1(v)[\frac{\partial \chi(v, x_1; y_1)}{\partial x_1}$$

Equation (17) can be easily solved[9]. With the initial condition $\chi(0, x_1; y_1) = \delta(y_1 - x_1)$ we find that

$$\chi(v, x_1; y_1) = B^{-1}(2\pi)^{-1/2} \tag{18}$$

$$\exp\{-(y_1 - x_1 - A)^2 / 2B^2\},$$

$$A = \int_0^v a[\bar{x}_1(s)]\, ds, \tag{19}$$

$$B^2 = \int_0^v b[x_1(s)]\, ds.$$

In the expressions for A and B^2, $x_1(s)$ designates the mean value of $\xi_1(s)$.

The determination of η ν_4) can be found in the work of Janossy[8].

For a practical application of the approximation in question we refer to one of some forthcoming papers.

Translated by R. Silverman
62

---

[9] L. Pal, Vestn. Moscow State University 6, 111 (1953)

SOVIET PHYSICS JETP VOLUME 3, NUMBER 2 SEPTEMBER, 1956

Matrix Aspects of Boson Theory

A. A. BORGARDT
Dnepropetrovsk State University

(Submitted to JETP editor November 17, 1954)
J. Exptl. Theoret. Phys. (U.S.S.R.) **30**, 334-341 (February, 1956)

Certain relations are presented which make it possible to change at any stage of a calculation from anticommuting matrices to Kemmer matrices. The paper shows the connection between the Γ_μ, the matrices of the irreducible representation of the Kemmer and Dirac algebra, and also the Tamm matrices.

1. TRANSITION FROM MATRIX TO FIELD DESCRIPTION

IN a previous paper[1] we have introduced the basic operators which convert from undor matrix notation to the usual tensor notation. The scalar projection operator R, which has the property

$$k_0^{-2} R\Psi = \psi, \tag{1}$$

can obviously be expressed in terms of the reflection matrices $R_\mu = 2\beta_\mu^2 - I$,

$$R = (^1/_2)^4 \prod_{\mu=1}^{4} (I - R_\mu) \tag{2}$$

(Reference 4 contains an evident error in the coefficient). By expanding the product, one can also obtain for R the formula

$$R = (^1/_2)^4 ((I + R_5)(I + M_1) + M_2), \tag{3}$$

where

$$M_1 = \sum_{\mu=1}^{4} R_\mu, \quad M_2 = \sum_{\mu\neq}^{4} \sum_{\nu=1}^{4} R_\mu R_\nu, \tag{4}$$

$$M_3 = R_5 M_1 = \sum_{\mu\neq}^{4} \sum_{\nu\neq}^{4} \sum_{\rho=1}^{4} R_\mu R_\nu R_\rho. \tag{5}$$

The matrices I, M_1, M_2, $R_5 M_1$ form the center of the Kemmer algebra, the quantities which commute with all elements of G_{16} being[2]

$$I, \ M = M_1 - M_2, \quad N = R_5 (I - M_1).$$

The traces of the matrices M_1, M_2, M_3 vanish.

The pseudoscalar operator R, with the property

$$k_0^{-2} \widetilde{R}\Psi = \widetilde{\psi}, \tag{6}$$

can be obtained from R by means of the generalized Larmor transformation[1] $\widetilde{R} = \Gamma_5 R \Gamma_5$.

Both these operators, by their definition, satisfy the obvious relations

$$R^n = R, \quad \widetilde{R}^n = \widetilde{R}, \quad \mathrm{Sp}\, R = \mathrm{Sp}\, \widetilde{R} = 1. \tag{7}$$

In working out the commutation relations between the Γ_μ and the operators M_1, M_2, one is forced to introduce the group of matrices $\overline{\Gamma}_\mu$, $\overline{G}_{16}$; this is reasonable since the commutative group R_μ connects Γ_μ and $\overline{\Gamma}_\mu (\overline{\Gamma}_\mu = R_\mu \Gamma_\mu$, n.s.*):

$$\begin{gathered} \{\Gamma_\mu M_1\} = 2\overline{\Gamma}_\mu, \ \{\overline{\Gamma}_\mu M_1\} = 2\Gamma_\mu, \\ [\Gamma_\mu M_2] = -2(M_1 \overline{\Gamma}_\mu - \Gamma_\nu), \\ [\overline{\Gamma}_\mu M_2] = -2(M_1 \Gamma_\mu - \overline{\Gamma}_\mu); \\ \{\Gamma_5 M_1\} = \{\overline{\Gamma}_5 M_1\} = [\Gamma_5 M_2] = [\overline{\Gamma}_5 M_2] = 0. \end{gathered} \tag{8}$$

With the help of these equations one can obtain the commutation rules between the Γ_μ and R:

$$[\Gamma_\mu R] = (^1/_2)^3 (I - R_5 + M_1)(\Gamma_\mu - \overline{\Gamma}_\mu), \tag{9}$$

and with the help of the latter one can prove that the vector operator

$$\begin{gathered} k_0^{-1} A_\mu \Psi = \psi_\mu, \\ A_\mu = (^1/_2)^4 (I - R_\mu) \prod_{\nu\neq\mu=1}^{4} (I + R_\nu) \end{gathered} \tag{10}$$

is equal to

$$A_\mu = \Gamma_\mu R \Gamma_\mu \ \text{(n.s.)} \tag{11}$$

By performing the Larmor transformation on the A_μ, we obtain the pseudovector operators. These operators have the obvious properties:

$$A_\mu^n = A_\mu, \quad \widetilde{A}_\mu^n = \widetilde{A}_\mu, \quad \mathrm{Sp}\, A_\nu = \mathrm{Sp}\, \widetilde{A}_\mu = 1. \tag{12}$$

The rules for commuting A_μ, $\widetilde{A}_\mu$ with the Γ_μ and with each other, and also the analogous relations for the tensor projection operators can easily be worked out from the formulae given above.

---

[1] A. A Borgardt, J. Exptl. Theoret. Phys. (U.S.S.R.) **24**, 24 (1953).

[2] N. Kemmer, Proc. Roy. Soc. (London) **173A** 94 (1939).

* "n. s." means no summation.

2. TRANSITION TO MIXTURES AND PURE FIELDS

It follows from (11) that the sum $\Gamma_\mu R\Gamma_\mu$ extracts from the undor* the matrix vector $k_0(\vec{\psi}, \psi_0)$. If we express the operator $\sum_{\mu=1}^{4} A_\mu$ in terms of the matrices β_μ we obtain the quantity β, which was at first introduced by Harish-Chandra[4]. Now it is easy to extract from the matrix equations in terms of the Γ_μ, the part relating, for example, to a pure scalar field.

If we construct the 16-dimensional unit matrix I from the scalar, vector, pseudovector, and pseudoscalar unit matrices, $I(s)$, $I(v)$, $I(v)$ and $I(s)$, $I(s)$, we see that the extraction of the pure scalar field from the Ψ field is accomplished by the operator $I(s)$

$$I(s) = R + \sum_{\mu=1}^{4} \Gamma_\mu R \Gamma_\mu. \qquad (13)$$

The addition of $\tilde{R} + I(s)$ to the 16-dimensional unit matrix obviously extracts the pseudovector field

$$I(\tilde{v}) = I - I(s) - \tilde{R}. \qquad (14)$$

The pseudoscalar and vector unit operators are obtained from $I(s)$ and $I(v)$ by a Larmor transformation.

The equations derived above can be used to obtain from the general equations

$$(\Gamma_\lambda \partial / \partial x_\lambda + k_0)\Psi = Q \qquad (15)$$

for example, the equation of the pseudoscalar field

$$(\Gamma_\lambda \partial / \partial x_\lambda - k_0)\tilde{R}\Psi + k_0 I(\tilde{s})\Psi = I(\tilde{s})Q - \tilde{R}Q. \qquad (16)$$

In the equations for mixed fields we can use at the same time both sets of anticommuting matrices Γ_μ and $\overline{\Gamma}_\mu$, and construct from them two reducible representations of the Kemmer algebra

$$\beta_\mu = {}^1/_2(\Gamma_\mu + \overline{\Gamma}_\mu), \quad \beta'_\mu = {}^1/_2(\Gamma_\mu - \overline{\Gamma}_\mu), \qquad (17)$$

where $[\Gamma_\mu \overline{\Gamma}_\nu] = 0$. In this way we are led to wave equations of the type

$$[{}^1/_2(\Gamma_\nu \pm \overline{\Gamma}_\lambda)\partial / \partial x_\lambda + k_0]\Psi = Q. \qquad (18)$$

3. COVARIENT FORM OF THE HAMILTONIAN

The use of Hamiltonian equations, instead of relativistically symmetric ones like (15), in explicit calculations has a number of substantial advantages. However, this method does not satisfy the covarience requirement of modern theory[5], because of the way the time coordinate is singled out. We introduce therefore a three-dimensional hypersurface σ with a normal unit vector n_μ, $n_\lambda^2 = -I$. Any four vector A_μ can then be resolved into a longitudinal part A_μ^L and a transverse part A_μ^T by the relations

$$A_\mu^L = -n_\mu n_\lambda A_\lambda, \quad A_\mu^T = -A_{[\mu} n_{\lambda]} n_\lambda, \qquad (19)$$

One verifies immediately that this resolution is correct and unique, since

$$A_\mu = A_\mu^L + A_\mu^T, \quad A^L = n_\lambda A_\lambda^L, \quad n_\lambda A_\lambda^T = 0.$$

Similarly we can form the matrix vectors Γ_μ and R_μ the purely longitudinal quantities

$$\Gamma_L = n_\lambda \Gamma_\lambda, \quad R_L = 2\beta_L^2 - I. \qquad (20)$$

The properties of these matrices follow from their definition:

$$\{\Gamma_L \Gamma_\mu\} = 2n_\mu, \quad \{\Gamma_L R_5\} = 0, \qquad (21)$$

$$\{\Gamma_L R_\mu\} = 2n_\mu \overline{\Gamma}_\mu.$$

The matrix R_L performs the transformation of the undor Ψ which represents a reversal of the direction of the normal to the hypersurfaces, and the operator ${}^1/_2(I + R_L)$ is therefore related to the separation of the field quantities into longitudinal and transverse parts. It may be calculated in the following way. We introduce for the β_μ the representation ${}^1/_2(\Gamma_\mu + \Gamma_\nu)$; then

$$\beta_L^2 = {}^1/_2(1 - n_\nu n_\sigma \hat{T}_{\lambda\sigma}), \qquad (22)$$

where

$$\hat{T}_{\mu\nu} = {}^1/_2(\overline{\Gamma}_\mu \Gamma_\nu + \Gamma_\mu \overline{\Gamma}_\nu). \qquad (23)$$

From the definition of R_L we find that

$${}^1/_2(I \pm R_L) = {}^1/_2(I \mp n_\nu n_\sigma \hat{T}_{\lambda\sigma}). \qquad (24)$$

---

* Here and in the following we use the term "undor" to denote a matrix which has as elements a scalar, a vector and the components of all completely antisymmetric tensors in four-dimensional space (total number 16) (cf. Ref. 3).

[3] F. Belinfante, Physica **6**, 849, 870 (1939).

[4] Harish-Chandra, Proc. Roy. Soc. (London) **184A**, 215 (1946).

[5] J. Schwinger, Phys. Rev. **74**, 1439 (1948).

The commutation relations and some other necessary equations are given below:

$$[\hat{T}_{\mu\nu}\hat{T}_{\rho\tau}] = {}^1\!/_2\,(-(\Gamma_\rho\Gamma_\mu - \bar{\Gamma}_\mu\bar{\Gamma}_\rho)\,\delta_{\nu\tau} - (\Gamma_\tau\Gamma_\nu - \bar{\Gamma}_\nu\bar{\Gamma}_\tau)\,\delta_{\mu\rho} \tag{25}$$

$$+ (\Gamma_\nu\Gamma_\rho - \bar{\Gamma}_\rho\bar{\Gamma}_\nu)\,\delta_{\mu\tau} + (\Gamma_\mu\Gamma_\tau - \bar{\Gamma}_\tau\bar{\Gamma}_\mu)\,\delta_{\nu\rho}), \tag{26}$$

$$\{\Gamma_\mu\hat{T}_{\nu\rho}\} = \Gamma_\nu\delta_{\mu\rho} + \bar{\Gamma}_\mu\delta_{\mu\nu},\quad \{\bar{\Gamma}_\mu\hat{T}_{\nu\rho}\} = \bar{\Gamma}_\nu\delta_{\mu\rho} + \Gamma_\rho\delta_{\mu\nu}, \tag{27}$$

$$[R_5\hat{T}_{\mu\nu}] = [R_\mu\hat{T}_{\nu\rho}]_{\mu\neq\nu,\,\rho} = \{R_\mu\hat{T}_{\mu\rho}\}_{\mu\neq\rho} = \{\Gamma_5\hat{T}_{\mu\nu}\} = 0, \tag{28}$$

$$\hat{T}_{\mu\lambda}\Gamma_\lambda = {}^1\!/_2\,(6\bar{\Gamma}_\mu - M_1\Gamma_\mu),\qquad \hat{T}_{\mu\lambda}\bar{\Gamma}_\lambda = {}^1\!/_2\,(6\Gamma_\mu - M_1\bar{\Gamma}_\mu).$$

The symmetric tensor operator $\hat{T}_{\mu\nu}$ forms a density, which is conserved in the absence of sources for the field. Indeed, the equations

$$\begin{aligned} &(\Gamma_\lambda\partial/\partial x_\lambda + k_0)\,\Psi = 0,\\ &(\bar{\Gamma}_\lambda\partial/\partial x_\lambda + k_0)\,\Psi = 0,\\ &(-\Gamma_\lambda^T\partial/\partial x_\lambda + k_0)\,\Psi^+ = 0,\\ &(-\bar{\Gamma}_\lambda^T\partial/\partial x_\lambda + k_0)\,\Psi = 0 \end{aligned} \tag{29}$$

lead to the continuity equation

$$\partial\,(\Psi^+(\bar{\Gamma}_\mu\Gamma_\lambda + \Gamma_\mu\bar{\Gamma}_\lambda)\,\Psi)/\partial x_\lambda = 0, \tag{30}$$

i.e., the conservation law for the energy-momentum tensor of the field described by equations (29). The complete Ψ field, with the anticommuting velocity matrices Γ_μ, possesses an energy-momentum density operator of the form $\Gamma_\mu\Gamma_\nu$. The operator $\hat{T}_{\mu\nu}$ enters also into the commutation laws for the components of Ψ. The commutator must be a solution of the wave equations of first order. In the case of the field described by the equations

$$[{}^1\!/_2\,(\Gamma_\lambda \pm \bar{\Gamma}_\lambda)\,\partial/\partial x_\lambda + k_0]\,\Psi = 0,$$

this requirement is satisfied by the undor

$$S^{(\pm)}(x) = (1/2\,k_0)\,[k_0^2 \pm \hat{T}_{\lambda\sigma}\,\partial^2/\partial x_\lambda\,\partial x_\sigma - k_0\,(\Gamma_\lambda \pm \bar{\Gamma}_\lambda)\,\partial/\partial x_\lambda]\,\Delta(x), \tag{31}$$

where

$$\Delta(x) = (2\pi)^{-3}\int e^{i\mathbf{k},\mathbf{x}}\,\frac{\sin\left(c\sqrt{\mathbf{k}^2 + k_0^2}\right)t}{c\sqrt{\mathbf{k}^2 + k_0^2}}\,(d\mathbf{k}). \tag{32}$$

For a field with an anticommutive algebra we obtain from (31), as expected,

$$S(x) = (-\Gamma_\lambda\,\partial/\partial x_\lambda + k_0)\,\Delta(x). \tag{33}$$

It is convenient to express the commutative laws by resolving Ψ into a potential Ψ^{I} and a tension Ψ^{II}. They then take the form

$$\begin{aligned} [\Psi_\alpha^{+\mathrm{II}}(x'),\ \Psi_\beta^{\mathrm{II}}(x)] &= -(i\hbar c^2/2)\,(k_0^2\delta_{\alpha\beta} \mp \hat{T}_{\lambda\sigma}^{\alpha,\,\beta}\,\partial^2/\partial x_\lambda\,\partial x_\sigma)\,\Delta(x - x'),\\ [\Psi_\alpha^{+\mathrm{I}}(x'),\ \Psi_\beta^{\mathrm{I}}(x)] &= -(i\hbar c^2/2)\,(\delta_{\alpha\beta} \mp k_0^{-2}\hat{T}_{\lambda\sigma}^{\alpha,\,\beta}\,\partial^2/\partial x_\lambda\,\partial x_\sigma)\,\Delta(x - x'),\\ [\Psi_\alpha^{+\mathrm{II}}(x'),\ \Psi_\beta^{\mathrm{I}}(x)] &= (i\hbar c^2/2)\,(\Gamma_\lambda \pm \bar{\Gamma}_\lambda)^{\alpha\beta}\,(\partial/\partial x_\lambda)\,\Delta(x - x'). \end{aligned} \tag{34}$$

The transition to a field with a purely anticommutive algebra can be carried out by omitting the terms with the alternative sign and doubling the even ones.

Because of the covariance of the division of the operator $\partial/\partial x_\mu$ into a longitudinal and a transverse part, the covarient form of the Hamiltonian equations is

$$\begin{aligned} &((\hbar c/i)\,\partial/\partial x_L + H_{0L})\,\Psi = Q_L,\\ &((\hbar c/i)\,\partial/\partial x_L + H_{0L}^+)\,\Psi^+ = Q_L^+, \end{aligned} \tag{35}$$

where

$$H_{0L} = -(i\hbar c/2)\,[\Gamma_\lambda\Gamma_\sigma]\,n_{[\lambda}\partial/\partial x_{\sigma]} - \mathcal{E}_0\Gamma_L.\qquad Q_L = -\Gamma_L Q, \tag{36}$$

$$H_{0L}^+ = -(i\hbar c/2)\,[\Gamma_\lambda\Gamma_\sigma]^T\,n_{[\lambda}\partial/\partial x_{\sigma]} + \mathcal{E}_0\Gamma_L^T,\quad Q_L^+ = +\Gamma_L^T Q^+. \tag{37}$$

In the equations of mixed Kemmer fields the Γ_μ must, as usual, be replaced by $^1/_2\,(\Gamma_\mu \pm \bar{\Gamma}_\mu)$.

4. CONNECTION BETWEEN Γ_μ AND FOUR-DIMENSIONAL QUATERNIONS

The separation of the wave function into a potential and a pressure by means of the operator $1/2(I \pm R_5)$ allows, besides the transition to photon theory, also the introduction of contracted, eight-row anticommuting matrices . Strictly speaking, there is no need to number the components of Ψ^{I} and Ψ^{II} differently in the equations

$$\Gamma_\lambda \partial\Psi^{I}/\partial x_\lambda + \Psi^{II} = Q^{II},$$

$$\Gamma_\lambda \partial\Psi^{II}/\partial x_\lambda + k_0^2\Psi^{I} = Q^{I}, \tag{38}$$

because of the difference in the superscripts. We may lable the components of Ψ^{I} and Ψ^{II} by the same set of numbers, if we change from Ψ^{I} to a new function $\bar{\Psi}^{I} = (1/i)\,\Gamma_4\Psi^{I}$. It is natural that the matrix Γ_4 has to be used for this purpose, since this is just the matrix which interchanges the canonically conjugate variables Ψ^{I} and Ψ^{II} ($\Psi^{+}R_5\Gamma_4\Psi$ is an action density, i.e., an invarient product of canonical coordinates and momenta). Equation (38) can now be put into the form*

$$\partial\bar{\Psi}^{I}/c\partial t + \vec{\Gamma}'\nabla\bar{\Psi}^{I} + \Psi^{II} = Q^{II},$$

$$-\partial\Psi^{II}/c\partial t + \vec{\Gamma}'\nabla\Psi^{II} + k_0^2\bar{\Psi}^{I} = \bar{Q}^{I}, \tag{39}$$

where $\bar{Q}^{I} = (1/i)\,\Gamma_4 Q^{I}$, and the eight-row matrices Γ' are defined by the relations

$$\vec{\Gamma}' = (1/i)\,\Gamma_4\vec{\Gamma}\cdot I(8) \tag{40}$$

and satisfy the anticommutive algebra

$$^1/_2\,\{\Gamma_i'\Gamma_k'\} - \delta_{ik}\cdot I = 0. \tag{41}$$

The product of all three matrices Γ_i' gives a matrix which commutes with the whole three-dimensional group G_8 formed by I, the Γ_k' and their products

$$\Gamma_0 = (1/i)\,\Gamma_1'\Gamma_2'\Gamma_3'. \tag{42}$$

From the definition of Γ_0 follows its main property:

$$^1/_2\,[\Gamma_i'\Gamma_k'] = i\Gamma_0\Gamma_l'. \tag{43}$$

(i, k, l being a permutation of 1, 2, 3). The group $\bar{G}_8$ ($[\bar{\Gamma}_i, \Gamma_k] = 0$) can be obtained by forming in analogy with (40), the eight-row matrices $\bar{\Gamma}_k'$ from the $\bar{\Gamma}_4\bar{\Gamma}_k$. The reflection matrices R_k are formed in the usual way

$$R_k = \bar{\Gamma}_k'\Gamma_k' \quad \text{(n.s.)} \tag{44}$$

their properties in relation to G_8, $\bar{G}_8$ being the same as in the 16-dimensional representation, except for the following new relations, which are absent in the latter case

$$R_i R_k = R_l, \quad M_1 = M_2, \tag{45}$$

$$M_3 = R_1R_2R_3 = I.$$

The scalar and pseudoscalar projection operators now cannot be separated (note that the Larmor transformation matrix Γ_5 commutes with Γ_k'!) and both occur in the form of the operator

$$R = R^n = (^1/_2)^3 \prod_{k=1}^{3} (I + R_k)$$

$$= {}^1/_4\,(I + M_1) \tag{46}$$

(the operator $\prod\limits_{k=1}^{3} (I - R_k) \equiv 0$ vanishing identically). The vector projection operators are found as usual: $A_k = \Gamma_k' R\Gamma_k'$ (n.s.), but the vectors and pseudovectors are again undistinguishable.

The eight-dimensional representation Γ_k' is reducible, and we can extract from the contents of G_8 three anticommuting four-row matrices, which belong to the group G_{16} of the Dirac matrices of electron theory.

It would now be possible to go directly from equation (39) to a pure quaternion notation, but we shall make this transition by starting directly from the original wave equation

$$(\Gamma_\lambda\,\partial/\partial x_\lambda + k_0)\,\Psi = Q. \tag{47}$$

We now introduce a wave function which is complex even for a neutral field, letting Γ_5 play the part of $\sqrt{-1}$:

$$\Phi = (I - \bar{\Gamma}_5)\,\Psi. \tag{48}$$

The equation

$$\Gamma_5\Phi = -\Phi, \ \Gamma_5\Phi = -R_5\Phi, \tag{49}$$

---

* In order to make the numbering of the elements of Ψ^{I}, Ψ^{II} continuous, it is better to choose a special representation, in which $\Psi = (\vec{\mathscr{E}},\ \psi,\ \vec{\mathscr{H}},\ \tilde{\psi},\ k_0\vec{\psi},\ k_0\psi_0,\ k_0\overleftarrow{\tilde{\psi}},\ k_0\psi_0)$.

which follows from (48), shows that one half of Φ repeats the other, apart from a sign. To spell this out, split Φ into a potential and a tension

$$\Phi^{\mathrm{I}} = (1/2\,k_0)\,(I - R_5)\,\Phi, \qquad \Phi^{\mathrm{II}} = {}^1\!/_2\,(I + R_5)\,\Phi. \tag{50}$$

Making use of (49), we then obtain

$$\Gamma_5\Phi^{\mathrm{I}} = \Phi^{\mathrm{I}}, \;\; \Gamma_5\Phi^{\mathrm{II}} = -\,\Phi^{\mathrm{II}} \tag{51}$$

If we now also split Φ^{I} and Φ^{II} into parts by means of the relations* (52)

$$\begin{aligned} {}^1\!/_2\,(I - R_4)\,\Phi^{\mathrm{I}} &= \varphi^{\mathrm{I}}, & {}^1\!/_2\,(I + R_4)\,\Phi^{\mathrm{I}} &= \varphi^{\mathrm{I}'}, \\ {}^1\!/_2\,(I + R_4)\,\Phi^{\mathrm{II}} &= \varphi^{\mathrm{II}}, & {}^1\!/_2\,(I - R_4)\,\Phi^{\mathrm{II}} &= \varphi^{\mathrm{II}'}, \end{aligned}$$

we find that $\Gamma_5\varphi^{\mathrm{I}} = \varphi^{\mathrm{I}'}$ and $\Gamma_5\varphi^{\mathrm{II}} = -\,\varphi^{\mathrm{II}'}$. Therefore φ^{I}, φ^{II} are equivalent with $\varphi^{\mathrm{I}'}$, $\varphi^{\mathrm{II}'}$

We now express the wave equation in terms of φ^{I} and φ^{II}:

$$\begin{aligned} (-\,i/c\Gamma_4\Gamma_5\partial/\partial t + \vec{\Gamma}\,\nabla)\,\varphi^{\mathrm{I}} + \varphi^{\mathrm{II}} &= q^{\mathrm{II}}, \\ (+\,i/c\Gamma_4\Gamma_5\partial/\partial t + \vec{\Gamma}\,\nabla)\,\varphi^{\mathrm{II}} + k_0^2\varphi^{\mathrm{II}} &= q^{\mathrm{I}}. \end{aligned}$$

We multiply both equations by $\Gamma_4\Gamma_5$ and remember the properties of Γ_4 and Γ_5 when operating on φ^{I} and φ^{II}. We find finally (Γ_4 leads to an identical labelling of the components of φ^{I} and φ^{II})

$$i\,\square\,\varphi^{\mathrm{I}} + \varphi^{\mathrm{II}} = q^{\mathrm{II}}, \;\; i\,\square^*\,\varphi^{\mathrm{II}} + k_0^2\varphi^{\mathrm{I}} = q^{\mathrm{I}}, \tag{53}$$

where $\square = \partial/c\partial t + \vec{\gamma}\,\nabla$; $\overline{\square} = \partial/c\partial t - \vec{\gamma}\,\nabla$,

and $${}^1\!/_2\,\{\gamma_i\gamma_k\} - \delta_{ik}I = 0, \;\; \gamma_i\gamma_k = -\,i\gamma_l. \tag{54}$$

The three matrices γ_k are connected with the Dirac matrices in the Kramers representation[6] by the relations

$$\gamma_1 = \beta, \;\; \gamma_2 = \alpha_1\alpha_2\alpha_3\beta, \;\; \gamma_3 = \alpha_1\alpha_2\alpha_3. \tag{55}$$

Amongst the elements of the same irreducible representation of G_{16} there exist three more matrices which have the same properties as the γ_k, but commute with them; they are

$$\overline{\gamma}_1 = i\alpha_1\alpha_2, \;\; \overline{\gamma}_2 = i\alpha_2\alpha_3, \;\; \overline{\gamma}_3 = i\alpha_3\alpha_1. \tag{56}$$

By carrying out similar operations on the equations

$$(\overline{\Gamma}_\lambda\,\partial/\partial x_\lambda + k_0)\,\Psi = \overline{Q},$$

we can show that their reduction to a four-row notation gives the equations

$$i\,\overline{\square}\,\varphi^{\mathrm{I}} + \varphi^{\mathrm{II}} = \overline{q}^{\mathrm{II}}, \quad i\,\overline{\square}^*\,\varphi^{\mathrm{II}} + k_0^2\varphi^{\mathrm{I}} = \overline{q}^{\mathrm{I}}. \tag{57}$$

Both systems (53) and (57) are equivalent to the corresponding Klein equation by virtue of the identity

$$\square^*\,\square = \overline{\square}^*\,\overline{\square} = -\,\nabla^2 + \partial^2/c^2\,\partial t. \tag{58}$$

Besides the condition of mutual commutability, a connection between $\overline{\gamma}_k$ and γ_k can be established by means of the reflection operators $r_k = \overline{\gamma}_k\gamma_k$ (n.s.). The properties of the r_k are the usual ones, but unlike the situation in the case of the 16-dimensional representation, multiplication of the r_k does not take us out of the framework of the four quantities (I, r_k) because of the relations $\gamma_i\gamma_k = -\,i\gamma_l$, $\overline{\gamma}_i\overline{\gamma}_k = -\,i\overline{\gamma}_l$; Therefore

$$r_ir_k = r_l, \quad r_1r_2r_3 = I, \quad M_1 \doteq M_2. \tag{59}$$

The projection operators have the same properties as the corresponding operators in the 8-dimensional representation (see above).

The elimination of the (non-covariant) longitudinal components of φ^{I} and φ^{II} is done by means of the operator

$$\begin{aligned} T = T^n &= {}^1\!/_2\,(I - R) \\ &= \sum_{h=1}^{3} \gamma_h R \gamma_h = {}^1\!/_4\,(3 + M_1), \end{aligned} \tag{60}$$

which converts the anticommuting four-row matrices into three-row matrices of the three-dimensional irreducible representation of the Kemmer algebra:

$$T\gamma_kT = \beta_k, \tag{61}$$

$$\beta_i\beta_k\beta_l + \beta_l\beta_k\beta_i - \delta_{ik}\beta_l - \delta_{lk}\beta_i = 0.$$

Since the matrices γ_k satisfy, in addition, the relations $\beta_i\beta_k = -\,i\beta_l$, they can be transformed into Tamm matrices[7].

In this variant of the theory there is no possibility of a Larmor transformation, but here again the anticommuting matrices γ_k, $\overline{\gamma}_k$ may be expressed, similarly to (17) in terms of two orthogonal sets of matrices β_k:

---

* This division is already not covariant; for covariance one has to use the operator ${}^1\!/_2\,(I \pm R_L)$, cf. Sec. 3. The further conclusions remain, since $\{\Gamma_5R_L\} = 0$.

[6] H. A. Kramers, Proc. Roy. Acad. Amsterdam **40**, 814 (1937).

[7] I. Tamm, Dokl. Akad. Nauk SSSR **23**, 551, 1940.

$$\gamma_k = \beta_k + \beta'_k, \quad \bar{\gamma}_k = \beta_k - \beta_k. \tag{62}$$

It must be pointed out that the four-dimensional quantities of the type $A = A_0 + \vec{\gamma}\mathbf{A}$ are not real quaternions, similar to Hamilton's quaternions in three-dimensional space, because of the special treatment of the time. This is due to the pseudo-Euclidean character of the Minkowski world. For the same reason the result of the multiplication of the Cauchy-Riemann equations (53) is a hyperbolic equation.

In this way the present formulation of the theory may, with good justification, be called a pseudoquaternion theory, at least in the case of non-static fields.

CONCLUSIONS

1. There exist relations which make it possible to use anticommuting matrices, not only in the theory of mixtures of meson fields, but also for "pure" fields.
2. It is possible to replace the sixteen-dimensional reducible representation of the Dirac algebra by an eight-dimensional one.
3. One may use, as kinematic matrices of photon or vector meson theory, the reflection matrices of electron theory, γ_4, $\gamma_1\gamma_2\gamma_3$ and $\gamma_1\gamma_2\gamma_3\gamma_4$. The connection of these with the Tamm matrices has been found.

Translated by R. Peierls
59

SOVIET PHYSICS JETP VOLUME 3, NUMBER 2 SEPTEMBER, 1956

Interrelation between the Anisotropy of the Hall Effect and the Change in Resistance of Metals in a Magnetic Field. I.

Investigation of Zinc

E. S. Borovik
Physico-Technical Institute, Academy of Sciences, Ukranian SSSR

(Submitted to JETP editor January 15, 1955)
J. Exptl. Theoret. Phys. (U.S.S.R.) 30, 262-271 (1956)

The dependence of the resistance and the Hall effect for zinc on the magnitude of the angle between the axis of symmetry of the sixth order and the magnetic field is investigated for magnetic fields of up to 25,000 oersteds and for temperatures of 4 and 20 °K. The possibility of explaining the observed regularities within the framework of present day theory is considered.

INTRODUCTION

A VERY large anisotropy of the resistance in a magnetic field has been observed for a number of metals. The resistance of a single crystal in a transverse magnetic field may change by 15 to 30 times when it is turned about an axis parallel to the current. Such a strong anisotropy, observed for certain orientations of single crystals of gallium, zinc, cadmium and tin[1-5], is unexpected, since in the absence of a magnetic field the anisotropy in the conductivity is small--of the order of tenths of a percent.[6]

The strong anisotropy is manifested by the occurrence of deep narrow minima, which we may call "anomalous minima," in the resistance, as plotted against angle of rotation. The position of the crystal which corresponds to the appearance of such an anomalous minimum is distinguished, as a rule, not only by the magnitude of the resistance, but also by the character of the dependence of the resistance on the magnetic field. In large fields the dependence on the field is not found to be quadratic, but weaker, approximately linear.[2-5]

It has previously been shown[7-9] that the delayed growth of the resistance in a magnetic field is

---

[1] W. J. de Haas and J. W. Blom, Physica 2, 952 (1935).

[2] B. G. Lazarev, N.M. Nakhimovich and E. A. Parfenova, J. Exptl. Theoret. Phys. (U.S.S.R.) 9, 1169 (1939).

[3] E. Justi, J. Kramer and R. Schulze, Physik. Z. 41, 308 (1940).

[4] E. S. Borovik, Dokl. Akad. Nauk SSSR 69, 767 (1949).

[5] E. S. Borovik, J. Exptl. Theoret. Phys. (U.S.S.R.) 23, 91 (1952).

[6] Halis, *Collection of Physical Constants*, ONTI, Moscow-Leningrad, 1937.

[7] E. S. Borovik, J. Exptl. Theoret. Phys. (U.S.S.R.) 23, 83 (1952).

[8] E. S. Borovik, Dokl. Akad. Nauk SSSR 75, 639 (1950).

[9] E. S. Borovik, J. Exptl. Theoret. Phys. (U.S.S.R.) 27, 355 (1954).

connected with the influence of the large Hall field. We might expect that the delayed growth of the resistance for orientations corresponding to anomalous minima would also be connected with the influence of the Hall field. Hence an investigation of the anisotropy of the Hall effect and of its relation to the anisotropy of the resistance in a magnetic field was undertaken. Zinc, a metal with a large anisotropy in its resistance[2], was chosen as one of the first objects of the investigation.

The anisotropy in the Hall effect in zinc was investigated for the temperatures 300 and 78 ° K by Noskov[10] and Lazarev[11], and for the temperature 20°K by Logan and Marcus.[12] The Hall effect in zinc has been investigated[13] at temperatures down to 4°K for one orientation of a single crystal. A brief communication of our results on the investigation of the anisotropy of the Hall effect in zinc and tin at 4°K has been published.[14,15]

1. METHODS OF MEASUREMENT AND CHARACTERISTICS OF THE OBJECTS OF THE INVESTIGATION

In works on the investigation of the anisotropy in the Hall effect either the magnitude of the Hall field for directions of the magnetic field parallel to the principal directions of the crystal is investigated or else, if the crystal is turned during the measurements, only one of the components of the Hall field is measured.[10-12] These methods may be considered satisfactory in the region of small magnetic fields.

In the region of large magnetic fields the situation becomes more complex. In the case, for example of the variation of the resistance in a magnetic field, it is clear that it is quite insufficient to know the magnitude of the effect for the principal directions in order to determine it for an arbitrary direction. One might expect that a similar situation would occur for the Hall field.

In order to obtain complete information concerning the magnitude and direction of the electric field in a metal located in a magnetic field when a current is passed through it, it is in general necessary to measure all three components of this electric field, E_x, E_y, E_z. The Hall field, in accorddance with the mechanism by which it arises, must be perpendicular to the current but not necessarily perpendicular to the magnetic field. The components of the Hall field must change sign when the direction of the magnetic field is reversed. In order to measure both components (E_y and E_z) of the Hall field and the electric field (E_x) in the direction of the current, the following setup was used.

Using a cylindrically shaped sample, we mounted two pairs of electrodes on the surfaces cut perpendicular to the axis of the cylinder. The electrodes were placed approximately at the ends of two mutually perpendicular diameters of these cuts. With this arrangement, a measurement of the difference in potentials for the two pairs of electrodes permits the determination of both components of the transverse electric field. In order to determine the component, E_x, of the electric field parallel to the current, two more electrodes were mounted at distances of ~ 1/4 of the length of the crystal from its ends. The electrodes were made from thin wire (d=0.03-0.05 mm) and were attached by spot welding. The positions of the transverse electrodes were determined by measurements made while the crystal was rotated under a microscope.

The samples, placed in a cooling liquid, could be turned about their longitudinal axis, perpendicular to the magnetic field.

Later, when we had confirmed the obvious fact that for a direction of the magnetic field parallel to one of the principal directions of the crystal the Hall field perpendicular to the magnetic field was zero ($E_z = 0$), we used a more convenient electrical method of determining the positions of the Hall electrodes. If the pairs of Hall electrodes are situated approximately along mutually perpendicular principal directions in the crystal, then from the results of measurements of the difference in the Hall potentials for both pairs of electrodes and their possible combinations in pairs for two positions of the crystal, with the magnetic field parallel to a principal direction, we may easily find the position of the electrodes corresponding to the condition that $E_z = 0$.

The setting up of a magnetic field parallel to a principal direction was done in accordance with the magnitude of the resistance in the magnetic field. The great sharpness of the minima which occur on rotation easily allows the setting up of the required direction with an accuracy of as little as 20 min. The error in the magnitude of the Hall field on account of the inaccuracy in the determination of the position of the electrodes is 1-3%. Differences in the Hall potentials were measured by a low resistance potentiometer with a scale of 10^{-8} volt per division. Secondary effects were excluded by reversing the direction of the current in the sample and the direction of the magnetic field.

---

[10] M. M. Noskov, J. Exptl. Theoret. Phys. (U.S.S.R.) 8, 717 (1938).

[11] B. Lazarev, Nature 134, 139 (1934).

[12] J. K. Logan and J. A. Marcus, Phys. Rev. 88, 1234 (1952).

[13] E. S. Borovik, Dokl. Akad. Nauk SSSR 70,601 (1950).

[14] E. S. Borovik, Dokl. Akad. Nauk SSSR 95, 485 (1954).

[15] E. S. Borovik, Dopovidi A. N. URSR 4, 354 (1955).

The single crystal of Zn-10 which was investigated had the form of a cylinder of elliptical cross section with transverse dimensions of 0.9 and 1.00 mm and a length (between the potential leads) of 9 mm. The axis of symmetry of the sixth order was perpendicular to the longitudinal axis of the sample, while one of the binary axes was parallel to it. The deviation from the indicated directions of orientations was less than the error in the measurements. The accuracy of the determination of orientation was within 1-2°.

The following are the data for the dependence of the resistance of Zn-10 on the temperature:

T°K:	20.38	4.22	1.81
r_{0T}/r_{00}:	$6.06 \cdot 10^{-3}$	$5.30 \cdot 10^{-4}$	$5.16 \cdot 10^{-4}$

(r_{00} is the resistance for 0°C; r_{0T} is the resistance for the temperature of the experiment and for $H = 0$.)

2. RESULTS OF THE MEASUREMENTS

In the sample of Zn-10 the axis of symmetry of the sixth order was perpendicular to the longitudinal axis of the sample. If we direct the x axis along the longitudinal axis of the crystal, according to the direction of the current in it, then when the sample is turned about its longitudinal axis the axis of symmetry of the sixth order will turn in the y,z plane. We designate as ψ the angle between the axis of symmetry of the sixth order and the magnetic field directed along the z axis.

The conditions of the experiment for zinc in the investigated temperature interval correspond to the region of essential change in the resistance in a magnetic field. Hence we will characterize the Hall effect by the magnitudes E_y/E_x and E_z/E_x[10,13]. Figure 1 shows the dependence of these quantities on the angle ψ between the axis of symmetry of the sixth order and the magnetic field for $T = 4.22$° K and a field H = 20, 200 oersteds. The variation of E_y/E_x is shown by curve 1 and that of E_z/E_x by curve 2. Curve 3 of the same figure shows, for comparison, the variation in resistance. Curve 3 is similar to curves obtained in reference 2 for crystals of corresponding orientation.

The absolute magnitudes of the Hall field have sharp maxima for values of the angle ψ corresponding to the principal minima in the resistance, that is, for $\psi = 0$ and 90°, and a less sharply defined maximum for the secondary minimum in the resistance at $\psi = 55$°.

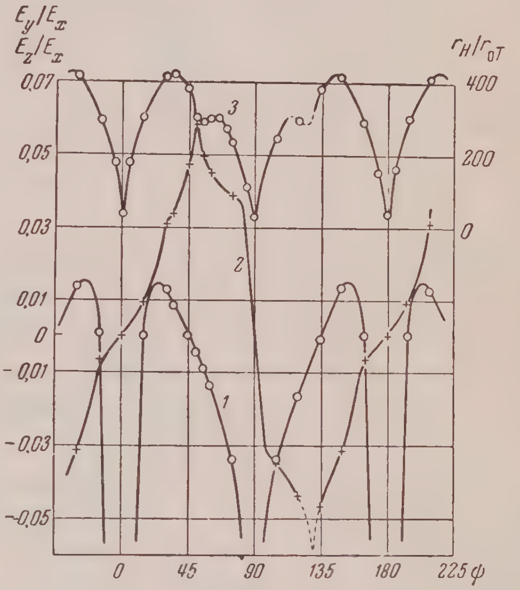

FIG. 1. Dependence of the Hall effect and the change in resistance on angle of rotation of the sample for Zn-10. ψ is the angle between the axis of symmetry of the sixth order and the direction of the magnetic field, $T = 4.22$ °K, $H = 20{,}200$ oersteds. Curve 1 gives E_y/E_x; Curve 2, E_z/E_x; curve 3, r_H/r_{0T}.

The Hall field vector is perpendicular to the direction of the magnetic field only when it is directed along one of the main crystallographic directions. The variation in the Hall field components E_y/E_x and E_z/E_x when the crystal is rotated is shown in Figs. 2 and 3 for a number of values of the magnetic field. Since the diagram for Zn-10 is sufficiently symmetrical (Fig. 1), we shall, in what follows, limit ourselves to a study of the interval in ψ lying between 0 and 90°.

It is curious to note that the Hall effect for a crystal with an axis of sixth order parallel to the current is positive down to helium temperatures, but for crystals with an orientation such as obtains in Zn-10 it is positive to $T = 20.4$° K[11,12]. For Zn-10 at $T = 4.22$ °K in a very high field (20, 200 oersteds) the magnitude of E_y/E_x is positive only in a narrow interval of angles ($\psi = 15$-45°). The magnitude of the Hall field for $\psi = 0$°, which is

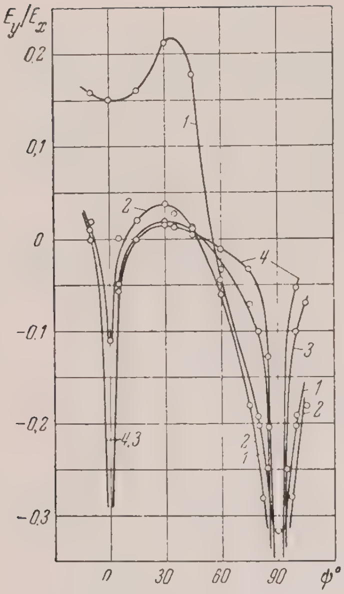

FIG. 2

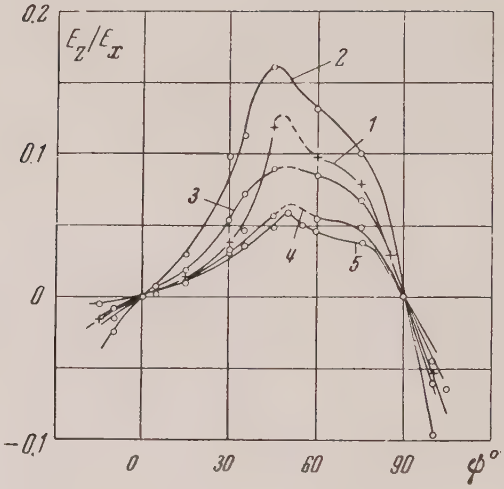

FIG. 3

FIG. 2. Dependence of the Hall field on angle of rotation for Zn-10. E_y/E_x for T=4.22 °K. Curve 1 is for H=2350, curve 2 for H=5000, curve 3 for H=9850, and curve 4 for H=15, 200 oersteds. At $\psi=0°$, $E_y/E_x=-0.465$ for curve 3 and $E_y/E_x=-0.56$ for curve 4. At $\psi=90°$, $E_y/E_x=-0.54$ for curve 2, $E_y/E_x=-0.575$ for cuve 3 and $E_y/E_x=-0.515$ for curve 4.

FIG. 3. Dependence of the Hall field on angle of rotation for Zn-10. E_z/E_x for T=4.22 °K. Curve 1 is for H=2350, 2 for H=5000, 3 for H=9850, 4 for H=15,200, and 5 for H=20,200 oersteds.

negative for high fields, first decreases rapidly in absolute value as the magnetic field is decreased, then changes sign and at $H=2350$ oersteds already has a rather large positive value. For $H=2350$ oersteds the magnitude of E_y/E_x is positive in the greater part of the angular interval.

The curves for the longitudinal component of the Hall field E_z/E_x (Fig. 3) give, as they should, zero values for directions of the magnetic field coinciding with the principal directions in the crystal: $\psi=0°$ and $\psi=90°$. The magnitude of E_z/E_x has a maximum in the region ψ=40-50°. As the magnitude of the magnetic field is decreased, the value of E_z/E_x for all orientations first increases, then passes through a maximum and begins to decrease.

The complex character of the dependence of the Hall field on the angle ψ shows that in a study of the anisotropy of the Hall effect in zinc we cannot limit ourselves to a study of the magnitude of the effect in the principal directions, but must obtain the entire picture of its variation with angle of rotation.

Diagrams showing the variation of the resistance of Zn-10 with angle of rotation in magnetic fields $H <$ 20,000 oersteds are presented in Fig. 4. The curves in Fig. 4 are similar to the curves obtained in Ref. 2 for crystals of the same orientation, but are distinguished from them by a rather greater value of the increase in the resistance, in conformity with the smaller value of the residual resistance of our sample.

Figure 5 shows the variation in the magnitude of the Hall effect and of the resistance with the angle ψ for Zn-10 at 20.38° K and H = 20,200 oersteds. Here E_y/E_x is positive for almost the entire angular interval and only becomes negative close to 90°. The conditions of the experiment from zinc at T = 20.4 °K still correspond to a region of essential increase in the resistance in a magnetic field ($\Delta r/r_{0T}$=2.5 -5). The character of the angular dependence of the Hall field is still sufficiently complicated that the study of the Hall effect cannot be limited to the principal directions.

The dependence of the Hall field and of the change in resistance in a magnetic field on the magnitude of the field is shown in Fig. 6 for T = 20.38 °K. The Hall field for $\psi=0°$ reaches its

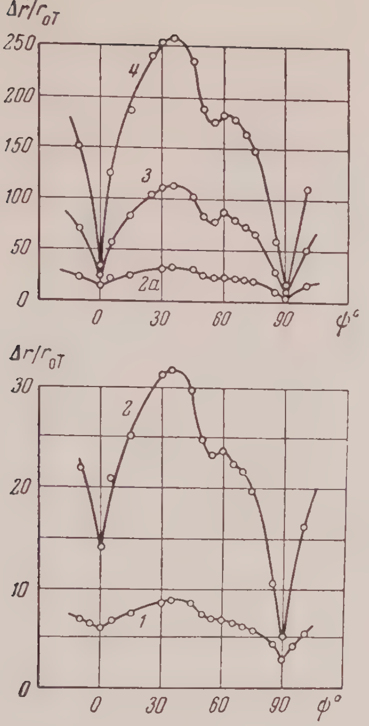

FIG. 4.

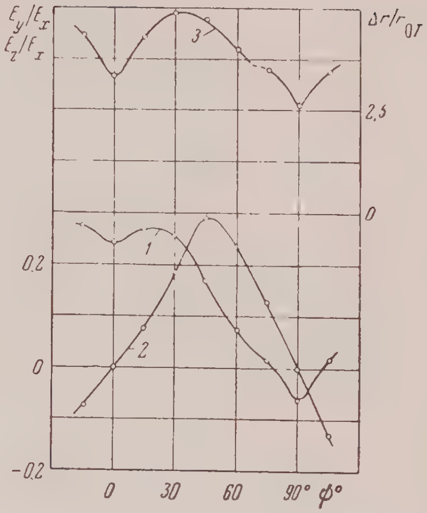

FIG. 5

FIG. 4. Dependence of the change in resistance of Zn-10 in a magnetic field on the angle of rotation. $T = 4.22\,°$ K. Curve 1 is for H=2350. 2 and 2a for H=5000, 3 for H = 9850 , and 4 for H = 15, 200 oersteds.

FIG. 5. Dependence of the Hall field and of the change in resistance on the angle of rotation for Zn-10. T=20.38 °K, H=20,200 oersteds. Curve 1 gives E_y/E_x, 2 gives E_z/E_x, and 3 gives $\Delta r/r_{0T}$.

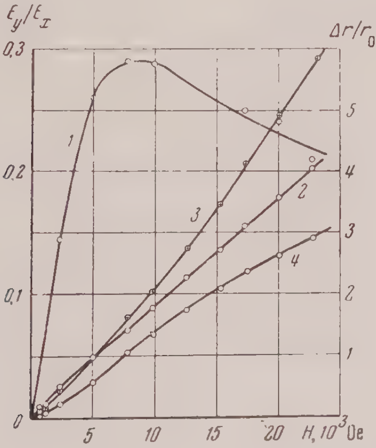

FIG. 6. Dependence of the Hall effect and of the change in resistance on the magnitude of the magnetic field for Zn-10 at 20.38 °K. Curve 1 gives E_y/E_x for ψ=0°, 2 gives $\Delta r/r_{0T}$ for ψ=0°, 3 gives $\Delta r/r_{0T}$ for ψ=35° 4 gives $\Delta r/r_{0T}$ for ψ= 90°.

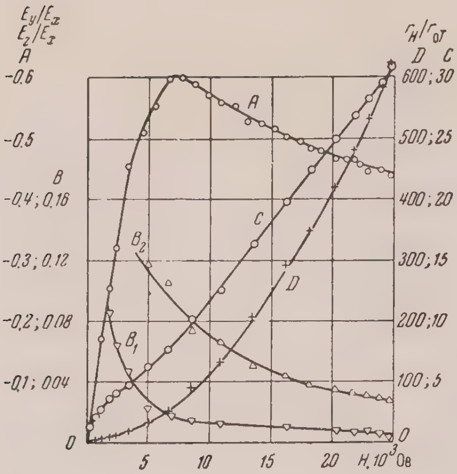

FIG. 7. Dependence of the magnitude of the Hall field and of the change in resistance on the magnitude of the magnetic field for Zn-10 at $T = 4.22$ °K, Curve A gives E_y / E_x for $\psi = 90°$, B_1 gives E_y / E_x for $\psi = 35°$, B_2 gives E_z / E_x for $\psi = 35°$, C gives r_H / r_{0T} for $\psi = 90°$, D gives r_H / r_{0T} for $\psi = 35°$. The scales for the curves are designated by the same letters.

maximum value $E_y / E_x = 0.29$ for $H \approx 9000$ oersteds. The values measured for $\psi = 90°$ had a large error and were not put on the graph. For $\psi = 90°$ the Hall field changes sign at $H \approx 9 \times 10^3$ oersteds and becomes positive at small fields, so that for small fields the magnitude of $E_y / E_x > 0$ for all values of the angle ψ. The crossing of curves 3 and 2 of Fig. 6 at $H \approx 5000$ oersteds is also noteworthy. It indicates that the minimum at $\psi = 90°$ on the diagram showing the variation of resistance with angle of rotation in a magnetic field disappears for $H < 5000$ oersteds.

Figure 7 shows the dependence of the magnitude of the Hall field and of the change in the resistance on the magnitude of the magnetic field for $T = 4.22°$ K and for two values of the angle ψ. For an orientation of the hexagonal axes of the crystal perpendicular to the field ($\psi = 90°$) the curve for the Hall field (curve A in Fig. 7) has the maximum which is typical of metals having equal numbers of holes and electrons.[15] At its maximum E_y / E_x has a large magnitude ($E_y / E_x \approx 0.6$), and after the maximum the Hall field falls slowly. The curve showing the variation of the resistance in a magnetic field is linear at large fields (curve c in Fig. 7).

For $\psi = 35°$, corresponding to the maximum in the plot of resistance *versus* angle of rotation (Fig.1), the magnitude of the Hall field is characteristically much smaller. Cf. curves B_1 and B_2 of Fig. 7, in which we observe only the decreasing portion of the curve after the maximum, this maximum lying somewhere in the region of small fields. The curve for the change in resistance is almost quadratic. In a field of 25,000 oersteds the resistance is increased by more than 600 times its magnitude in the absence of field and exceeds by more than 20 times the value of the resistance at the same field for $\psi = 90°$.

Figure 8 gives the results obtained for $\psi = 0°$ (hexagonal axis parallel to the magnetic field) for temperatures of 4.22 and 1.81 °K. The curves for the change in resistance (curves 3 and 4) are similar to the curves obtained in references 2 and 16; the irregularities are obviously connected with quantum oscillations which occur at the particular values of the field involved. These quantum oscillations are most noticeable on the curves for the Hall field (curves 1 and 2). Just as for $\psi = 90°$, the absolute magnitude of the Hall field is large (the maximum observed values of $E_y / E_x \approx 0.8$) and in the region of fields investigated E_y / E_x increases steadily with field. The change in sign of the Hall field at $H = 3600$ oersteds is noteworthy.

Figure 8 also gives, for comparison, the dependence of the magnetic susceptibility on the field (curves 5 and 6), according to results obtained in references 17 and 18. Although there is not complete correspondence between the oscillations in

---

[16] N. M. Nakhimovich, J. Exptl. Theoret. Phys. (U.S.S.R.) 12, 539 (1942).

[17] J. A. Marcus, Phys. Rev. 76, 413 (1949).

[18] B. I. Verkin, Dokl. Akad. Nauk SSSR 81, 529 (1951).

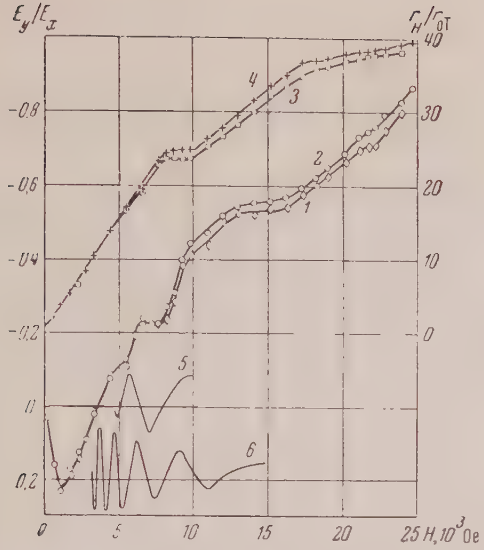

FIG. 8. Dependence of the magnitude of the Hall field and of the change in resistance on the magnitude of the magnetic field for Zn-10. $\psi=0°$. Curve 1 gives E_y/E_x for $T=1.81$, 2 gives E_y/E_x for $T=4.22$, 3 gives r_H/r_{0T} for $T=1.81$, 4 gives r_H/r_{0T} for $T=4.22$ °K; 5 is the curve of the magnetic susceptibility χ for $\psi=0°$ at $T=14$ °K[17]; 6 is the curve of the difference of the principal susceptibilities for $T=4.22$ °K.[18]

the two curves, the periods of the oscillations in the curves for the Hall field and for the magnetic susceptibility are quite the same in order of magnitude. Results involving quantum oscillations have been discussed in previous communications.[15]

3. DISCUSSION OF RESULTS

The results obtained indicate that for zinc, just as for tin,[14] the minima in the resistance correspond to increased values of the Hall field. However, these increased values of the Hall field cannot completely explain the slow increase in resistance in a magnetic field for $\psi=0°$ and $\psi=90°$, since, for example, for $\psi=90°$, the slow increase in resistance in a magnetic field continues even after E_y/E_x has passed through a maximum and has begun to decrease.

We shall try to explain, at least qualitatively, the connection between the electronic structure of the metal and the character of the diagrams showing the variation of properties with angle of rotation (Figs. 1 through 5).

A model in which account was taken of the anisotropy of the effective mass for the electrons in the upper energy zone has already been considered in the early works of Blochinzev and Nordheim[19] and Kontorova and Frenkel'[20]; the mass of the holes was considered isotropic. A much more general consideration of the question of the effect of the anisotropy on galvanometric phenomena in metals with overlapping Brillouin zones has been given in an article by Dimitriev[21]; unfortunately the author came to the mistaken conclusion that the phenomenon of saturation should be observed for all metals. The question in which we are interested, that of the anomalous minima and, in general, of the form of the diagrams showing the variation of properties with angle of rotation, has not been treated in the literature.

In considering a metal in which the overlapping of zones is small and the number of electrons in the upper zone is small, it is expedient to consider separately in the upper zone groups of electrons the excited members of which lie close to each pair of opposite surfaces of the polyhedron bounding the first zone. Of course, such a division of the electrons into groups is possible only if the Fermi surface is cut into separate isolated sections by the polyhedron bounding the first zone, that is, if the number of holes as well as electrons is small.

If the binding of the electrons in the lattice may be considered weak, then for such a separate group the components of the reciprocal mass tensor for directions parallel to the bounding surface of the zone must be only slightly different from the free electron values $1/m_0$. The component of the reciprocal mass tensor for the direction perpendicular to the bounding surface $h^{-2}\,\partial^2 E/\partial k_z^2$ must be larger, and the corresponding component of the effective mass $m_z{}^*$ must be smaller, than the free electron mass. It is clear that if the condition of weak binding is not observed, we may still consider as true in the general case the statement that the effective mass for acceleration in a direction perpendicular to the surface of discontinuity in the energy must, for such individual groups of electrons, be smaller than in other directions. A decrease in the value of the effective mass also obtains for holes situated near the surface of discontinuity in the energy. However, in their case the value of the effective mass grows very quickly with distance from the surface of discontinuity and, in the case of weak binding, may become substantially greater than the free electron mass even at a fairly small distance from this surface. Hence we may expect an especially large anisotropy of the effective mass for holes.

---

[19] D. Blokhintsev and L. Nordheim, Z. Physik **84**, 168 (1933).

[20] T. A. Kontorova and Ia. I. Frenkel', J. Exptl. Theoret. Phys. (U.S.S.R.) **11**, 666 (1941).

[21] V. A. Dimitriev, J. Exptl. Theoret. Phys. (U.S.S.R.) **20**, 1019 (1950).

Under experimental conditions of very low temperature, when we are in the region where the resistance is almost independent of temperature, the electron distribution is determined mainly by alterations of the lattice due to impurities. In this case we may with sufficient accuracy consider the probability of collision of an electron with the lattice as isotropic, independent of the electron's direction or movement. If the average time between collisions is isotropic, then we may generalize the formulas given in Refs. 19 and 20 and consider the general case with certain groups of electrons with anisotropic effective masses. However, as is clear from the work of Dimitriev,[21] these general formulas will be of only limited applicability. On the other hand, in the present state of the theory excessive detailization might seem premature. Hence we limit ourselves to the particular cases which we need.

Let us consider the properties of a metal which has one group of holes with concentration n_1 and one group of electrons in the upper zone with concentration n_2. We suppose that our coordinate axes are chosen directed along the principal axes of the tensor $\frac{1}{h^2}\frac{\partial^2 E(\mathbf{k})}{\partial k_2 \partial k_1}$. The current flows along the x axis, and the magnetic field is parallel to the z axis ($H = H_z$). We designate the magnitudes of the effective masses for the holes by μ_{ii} and for the electrons by m_{ii} ($i = 1,2,3$). The average time between collisions we call τ_1 for the holes and τ_2 for the electrons. Then in the absence of the magnetic field the electric conductivity is

$$\sigma_{0T} = \frac{n_1 e^2 \tau_1}{\mu_{11}} + \frac{n_2 e^2 \tau_2}{m_{11}} = \sigma'_{11} + \sigma''_{11}. \tag{1}$$

The electric conductivity in the magnetic field is

$$\sigma_H = \frac{\sigma'_{11}}{1+\varphi_1^2} + \frac{\sigma''_{11}}{1+\varphi_2^2} + \left(\frac{\sigma'_{22}}{1+\varphi_1^2} + \frac{\sigma''_{22}}{1+\varphi_2^2}\right)\left(\frac{E_y}{E_x}\right)^2 \tag{2}$$

and the Hall field, from the condition $j_y = 0$, is

$$\frac{E_y}{E_x} = \frac{n_1\varphi_1^2/(1+\varphi_1^2) - n_2\varphi_2^2/(1+\varphi_2^2)}{n_1\sqrt{\mu_{11}/\mu_{22}}\,\varphi_1/(1+\varphi_1^2) + n_2\sqrt{m_{11}/m_{22}}\,\varphi_2/(1+\varphi_2^2)}, \tag{3}$$

where $\sigma'_{11} = n_1 e^2 \tau_1/\mu_{11}$ and $\sigma''_{11} = n_2 e^2 \tau_2 / m_{11}$ are the electric conductivities in the direction of the x axis, with σ'_{11} depending on the holes and σ''_{11} depending on the electrons, while $\sigma'_{22} = n_1 e^2 \tau_1/\mu_{22}$; and $\sigma''_{22} = n_2 e^2 \tau_2 / m_{22}$ are the corresponding conductivities in the direction of the y axis. Here

$$\varphi_1 = eH\tau_1 / c\sqrt{\mu_{11}\mu_{22}}; \tag{4}$$

$$\varphi_2 = eH\tau_2 / c\sqrt{m_{11}m_{22}}.$$

Formulas (1) through (4) are not very different from the formulas for the isotropic model.

The effective magnitude of the magnetic field, which is determined by the dimensionless variables φ depends on the geometric mean of the effective masses for the directions x and y.

If the principal directions of the reciprocal effective mass tensor do not coincide with the chosen coordinate axes, a z-component of the electric field will occur, and the expressions will become notably more complicated. Although we have not determined the exact form of these expressions, we may make some general remarks.

From what has been seen above, the solutions of the equations of motion must contain periodic terms, functions of dimensionless parameters φ' and φ'', of the type of the magnitudes φ_1 and φ_2 introduced in (4). These magnitudes φ' and φ'' must now also be contained in the non-diagonal components of the reciprocal effective mass tensor. The magnitudes φ', φ'' characterize the effective magnitude of the magnetic field. In the general case of arbitrary direction of coordinate axes, it follows from considerations of symmetry and dimensionality that

$$\sigma_H = \frac{\sigma'_{11}}{1+(\varphi')^2} + \frac{\sigma''_{11}}{1+(\varphi'')^2} + \left(\frac{\sigma'_{22}}{1+(\varphi')^2} + \frac{\sigma''_{22}}{1+(\varphi'')^2}\right)\left(\frac{E_y}{E_x}\right)^2 + \left(\frac{\sigma'_{33}}{1+(\varphi')^2} + \frac{\sigma''_{33}}{1+(\varphi'')^2}\right)\left(\frac{E_z}{E_x}\right)^2, \tag{5}$$

where the magnitudes φ' and $\varphi'' \sim eH\tau/c$ go over into φ_1 and φ_2, which were introduced in (4), when the coordinate axes coincide with the principal directions of the reciprocal effective mass tensor.

It should be noted that for orientations of magnetic field and current coinciding with the principal directions of the effective mass tensor, the geometrical average of the effective masses in a direction perpendicular to the surface of discontinuity in the energy will enter into the magnitude φ. If the conclusion that the effective mass in a direction perpendicular to the surface of discontinuity in the energy should be less than in other directions is correct, then for a direction of the magnetic field perpendicular to the boundary of the zone, $\sqrt{m_{11}m_{22}}$ will have a maximum value in comparison with orientations of the field parallel to other principal directions. The magnitude of the effective value for this direction will be less than for other directions, and the increase in resistance in the magnetic field will also be less.

In the general case of several groups of electrons and holes a sum of terms similar to those introduced in (5), each of which will correspond to a single group of holes or electrons, will enter into the expression for σ_H. We will have a minimum on the diagram showing change in resistance in the magnetic field *versus* angle of rotation each time one of the surfaces of the polyhedron of the first zone becomes perpendicular to the field. The minima will be obtained only for those surfaces which intersect the Fermi surface. These qualitative observations give a picture which corresponds in general to the experimental rules for the change in resistance in a magnetic field formulated in Refs. 5 and 14, and to the results obtained here for zinc. An exact comparison with the results of experiment is made difficult by the fact that because of the behavior of the remaining groups the position of the minimum in the resistance may be displaced and field-dependent. Metals which have a very complicated structure in their angular-dependence diagrams, with a great number of minima (Sn, Ga) have a complex crystalline cell and the form of their energy zones has not been calculated.

This explanation seems to be contradicted to a certain extent by the disappearance of most of the minima in the angular-dependence diagrams at low fields.

With respect to the Hall effect, it follows from the indicated considerations only that for points of minimum resistance E_y / E_x will have an extreme value, but it is impossible to say whether it will be a maximum or a minimum, since the Hall field is determined by a difference in terms corresponding to the behavior of groups of electrons and holes.

We limit ourselves here to just these qualitative indications as to the possibility of theoretical explanation of the experimental results.

CONCLUSIONS

As a result of this investigation of the interrelation between the anisotropy of the Hall effect and the change in resistance in a magnetic field, it has been established that the minimum in the plot of resistance *versus* angle of rotation corresponds to a maximum in the Hall field. It is shown that for zinc at $T \leq 20\,^\circ$K it is impossible to derive complete information about the Hall effect from measurements of its magnitude made only for the principal crystallographic directions, and that it is necessary to study the complete variation with angle of rotation. By qualitative consideration of the properties of a zone model for a metal, the Fermi surface of which intersects the polyhedron bounding the Brillouin zone, it is shown that this model can explain the experimentally observed form of the angular-dependence diagrams.

In conclusion the author expresses his thanks to Professor B. G. Lazarev for his interest in the work and to V. I. Sharonov for help in the measurements.

Translated by M. G. Gibbons
49

SOVIET PHYSICS JETP VOLUME 3, NUMBER 2 SEPTEMBER, 1956

Probe Studies of Rarefied Flames

V. I. TVERDOKHLEBOV
Dnepropetrovsk Mining Institute

(Submitted to JETP editor, January 3, 1955)
J. Exptl. Theoret. Phys. (U.S.S.R.) 30, 252-255 (February, 1956)

We have investigated the changes in the probe current in relation to the location of the probe within a rarefied flame. An assumption is introduced pertaining to the mechanism of ionization in the reaction zone of a flame.

Physicists are interested in two phenomena taking place within flames--radiation and ionization. Spectrum investigations have given us means for studying a large number of molecules, atoms, and radicals present in flames, and also allowed us to gain an understanding of some elementary processes taking place in a flame. Ionization of flames is less thoroughly understood. For the investigation of this phenomenon we have employed the method devised and described by J. J. Thomson and G. P. Thomson[1], and by H. A. Wilson.[2] Andrew, Axford, and Sugden,[3] and later Shuler and Weber[4] have developed a new method based on the measurement of the damping of ultrashort radio waves passing through the flames. All the investigations of flame ionization have been carried out at atmospheric pressure. Only recently, Rossikhin, Protopopov, Martyniuk and Tsikora[5] investigated electrical conductivity of a non-stationary flame under the pressure of 200-400 mm Hg, while Jost and Wagner[6] have studied ionization of a cold flame under the pressure of 200-700 mm Hg.

In our present work we have investigated electrical properties of flames under pressures of 30-50 mm Hg by means of a probe similar to that used by Heumann[7] in his studies of flames burning under atmospheric pressure.

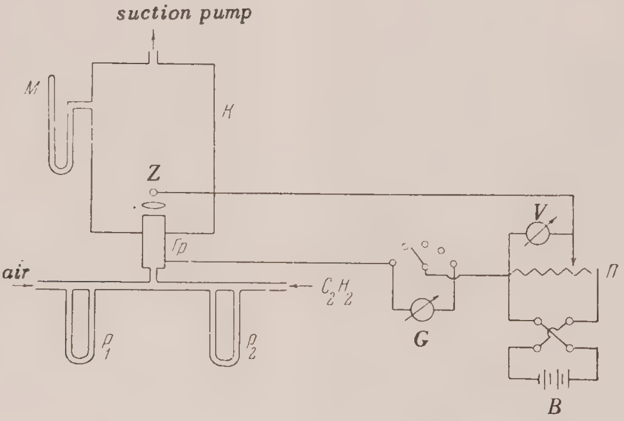

FIG. 1. Schematic drawing of the apparatus: *K*-camera of burning, *M*-manometer, P_1 P_2 -rheostats, *Z*-probe, *V*-voltmeter, *G*-galvanometer, *B*-batteries.

Figure 1 shows the schematic drawing of the apparatus; camera of combustion is cylindrical in shape and is made of 3 mm thick iron. Its diameter is 30 cm, and its height 40 cm. The metallic hearth is covered by a removable copper lid coated with nickel. The lid contains several openings of

---

[1] J. J. Thomson and G. P. Thomson, *Conduction of Electricity through Gases*. 3rd ed., Cambridge, 1928.

[2] H. A. Wilson, Revs. Mod. Phys. 3, 156 (1931); *Modern Physics*, Blackie, 1944.

[3] E. R. Andrew, D. W. E. Axford, And T. M. Sugden, Trans. Farad. Soc., 44, 427 (1948).

[4] K. E. Shuler and J.Weber, J. Chem. Phys., 22, 491 (1954).

[5] S. Rossikhin, A. K. Protopopov, L. A. Martyniuk and I. L. Tsikora, Nauchn. Zap. Dnepropetrovsk Mining Institute, 41, 9 (1953).

[6] W. Jost and H. G. Wagner, Naturwiss 40, 435(1953).

[7] T. Heumann, Spectrochimica Acta. 1, 293 (1940).

2 mm diameter. The inflammable mixture is ignited by means of an induction coil. We have investigated the inflammable mixture of C_2H_2 and air, with the volumetric concentration of the former, $c = 7$ per cent. The rarefied flame may be divided into three parts: the bright-green part in the shape of a disc with a diameter of 40 mm and thickness of 5-7 mm (this part is known as the zone of reaction); the part between the zone of reaction and the surface of the hearth; and the region above the zone of reaction. The last has a barely visible violet tinge.

The probe, which was in the form of a platinum sphere of 0.95 mm diameter, was moved along the height of the flame, and its location was fixed by means of a viewing tube. The system of the probe and the hearth was subjected to a current of known intensity.

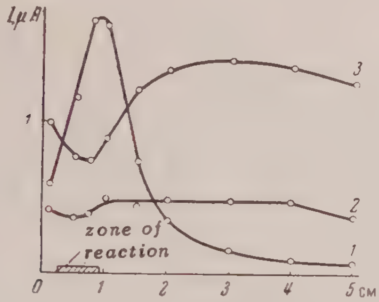

FIG. 2. Dependence of the probe current on the position of the probe in the C_2H_2-air flame burning at a pressure of 30mm Hg

Figure 2 shows the curves which depict the relationship of the current to the location of the probe.* Curve 1 was produced at the probe potential $V_1 = -5V$, curve 2 at the potential $V_2 = 0$, curve 3 at the potential $V_3 = +5$ V. The flame was burning under the pressure of 30 mm Hg. Investigation of the curves indicates that the maximum current in case of a negative probe occurs at the zone of reaction, and that it does not coincide with the maxima of the positive and the zero probe; for the latter two the maxima lie above the zone of reaction. Diffusional flow of electrons and negative ions onto the zero probe invariably produces a stream of positive ions.

Figure 3 shows curves which depict the relationship of the current to the location of the probe under the pressure of $p = 50$ mm Hg, with all other conditions remaining unaltered. Comparison of

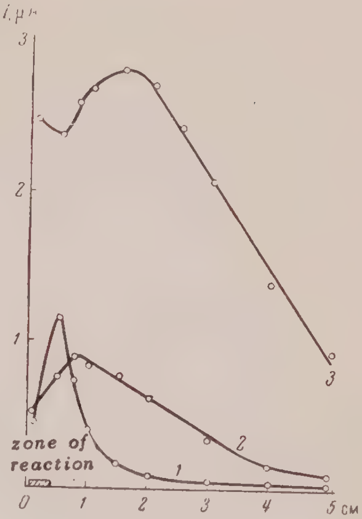

FIG. 3. Dependence of the probe current on the position of the probe in the C_2H_2-air flame burning at a pressure of 50 mm Hg

Figs. 2 and 3 shows that: 1) with the increase of pressure the current on the negative probe diminishes; 2) as the pressure mounts higher the current on the positive probe increases pronouncedly while the current on the zero probe increases less markedly; 3) the distance between the maxima of currents on the negative, the positive, and the zero probes diminishes with the increase of pressure.

This experimental material can be explained if we accept the assumptions listed below.

1. Formation of the positive and the negative electrons takes place in the zone of reaction. The most plausible reaction leading to the formation of the positive and the negative ions appears to be

$$M + \mathrm{OH}' \rightarrow M \ + \mathrm{OH}^-, \tag{1}$$

where M represents carbohydrogen molecules or radicals of the type C_nH_m and C_n, with a considerable store of inner energy; OH' represents excited hydroxyl. Potential of excitation of the band OH $\lambda = 3064$ is equal to 4 ev; for the other bands of OH, potentials of excitation were quite high. According to the data obtained by Smith and Sugden,[8] electronic affinity of OH is equal to 3 ev. Carbohydrogen molecules and radicals present in the zone of reaction are known to have ionization potentials of 8 to 12 ev. It should be noted that, according to the rule, radicals have ionization potentials smaller than the ionization potentials of the corresponding molecules. For this reason the energy reaction (1) becomes acceptable.

---

*Current of curve 1 is opposite in direction to the currents of cuves 2 and 3.

[8] H. Smith and T. M. Sugden, Proc. Roy. Soc. A211, 31 (1952).

2. Ion-radical OH enters the reaction fairly rapidly, and produces a more complex molecule containing an extra electron,

$$M_1 + OH^- \rightarrow M_1OH^- \quad (2)$$

or else produces free electrons

$$M_1 + OH^- \rightarrow M_1OH + e. \quad (3)$$

3. Positive ions are formed in response to the process of polymerization, as a result of which particles with diameters of the order of 100-500 Å can be produced. Figures 2 and 3 show that the stream of positive ions flowing onto the probe diminishes sharply after the departure from the zone of reaction. This is caused by the diminution of mobility of the positive ions.

This analysis of the experimental data can be countered by the following possible processes: 1) thermoelectronic emission from the probe, 2) thermoeffect produced in the electric circuit, 3) photoeffect, 4) exothermal reactions originating on the surface of the probe, 5) removal of the conduction electrons from the surface of the probe by the excited particles.

A thermocouple introduced into the rarefied flame gives a temperature reading of ~ 1000° K. The probe placed in this flame assumes the same temperature. Under this condition the current of thermoelectronic emission off the probe is smaller by several orders than the current observed.

Thermoeffect on the electric circuit has also no conspicuous influence on the probe current; this has been proven by the work of Heumann[7] who has studied various interferences in detail.

The probes were made of material in which work of emission is high and which is consequently characterized by a short limiting wavelength of the photoeffect. For example, the limiting wavelength for platinum is $\lambda_0 = 1900$ Å, and for nickel $\lambda_0 = 2490$ Å. The reducing part of the flame's rays falls within the visible region and is near the ultraviolet; for this reason the photoeffect plays no great part in our work.

Any important influence exercised by the exothermal reactions on the probe current is eliminated by the fact that with the increase of pressure, the current on the negative probe diminishes.

The most conspicuous influence can be produced by the excited radicals, atoms and molecules. In the first place such an influence could be exercised by the excited hydroxyl. When the molecules or atoms of a negatively charged gas collide with a metallic surface, the removal of an electron and formation of a negative ion is quite possible. To have this process accomplished it is necessary to satisfy the condition

$$E_c + E_B \geqslant \varphi, \quad (4)$$

where E_c is the affinity of the particle for an electron, E_B is the energy of excitation, φ is the work function for the metallic surface. For most metals the latter is of the order of 4--5 ev. For this reason condition (4) for the excited hydroxyl is fulfilled. While dealing with experimental data we should take into consideration the possibility of the process of removing the electrons from the probe by the excited hydroxyl.

A layer of gas forms around a probe placed in the flames. Excited particles are not produced in this layer. If the thickness, l, of this layer satisfies the condition $l > r\lambda$, the removal of the electrons from the probe by the excited particles does not take place (λ represents the mean free path of the gas molecules, r the number of collisions necessary for the deactivation of an excited particle). According to the data of Gaydon and Wolfhard,[9] r= 40--100 for the excited hydroxyl.

On the bases of these deductions the current on the negative probe should diminish with the dimunition of pressure, which fact was indeed observed in our experiment. However, the inspection of curves on Figs. 2 and 3 shows that the process of removal of the electrons is not of paramount importance. If this process were of stronger influence than the others, then the current on the zero probe would have the direction opposite to that observed in the experiment.

In conclusion we would like to express our deep gratitude to V. S. Rossikhin for his valuable help in this work.

---

[9] A. G. Gaydon and H. G. Wolfhard, Proc. Roy. Soc. (London) A194, 169 (1948); A208, 63 (1951).

Translated by R. G. Huzarski
47

SOVIET PHYSICS JETP VOLUME 3, NUMBER 2 SEPTEMBER, 1956

Paramagnetic Resonance in Anthracite and Other Carbonaceous Substances

N. S. GARIF'IANOV AND B. M. KOZYREV
Physico-Technical Institute, Kazan' Branch, Academy of Sciences, U.S.S.R.

(Submitted to JETP editor January 18, 1955)
J. Exptl. Theoret. Phys. (U.S.S.R.) 30, 272-276 (February, 1956)

Paramagnetic resonance was measured in a number of substances containing free carbon. The measurements were carried out at 295° and 90° K at the frequencies 9450, 536.76 176.1 and 20 mc.

IN 1953 Castle[1] detected paramagnetic resonance in thin layers of graphite. In 1954 a number of investigators[2-5] established that paramagnetic resonance is present in certain other forms of carbon (in activated wood charcoal, charred organic substances). We undertook to investigate various types of coal, organic tars and certain other substances containing free carbon.

1. Procedure

A block diagram of the installation is shown in Fig. 1. High frequency vibrations were produced by a klystron generator which was fed by a stabilized source of current. The frequency of the generator was measured by a wave meter with an accuracy of ± 0.03%. The high frequency power of the generator was controlled by a thermistor bridge. The high frequency signal from the generator was introduced to the resonance cavity through an attenuator (5-10 db). After the signal emerged from the cavity it was rectified, amplified, and finally introduced to the vertical plates of an oscillograph. In the different measurements two types of amplifiers were used: 1) a narrow band amplifier at 400 cycles for observing the maxima of the curves $X''=X''(H)$ and 2) a broad band amplifier for observing the overall shape of the curves $X''=X''(H)$

The specimen of the substance under investigation was placed into the resonance cavity, which was located between the poles of the electromagnet producing the static magnetic field H of a strength up to 10000 oersteds. The magnetic field was modulated by coils wound on the pole pieces of the electromagnet. The modulations coils were fed by a 50 cycle current from the line circuit (during broad band amplification) or a 200 cycle current from a sonic frequency generator (during narrow band amplification). The amplitude of modulation was kept strictly constant during the experiment. During narrow band amplification, values from 0.1 to 50 oersteds could be assigned to it and during broad band amplification values from 0.5 to 700 oersteds. The modulated current was introduced through a phase changer to the horizontal plates of an oscillograph. The determination of the H^* values was carried out by proton resonance. For this purpose a generator was used the frequency of which could be varied gradually from 10 to 20 mc. The measuring coil of the proton generator, containing an ampoule with a weak aqueous solution of $MnCl_2$ (0.01 mole / l) was placed in the field of the electromagnet, directly under the resonance cavity. The uniformity of the static magnetic field was such that when the measuring coil containing the solution of $MnCl_2$ was placed into that position in the field which (during measurements) was occupied by the specimen of the substance under investigation, there was hardly any change in the picture of the proton resonance on the screen of the oscillograph. Proton resonance was registered by the method of Zavoiskii from the changes in the anode current.[6] By means of successive switching it was possible to obtain signals on the screen of the oscillograph from the three centimeter generator and from the proton generator. The amplitude of modulation in the measurements of proton resonance had the value 0.2 oersted. For a value of field $H=H^*$; corresponding to electron resonance, the frequency of the proton generator was changed until such time when no proton resonance line appeared on the screen of the oscillograph.

The frequency, corresponding to proton resonance, at a given value of H^*, was measured by a heterodyne wave meter with an accuracy up to 0.1%. It is this value which mainly determines the accuracy of the experiment. The calibration of the magnetic

---

[1] J. G. Castle, Phys. Rev., 92, 1063 (1953).

[2] J. G. Castle, Phys. Rev., 95, 846 (1954).

[3] F. R. Henning, B. Smaller and E. L. Yasaitis, Phys. Rev. 95, 1088 (1954).

[4] D. J. E. Ingram and J. E. Bennett, Phil. Mag. 45, 545 (1954).

[5] D. J. E. Ingram and J. M. Tapley, Phil Mag., 45, 1221 (1954).

[6] E. K. Zavoiskii, Dissertation, Phys. Inst., Academy of Sciences, 1944.

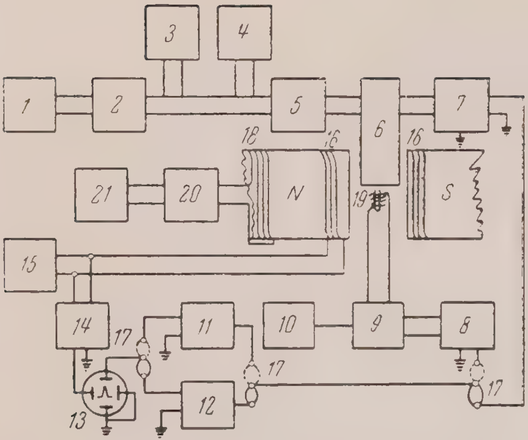

FIG. 1. Block diagram of the high frequency apparatus. *1*-stabilized power of supply, *2*-klystron generator, *3*-wave meter, *4*-power control, *5*-attenuator, *6*-resonance cavity, *7*-crystal detector, *8*-stabilized power supply, *9*-generator of proton resonance, *10*-heterodyne wave meter, *11*-narrow band amplifier, *12*-wide band amplifier, *13*-oscillograph, *14*-phase changer, *15*-audio frequency generator, *16*-modulation windings of the electromagnet, *17*-change-over switches, *18*-electromagnet windings, *19*-measuring coil of the proton generator, *20*-apparatus for the field strength H of the electromagnet, *21*-source of supply for the electromagnet.

field during broad band amplification was carried out by the luminous modulation of the oscillograph tube.

The measurements at the frequencies 536.71 and 176.1 mc were carried out by the Zavoiskii method of the grid current.[6] The grid current of the appropriate generator was connected to the input of the narrow band amplifier instead of the current from the detector of the three centimeter installation. The calibration of the magnetic field in this case was carried out by the free radical α,α-diphenyl-β-trinitrophenylhydrazyl, the g-factor of which was determined at the frequency 9450 mc by means of proton resonance and found to equal 2.004 ± 0.002, which is in agreement with the measurements of other authors.[7]

The width of line in the free radical, determined at the frequency of 9450 mc, was found to equal 2 ± 0.5 oersteds, which is in agreement with the data of Chu et al.[7] The absorption curve of the free radical obtained at the frequency 9450 mc is given in Fig. 2a.

2. Measurements of paramagnetic resonance in anthracite

An easily measurable effect with a very narrow resonance line was found in the anthracite specimens. The shape of the absorption curves was found to be strongly dependent on the form of the specimens and on the frequency of the oscillating magnetic field.

The photographs of the signals observed on the screen of the oscillograph by the method of broad band amplification at 9450 mc are shown in Fig. 2. The anthracite specimens had equal areas 11.3 x 4.4 mm and differed in the thickness ($2d$). For the specimen b the thickness $2d = 0.25$ mm, for $c = 0.5$ mm, for d $= 0.8$ mm, for $e = 1$ mm and for $f = 2$ mm.

The specimens were located on the bottom of the resonator with the long axis along the magnetic lines of force. They were insulated from the metallic bottom of the cavity with parchment. The characteristic distortion of the shape of the absorption line, which was observed in the thicker specimens and which becomes almost unnoticeable in the samples with the thickness of $2d \leq 0.25$ mm, finds an explanation in the considerable electroconductivity of the anthracite. The effect of the electroconductivity on the shape of the line of magnetic absorption was theoretically analyzed by Bloembergen.[8]

For an infinite flat conducting plate he found that in the limiting case, when the depth of penetration of the field into the plate $\delta \gg d$, the magnetic losses should be proportional to $1 + 2\pi(X'+X'')$. In the other limiting case, when $\delta >> d$, the magnetic losses should be the same as in semiconductors.

A qualitatively experimental substantiation of the effect of conductivity on the shape of the absorption line was obtained by Bloembergen by comparing the curves of the derivative of the coefficient of paramagnetic absorption, produced by the Cu^{63} nuclei in metallic copper when taken as a fine powder. Our experiments represent one of the first verifications of the effect of conductivity in electronic paramagnetics.

As is evident from curve b (Fig. 2), at a thickness of plate $2d \leq 0.25$ mm the influence of X' on the effective absorption coefficient is negligible. As d increases, the part of X' in the absorption effect increases and at $2d \geq 2$ mm it becomes sharply predominating, since the shape of curve f practically coincides with the predicted shape for $X'(H)$.

Thus the effective coefficient of absorption X''_{eff} in anthracite can be expressed as $A(d)X'+X''$, where the numerical coefficient $A(d) \ll 1$ when $\delta > d$ and $A(d) \gg 1$ when $\delta < d$. The discrepancy

---

[7] T. L. Chu, E. Pake, D. E. Paul, J. Tawsend and S. I. Weissman, J. Phys. Chem. 57, 504 (1953).

[8] N. Bloembergen, J. Appl. Phys. 23, 1383 (1952).

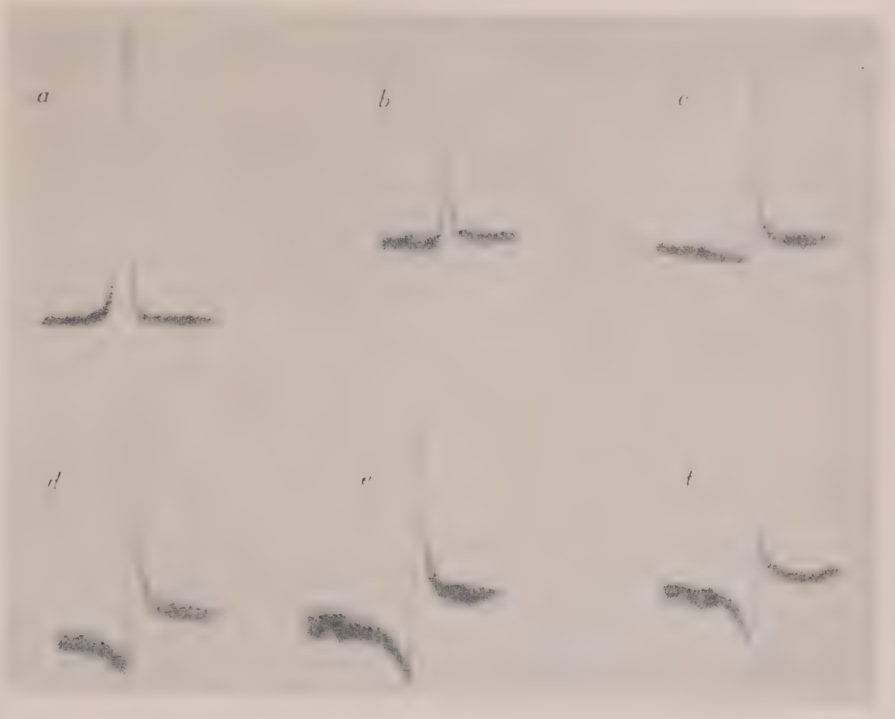

FIG. 2.

in the result we obtained and the Bloembergen formula for the latter case is not surprising, since in our experiments with the thick specimens the thickness of the plate was commensurable with the linear dimensions of its area.

At the lower frequencies, the distortion in the shape of the absorption line in anthracite becomes much less noticeable owing to the increase in the depth of penetration δ. It was possible to observe this distortion in the thick cylindrical specimen (diameter 8 mm) at the frequency $\nu = 536$ mc. The same specimen at the frequencies 176 and 20 mc gave the ordinary curve $X'' = X''(H)$.

The effective *g*-factor of the absorption line in anthracite was determined on the specimen *b* by the method of proton resonance at the frequency 9450 mc. It was found to equal 2.004 ± 0.002.

The measurement of the width of the absorption line* ΔH in anthracite was carried out at the frequency 9450 mc in the specimen *b*, as well as at the frequencies 176 and 20 mc. The width was determined by comparing with the line resulting from the free radical. It was found that for anthracite the value $\Delta H = 0.7$ oersted over the entire range of frequencies investigated. The relative error in the determination of ΔH did not exceed 20%, (The absolute value of ΔH cannot claim to such accuracy owing to the possible error in the determination of ΔH for the free radical)

The fact that the width of the line in anthracite is independent of frequency shows that the main share of the effect cannot be ascribed to the electrons of the conductivity, since in graphite, in accord with Refs. 1,2, the width of line varies from 40 oersteds at $\nu = 9000$ mc to 0.1 oersted in the region of radio frequencies.

Thus, either the free radicals or the "broken bonds" between the carbon atoms can be responsible for the effect. A substantiation of this statement is given by the experiment with the anthracite which was finely pulverized in an agate mortar. When the pulverization is carried out in the presence of air, the effect is greatly diminished and in a short time (10-15 min.) it cannot be observed at all. When, however, the pulverization of the anthracite in the mortar is carried out under a layer of liquid, preventing oxidization, then the effect continues to be observed for a long time. Twenty four hours later it can still be measured; however, the absorption curve has broadened considerably. After anthracite had been heated to a temperature of red heat and then allowed to cool to room temperature, the effect disappears completely.

At the temperature of liquid oxygen the effect in anthracite increases by approximately 3 times as compared with its value at room temperature; moreover, the width of the absorption curve remains unchanged. This can also be observed in the free radical, the susceptibility of which obeys the Curie law.

---

* By width of line we mean the distance in oersteds between the points, corresponding to an intensity of the effect equal to one half the maximum intensity.

On the basis of all of the results given above, one can consider that it has been established that either the free radicals present in the anthracite or the ‘‘broken bonds’’ are responsible for the effect observed in anthracite. Evidently, between the paramagnetic particles in anthracite there exist very strong exchange interactions.

3. Measurements of paramagnetic resonance in other substances

We have also observed paramagnetic resonance in a number of other substances containing carbon: coal, freshly prepared wood charcoal, petroleum asphalt, carbolite and black rubber. Of the substances named, the most intense effect was observed in petroleum asphalt and in carbolite. At 90° K a weak effect $g \approx 2$ was found in specimens of petroleum from Bavlinskii region (Tartariia).

The effective g-factor for all of the substances mentioned was found to equal 2.004 ± 0.002. It was established that, upon cooling to the temperature of liquid air, the intensity of the effect in all cases increases by approximately 3 times, in the free radical as well as in the anthracite. No distortion of any kind in the shape of line was observed in the above substances. The width of lines was measured at the frequency 9450 mc by comparing with the free radical. The widths of lines obtained for the substances investigated are given below (in oersteds):

1. Coal (gaseous)	4.4 ± 0.5
2. Freshly prepared wood charcoal	4.8 ± 0.5
3. Petroleum Asphalt	4.3 ± 0.5
4. Carbolite	3.8 ± 0.5
5. Black Rubber	11 ± 2

Thus the substances we studied can be subdivided into 3 types differing in width of line. Anthracite belongs to the first type having the narrowest curve (0.7 oersted). To the second type belong the substances 1-4 given in the Table above; in these the width of lines is equal, within the limits of experimental error, and on the average it is approximately 4.4 oersted. Finally, black rubber belongs to the third group of substances having the broadest curve.

The agreement in the value of the g-factors and identical temperature dependence of the intensity of the effect make plausible the assumption that in all cases the free radicals or the ‘‘broken bonds’’ between the carbon atoms are responsible for the effect.

In conclusion the authors wish to express their deep gratitude to Academician A. E. Arbuzov and to F. G. Valitova for the preparation of the substance ∝ ∝ -diphenyl- β - trinitrophenylhydrazyl, which made it possible to carry out easily quantitative determinations of the width of lines in the substances investigated.

Translated by E. Rabkin
50

SOVIET PHYSICS JETP VOLUME 3, NUMBER 2 SEPTEMBER, 1956

Some Hydrodynamical Phenomena Accompanying the Passage of a Current Through Insulating Liquids

Ġ. A. Ostroumov
Molotov State University

(Submitted to JETP editor, March 1, 1955)
J. Exptl. Theoret. Phys. (U.S.S.R.) 30, 282-286 (February, 1956)

Experiments are described, conducted with turpentine, benzene, nitrobenzene, benzine and transformer oil, which indicate that in a strong, almost homogeneous electric field these liquids are set into motion, independent of the sign of the applied voltage.

SOME theoretical considerations[1] lead to the conclusion that electro-insulating liquids in a sufficiently strong electric field cannot be at rest. The usual methods of study of the motion of a liquid are difficult to apply for the observation of the hydrodynamical phenomena arising here. In particular, the mixing of colored additives inevitably changes the dielectric permeability of the electro-conductivity of the separate parts of the liquid and hence disturbs its homogeneity. Therefore, other phenomena, as for example, electroconductive convection[2], will be admixed with the phenomenon under investigation. The addition of light-scattering particles leads to the occurrence of cataphoresis as a masking action, and so must also be excluded.

free as far as possible from the indicated deficiencies, and controlled, so that the method, at least in principle, would record just the process under investigation.

After numerous trials, the goal was succesfully attained by the combination of an optical method of high sensitivity[3] and the introduction into the liquid of a negligible (as far as possible) thermal nonuniformity. The vessel (Fig. 1), with dimensions 95 x 100 x 38 mm, has a metallic bottom and two metallic side walls. The front and back walls are of plane-parallel glass. An aluminum electrode in the form of an upside down umbrella with a maximum diameter of 50 mm is lowered into the vessel. This electrode is provided with a heater consisting of several tens of turns of enameled constantan wire, indicated in the figure by dots. The heater resistance is 12.6 ohms. The vessel is half filled with the liquid being studied, and is placed in the path of a beam of light in a partially shaded mounting with a grating. The source of light is represented by a horizontal slit, with dimensions 0.7 x 11 mm, on which is focussed the filament of an incandescent lamp for an alloscope. The collimator has a focal length of 140 cm, and an objective diameter of 95 mm. The parallel rays leaving the collimator traverse the vessel and continue further through an objective with a diameter of 110 mm and a focal length of 165 cm. A grating with horizontal rods is placed in the focal plane of this objective. There are 12 rods, 1.281 ± 0.003 mm in diameter, 38 mm long, and separated by 2.95 ± 0.05 mm between their axes. A telescope with a focal length of 35 cm and with a Ramsden ocular was placed behind the grating. The vessel, which is translucent throughout, can be observed visually and photographed through the telescope and grating. The exposure time required for film with a sensitivity of 90 units GOST was of the order of 0.5 sec. The location of the grating was controlled in such a way that in the absence of the process, the liquid appeared dark.

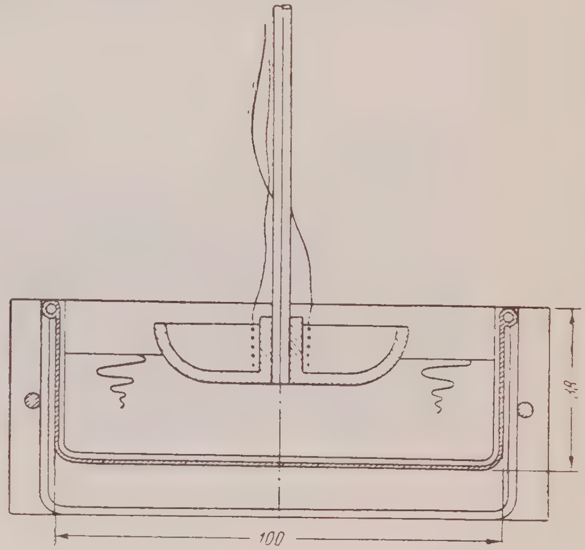

FIG. 1. Section of the model vessel

When the electrode is heated, a temperature gradient arises in the liquid, the field becomes clear

---

[1] G. A. Ostroumov, J. Tech. Phys. (U.S.S.R.) 24, 1916 (1954), Sec. IV, Eq. (18).

[2] G. A. Ostroumov, J. Exptl. Theoret. Phys. (U.S.S.R.) 29, 529 (1955); Soviet Phys. 2, 428 (1956).

[3] G. A. Ostroumov, J. Tech. Phys. (U.S.S.R.) 24, 2045 (1954).

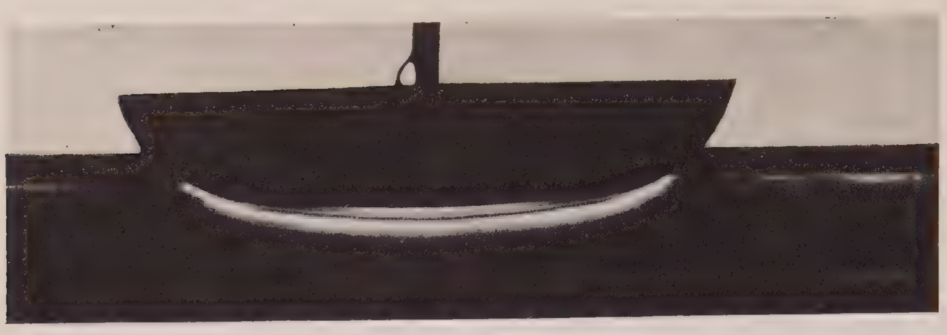

FIG. 2. Photograph of the initial stage of heating of the electrode, without high voltage

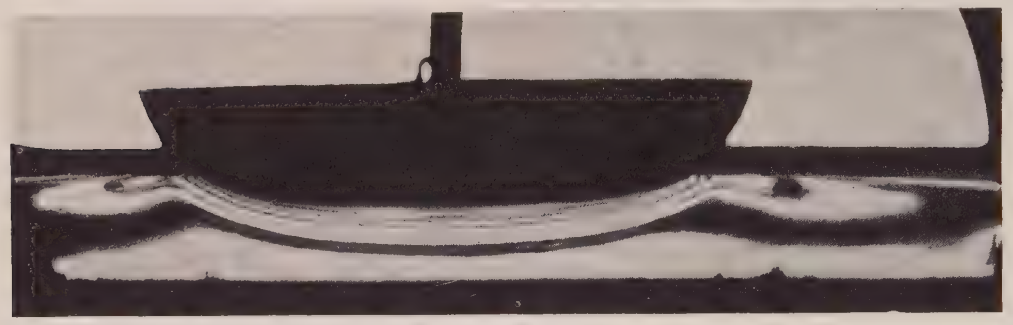

FIG. 3. Photograph of the final stage of heating of the electrode, without high voltage. Heating power, 0.2 W.

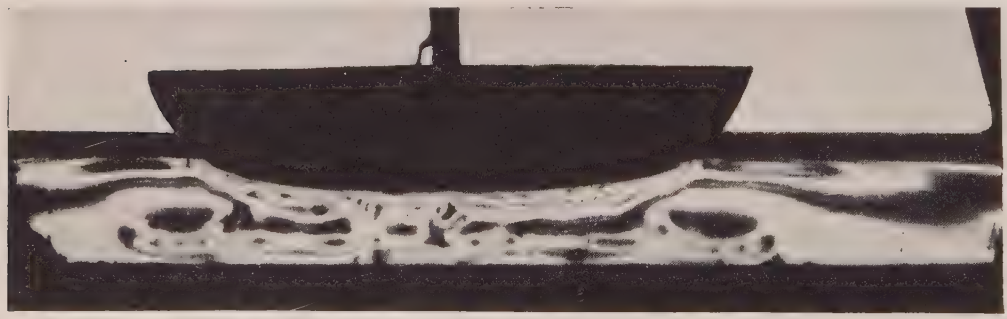

FIG. 4. Heating power, 0.2 W. High voltage around 3000 V.

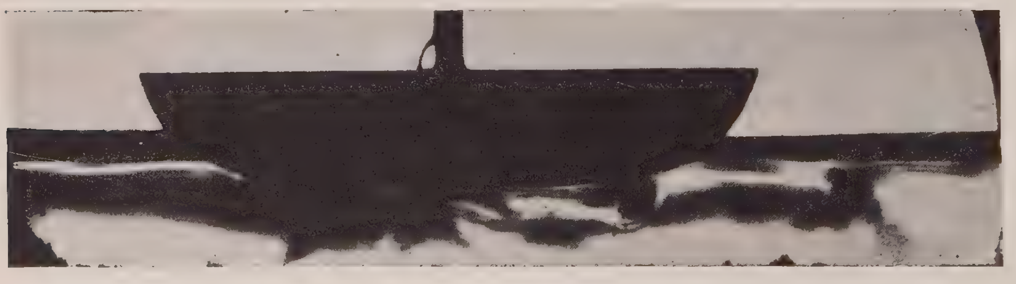

FIG. 5. Heater switched off. High voltage around 3000 V.

in certain places, and thermal convection begins. Figure 2 is a picture corresponding to an initial stage of heating of the electrode in turpentine. Fig. 3 represents the final stage of heating, the power expended being 0.20 w.

If a constant voltage of the order of several hundred volts is now applied between the electrode and the bottom of the vessel, the stable picture will be markedly distorted, as reflected in Fig. 4. The dark and light streaks move rapidly, and vigorously change their configuration, disclosing an intensive hydrodynamic process. The most vigorous motion is noticeable under the central part of the electrode.

The motion in general gives the impression of being irregular; however, certain peculiar details are noticed. In particular, through the motion of certain dust particles (the rest of the dust sticks to the electrode) it is possible to follow the general circulation of the liquid--from the free surface it constricts towards the upper electrode, generally sinks downward under it, spreads along the bottom, and rises to the surface again along the walls. The direction of this motion does not depend on the sign of the applied voltage. The intensity of the motion did not appear to depend on the sign of the applied voltage. However, the intensity of the motion of course increased with increased voltage. This general motion is comparatively slow, but it is still more rapid than the convective thermal motion which could be noticed during the heating of the electrode in the absence of the field, and which was exactly in the opposite direction.

In the course of not many seconds after the switching off of the high voltage, the normal picture of thermal convection is re-established (see Fig. 3). This lapse of time is in good agreement with the magnitude of the thermal conductivity of turpentine--8 10^{-4} $cm^2/sec.$[4] The re-establishment is the resolution of thermal nonuniformities, caused by the hydrodynamic process.

It might have been expected that with the heater switched off and with a sufficiently large voltage, conduction current and Joule heating of the liquid would occur, leading to approximately the same effect of thermal convection as with a warm heater: the greatest heating being obtained under the electrode, the warmed liquid would rise upwards and spread under the free surface. Actually, things take place otherwise: large, irregular regions of translucence of the field of view in the liquid arise, move about, and fade away (Fig. 5), voltage around 3000v). The motes disclose an irregular mixing of the liquid generally in the same direction as described above (see Fig. 4). Hence, it may be concluded that the electrical causes of the motion of the liquid are far stronger than the gravitational effects associated with uneven heating, and in general are directed opposite to the latter.

If a variable voltage at industrial frequency is applied to the electrode, the change in the picture of thermal convection (Fig. 3) is scarcely noticeable, the motion of the motes being slightly less regular. At large voltages hydrodynamic effects were noticed, produced by the quivering of motes with one end adhering to the electrode and oriented along the field, and also by the phenomenon of "electric wind" (in a liquid!) arising in the neighborhood of the ends of some motes. Sometimes these motes undergo an amusing boring motion of an astonishingly large velocity (many tens of revolutions per second).

These effects were also observed in certain other liquids, not subjected to any special purification.

Benzene has a very large specific resistance (therefore the conduction current is extremely small). It is set into intensive motion at small voltages. This motion is readily observed with a hot as well as with a cold electrode.

An enormous current, 3 ma at 600 v, flows through nitrobenzene (in contrast with benzene). With a hot electrode, electrical convection develops mainly around the electrode, and is very intensive. With a cold electrode it spreads through the entire thickness of the liquid. With a cold electrode, the general direction of flow coincides with the direction of purely thermal convection (and not the reverse as with turpentine and benzene). Thanks to the large number of motes not adhering to the electrodes, the hydrodynamic motion in the space between the electrodes is readily traced,--it calls to mind the Benar cell. Through the motion of motes, which skip between the electrodes, one may readily observe how the motes that become charged by contact with one electrode tear away from it, not getting as far as the other electrode, giving up their charge to the liquid, and in time coming to a standstill.

In aviation benzine, the same effects are noted as in benzine or turpentine, but especially clearly seen is the rotary motion of the adhering motes. In transformer oil, in consequence of its large viscosity, the hydrodynamic effects are slowed down considerably, and the thermal effects are somewhat accelerated. In ethyl alcohol, in view of its comparatively large electro-conductivity, the hydrodynamic effects are different, and merit separate investigation.

It is evident from the above-mentioned photographs that in many places the dark stripes are cut by narrow light lines, and conversely. This indicates that the phenomenon of optical diffraction is taking place. Through this effect we can estimate the sensitivity of the method, used with photography. Let us assume that in some region of the photographed model, its optical thickness varies according to the law

$$nS = a_0 + a_1 y + a_2 y^2. \qquad (1)$$

where y denotes a vertical coordinate on the model. Then the region around $y=0$ is projected on the zeroth rod of the grating, the region around $y=y_1$ is projected on the first rod of the grating, the region around $y=y_2$ --on the second, and so on. The zeroth of these regions will be distinguished in that for it, $(d(nS)/dy)_0 \approx 0$, the first in that for it, $(d(nS)/dy)_1 \approx d/p$, the second in that $(d(nS)/dy)_2 \approx 2d/p$, and so forth.

Each of these regions will be registered on the picture by dark stripes with light spaces between them. The smallest angular distance between neighboring stripes, still providing sharpness of the stripes, is obtained thus:[3]

$$(y_2 - y_1)/p \qquad (2)$$

$$= (y_1 - y_0)/p = x/f = \lambda/d.$$

where p is the distance from the model to the grating, f is the focal distance of the camera, x is the distance between the rods of the grating, and λ is the wavelength of light in the cavity of the camera. Writing explicitly the three relations presupposed by Eq. (1), we find,

$$y_0 = 0;$$

$$(d(nS)/dy)_1 = a_1 + 2a_2 y_1 = d/p; \qquad y_1 = (d/p - a_1)/2a_2;$$

$$(d(nS)/dy)_2 = a_1 + 2a_2 y_2 = 2d/p; \qquad y_2 = (2d/p - a_1)/2a_2.$$

Hence the distance between stripes is

$$y_1 - y_0 = (d/p - a_1)/2a_2; \quad y_2 - y_1 = d/2pa_2.$$

The stripes will be equi-distant if $a_1 = 0$. Then taking account of Eq. (2), $\Delta y \equiv y_2 - y_1 = y_1 - y_0 = d/2a_2 p = \lambda p/d$. Hence $a_2 = \lambda/2(\Delta y)^2$. Setting this in Eq. (1), we find for the first stripe

$$(nS)_1 - (nS)_0 = a_2 y_1^2 = \lambda/2. \qquad (3)$$

For the second stripe

$$(nS)_2 - (nS)_0 = a_2 y_2^2 = 2\lambda$$

and so forth. Hence it is evident that in our case, when the sharpness of the stripes already suffers from diffraction, the first dark stripe after the initial zeroth darkening corresponds to a path difference through the model of less than half a wavelength.

According to the Lorentz-Lorenz formula for the square of the index of refraction, we find for small changes of the temperature around $t=0$.

$$\frac{n^2-1}{n^2+2} = A\rho_0(1 - \alpha t); \qquad (4)$$

$$\frac{dn}{dt} = -\frac{(n^2+2)(n^2-1)}{6n}\alpha.$$

For the first stripe according to Eq. (3), and taking into account that $n_1 < n_0$,

$$(n_1 - n_0)S = -\Delta n S = -(dn/dt)S\Delta t = \lambda/2,$$

or, according to Eq. (4),

$$\Delta t = -\frac{\lambda}{2S(dn/dt)} = \frac{3\lambda n}{S(n^2+2)(n^2-1)\alpha}.$$

The geometrical length of the path of a beam of light between the electrodes can be estimated by the diameter of the electrode, $S=5$ cm. For turpentine,[4] the index of refraction is $n=1.47$ and the thermal coefficient of expansion is $\alpha = 0.94 \times 10^{-3}$ deg.$^{-1}$ Hence the first dark stripe corresponds to a mean temperature rise of $\Delta t = 0.98 \times 10^{-2}$ degree along the ray. This estimate illustrates the sensitivity of the applied optical method. It forces us to believe that the intense hydrodynamic process observed could not be due to such a small temperature gradient. This is not that process in strongly non-uniform fields which was studied earlier in gases and is now investigated in liquids.[5] It should be expected that this process is conditioned not only by some inhomogeneity of the field, but also by peculiarities of the electric field in mobile

---

[4] D. Kei and T. Lebi, *Handbook of Experimental Physics*, IIL, Moscow, 1949.

[5] H. Senftleben and E. Bultmann, Physik Z. 136, 389 (1953).

(fluid) imperfect (conducting) dielectrics.

In this connection it should be expected that the molecular nature and chemical composition of the liquid does not play a decisive role here. This process must take place not only in pure liquids, but also in mixtures and solutions. The only requirement is that there be no evident phase division (a solution must not be turbid or opalescent). By this token, this investigation should be demarcated from the investigation of the passage of current through pure liquids where all of the effects can be accounted for by the molecular composition and degree of purity of the given chemical substance.[6,7] On the other hand, the investigated effect is demarcated also from those specific effects where a many-phase liquid plays the essential role, for example, cataphoresis or electromagnetophoretic effects.[8]

---

[6] A. Nikuradse, Z. Physik 34, 97 (1933).

[7] E. Schmidt u. W. Leidenfrost, Forsch. Geb. Ing. 19, 65 (1953).

[8] A. Kolin, J. Appl. Phys. 25, 1065, (1954).

Translated by D. Lieberman
52

SOVIET PHYSICS JETP VOLUME 3, NUMBER 2 SEPTEMBER, 1956

Application of the Theory of Stochastic Processes to the Investigation of Nuclear Fission

L. PAL
Budapest

(Submitted to JETP editor, December 23, 1954)
J. Exptl. Theoret. Phys. (U.S.S.R.) 30, 367-373 (February, 1956)

The statistical theory of the ionization chamber is considered for the investigation of nuclear fission. The mean number of pulses produced by the ∝ particle background is determined. A theory of random processes is developed in connection with the investigation of this stochastic process.

IN the construction of ionization chambers for the study of fission processes, the problem of excluding (or at least minimizing) the ionizing action of ∝-particles occupies a central place. The energy of the fission fragments can vary within wide limits, but their mean energy, in each case, is an order of magnitude larger than the energy of the ∝-particles. However, the superposition of pulses from several ∝-particles can create a pulse which is comparable with those from the fragments. The pulses are recorded as a pulse which is created by the fission fragments; therefore, it is necessary to give at least an approximate estimate of the number of such cases.

The problem of the correction of the number of fissions was considered by Rossi and Staub.[1] Under the assumption that the pulses have rectangular shape and duration τ, they determined the number of readings per unit time which contained unwanted pulses of ∝-particles. For practical purposes, their formula is satisfied only approximately, since in most cases the pulses have an exponential shape. The purpose of the present research was to consider the effect of the exponential shape on the number of readings.

1. Let $H(x)$ be the probability that the amplitude of the pulse produced by the ∝-particles be less than x. For simplicity, we assume that the number of pulses satisfies a Poisson distribution.* If N is the pulse density and $R(x,t)$ is the probability that the sum of pulses produced by the ∝-particles in the time interval $(0,t)$ is less than x at the time t, one can easily convince oneself that $R(x,t+\Delta t)$ is composed of the probabilities of two mutually incompatible events, as follows:

1) either the sum of pulses is less than $xe^{\Delta t/\tau}$ at time t, and no new pulse appears in the time interval $(t,t+\Delta t)$,

2) or, the sum of pulses is less than $(x-y)e^{\Delta t/\tau}$ at the time t and a new pulse appears in the time interval $(t,t+\Delta t)$ with amplitude lying in the interval $(y,y+dy)$. It is evident ** that

$$R(x,t+\Delta t)=(1-N\Delta t)\,R(xe^{\Delta t/\tau},t) \quad (1)$$

$$+N\Delta t\int_0^x R[(x-y)e^{\Delta t/\tau},t]\,dH(y)+o(\Delta t).$$

It follows from Eq. (1) that

$$\frac{\partial R}{\partial t}=\frac{x}{\tau}\frac{\partial R}{\partial x} \quad (2)$$

$$+N\left\{\int_0^x R(x-y,t)\,dH(y)-R(x,t)\right\}$$

If $\lim R(x,t)\to R(x)$ as $t\to\infty$, then the following relation results from Eq. (2):

$$\frac{x}{\tau}\frac{dR}{dx} \quad (3)$$

$$=N\left\{R(x)-\int_0^x R(x-y)\,dH(y)\right\}$$

By virtue of the independence of the pulses of ∝-particles from the pulses of fission fragments, the distribution function of the sum of pulses of fission fragments $S(x)$ is defined in similar fashion by the equation

$$\frac{x}{\tau}\frac{dS}{dx}=M\left\{S(x)-\int_0^x S(x-y)\,dK(y)\right\}, \quad (4)$$

where $K(y)$ is the pulse amplitude distribution function and M is the pulse density. Knowing the distribution functions $R(x)$ and $S(x)$, we can determine the distribution function $P(x)$ of the output voltage of the ionization chamber:

$$P(x)=\int_0^x R(x-y)\,dS(y). \quad (5)$$

---

*It is shown in Appendix A that these results are easily generalized to the case of certain non-Markovian processes. A similar generalization has been given by Takacs.[2]

[1] B. B. Rossi and H. H. Staub, *Ionization Chambers and Counters*, New York, 1949.

[2] L. Takacs, MTA III, Oszt. Közlemenyei. 4, 473 (1954).

**The probability that more than one pulse appears in the time interval $(t, t+\Delta t$ is equal to $o(\Delta t)$.

We denote by V the recording level of the discriminator which follows the ionization chamber. If the voltage at the input of the discriminator increases above the recording level V, this fact is recorded as a "nuclear fission". Naturally, in this case we also count those pulses which are connected with the superposition of pulses from α-particles. We denote by Q_1 the density of pure fissions and by Q_2 the density of pulses connected with the superposition of pulses from α-particles. It is evident that the number of readings Q is equal to $Q_1 + Q_2$. The quantities Q_1 and Q_2 are determined by the following expressions:

$$Q_1 = M \int_0^V \{1 - K(y)\}\, dP(V - y); \tag{6}$$

$$Q_2 = N \int_0^V \{1 - H(y)\}\, dP(V - y). \tag{7}$$

By appropriate choice of the recording level V and other parameters, one can also bring about the condition that $Q_1 \gg Q_2$.

2. Let us choose the amplitude distribution function of the α-particles in the following form:

$$H(x) = 1 - e^{-ax}, \tag{8}$$

where $1/a$ is the mean value of the amplitude of the pulses. Since the ionizing effects of the fission fragments are cancelled out, we obtain the following expression for the distribution function $K(x)$:

$$K(x) = b \int_0^x \{1 - e^{-a(x-y)}\}\, e^{-by} dy, \tag{9}$$

where $2b^{-1}$ is the mean value of the amplitude of the pulses of fission fragments. Making use of Eq. (8), we get from Eq. (3):

$$d \ln \bar{r}(z) / dz = - N\tau (z + a)^{-1}, \tag{10}$$

where
$$r(z) = \int_0^\infty e^{-zx} dR(x).$$

We then obtain immediately

$$\bar{r}(z) = a^{N\tau} (z + a)^{-N\tau}. \tag{11}$$

The original function $r(x)$ is defined in elementary fashion:

$$r(x) = a e^{-ax} (ax)^{N\tau - 1} / \Gamma(N\tau), \tag{12}$$

and the distribution function $R(x)$ has the form:

$$R(x) = \Gamma(ax, N\tau) / \Gamma(N\tau), \tag{13}$$

where $\Gamma(ax, N\tau)$ is the so called incomplete gamma function.

The function $s(x)$ is defined in similar fashion. It is easy to show that $s(z)$ satisfies the following equation:

$$d \ln \bar{s}(z) / dz = - M\tau \{(z + b)^{-1} + b(z + b)^{-2}\}. \tag{14}$$

From Eq. (14) we obtain

$$\bar{s}(z) = b^{M\tau} \times \exp\{- M\tau z (z + b)^{-1}\} (z + b)^{-M\tau}, \tag{15}$$

whence

$$s(x) = b(xb / M\tau)^{(M\tau - 1)/2} \times \exp\{-(M\tau + bx)\}\, I_{M\tau - 1}(2\sqrt{M\tau b x}), \tag{16}$$

where

$$I_\nu(x) = i^{-\nu} J_\nu(ix).$$

The basic problem consists in the determination of the function $Q(V)$. Making use of the results of Eq. (5) and Eq. (11), we find from Eqs. (6) and (7) that

$$\bar{Q}_1(z) = (M/N)\, \bar{Q}_2(z)(z + a) \times (z + b)^{-1} \{1 + b(z + b)^{-1}\}; \tag{17}$$

$$\bar{Q}_2(z) = N a^{N\tau} b^{M\tau} \exp\{- M\tau z (z + a)^{-1}\} \times (z + a)^{-(N\tau + 1)} (z + b)^{-M\tau}, \tag{18}$$

where

$$\bar{Q}_1(z) = \int_0^\infty e^{-zx} Q_1(x)\, dx;$$

$$\bar{Q}_2(z) = \int_0^\infty e^{-zx} Q_2(x)\, dx.$$

To simplify the formula, we introduce the notation $N\tau = \alpha$; $M\tau = \beta$. It should be noted that $\alpha > \beta$ and $\alpha \ll 1$. To determine $Q_1(V)$ and $Q_2(V)$ we must calculate the following integrals (see appendix B):

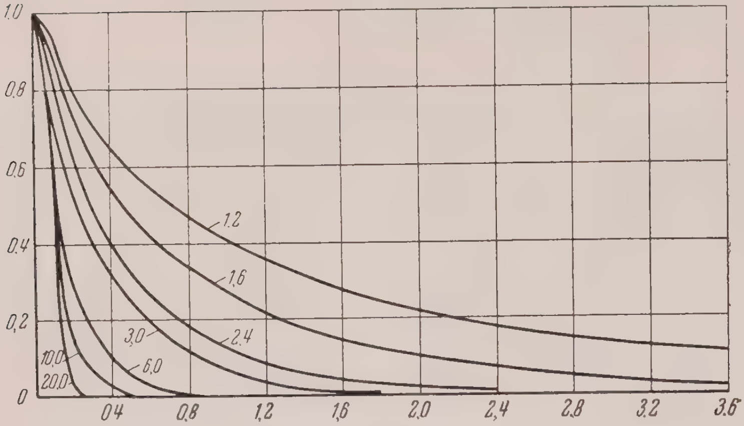

FIG. 1. Dependence of the ratio $MQ_2(N)/NQ_1(V)$ on the potential V of the discriminator (horizontal axis) for different values of a which are shown on the curves). The potential is in units of b^{-1}

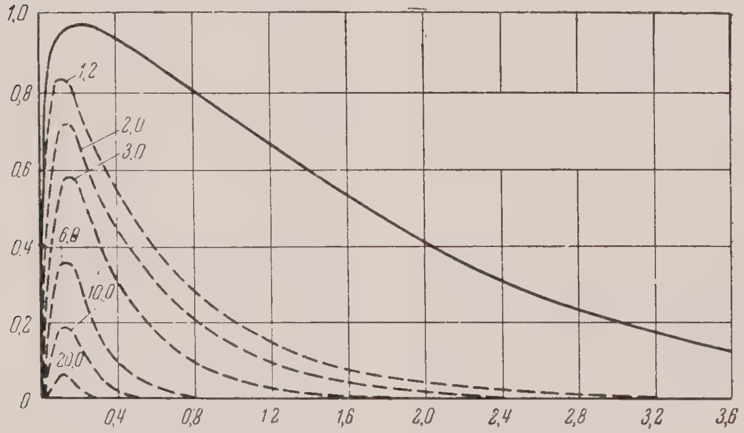

FIG. 2. The solid curves show the dependence of the number of true fissions (Q_1M^{-1}), and the broken lines. The dependence of the number of false fissions, associated with the superposition of α-particles pulses (Q_2N^{-1}) on the potential V of the discriminator (horizontal axis) for different values of a, shown on the curves, in the case $M\tau = 10^{-4}$ $N\tau = 10^{-3}$. The potential is in units of b^{-1}

$$Q_2(x) = \frac{Na^{\alpha}b^{\beta}e^{-\beta}}{2\pi i}\int\limits_{\sigma-i\infty}^{\sigma+i\infty} \exp\{zx+\beta b(z+b)^{-1}\}(z+b)^{-\beta}(z+a)^{-(\alpha+1)}\,dz, \qquad (19)$$

and

$$Q_1(x) = u_{11}(x) + u_{12}(x),$$

$$u_{11}(x) = (2\pi i)^1 \frac{M}{N}\int\limits_{\sigma-i\infty}^{\sigma+i\infty} e^{zx}Q_2(z)(z+a)(z+b)^1\,dz; \qquad (20)$$

$$u_{12}(x) = (2\pi i)^1 \frac{M}{N}\int\limits_{\sigma-i\infty}^{\sigma+i\infty} e^{zx}Q_2(z)(z+a)(z+b)^2\,dz. \qquad (21)$$

By virtue of the fact $V\beta b \ll 1$ for values of V of practical importance, we can obtain approximate expressions for $Q_1(V)$ and $Q_2(V)$ in the form

$$Q_1(V) \sim M \exp\{-(M\tau + bV)\} \times (Va)^{N\tau}(Vb)^{M\tau}(1 + bV); \tag{22}$$

$$Q_2(V) \sim N \exp\{-(M\tau + aV)\} \times (Va)^{N\tau}(Vb)^{M\tau}. \tag{23}$$

Equation (22) gives the number of readings of true fissions, and Eq. (23) gives the number of false fissions, connected with the superposition of pulses from α-particles, both per unit time.

In Fig. 1 we have plotted the dependence of $MQ_2(V)/NQ_1(V)$ on the voltage of the discriminator for a given value of M/N and for difference values of a/b. It should be noted that the voltage b^{-1} was chosen as the unit voltage. If the value of a/b is known from experimental data, then we can easily find the best recording conditions with the aid of Fig. 1. The curves in Fig. 2 show the dependence of the number of true fissions and false fissions (dotted curves) connected with the superposition of pulses from α-particles, on the voltage of the discriminator for various values of a/b (b^{-1} is taken here to be of unit voltage).

It should be noted that these calculations have a much more general character and can be used successfully in the analysis of the results of an arbitrary discriminator amplitude.

At the present time there are no reliable experimental data on the distribution law of the amplitudes of pulses from α-particles and fission fragments, and therefore we used an exponential (as a very general) distribution law.

APPENDIX A

Let $F(t)$ be the distribution function of time intervals between two successful voltage pulses. If we note by $G_n(x)$ the probability that the voltage on the output resistor at the time of time of realization of the nth pulse be less than x, and consider an exponential decay (with the law $e^{-t/\tau}$) of the voltage between two successive pulses, then we can describe $G_n(x)$ by the following recurrence relation:

$$G_n(x) = \int_0^\infty \int_0^x G_{n-1}[(x-y)e^{t/\tau}]\, dF(t)\, dH(y). \tag{A1}$$

With the help of the Laplace-Stieltjes representation, we get from Eq. (A1):

$$\bar{g}_n(z) = \bar{h}(z) \int_0^\infty \bar{g}_{n-1}(ze^{-t/\tau})\, dF(t); \tag{A2}$$

$$\bar{g}_n(z) = \int_0^\infty e^{-zx}\, dG_n(x), \tag{A3}$$

$$\bar{h}(z) = \int_0^\infty e^{-zx}\, dH(x).$$

If $\lim \bar{g}_n(z) \to \bar{g}(z)$ for $n \to \infty$, then we have the following integral equation for $\bar{g}(z)$:

$$\bar{g}(z) = \bar{h}(z) \int_0^\infty \bar{g}(ze^{-t/\tau})\, dF(t). \tag{A4}$$

From Eq. (A4) we can determine the distribution function $G(x)$, with the help of which we can easily find the distribution function $R(x)$, i.e.,

$$R(x) = \lambda \int_0^\infty \{1 - F(t)\}\, G(xe^{t/\tau})\, dt, \tag{A5}$$

where

$$\lambda = \int_0^\infty \{1 - F(t)\}\, dt. \tag{A6}$$

For an exponential distribution of the intervals between successive pulses ($F(t) = 1 - e^{-Nt}$) Eq. (A6) coincides with Eq. (3) from Sec. 1.

APPENDIX B

In Eqs. (19)-(21) it was necessary to determine integrals of the following type:

$$\Phi(x) = (2\pi i)^{-1} \times \int_{\sigma - i\infty}^{\sigma + i\infty} \exp\{zx + \beta b(z+b)^{-1}\} (z+a)^{-(r+\alpha)}(z+b)^{-(l+\beta)}\, dz. \tag{B1}$$

Assuming that $\beta bx \ll 1$ and $\beta < \alpha \ll 1$, and with the aid of the rapidly converging expansion

$$\exp\{\beta b(z+b)^{-1}\} = \sum_{m=0}^{\infty} \frac{(\beta b)^m}{m!}(z+b)^{-m}$$

calculation of the integral (B1) reduces to the determination of the following integral:

$$\Phi_m(x) = (2\pi i)^{-1} \times \int_{\sigma - i\infty}^{\sigma + i\infty} e^{zx}(z+a)^{-(r+\alpha)}(z+b)^{-(m+l+\beta)}\, dz. \tag{B2}$$

It is not difficult to show that the integral (B2) has the form

$$\Phi_m(x) = e^{-ax}\frac{x^{\nu_m+\mu-1}}{\Gamma(\nu_m+\mu)}\,{}_1F_1(\nu_m, \nu_m+\mu, cx), \tag{B3}$$

where

$$\nu_m = m+l+\beta, \quad \mu = r+\alpha, \qquad \times\; c = a-b, \tag{B4}$$

and ${}_1F_1(\nu_m, \nu_m+\mu, cx)$ is the degenerate hypergeometric function (see Ref. 3). In this way, Eq. (B1) is represented in the form of a rapidly converging series:

$$\Phi(x) = e^{-ax} \times \sum_{m=0}^{\infty}\frac{(\beta b)^m}{m!}\frac{x^{\nu_m+\mu-1}}{\Gamma(\nu_m+\mu)}\,{}_1F_1(\nu_m, \nu_m+\mu, cx); \tag{B5}$$

Making use of Eq. (B5), we get for $Q_1(V)$ and $Q_2(V)$ the expressions

$$Q_1(V) = Ma^\alpha b^\beta \exp\{-(aV+\beta)\}\left\{\sum_{k=0}^{\infty}\frac{(\beta b)^k}{k!}\frac{V^{\alpha+\beta+k}}{\Gamma(\alpha+\beta+k+1)}\right. \tag{B6}$$

$$\times\,{}_1F_1(\beta+k+1, \alpha+\beta+k+1;\ cV) + bV\sum_{k=0}^{\infty}\frac{(\beta V)^k}{k!}\frac{V^{\alpha+\beta+k}}{\Gamma(\alpha+\beta+k+2)}$$

$$\left.\times\,{}_1F_1(\beta+k+2, \alpha+\beta+k+2;\ cV)\right\}$$

and

$$Q_2(V) = Na^\alpha b^\beta \exp\{-(aV+\beta)\}\sum_{k=0}^{\infty}\frac{(\beta b)^k}{k!}\frac{V^{\alpha+\beta+k}}{\Gamma(\alpha+\beta+k+1)} \tag{B7}$$

$$\times\,{}_1F_1(\beta+k, \alpha+\beta+k+1;\ cV).$$

It is not difficult to be convinced that for sufficiently small values of α and β:

$${}_1F_1(\beta+k, \alpha+\beta+k;\ cV) \tag{B8}$$

$$\sim e^{cV} - \alpha\sum_{m=1}^{\infty}\frac{\lambda_m^k}{1+(\alpha+\beta)\lambda_m^k}\frac{(cV)^m}{m!},$$

where

$$\lambda_m^k = \sum_{j=k}^{k+m-1}\frac{1}{j}$$

Furthermore,

$${}_1F_1(\beta+k, \alpha+\beta+k+1; cV) \tag{B9}$$

$$\sim k\int_0^1 t^{k-1}e^{cVt}\,dt$$

$$-\,\alpha k\sum_{m=1}^{\infty}\frac{\lambda_{m+1}^k}{(m+k)[1+(\alpha+\beta)\lambda_{m+1}^k]}\frac{(cV)^m}{m!}$$

$$-\,\beta k\sum_{m=1}^{\infty}\frac{1}{(m+k)^2[1+(\alpha+\beta)\lambda_{m+1}^k]}\frac{(cV)^m}{m!}.$$

If we neglect terms which are linear in α and β we get

$$Q_1(V) \sim M\exp\{-(M\tau+bV)\} \tag{B10}$$

$$\times\,(Va)^{N\tau}(Vb)^{M\tau}(1+bV),$$

$$Q_2(V) \sim N\exp\{-(M\tau+aV)\} \tag{B11}$$

$$\times\,(Va)^{N\tau}(Vb)^{M\tau}.$$

With the aid of Eqs. (B8) and (B9) we can estimate the inaccuracy of Eqs. (B10) and (B11). For the values $M\tau = 10^{-4}$ and $N\tau = 10^{-3}$ this inaccuracy is less than 2%.

---

[3] V. A. Ditkin and P. I. Kuznetsov, *Handbook of Operational Calculus*, Moscow-Leningrad, 1951.

Translated by R. T. Beyer
63

SOVIET PHYSICS JETP VOLUME 3, NUMBER 2 SEPTEMBER, 1956

Theory of Elliptic Polarization of Light Reflected from Isotropic Media

D.V. SIVUKHIN
Institute of Physics Problems, Academy of Sciences, USSR

(Submitted to JETP editor November 2, 1954)
J. Exptl. Theoret. Phys. (U.S.S.R.) 30, 374-381 (February, 1956)

With reflection of light viewed as interference of waves radiated by molecules and atoms of a medium, equations that take into account the effect of the transition layers are derived for the amplitudes of the reflected light. No special assumptions are made concerning the molecular structure of the medium or of the transition layer. The equations are valid for layers of any thinness, including monomolecular layers. At the end of the work, the equations are supplemented by second order terms in $f\gamma_m$. Complex mathematical calculations are avoided by converting radiation from volume sources to radiation from surface sources.

1. THE latest investigations by Kizel'[1] make timely the development of a theory of elliptic polarization of light reflected by an isotropic medium. This theory is free of the limitations imposed by the phenomenological treatment and does not introduce simplified concepts with respect to the molecular structures of the reflecting medium and of the transition layer. Results following from this theory were given in part in Ref. 2. However, the proof given there is easier stated than derived. Here we introduce the single hypothesis that the elliptic polarization is the result of the existence of transition layer on the reflecting surface of the medium, with no assumptions made at all concerning the molecular structure of the medium or of the transition layer. To free ourselves of the restrictions of the phenomenological theory, we shall dispense also with phenomenological description of the transition layer in terms of the dielectric constant or the index of refraction. At the same time no limitations whatever are imposed on the lower thickness limit of the transition layer. To exhibit more clearly the physical nature of the theory, we propose to employ elementary calculations almost exclusively or to avoid calculations where possible

2. We know that the reflected wave is the result of interference of secondary waves, radiated by the molecules or atoms of the medium. Under the influence of the incident wave and of the radiation of the remaining molecules and atoms these molecules or atoms acquire dipole moments and therefore produce radiation. Since we are interested in the radiation field at distances from the medium that are very large compared with the molecular dimensions and the intermolecular distances, we can replace the discrete radiation centers in the medium by continuously distributed sources. Let us introduce two types of such sources--volume sources and surface sources. If a plane monochromatic wave is incident on the medium the polarization vector of the medium consists of a homogeneous-wave term:

$$\mathbf{P} = \mathbf{P}_0 e^{i(\omega t - kr)} \qquad (1)$$

and of a supplementary polarization of the transition layer. By virtue of the polarization term (1), each volume element of the medium can be considered as a radiating Hertz dipole of moment $\mathbf{P}\,dV$. In addition to these volume sources, it is also necessary to account for the radiation from the transition layer. This can be done numerically by assuming that each elementary area dS on the surface of the body is a radiating Hertz dipole of moment $\vec{\tau}\,ds$. The vector is the supple-

$$\vec{\tau} = \vec{\tau}_0 \exp\{i(\omega t - k_x x)\} \qquad (2)$$

mentary dipole moment per unit surface of the body (the surface of the medium is taken to be the XY coordinate plane; the Z axis is directed downward inside the medium; X and Z lie in the plane of incidence). This vector and the proposed theory make possible a description of the properties of transition layer, inasmuch as we deal with a first-order approximation. The question of the origin of this layer is not touched upon in this theory. The layer may be either the result of soiling or processing the reflecting surface, or the result of the molecular structure of the medium near the surface, or finally the result of a difference between the effective field near the surface and the effective field inside the medium.

3. The radiation from the volume sources can be reduced formally to a radiation from surface sources Let us subdivide the entire medium into plane-parallel layers of equal thickness. These layers we shall call zones, in analogy with the Fresnel zones. The radiation field in the upper half space

---

[1] V. A. Kizel', J. Exptl. Theoret. Phys. (U.S.S.R.) 26, 228 (1954); 29, 658 (1955).

[2] D. V. Sivukhin, J. Exptl. Theoret. Phys. (U.S.S.R.) 18, 976, (1948); 21, 367 (1951).

due to each of these zones is a plane wave, propagating in the direction of the wave vector f′ of the reflected wave. The direction and length of this vector as well as of the wave vector f of the incident wave are determined by the following conditions:

$$f^2 = f'^2 = \omega^2 / c^2,\ f_x = f'_x = k_x; \qquad (3)$$

$$f_z = -f'_z = \sqrt{f^2 - f_x^2}\,.$$

Let the thickness of each zone be $L = \pi / (k_z + f_z)$. The plane waves radiated by the neighboring zones are then of opposite phase, and the radiation field in the upper half space is represented by an alternating series:

$$\mathbf{E} = \mathbf{E}_1 - \mathbf{E}_2 + \mathbf{E}_3 - \ldots, \qquad (4)$$

in which every term represents the radiation field due to the corresponding zone. Were the polarization wave (1) strictly homogeneous, and were the spherical waves radiated by the volume elements of the medium to experience no absorption at all, the absolute values of all terms of series (4) would be equal and the series itself would diverge (oscillate). Actually, however, absorption should cause the terms of series (4) to decrease monotonically, thereby insuring its convergence. If the absorption is slight, the decrease should be in geometric progression, since the attenuation of a plane wave of light passing through an infinitesimally thin layer of a medium is proportional to the thickness *dx* of this layer, owing to the linearity of the field equations. Denoting the denominator of the progression by q, we can therefore write $E = E_1 / (1-q)$. In the limiting case of infinitely small absorption $q = -1$, and we obtain $E = E_1 / 2$. Thus the field intensity produced by radiation from the entire medium in the upper half space is equal to half the field intensity produced by radiation from the first zone.

Let us subdivide the first zone into a large number of subzones of equal thickness and employ the vector-diagram nethod (Fig. 1). The complex amplitudes of the waves produced in the upper half space by the individual subzones are represented on the vector diagram by small arrows, forming half a regular polygon, and becoming a semicircle in the limit. The diameter $AB = D$ of this semicircle, is the complex amplitude of the wave radiated by the entire first zone. Were all phases of the waves radiated by the individual subzones identical and equal to the phase of the wave radiated by the first subzone, we would obtain (instead of a semicircle) a straight-line segment of length $\pi D/2$. This would increase the wave $\pi/2$ times, and the phase of the resultant wave would lead the phase of the wave radiated by the entire first zone by $\pi/2$. Considering that the amplitude of the wave radiated by the entire medium is equal to half the amplitude of the wave radiated by the first zone, we obtain the following theorem: If a half space bounded by a plane is filled with a medium the polarization vector of which is given by the plane wave (1), the radiation produced outside the medium is equivalent to the radiation due to an infinitely thin layer, placed on the surface of the medium, provided the dipole moment per unit area of this surface is:

$$\mathbf{A} = \frac{L}{\pi}\mathbf{P}_0 \exp\{i(\omega t - k_x x - \pi/2)\} \qquad (5)$$

$$= -\frac{i}{f_z + k_z}\mathbf{P}_0 \exp\{i(\omega t - k_x x)\}\,.$$

The proven theorem is valid for the radiation field only at distances from the surface of the radiating medium that are large compared with the molecular dimensions and intermolecular distances. Incidentally, this limitation is not as rigid as appears at first glance. Exact calculations by Ewald[3] have shown that the radiation field of a crystal lattice is practically equal to the radiation of a solid medium even at distances on the order of the lattice constant.

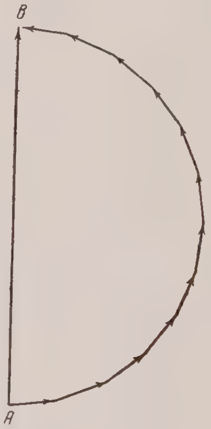

FIG. 1.

4. To obtain the field of the reflected wave, it is necessary also to take into account the added radiation produced by the transition layer. This can be done by adding the vector $\vec{\tau}$ to expression (5). This leads to the following theorem. The

---

[3] P. P. Ewald, Ann. Physik 49, 117 (1916).

field of the reflected wave is equivalent to the field due to an infinitesimally thin layer, placed on the surface of the medium and having the following dipole moment per unit area:

$$\mathbf{A}^{(r)} = (\vec{\tau}_0 - \frac{i}{f_z + k_z}\mathbf{P}_0)\exp\{i(\omega t - k_x x)\}. \quad (6)$$

This theorem is valid not only for infinitesimally thick transition layers, but also for layers of any thickness. In fact, in a manner similar to that used for the radiation due to the medium, the radiation produced by the transition layer in the upper half space can be replaced by the radiation due to an infinitesimally thick layer on the surface of the medium, provided only that $\vec{\tau}_0$ is suitably defined.

5. Let us now replace the field of the incident wave by the radiation from an infinitely thin layer, also placed at the boundary of the medium. This can be done in the following manner: The field at point Q, located within the medium where the polarization wave is practically homogeneous, i.e., far from the boundary, it can be represented in the form $E_Q = E^{(e)} + E_{lo} + E_{la}$, where $E^{(e)}$ is the field intensity produced at Q by the incident wave; E_{lo}--the field intensity due to radiation from the medium filling the lower half space, calculated under the assumption that the polarization wave of the medium is homogeneous everywhere; E_{la}--intensity of the additional radiation field due to the transition layer.

If we now imagine for an instant that the medium fills all the infinite space both above and below the coordinate plane XY, and that a homogeneous polarization wave (1) is propagated in this medium, then it is obvious that the field at point Q remains unchanged, since, by assumption, the polarization of the medium does not vary at this point. But in this case we can write $E_Q = E_{lo} + E_u$, where E_u is the radiation field due to the upper half of the medium. Comparison with the preceding equation gives: $E^{(e)} = E_u - E_{la}$. The effect of the upper half of the medium can be reduced to the radiation field due to an infinitely thin layer, placed in the coordinate plane XY, similar to the manner used for the lower half of the medium. The effect of the transition layer in the lower half space can be reduced to the radiation due an infinitely thin layer with a dipole-moment surface density:

$$\vec{\tau}' = \vec{\tau}_0{}' \exp\{i(\omega t - k_x x)\}. \quad (7)$$

This leads to the following theorem: The field due to an incident wave in the lower half space is the same as the field radiated by an infinitely thin layer, placed at the boundary of the medium, provided the dipole moment per unit surface area is:

$$\mathbf{A}^{(e)} = (-\vec{\tau}_0{}' + \frac{i}{k_z - f_z}\mathbf{P}_0)\exp\{i(\omega t - k_x x)\}. \quad (8)$$

Where we write $\vec{\tau}'_0$ instead of $\vec{\tau}_0$, since we deal with radiation produced by the transition layer in the lower half space. If the transition layer is thick the decrease in the phases of the sources in the Z direction causes the radiation in the upper and lower half space to be different. Consequently $\vec{\tau}'_0 \neq \vec{\tau}_0$ in general. Only in the case of very thin transition layers, when the thickness is quite small compared with the wave length, can we neglect the changes in phase over the thickness of the layer; in this approximation we can assume $\vec{\tau}'_0 = \vec{\tau}_0$.

6. The problem of computing the amplitudes of the reflected light has thus been reduced to a comparison of the radiation produced by two infinitesimally thin layers with dipole-moment surface densities (6) and (8). It is necessary to recall here that the radiation from a dipole depends on the relative orientation of the dipole and of the radiation: the only effective dipole-moment component is the one perpendicular to the direction of the radiation; the parallel component produces no radiation. Taking this into account, let us introduce the following symbols:

$$a_m = \tau_{0m} / P_{0m}; \quad a'_m = \tau'_{0m} / P_{0m}$$
$$(m = x, y, z)$$

(by virtue of the symmetry $a_x = a_y$; $a'_x = a'_y$) and let us examine two cases.

First case. Electric vector perpendicular to the plane of incidence. Evidently,

$$R_s/\mathscr{E}_s = A_y^{(r)}/A_y^{(e)},$$

where $\mathscr{E}_s$ and R_s are the complex amplitudes of the incident and reflected waves. Inserting (6) and (8) we obtain by simple transformations

$$\frac{R_s}{\mathscr{E}_s} = -\frac{\sin(\varphi - \psi)}{\sin(\varphi + \psi)} \frac{1 + ia_y f(\cos\varphi + n\cos\psi)}{1 - ia'_y f(\cos\varphi - n\cos\psi)}, \quad (10)$$

where φ is the angle of incidence, ψ the angle of refraction, and n the index of refraction of the medium.

Second case. Electric vector lies in the plane of incidence. Let e and e′ be unit vectors in the plane of incidence, perpendicular to the incident and reflected waves respectively, and directed toward the normal to the surface of the medium. Then

$$R_p/\mathscr{E}_p = (\mathbf{A}^{(r)}\mathbf{e}')/(\mathbf{A}^{(e)}\mathbf{e}),$$

where $\mathscr{E}_p$ is the complex amplitude of the incident wave, and R_p that of the reflected wave. Inserting (6) and (8) and allowing for the transverse nature of the reflected wave ($\mathbf{k}\cdot\mathbf{P}=0$) we obtain by a simple transformation:

$$\frac{R_p}{\mathscr{E}_p} = \frac{\operatorname{tg}(\varphi-\psi)}{\operatorname{tg}(\varphi+\psi)} \cdot \frac{1 - if(a_z \sin\varphi - a_x \cos\varphi \operatorname{ctg}\psi)\operatorname{tg}(\varphi+\psi)}{1 + if(a'_z \sin\varphi + a'_x \cos\varphi \operatorname{ctg}\psi)\operatorname{tg}(\varphi-\psi)}. \tag{11}$$

7. For all their generality Eqs. (10) and (11) have the substantial shortcoming that the quantities a_m and a'_m remain undetermined. However, in the case of thin transition layers it is possible to make definite conclusions concerning these quantities. They have the dimensionality of length, and we shall call the transition layer thin if a_m and a'_m are quite small compared with the wave length. Let us expand a_m and a'_m in power series in f and let us keep only the zero-order terms of these expansions. In this approximation we neglect the variation of the phase of the source with the thickness of the layer. Therefore $a_m = a'_m = \gamma_m$, where γ_m is the common zero-order term in the expansions for a_m and a'_m. Substituting this value into (10) and (11) and disregarding the terms in $(f\gamma_m)^2$ we obtain:

$$\frac{R_s}{\mathscr{E}_s} = -\frac{\sin(\varphi-\psi)}{\sin(\varphi+\psi)}[1 + 2if\gamma_y \cos\varphi]; \tag{12}$$

$$\frac{R_p}{\mathscr{E}_p} = \frac{\operatorname{tg}(\varphi-\psi)}{\operatorname{tg}(\varphi+\psi)} \times \left[1 + 2if\cos\varphi\,\frac{\gamma_x\cos^2\psi - \gamma_z\sin^2\varphi}{\cos^2\psi - \sin^2\varphi}\right]. \tag{13}$$

The parameters $\gamma_x = \gamma_y$ and γ_z are independent of the field intensity and of the frequency of the incident wave (neglecting dispersion). These parameters indeed characterize the properties of the transition layer in the approximation employed here.

8. Assume that the incident light is linearly polarized at a 45° angle with the plane of incidence, i.e., $\mathscr{E}_s = \mathscr{E}_p$. Let us introduce the designation

$$R_p/R_s = \eta e^{i\delta}. \tag{14}$$

The polarization of the reflected light will in general be elliptic. We shall call the ratio of the minor to the major axes of the corresponding ellipse the ellipticity coefficient of the reflected light. If the reflected light is passed through a Nicol-prism analyzer, it becomes again linearly polarized, whereby η (which can always be made positive by proper choice of δ) will equal to the ratio of the p and s components of the electric vector of the reflected waves, i.e., to the tangent of the azimuth of the restored polarization of the reflected light. In the experiments one usually measures η and δ. The ellipticity coefficient ρ is calculated from the following equation:

$$\rho^2 = \frac{1+\eta^2 - [(1+\eta^2)^2 - 4\eta^2\sin^2\delta]^{1/2}}{1+\eta^2 + [(1+\eta^2)^2 - 4\eta^2\sin^2\delta]^{1/2}}. \tag{15}$$

We stopped to discuss these known definitions and relationships because in the literature (see, for example, Ref. 1), ρ is sometimes confused with η. Actually, η characterizes only the position of the planar polarization of the reflected light after its linear polarization has been restored by a Nicol-prism analyzer. The quantity η alone cannot establish the form and orientation of the ellipse of oscillations, and δ must also be known for this purpose. In particular, if $\delta = \pi/2$, we have $\rho = \eta$.

9. If we determine R_p/R_s from (12) and (13) and compare the results with (14), we readily obtain

$$\eta\cos\delta = -\frac{\cos(\varphi+\psi)}{\cos(\varphi-\psi)}; \tag{16}$$

$$\eta\sin\delta = 2f(\gamma_z - \gamma_x)\frac{\cos\varphi\sin^2\varphi}{\cos^2(\varphi-\psi)}.$$

These relationships are accurate as long as the $(f\gamma_m)$ terms do not exceed the first power; they yield:

$$\operatorname{tg}\delta = 2f(\gamma_z - \gamma_x)\cos\varphi\sin^2\varphi/(\sin^2\varphi - \cos^2\psi). \tag{17}$$

As far as η goes, equations (16) cannot be used to compute this quantity with an accuracy greater than that given by the simple Fresnel equations. It would be necessary for this purpose to carry out all calculations with an accuracy up to $(f\gamma_m)^2$.

The only exception occurs when the light is incident at the Brewster angle or very nearly so. In this case the zero term in the expansion for $\eta \cos \delta$ vanishes, so that the expansion itself starts with a second-degree term which affects only the third-order quantities in the expression for ρ and can be discarded. If the incidence in this approximation is at the Brewster angle, the second equation of (16) yields

$$\eta = \rho = (\pi/\lambda)\sqrt{n^2+1}\,(\gamma_z - \gamma_x), \qquad (18)$$

since in this case $\delta = \pi/2$. Here n is the index of refraction of the medium, and λ is the wavelength in vacuum.

Thus, independently of the structure of the medium and of the transition layer, relationships (17) and (18) should hold, provided only that the causes of ellipticity are the transition layers at the reflecting surface of the medium. There are not enough experimental data available to decide with full assurance whether these relationships are true or not. In particular, the corrolary of Eq. (18), that the ellipticity of the reflected light is inversely proportional to the wavelength, has never been checked at all. According to Eq. (17), tan δ is inversely proportional to λ. This consequence has also not been checked. The dependence of δ on the angle of incidence φ has not been studied sufficiently. Before we can study the structure of the reflecting surfaces of media by reflected light it is necessary to investigate all these problems and thus corroborate or reject the basic initial premises of the theory, namely that the ellipticity of the reflected light results from the existence of transition layers. We can hope that the continuing investigations by Kizel' will throw light on this problem.

The dependence of the ellipticity coefficient ρ or of the quantity η on the angle of incidence φ in the vicinity of the Brewster angle cannot serve as a criterion for the correctness of the theory proposed, for the theory is true only with an accuracy to within first-order terms in $f\gamma_m$. To determine ρ or η in the vcinity of the Brewster angle it is necessary to carry out all the calculations with an accuracy at least including second-order terms. We shall therefore dwell on the form of the equations in the "second approximation."

Since we are interested in the radiation far away from the transition layer, we can replace the discrete radiation centers by sources that are continuously distributed through the volume of the layer. This can be done if we assume that within the transition layer we add to the polarization (1) a supplementary polarization

$$\mathbf{P}' = \mathbf{P}'_0(z)\, e^{i(\omega t - \mathbf{kr})} \qquad (19)$$

It is easy to see that the radiation in the upper half space, due to such a polarization, is equivalent to the radiation, due to an infinitesimally thin layer, placed in the XY coordinate plane, provided the dipole moment (2) per unit area has the amplitude

$$\vec{\tau}_0 = \int_0^l \mathbf{P}'_0(z) \exp\{-i(k_z + f_z)z\}\, dz, \qquad (20)$$

where l is the thickness of the transition layer. In fact, the phase of the wave radiated from point 0 (Fig. 2) to point A is equal to $\omega t - f'r$. Let us isolate an infinitesimally thin layer of thickness dz and let us extend the radius vector r in the backward direction until it intersects this layer. The phase of the wave radiated from B (R) to A (r) is $\Phi = \omega t - f'(r+R) - \mathbf{k}\cdot\mathbf{R} = \omega t - f'r + (\mathbf{f}' - \mathbf{k})\cdot\mathbf{R}$, or since $f'_x = f_x = k_x$ and $f'_z = -f_z$, we have

$$\Phi = \omega t - f'r - (k_z - f_z)\, z.$$

Integrating with respect to z and taking the phases of the radiated waves into account, we obtain Eq. (20).

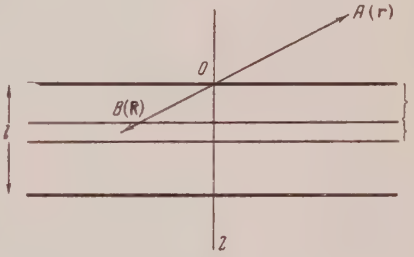

FIG. 2.

Analogously, the wave due to the supplementary polarization (19) radiated from the transition layer into the lower half space is equivalent to the radiation from an infinitely thin layer with a surface density of dipole moment (7), whereby

$$\vec{\tau}'_0 = \int_0^l \mathbf{P}'_0(z) \exp\{-i(k_z - f_z)z\}\, dz. \qquad (21)$$

The vector $\mathbf{P}'_0(z)$ depends on the frequency of the incident wave and also on the angle of incidence. However, rather than introduce these two arguments it is more convenient to use the arguments k_z and f_z. Let us expand the vector $\mathbf{P}'_0(z)$ in powers of k_z and f_z and let us terminate the expansion with the first-degree terms:

$$\mathbf{P}_0'(z) = \mathbf{P}_{00}'(z) - ik_z\mathbf{P}_{01}'(z) - if_z\mathbf{P}_{02}'(z),$$

where $P'_{00}, P'_{01}, P'_{02}$ no longer depend on the frequency (neglecting dispersion) or on the angle of incidence. In this approximation we can replace (20) and (21) by

$$\vec{\tau}_0 = \mathbf{d} - ik_z\mathbf{q}_1 - if_z\mathbf{q}_2, \qquad (22)$$

$$\vec{\tau}_0' = \mathbf{d} - ik_z\mathbf{q}_1 + if_z\mathbf{q}_2,$$

$$\mathbf{d} = \int_0^l \mathbf{P}_{00}'(z)\,dz; \quad \mathbf{q}_1 = \int_0^l (\mathbf{P}_{01}' + z\mathbf{P}_{00}')\,dz; \qquad (23)$$

$$\mathbf{q}_2 = \int_0^l (\mathbf{P}_{02}' + z\mathbf{P}_{00}')\,dz.$$

It is important to note that in the case of non-absorbing media the vectors d, q_1, and q are all real. It is enough to prove that P'_{00}, P'_{01}, and P'_{02} are real. This follows from the reversibility principle for non-absorbing media. Let us reverse at the instant $t=0$ the magnetic field in all points of space. Then, according to the reversibility principle, the electric field, and consequently also the polarization vector of the medium, will have at the instant t exactly the same values that they had at the instant $-t$. In particular, the supplementary polarization vector is obtained at the instant t by replacing t in (19) by $-t$. This gives

$$\mathbf{P}'(t, \mathbf{r}) = \mathbf{P}_0'(z, \mathbf{f}, \mathbf{k})\, e^{-i(\omega t + \mathbf{kr})}.$$

On the other hand, the above reversal of vector H also reverses the vectors f, f′, and k. Therefore the value of $P'(t, \mathbf{r})$ can be also obtained by reversing the signs of f and k in (19):

$$\mathbf{P}'(t, \mathbf{r}) = \mathbf{P}_0'(z, -\mathbf{f}, -\mathbf{k})\, e^{i(\omega t + \mathbf{kr})}.$$

Comparison with the preceding expression gives:

$$\mathbf{P}_0'(z, \mathbf{f}, \mathbf{k}) = \mathbf{P}_0'^{*}(z, -\mathbf{f}, -\mathbf{k}), \qquad (24)$$

from which the above statement follows directly.

The vector d can be considered as the dipole moment per unit area of the transition layer. On the other hand, the vectors q_1 and q_2 have the sense of quadrupole moments per unit area of the same layer, Thus the second-order theory differs from the first-order theory by further inclusion of the quadrupole radiation from the transition layer.

If we introduce along with parameters γ_x and γ_z the four new parameters:

$$\gamma_m' = q_{1m}/P_{0m}; \; \gamma_m'' = q_{2m}/P_{0m} \quad (m = x, z), \qquad (25)$$

we obtain

$$a_m = \gamma_m - ik_z\gamma_m' - if_z\gamma_m''; \qquad (26)$$

$$a_m' = \gamma_m - ik_z\gamma_m' + if_z\gamma_m''.$$

In the second approximation the properties of the transition layer are thus characterized by six parameters: $\gamma_x, \gamma_z, \gamma'_x, \gamma'_z, \gamma''_x$ and γ''_z. As to second order effects which may occur in experiments, this problem is exhaustively discussed in Ref. 4, and I will not dwell on it any further. These effects reduce to slight differences in the values of the polarization angle, of the principal angle of incidence, and of the Brewster angle, which according to the first-order theory should all equal each other.

11. If the thickness of the transition layer is large compared with the molecular dimensions and intermolecular distances (but naturally small compared with the wavelength), the transition layer can be phenomenologically characterized by the index of refraction. Equations (13) and (12) then become the Drude equations[2]; in second-order theory we obtain the Maclaurin equation.[4] On the other hand, if this condition is not satisfied, such a method is not suitable, and it becomes necessary to know the molecular structure of the medium and of the transition layer before the parameters γ_m can be calculated. These data cannot be obtained by optical investigations alone. An investigation of the reflected field can hardly serve as a basis for single-value conclusions concerning the molecular structure of the reflecting medium and of the transition layer. An attempt to calculate γ_x and γ_z making very rough assumptions concerning this structure is found in reference 2 (let us note that parameters γ_m employed there differ in sign from the parameters used here). In this respect the theory requires further development and refinement.

---

[4] D. V. Sivukhin, J. Exptl. Theoret. Phys. (U.S.S.R.) 13, 361 (1943).

Translated by J. G. Adashko
64

SOVIET PHYSICS JETP VOLUME 3, NUMBER 2 SEPTEMBER, 1956

The Solution of Inhomogeneous, One-Dimensional Motion Problems in Magnetic Gasodynamics

S. A. KAPLAN AND K. P. STANIUKOVICH
Lvov State University

(Submitted to JETP editor November 3, 1954)
J. Exptl. Theoret. Phys. (U.S.S.R.) 30, 382-385 (February, 1956)

An account is given of particular solutions, describing the motion of gases in a magnetic field for the case of variable entropy. At the same time the motions of a gas are investigated for the instance when the coefficient of proportionality between the field intensity and the gas density depends on the entropy.

IN Ref. 1 it is demonstrated that if the solution of any problem of uniform motion in gas dynamics is known, it is easily possible to obtain a solution of the corresponding problem in magnetic gasodynamics, i.e., in the theory of motion of an electroconductive gas in a magnetic field. Such a generalization is possible as a result of the existence in this case of the integral:

$$H/\rho = Hv = b, \tag{1}$$

where the factor b, which remains in force during the motion, is determined by the initial conditions. Here H is the intensity of the magnetic field, ρ is the density of the gas, and v is its specific volume. As a result of Eq. (1), the equations of uniform motion in magnetic gasodynamics can be related to the classical equations of uniform motion in gasodynamics, where, however, instead of the gas pressure ρ_r it is necessary to use the full pressure p:

$$p = p_r + (\mu/8\pi)H^2 \tag{2}$$

$$= p_r + (\mu/8\pi)b^2/v^2,$$

by means of which the aforementioned generalization is obtained. In the light of Eq. (1), the total pressure for polytropic motions (including adiabatic or isothermic motions) as well as the gas pressure is a single-valued function of the specific volume or density.

However, the solutions of the equation of uniform motion in magnetic gasodynamics examined in Ref. 1, as well as the corresponding solutions of the equation in classical gasodynamics, can be applied in practical computations only in cases of uniform distribution of the gas parameters at the initial moment of time, i.e., in those cases where the density, entropy, velocity of the gas, intensity of the magnetic field, and so forth, in their initial condition, are constant in regions separated from each other by initial discontinuities. In other words, the solutions of Eq. (1) can be employed only in those cases, where the magnitude b in (1) does not change upon transition from one element of mass to the other, i.e., is constant (however, b can change abruptly in the initial discontinuities). However, the necessity frequently arises for the solution of such equations also, in which the factor b, which is preserved for the given element of mass during its motion, changes during the transition of one element of mass into another. We will call such problems homogeneous.

The general method of solving inhomogeneous problems of one-dimensional motion in classical gasodynamics has been adequately demonstrated in Ref. 2. (Examination shows that Ref. 2 refers to those instances in which the inhomogeneity is due to inequality of the value of entropy, density, and other such parameters in various elements of mass under the initial conditions.) In the present work, this method is employed for the solution of inhomogeneous problems of magnetic gasodynamics.

Let us first convert the equations of one-dimensional motion in magnetic gasodynamics[1] to Lagrangian form. As one may easily see, they have the form:

$$u_t + \left(p_r + \frac{\mu}{8\pi}H^2\right)_h = 0, \quad u_h = v_t; \tag{3}$$

$$S_t = 0, \quad (vH)_t = 0 \quad \text{or} \quad S = S(h),$$

$$Hv = b(h).$$

Here, as usual, the derivatives are designated by a subscript; u_x is the velocity of the gas, t is the time, S is entropy, and $h = \int_0^x \rho\, dx$ is the Lagrange coordinate (the mass of the gas contained between the sections $x=0$ and the current section). As can be seen from the third equation in (3), the factor b in (1) is, as was to have been expected, a function of h. In Ref. 1 the case was examined in which $b(h)$=constant and $S(h)$=constant. Here we will consider them as given functions; in the particular case, one of them may be a constant.

---

[1] S. A. Kaplan and K. P. Staniukovich, Dokl. Akad. Nauk SSSR 95, 769 (1954).

The precise solution of (3) is as yet unknown. It is possible to obtain an approximate solution, however, if the total pressure is approximated by an expression of the form:

$$p = p_r + \frac{\mu}{8\pi}\frac{b^2(h)}{v^2} \tag{4}$$

$$= \left[\frac{A^2 k}{v-\sigma(h)}\right]^k \left(\frac{h_0}{h+h_0}\right)^{3k-1},$$

where A, k and h_0 are certain constants, and $\sigma(h)$ is a function selected, like these constants, from conditions of optimum approximation of the total pressure. Since (4) contains three arbitrary constants and a single arbitrary function, the accuracy of this approximation is entirely satisfactory for the solution of many problems of magnetic gasodynamics. The further solution of (3) simultaneously with (4), according to the method in Ref. 2 is accurate. A particularly important part is played by the constant h_0, which characterizes the degree of inhomogeneity. For large h_0, the initial distribution approaches uniformity; at small h_0, it is strongly inhomogeneous.

Transforming (3) and (4) to new variables with the aid of the substitutions of Ref. 2

$$\tau = (h+h_0)^{-1}, \tag{5}$$

$$z = p\tau, \quad w = u/\tau + \int p\,dt,$$

we obtain the system:

$$w_t = z_\tau, \quad w_\tau = A^2 h_0{}^{(3k-1)/k} z^{-(k+1/k)} z_t, \tag{6}$$

the solution of which determines both the motion of the gas and the change in the magnetic field in the problems examined.

In order to find the special solution describing a uniformly propagating wave (analogous to the Riemann solution), we multiply the first equation in (6) by

$$A h_0{}^{(3k-1)/2k} z^{-(k+1)/2k} \tag{6A}$$

or add (or subtract) it to (from) the second. We then obtain:

$$A h_0^{(3k-1)/k} z^{-(k+1)/2k}\left[w \pm \frac{2kA}{k-1} h_0^{(3k-1/k)} z^{(k-1/2k)}\right]_t + \left[w \pm \frac{2kA}{k-1} h_0^{(3k-1)/2k} z^{(k-1)/2k}\right]_\tau = 0. \tag{7}$$

from this we find that the values of the factors

$$w \pm \frac{2kA}{k-1} h_0^{(3k-1)/2k} z^{(k-1)/2k} = \text{const} \tag{8}$$

and that they are propagated with a speed

$$\frac{dx}{dt} = \frac{(h+h_0)^2}{A\rho} \cdot \frac{z^{(k+1)/2k}}{h_0^{(3k-1)/2k}} \tag{9}$$

$$= \frac{p^{(k+1)/2k}}{A\rho}\left(\frac{h+h_0}{h_0}\right)^{(3k-1)/2k},$$

i.e., Eq. (9) is the velocity of propagation of a disturbance in the problems under consideration.

Integrating (7) with the aid of (8), we obtain:

$$t = \pm A h_0^{(3k-1)/2k} z^{-(k+1)/2k} \tau + F(z), \tag{10}$$

where F is an arbitrary function. Returning to the old variables:

$$t = \pm\left(\frac{h_0}{h+h_0}\right)^{(k-1)/2k} \frac{A h_0}{p^{(k+1)/2k}} + F\left(\frac{p}{h+h_0}\right). \tag{11}$$

This is then the special solution, describing in implicit form the dependence of the total pressure on time and h. The dependence of the velocity of the gas u on time and h is found by the substitution of (11) in the first equation of (3):

$$u = \pm\left(\frac{h_0}{h+h_0}\right)^{(3k-1)/2k} \tag{12}$$

$$\times A p^{(k-1)/2k} + \Phi\left(\frac{p}{h+h_0}\right),$$

where the function $\Phi(z)$ satisfies the condition

$$d\Phi/dz = -z dE/dz. \tag{12a}$$

As an example, let us examine the case in which F=0, which is the analogue of self-simulated motion in inhomogeneous problems. From (11) and (12) we then find:

---

[2] K. P. Staniukovich, Dokl. Akad. Nauk SSSR 96, 441 (1954).

$$p=\left(\frac{h_0}{h+h_0}\right)^{(k-1)/2k}\left(\frac{Ah_0}{t}\right)^{2k/(k+1)}, \tag{13}$$

$$u=u_0-\left(\frac{h_0}{h+h_0}\right)^{2k}A\left(\frac{Ah_0}{t}\right)^{(k-1)/(k+1)}$$

$$u_0=\text{const.}$$

The initial values of p and u are found at some value $t=t_0$. The formulas in (13) make it possible to examine qualitatively the peculiarities of motion in inhomogeneous problems. In particular, as may be deduced from (13) and (12), the total pressure decreases with time according to the law $t^{-2k(k+1)}$; whereas the velocity increases from its zero value to

$$u_{\max}=\left(\frac{h_0}{h+h_0}\right)^{(3k-1)/2k}Ap_0^{(k-1)/2k}, \tag{14}$$

where p_0 is the initial value of the full pressure. Thus the maximum velocity of propagation depends, generally, on h. This circumstance can lead to the formation of rarefaction shock waves, described in Eq. (13).

In fact, since $u=(\partial t/\partial t)_h$ then, integrating the second equation of (13), we arrive at a relationship which is determinant for x:

$$x=-\frac{k+1}{2}\left(\frac{h_0}{h+h_0}\right)^{2k} \tag{15}$$

$$\times A\left(\frac{Ah_0}{t}\right)^{(k-1)/(k+1)}t+u_0t+\varphi(h),$$

or

$$x=\frac{k+1}{2}(u-u_0)t+u_0t+\varphi(h) \tag{16}$$

$$=\frac{k+1}{2}ut-\frac{k-1}{2}u_0t+\varphi(h),$$

where

$$t=t_0,\ x=x_0(h), \tag{17}$$

$$p_0=\left(\frac{h_0}{h+h_0}\right)^{(k-1)/(k+1)}\left(\frac{Ah_0}{t_0}\right)^{2k/(k+1)},$$

$$u=u_0-\left(\frac{h_0}{h+h_0}\right)A\left(\frac{Ah_0}{t_0}\right)^{(k-1)/(k+1)};$$

then from (4) we find $v=v_0=dx_0/dh$, from which we determine $h=h(x_0)$ and $\varphi(h)$. However, since $\sigma(h)$ can be arbitrary in the given problem, then we will on the contrary set $t=t_0$ $\varphi(h)$, from which we determine $h=h(x_0)$. Therefore, let $\varphi(h)$ be given.

The conditions for the formation of the shock wave in Lagrange coordinates can be described extremely simply. As a matter of fact, the trajectories of the various particles must intersect, and consequently, knowing that $x=x(h,t)$, we require that

$$\left(\frac{\partial x}{\partial h}\right)_t=A(k+1)\left(\frac{h_0}{h+h_0}\right)^{2k+1} \tag{18}$$

$$\times\left(\frac{t}{h_0}\right)^{2/(k+1)}+\frac{\partial\varphi}{\partial h}=0.$$

As an example, let us suppose that

$$\varphi=B\left(\frac{h_0}{h+h_0}\right)^{\alpha}; \tag{18a}$$

then we arrive at the following expression

$$(k+1)A^{2k/(k+1)}\left(\frac{t}{h_0}\right)^{2/(k+1)}\left(\frac{h_0}{h+h_0}\right)^{2k+1} \tag{19}$$

$$=\frac{B\alpha}{h_0}\left(\frac{h_0}{h+h_0}\right)^{\alpha+1}$$

This condition relates the Lagrange coordinate h with the time of the beginning of the formation of the shock wave for the given particle. In the particular case, when $d=2k$, we arrive at the conclusion that the shock wave forms at the moment of time

$$t=\left(\frac{2k}{k+1}BA^{-2k/(k+1)}h_0^{-(k-1)/(k+1)}\right)^{(k+1)/2}, \tag{20}$$

i.e., simultaneously over the entire region of existence of the wave. As we see, the influence of a strong magnetic field on the motion of a gas can be extremely significant.

In conclusion we may note that if k satisfies the condition $k=(2n+3/(2n+1)$, where $n=-1, 0, 1, 2, \ldots$, then it is also possible to obtain a general solution for the system (6), depending on two arbitrary functions. Referring the reader to Ref. 2 for details, we immediately write the final result:

$$t=\frac{\partial^{n+1}}{\partial\theta^{2(n+1)}}\left[F_1(\theta+w)+F_2(\theta-w)\right], \tag{21}$$

$$\theta=\frac{2kA}{k-1}h_0^{(3k-1)/2k}\ z^{(k-1)/2k}$$

$$=\frac{2kh_0}{k-1}\left[\frac{h_0p}{h+h_0}\right]^{(k-1)/(k+1)}.$$

With the aid of this solution it is possible to investigate the motion of a gas in magnetic gasodynamics after the formation of shock waves.

Translated by A. Certner
65

SOVIET PHYSICS JETP VOLUME 3, NUMBER 2 SEPTEMBER, 1956

The Theory of the Interaction of an Electron Gas with the Vibrations of the Crystalline Lattice

V. L. BONCH-BRUEVICH
Moscow Electrotechnical Institute

(Submitted to JETP editor October 6, 1954)
J. Exptl. Theoret. Phys. (U.S.S.R.) **30**, 342-350 (February, 1956)

The method of the Green's function is applied to the problem of the interaction of electrons with the phonon field. The electron energy spectrum and electron momentum spectrum at absolute zero have been computed.

1. INTRODUCTION

THE question of the interaction of conduction electrons with the vibrations of the crystalline lattice has in recent years acquired considerable importance for a whole series of problems. It has been observed repeatedly (see, for example, references 1-3) that, within the framework of the phonon picture of the crystal, this problem is anologous to problems considered in contemporary quantum field theory (only with this difference, that the momentum of the phonon has, of course, an upper limit). Salam[3], with the help of the usual technique of Feynman diagrams formally constructed an *S* matrix for the electron-phonon field. However, the calculation of just one *S* matrix does not always present immediate interest. In a series of cases, there is physical interest in the energy spectrum of the electron which interacts with the vibrations of the lattice, and the state distribution functions of the electrons. These problems are most simply solved by the Green's function method, since the distribution function can be obtained directly from the latter.

In the present research, the connection is established between the Green's function and the distribution function, and the state of the system at absolute zero is investigated. For concreteness, we consider a system of electrons that are not directly interacting (an electron gas). However, it must be kept in mind that all considerations can, by a simple change of notation, carry over also to the case in which arbitrary elementary excitations of the Fermi type interact with phonons.

2. GREEN'S FUNCTION AND THE DISTRIBUTION FUNCTION

We denote by $\psi_s(x)$ and $A(x)$ the quantum wave functions of the electron and the phonon fields ($x = \{x, x_0\}$, s = spin index; only longitudinal vibrations of the lattice are taken into consideration, because the interaction of electrons with the transverse vibrations can usually be neglected). The Lagrangian of the interaction with the acoustical vibrations has the form ($\hbar = c = 1$; c=velocity of sound):

$$\mathcal{L}_{\text{int}} = \{g\psi_s^*(x)\,\psi_s(x) + \rho(x)\}\,\varphi(x); \tag{2.1}$$

$$\varphi = \partial A/\partial x_0.$$

Here $\rho(x)$ is the "external charge density" (analogous to the "external current" in quantum electrodynamics), g = coupling constant (it can be expressed by the known constant C which enters into the theory of electrical conductivity[4]). The matrix S is given by the well known expression (we make use of the interaction representation)

$$S = T\{\exp(i\int L(x)\,dx)\}, \tag{2.2}$$

where the symbol $T\{\ldots\}$ denotes the T product. Naturally, S is an eigenfunctional of $\rho(x)$. The electron Green's function G and the "potential" $a(x)$ are obtained in the same way as in quantum electrodynamics (see, for example, reference 5):

$$G_{ss'}(x, y) = \frac{i}{\langle S_0\rangle}\langle T\{\psi_s(x)\,\psi^*_{s'}(y)S\}\rangle_0, \tag{2.3}$$

$$a(x) = -i\,\partial \ln\langle S\rangle_0/\partial\rho(x) \tag{2.4}$$

(the symbol $<\ldots>_0$ means "averaged over the ground state of the system in the absence of interaction"). The Green's function for phonons could also be introduced, but it is not necessary for us in the present research.

It is easy to see that the Green's function $G_{ss'}(x, y)$ directly describes the state distribution

---

[1] H. Frölich, Phys. Rev. **79**, 845 (1950).

[2] S. B. Tiablikov, J. Exptl. Theoret. Phys. (U.S.S.R.) 21, 377 (1951).

[3] A. Salam, Progr. Theoret. Phys. **9**, 550 (1953).

[4] H. Bethe and A. Sommerfeld, *Electron Theory of Metals*.

of the electrons (taking into account the interaction with the phonons).

Thus

$$\lim_{\substack{x_0\to y_0=t\\ x_0<y_0}} G(x,\ y) = -iR_1^e(\mathrm{x},\ \mathrm{y};\ t); \qquad \lim_{\substack{x_0\to y_0=t\\ x_0>y_0}} G(x,\ y) = iR_1^h(\mathrm{x},\ \mathrm{y};\ t), \tag{2.5}$$

where R_1^e and R_1^h are "single particle" density matrices for electrons and holes, respectively (calculated with consideration of the interaction with phonons). We now put $\psi(x)$ in the form

$$\psi_s(x) = \int d\lambda a_s(\lambda)\varphi_\lambda(x) \tag{2.6}$$

($a_s(\lambda)$ are the Fermi operators, which operate on the occupation numbers, $\varphi_\lambda(x)$ are the eigenfunctions of a certain additive operator, the eigenvalues of which are λ; the index λ can also denote the set of several quantities). Then (for $x_0 < y_0$):

$$G_{ss'}(x,\ y) = -i\int d\lambda d\lambda' f_{ss'}(\lambda,\ \lambda')\varphi_\lambda(x)\varphi^*_{\lambda'}(y), \tag{2.7}$$

$$f_{ss'}(\lambda,\ \lambda') = \frac{1}{\langle S\rangle_0}\langle a^*_{s'}(\lambda')a_s(\lambda)S\rangle_0\,. \tag{2.8}$$

If the dynamical variable λ has a definite meaning even in the presence of interaction of the electrons with the phonons, then

$$f_{ss'}(\lambda,\ \lambda') = f_{ss'}(\lambda)\delta(\lambda-\lambda'), \tag{2.9}$$

$$G_{ss'}(x,\ y) = -i\int f_{ss'}(\lambda)\varphi_\lambda(x)\varphi^*_\lambda(y)\,d\lambda. \tag{2.10}$$

Passing to the limit $x_0 \to y_0$ in accord with Eq. (2.5), we see that, to find the distribution of the electrons over the values of the "quantum number" λ, it suffices to expand $G_{ss'}(x,y)$ in terms of the eigenfunctions $\varphi_\lambda(x)\varphi^*_{\lambda'}(y)$; in such a case, it will immediately become clear whether or not it is possible to speak generally of such a distribution (i.e., whether the given dynamical variable makes sense). Similarly, for $x_0 > y_0$, the expansion of the Green's function in terms of the $\varphi_\lambda(x)\varphi^*_{\lambda'}(y)$ gives the distribution of "free places".

3. EQUATION FOR THE GREEN'S FUNCTION AND FOR THE "POTENTIAL"

The equations for the functions $G_{ss'}(x,y)$ and $a(x)$ can easily be obtained (if only in the model of Anderson[5]). With the use of Eq. (2.3), we have*

$$G_{s_1s_2}(x,\ y) = iK_{s_1s_2}(x,\ y) - g\int dzK_{s_1s'}(x,\ z)\left\{\frac{\delta G_{s's_2}(z,\ y)}{\delta\rho(z)} + ia(z)G_{s's_2}(z,\ y)\right\}, \tag{3.1}$$

$$a(x) = i\int dzF(x,\ z)\rho(z) \tag{3.2}$$

(Summation is carried out over the repeated spin indices). Here $K_{ss'}(x,y)$ and $F(x,y)$ are the distribution functions of the "free" electron and of the phonon field:

$$K_{ss'}(x,\ y) = \langle T\{\psi_s(x)\psi^*_{s'}(y)\}\rangle_0, \tag{3.3}$$

$$F(x,\ y) = \langle T\{\varphi(x)\varphi(y)\}\rangle_0 \tag{3.4}$$

Writing $\psi_s(x)$ in the form (2.6), and introducing the notation

$$f^{(0)}_{ss'}(\lambda) = \langle a^*_s(\lambda)a_{s'}(\lambda)\rangle_0, \tag{3.5}$$

we obtain

$$K_{ss'}(x,\ y) = \begin{cases} \int d\lambda\varphi_\lambda(x)\varphi^*_\lambda(y)\{\delta_{ss'} - f^{(0)}_{ss'}(\lambda)\}, & x_0 > y_0, \\ -\int d\lambda\varphi_\lambda(x)\varphi^*_\lambda(y)f^{(0)}_{ss'}(\lambda), & x_0 < y_0. \end{cases} \tag{3.6}$$

---

* In Eq. (3.2), the components corresponding to closed loops are omitted. It is easy to show, however, that in the approxomation employed below ,consideration of such terms leads only to the renormalization of the Fermi energy. Assuming the latter operation to be completed, one can omit this term.

[5] J. L. Anderson, Phys. Rev. **94**, 703 (1954).

This expression can be written in more compact form if the functions $\varphi_\lambda(x)$ describe stationary states (this particular case also represents fundamental interest). Let $W(\lambda)$ be the energy eigenvalue which corresponds to the "quantum number" λ. Then $\varphi_\lambda(x) = U_\lambda(\mathrm{x}) \exp\{-iW(\lambda)x_0\}$ and, as can easily be seen, the function $K_{ss'}(x, y)$ can be written in the form

$$K_{ss'}(x, y) = \frac{i}{2\pi} \lim_{\substack{\varepsilon\to 0\\ \varepsilon>0}} \int d\lambda U_\lambda(\mathrm{x})\, U_\lambda^*(\mathrm{y}) \tag{3.7}$$

$$\times \int_{-\infty}^{+\infty} ds e^{-is(x_0-y_0)} \frac{\delta_{ss'}[s-W(\lambda)] + i\varepsilon[2f^0_{ss'}(\lambda) - \delta_{ss'}]}{[s-W(\lambda)]^2+\varepsilon^2}.$$

This formula is suitable for use if the structure function $f^{(0)}_{ss'}(\lambda)$ is continuous. In some cases, however (for example, in the investigation of a degenerate electron gas), this function is discontinuous:

$$f^{(0)}_{ss'}(\lambda) = \begin{cases} \delta_{ss'}, & W < W_0, \\ 0, & W > W_0, \end{cases} \tag{3.8}$$

where W_0 is some limiting value. It is then appropriate to replace Eq. (3.7) with

$$\times K_{ss'}(x, y) = \frac{i}{2\pi}\delta_{ss'} \tag{3.9}$$

$$\int d\lambda U_\lambda(\mathrm{x})\, U_\lambda(\mathrm{y}) \int_L ds \frac{\exp\{-is(x_0-y_0)\}}{s-W(\lambda)},$$

where the contour of integration L is drawn in the figure. (This formula is entirely analogous to the well known expression for the function $S_c(x-y)$[6].)

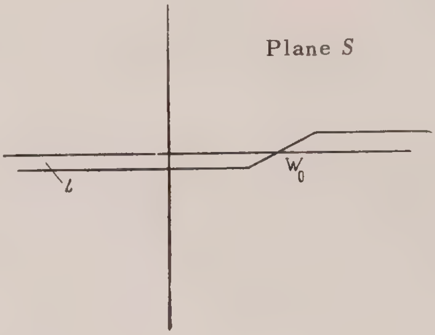

The quantum function of the phonon field $A(x)$ has the form[3]

$$A(x) = \frac{1}{\sqrt{2\pi^3}} \int \frac{d\mathfrak{f}}{|\mathfrak{f}|} \{b_{\mathfrak{f}} e^{ifx} + b^*_{\mathfrak{f}} e^{-ifx}\}. \tag{3.10}$$

Here $b_{\mathfrak{f}}$, $b^*_{\mathfrak{f}}$ are the usual Bose operators, $fx = \mathfrak{f}\cdot\mathbf{x} - |\mathfrak{f}|x_0$ and the possible values of the quasi-momentum of the phonon, $|\mathfrak{f}|$, are bounded above by the Debye value f_0. Introducing the expression

$$B(\mathfrak{f}) = \langle b^*_{\mathfrak{f}} b_{\mathfrak{f}}\rangle_0, \tag{3.11}$$

we obtain

$$F(x, y) = \begin{cases} \frac{1}{2\pi^3}\int d\mathfrak{f}\,|\mathfrak{f}|\,\{2iB(\mathfrak{f})\sin(f, x-y) + e^{i(f, x-y)}\}, & x_0 > y_0, \\ \frac{1}{2\pi^3}\int d\mathfrak{f}\,|\mathfrak{f}|\,\{-2iB(\mathfrak{f})\sin(f, x-y) + e^{-i(f, x-y)}\}, & x_0 < y_0. \end{cases} \tag{3.12}$$

In what follows, it will be more appropriate to use these integral representations for the functions $K_{ss'}(x, y)$ and $F(x, y)$ and not the explicit expressions for them.

4. "OPERATOR OF THE ENERGY OF INTERACTION." THEORY OF WEAK COUPLING

For the application of any particular form of perturbation theory, it is convenient to deal with the functional derivative not of the Green's function itself but of its inverse matrix. It is easy to see that

$$\delta G_{s's_2}(z, y)/\delta\rho(z)$$

$$= -\int dz' dx' dx'' \frac{\delta a(z')}{\delta\rho(z)} G_{s's'''}(z, x'') \tag{4.1}$$

$$\times \frac{\delta G^{-1}_{s'''s''}(x'', x')}{\delta a(z')} G_{s''s_2}(x', y).$$

If we introduce the notation

---

[6] A. I. Akhiezer and B. V. Berestetskii, *Quantum Electrodynamics*, Moscow, 1953.

$$\Delta E_{s's''}(z, x') = ig \int dz' dx'' \frac{\delta a(z')}{\delta \rho(z)} G_{s's'''}(z, x'') \frac{\delta G^{-1}_{s'''s''}(x'', x')}{\delta a(z')}, \tag{4.2}$$

then Eq. (3.1) reduces to the form

$$G_{s_1s_2}(x, y) = iK_{s_1s_2}(x, y) - ig \times \int dz K_{s_1s'}(x, z)\, G_{s's_2}(z, y)\, a(z) - i \int dz dx' K_{s_1s'}(x, z)\, \Delta E_{s's''}(z, x')\, G_{s''s_2}(x', y). \tag{4.3}$$

Multiplying Eq. (4.3) by G^{-1} and varying the result with respect to $a(z')$, we get the expression

$$\int K_{s''s'''}(z, x'') \frac{\delta G^{-1}_{s'''s''}(x'', x')}{\delta a(z')} dx'' = gK_{s's''}(z, x')\, \delta(x' - z') + \int dz'' K_{s's'''}(z, z'') \frac{\delta \Delta E_{s'''s''}(z'', x')}{\delta a(z')}, \tag{4.4}$$

which is of use in what follows. The matrix $\Delta E_{ss'}(z, x')$ characterizes the additional energy which is transformed by the electron into the phonon field and itself represents the analogue of the mass operator of quantum field theory. In this connection it is pertinent to call ΔE the operator of the energy of interaction.

To solve the nonlinear equation (4.3), we must make use of some form of perturbation theory. In the present work, we limit ourselves to the case of weak coupling. It should be borne in mind, however, that even under these conditions, direct expansion of the Green's function in a power series of the coupling constant is, generally speaking, hazardous. It is more accurate to expand not the Green's function itself, but the equation by which it is defined, i.e., the operator of the energy of interaction ΔE (or the inverse matrix G^{-1}, which amounts to the same thing).

In accordance with what we have said, we write

$$\Delta E = \Delta E^{(0)} + g\Delta E^{(1)} + g^2 \Delta E^{(2)} + \cdots \tag{4.5}$$

Noting that, by Eq. (3.2),

$$\frac{\delta a(x)}{\delta \rho(z)} = iF(x,z); \quad a(x)|_{\rho=0} = 0, \tag{4.6}$$

we get (the indices on G denote that this function satisfies the equation expanded in corresponding fashion):

$$\Delta E^{(0)} = \Delta E^{(1)} = 0, \tag{4.7}$$

$$G^{(0)}_{s_1s_2}(x, y) = G^{(1)}_{s_1s_2}(x, y) = iK_{s_1s_2}(x, y), \tag{4.8}$$

$$\Delta E^{(2)}_{s's''}(z, x') = -\frac{i}{g} \int dz' dx'' F(z', z)\, K_{s's'''}(z, x'') \frac{\delta G^{-1}_{s'''s''}(x'', x')}{\delta a(z')} {}_{g\to 0}. \tag{4.9}$$

By reason of Eq. (4.4), Eq. (4.9) takes the form

$$\Delta E^{(2)}_{s's''}(z, x') = -iF(x', z)\, K_{s's''}(z, x'), \tag{4.10}$$

and correspondingly, we find the following linear equation for $G^{(2)}_{s_1s_2}(x, y)$:

$$G^{(2)}_{s_1s_2}(x, y) = iK_{s_1s_2}(x, y) - g^2 \int dz' dz K_{s_1s'}(x, z)\, F(z', z)\, K_{s's''}(z, z')\, G^{(2)}_{s''s_2}(z', y). \tag{4.11}$$

This equation can be solved exactly.

5. FERMI DISTRIBUTION FOR AN ELECTRON GAS IN A CRYSTAL AT ABSOLUTE ZERO

The general relations obtained above permit us to solve without difficulty the problem of the effect of the zero vibrations of the crystalline lattice on the electron distribution function. As a first step, we "smooth out" the periodic potential of the lattice, considering it only formally – by replacing the real mass of the electron by an effective mass (m). For the functions $\varphi_\lambda(x)$ it is reasonable to take plane waves (the index λ denotes the three components of the momentum of the electron):

$$\varphi_\lambda(x) = (2\pi)^{-3/2} e^{i\mathbf{p}\mathbf{x} - ip_0 x_0}; \tag{5.1}$$

$$p_0 \equiv W(\lambda) = \mathbf{p}^2/2m.$$

The structure function $f_{ss'}^{(0)}(\lambda)$ has the form of Eq. (3.8), where $W_0 = E_F = p_F^2/2m$ is the Fermi energy. The function $B(f)$ is zero at absolute zero. Thus the distribution functions $K_{ss'}(x, y)$ and $F(x, y)$ take the form

$$K_{ss'}(x, y) = \delta_{ss'} K(x - y), \tag{5.2}$$

$$K(x - y) = \frac{i}{(2\pi)^4} \int d\mathbf{p} \int\limits_L ds \, \frac{\exp\{i(\mathbf{p}, \mathbf{x} - \mathbf{y}) - is(x_0 - y_0)\}}{s - \mathbf{p}^2/2m}, \tag{5.3}$$

$$F(x - y) = \frac{1}{2\pi^3} \int d\mathbf{f} \, |\mathbf{f}| \, \exp\{i(\mathbf{f}, \mathbf{x} - \mathbf{y}) - i|\mathbf{f}||x_0 - y_0|\}. \tag{5.4}$$

Equation (4.11) is easily solved in this case. First, it is clear that the Green's function is diagonal in the spin indices and depends only on the difference of the arguments

$$G^{(2)}_{s_1 s_2}(x, y) = \delta_{s_1 s_2} G(x - y). \tag{5.5}$$

From Eq. (4.11) we get for the function $G(x - y)$

$$G(x-y) = iK(x-y) - g^2 \times \int dz dz' K(x-z) F(z'-z) K(z-z') G(z'-y). \tag{5.6}$$

The boundary condition in this equation is clear from a consideration of Eq. (5.3). Setting $s = E_F + s'$ in that case, we see that in the new variables $(\mathbf{p}, s')$ the boundary condition takes the usual form: for $x_0 > y_0$ we must get diverging waves, for $x_0 < y_0$, converging (one does not have to pay attention to the factor $\exp\{-iE_F(x_0 - y_0)\}$, which appears in front of the integral, in this case).

The solution of Eq. (5.6) for the given boundary condition has the form

$$G(x - y) = -\frac{1}{(2\pi)^4} \int d\mathbf{p} \int\limits_L dp_0 \, \frac{\exp\{i(\mathbf{p}, \mathbf{x} - \mathbf{y}) - ip_0(x_0 - y_0)\}}{p_0 - (\mathbf{p}^2/2m) + ig^2 f(\mathbf{p}, p_0)}, \tag{5.7}$$

where the contour L is drawn in the figure (for $W_0 = E_F$), and

$$f(\mathbf{p}, p_0) = \int K(x) F(-x) \exp\{-i\mathbf{p}\mathbf{x} + ip_0 x_0\} \, dx. \tag{5.8}$$

Calculation of the integral gives (we limit ourselves to the case $p_F > f_0$):

1) for $p_F - f_0 < p < p_F + f_0$:

$$\begin{aligned} f(\mathbf{p}, p_0) = &-\frac{im}{\pi^2 p} \left\{ \frac{f_0^3}{3} \ln \frac{(f_0 + p)^2 + 2m(p_0 + f_0)}{(f_0 - p)^2 + 2m(p_0 - f_0)} + \frac{f_0^3}{3} \ln \frac{E_F + p_0 - f_0}{E_F + p_0 + f_0} \right. \\ &+ (p + m)\left[\frac{(p + m)^2}{3} + |a|^2\right] \ln \frac{(f_0 + p)^2 + 2m(p_0 + f_0)}{p_F^2 + 2m(p_0 + p_F - p)} \, \frac{(f_0 - p)^2 + 2m(p_0 - f_0)}{p^2 + 2mp_0} \\ &+ (p - m)\left[\frac{(p - m)^2}{3} + |b|^2\right] \ln \frac{p_F^2 + 2m(p_0 - p_F + p)}{p^2 + 2mp_0} \\ &+ a\left[\frac{|a|^2}{3} + (p + m)^2\right] \ln \left(\frac{f_0 + p + m + a}{f_0 + p + m - a} \, \frac{p_F + m - a}{p_F + m + a} \, \frac{p + m - a}{p + m + a} \right. \\ &\times \left. \frac{p + m - f_0 + a}{p + m - f_0 - a}\right) + b\left[\frac{|b|^2}{3} + (p - m)^2\right] \ln \left(\frac{p_F - m + b}{p_F - m - b} \, \frac{p - m - b}{p - m + b}\right) \\ &+ \frac{(E_F + p_0)^3}{3} \ln \frac{(E_F + p_0)^2 - (p_F - p)^2}{(E_F + p_0)^2 - f_0^2} + \frac{8}{3} mp(p_F - p) \\ &+ 2p(p_F - p)^2 + [f_0^2 - (p_F - p)^2]\left[2(p + m) - \frac{E_F + p_0}{3}\right] \\ &\left. - \frac{4}{3}[p^2 m + (p + m) f_0^2 - mp_F^2] \right\}, \end{aligned} \tag{5.9}$$

where

$$a = \sqrt{m^2 - 2m(p_0 - p)}; \quad b = \sqrt{m^2 - 2m(p_0 + p)}; \quad p = |\mathbf{p}|.$$

2) for $p < p_F - f_0$:

$$\begin{aligned} f(\mathbf{p}, p_0) = & -\frac{im}{p\pi^2}\left\{\frac{f_0^3}{3}\ln\frac{(p+f_0)^2 + 2m(p_0 - f_0)}{(p-f_0)^2 + 2m(p_0 - f_0)}\right. \\ & + (p-m)\left[\frac{(p-m)^2}{3} + |b|^2\right]\ln\frac{(p+f_0)^2 + 2m(p_0 - f_0)}{p^2 + 2mp_0} \\ & + (p+m)\left[\frac{(p+m)^2}{3} + |a|^2\right]\ln\frac{(p-f_0)^2 + 2m(p_0 - f_0)}{p^2 + 2mp_0} \\ & + b\left[(p-m)^2 + \frac{|b|^2}{3}\right]\ln\frac{p+f_0-m+b}{p+f_0-m-b}\,\frac{p-m-b}{p-m+b} \\ & \left. - a\left[(p+m)^2 + \frac{|a|^2}{3}\right]\ln\frac{f_0+a-p-m}{f_0-a-p-m}\cdot\frac{p+m+a}{p+m-a} + \frac{16}{3}mpf_0 + \frac{2}{3}pf_0^2\right\}. \end{aligned} \tag{5.10}$$

3) for $p > p_\Phi + f_0$:

$$\begin{aligned} f(\mathbf{p}, p_0) = & -\frac{im}{p\pi^2}\left\{\frac{f_0^3}{3}\ln\frac{(f_0+p)^2 + 2m(p_0 + f_0)}{(f_0-p)^2 + 2m(p_0 + f_0)}\right. \\ & + (p-m)\left[\frac{(p-m)^2}{3} + |b|^2\right]\ln\frac{(p-f_0)^2 + 2m(p_0 + f_0)}{p^2 + 2mp_0} \\ & + (p+m)\left[\frac{(p+m)^2}{3} + |a|^2\right]\ln\frac{(p+f_0)^2 + 2m(p_0 + f_0)}{p^2 + 2mp_0} \\ & + b\left[(p-m)^2 + \frac{|b|^2}{3}\right]\ln\frac{f_0-p+m-b}{f_0-p+m+b}\,\frac{p-m-b}{p-m+b} \\ & \left. - a\left[(p+m)^2 + \frac{|a|^2}{3}\right]\ln\frac{f_0+p+m-a}{f_0+p+m+a}\,\frac{p+m+a}{p+m-a} + \frac{2}{3}pf_0^2 - \frac{16}{3}mpf_0\right\}. \end{aligned} \tag{5.11}$$

Comparing Eq. (5.7) with Eq. (2.10), we can find the electron momentum distribution function $f(\mathbf{p})$ where the interaction with the vibrations of the lattice is taken into account. It will be more useful for us, however, to compute not $f(\mathbf{p})$ but the hole distribution function $\Phi(p)$ which is related to $f(\mathbf{p})$ by the relation $\Phi(\mathbf{p}) = 1 - f(\mathbf{p})$. From Eq. (5.7) we get

$$\Phi(\mathbf{p}) = \frac{i}{2\pi}\int_L dp_0 \frac{\exp\{-ip_0(x_0 - y_0)\}}{p_0 - (p^2/2m) + ig^2 f(\mathbf{p}, p_0)} \tag{5.12}$$

(for $x_0 > y_0$; $x_0 \to y_0$).

Comparing Eq. (5.7) with Eqs. (4.10) and (5.8), it is easy to see that the pole of the integrand in Eq. (5.7) determines the energy $W(\mathbf{p})$ of the electron which interacts with the phonons:

$$W(\mathbf{p}) = (\mathbf{p}^2/2m) - ig^2 f(\mathbf{p}, \mathbf{p}_0^*), \tag{5.13}$$

where p_0^* is the square root of the denominator in Eq. (5.7). We note that the following inequalities are practically always valid:

$$E_F \gg p_F; \quad f_0 \gg m. \tag{5.14}$$

Therefore the expression for $W(\mathbf{p})$ can be written in the comparitively simple form:

$$\begin{aligned} W(p) = & \frac{p^2}{2m} - \frac{g^2}{\pi^2}\,\frac{m}{p}\left\{\frac{2}{3}pf_0^2 + \frac{f_0^3}{3}\ln\frac{f_0^2 + 2pf_0 + 2p^2}{f_0^2 - 2pf_0 + 2p^2}\right. \\ & \left. + \frac{4}{3}p^3\ln\frac{f_0^2 + 4p^2}{4p^2} + \frac{8}{3}p^3\left[\operatorname{arc\,tg}\frac{p+f_0}{p} + \operatorname{arc\,tg}\frac{p-f_0}{p} - \frac{\pi}{2}\right]\right\}. \end{aligned} \tag{5.15}$$

(This formula is valid for $p \gg m$.)

It is further clear from Eq. (5.14) that for

$p < E_F + {}^1/_2\, m$ all the branch points of $F(\mathrm{p}, \mathrm{p}_0)$ (considered as a function of the complex variable p_0) lie to the left of E_F. By drawing the curve along the real axis from $-\infty$ to $p + 1/2\, m$, we can compute the integral (5.12) directly for values of p in the interval $0 \leqslant p < E_F + {}^1/_2\, m$ (i.e., in all regions of practical interest). It must only be kept in mind that the pole of the integrand in Eq. (5.12) is generally simple (because reduction to zero (for one and the same value of p_0) both of the denominator itself and its derivative with respect to p_0 is possible only for a certain definite g). Thus we obtain for $p < E_F + {}^1/_2\, m$ (here and below, we keep only the first terms of the expansion in small quantities of the type m/p_F, etc.):

$$\Phi(\mathrm{p}) = 0; \quad p < p_c; \tag{5.16}$$

$$\Phi(\mathrm{p}) = \Bigg\{1 + \frac{2g^2m^2}{\pi^2}\Bigg[\ln \frac{f_0^4 + 4p^4}{4p^4} + 2\left(\operatorname{arc\,tg} \frac{p + f_0}{p} + \operatorname{arc\,tg} \frac{p - f_0}{p} - \frac{\pi}{2}\right) + \frac{4}{3}\,\frac{4p^2f_0^2 - f_0^4}{f_0^4 + 4p^4}\Bigg]\Bigg\}^{-1}, \quad p > p_c \tag{5.17}$$

where

$$p_c = p_F\Bigg\{1 + \frac{2g^2m^2}{\pi^2}\Bigg[\frac{2}{3}t^2 + \frac{t^3}{3}\ln\frac{t + 2 + 2t^2}{t - 2 + 2t^2} + \frac{4}{3}\ln\left(1 + \frac{t^4}{4}\right) + \frac{8}{3}\left(\operatorname{arc\,tg}(1 + t) + \operatorname{arc\,tg}(1 - t) - \frac{\pi}{2}\right)\Bigg]\Bigg\}, \tag{5.18}$$

$$t = f_0/p_F.$$

In particular, if $p_F \gg f_0$ (generally speaking this inequality does not occur), then Eq. (5.17) has the simple form

$$\Phi(\mathrm{p}) = \left[1 + \frac{2g^2m^2}{3\pi^2}\,\frac{f_0^2}{p^2}\right]^{-1} \tag{5.19}$$

(if $p > p_c$). In this case,

$$p_c = p_F\left\{1 - \frac{4}{3}\,\frac{g^2m^2}{\pi^2}\,t^2\right\}. \tag{5.20}$$

It follows from Eq. (5.17) that, because of the interaction with the zero vibrations of the lattice, the electron momentum distribution is somewhat "smeared out"; even at absolute zero some of the electrons possess momentum which exceeds the Fermi limit. Analogous results are obtained also in the calculation of the interaction of electrons with optical vibrations.

I take this opportunity to thank N. N. Bogoliubov for his criticism of the work and for a number of valuable suggestions.

Translated by R. T. Beyer
60

Letters to the Editor

Some Electrical Properties of Water and Ice

V. I. ARABADZHI

(Submitted to JETP editor, June 8, 1954)
J. Exptl. Theoret. Phys. (U.S.S.R.) 30, 193-195 (January, 1956)

THE problem of the electrical properties of water and ice is of paramount importance in the study of atmospheric electricity, particularly with regard to storm formation, since it is directly due to the interaction of droplets of water and crystals of ice in the cloud that the storm process develops. In this connection, we undertook a series of experiments for the investigation of the properties of water and ice.

1. When ice was reduced to small particles with a saw or scraped with a metallic scraper, and particularly by glass, the small ice chips falling into the container of an electrometer displayed a positive charge. At ice temperatures within the limits of -12° to -18° C, a positive charge from the ice particles appeared on the receptor surface of the electrometer of an order of magnitude of 10^{-9} coulombs per gm of ice particles as a result of this scraping. When glass was used for scraping, a somewhat greater charge developed than when metal was used, but of the very same order of magnitude. When the temperature of the ice was lowered with the aid of a cooling mixture to -55° C, a positive charge appeared on the receptor surface of the electrometer, as a result of the scraping, which was an order of magnitude greater than in the foregoing case. (It is a noteworthy fact that during this procedure, after only 30 scrapings of glass on ice, the receptor surface of the electrometer charged up from the particles of ice\to a potential having an order of magnitude of 2000 V). However, upon further reduction of the temperature of the ice to -190° C with the aid of liquid air, the ice became brittle and instead of forming ice dust during scraping cracked off along its planes of juncture. The charge of the chips during this process was also positive, but approximately 300 times smaller than at a temperature of -55° C.

The scraping of the ice in all these experiments took place in the open air at temperatures of the order of -10° / -18° C, and also immediately after carrying the cooled ice from the refrigerator or from the open air into a laboratory with an air temperature of 18° C. In the experiments described, two forms of ice were utilized: ice which had formed in the open air during the freezing of water at the edges of roofs, and ice artificially prepared from distilled water in the laboratory. The character of the electrification of the ice chips did not vary essentially during the process.

2. For the characteristic curves of the electrical properties of ice it is important also to have some idea of its polarization, which we studied in a cylindrical specimen having a radius of 1 cm and a height of 3.5 cm. This specimen of ice was connected into a dc circuit in series with a resistor having a value of the order of 10^6 ohms for a period of approximately 1 hour, and its polarity was noted by reading an electrometer which was hooked up in the circuit between the specimen and the resistor. Computation of the emf of polarization was carried out according to the formula

$$P = u - u_{\text{э}t}(u - u_{\text{э}})/u_{\text{э}},$$

where u is the difference in potential between the terminals of the current source, and u_e and u_{et} are the potentials to ground established by means of the electrometer at the start and at the conclusion of measurement after time t. The results of measurement of the emf of polarization for two temperatures are shown in Fig. 1. The relative error of these measurements did not exceed 15%. In order to prevent oxidation of the electrodes between which the ice was compressed from having any effect on the measurements, the electrodes were tinned, and their condition was checked during every measurement. The ice was obtained from

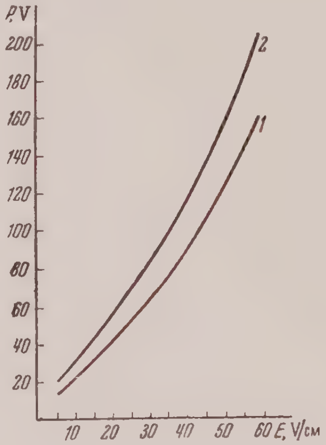

FIG. 1. Dependence of the emf polarization of ice P on the intensity of the applied field E. *1* – at 10°C *2* – at 18°C.

distilled water and together with the electrodes frozen to the ice remained in a thermostat where the necessary temperature was maintained constant with the aid of a cooling mixture.

3. The mutual electrical properties of water and ice are characterized by the contact difference in potentials between them.[1] Measurement of the contact difference in potentials was undertaken by us in the open air and was carried out at air temperatures within the limits of -8 to 12° C. The radiator-type collector was positioned at a height of approximately 0.5 cm above the surface of the water or ice and was connected to the electrometer. The water or ice in the glass container under the collector was grounded. First, water which had previously been cooled to approximately +4° C was placed under the collector, and the electrometer was read at a time 2-4 minutes after activating the test setup, when the needle had attained a fixed position. After this, in order to prevent the formation on the collector of a deposit of water or frost and to accelerate freezing, air was blown through the space between the water and the collector at a speed of 2.5 m/sec by means of a fan.

In order to clarify the possible effect of the blowing of air over the water on the results of the measurement, control experiments were carried out for measuring the contact difference in potentials with and without the blower, and these demonstrated that the blower had no effect on the results of measurement. When the water surface had become covered with a solid layer of ice, the blower was turned off and the stable reading of the electrometer was once again recorded. The difference in the readings of the electrometer represents the contact difference in potentials between water and ice. In all the experiments described we used distilled water and the ice obtained from the latter. The freezing of the water under the conditions of our experiments took place over a period of 8 to 16 minutes. The average of the 20 measurements carried out by means of the indicated setup results in a value of 0.15 V with amplitudinal values of 0.2 and 0.1 V for the contact difference in potentials between water and ice. As a check, a series of experiments was carried out replacing the water under the collector with prepared ice, and vice versa. The results obtained were identical with the foregoing.

4. Electrification during the exhaust of a droplet-steam jet from a nozzle has been known since the time of Faraday. A similar phenomenon was later observed in the exhaust into the atmosphere of compressed gases through a nozzle. However, in this case, as Drozdov[2] notes, the electrification is observed only under conditions of contamination of the gas flow by a liquid or particles of a solid aerosol. In order to obtain the characteristic curves of this phenomenon supplementing those already known, we carried out the measurements which are described below. Steam was produced in a steam boiler where the pressure could be raised to 6 atm. Filling of the steam boiler was done with ordinary tap water. In all the experiments the output of steam was accomplished over a period of 4 sec through a nozzle with a diameter of 0.5 cm, and during the course of the experiments the boiler was grounded. The pressure drop in the boiler during steam output amounted to 1-2 atm, if the initial pressure of steam at the beginning of output was within the limits of 3-6 atm; the drop was 0.5 atm at an initial steam pressure of less than 3 atm. In the experiments conducted, the potential gradient with respect to ground was recorded immediately after the cessation of steam output with the aid of a radio-thorium collector used in conjunction with an electrometer. The results are given in Fig. 2 for various steam pressures and for various distances from the nozzle. As can be seen from Fig. 2, with an increase in pressure, the zone of maximum potential gradient moves away from the nozzle along the axis

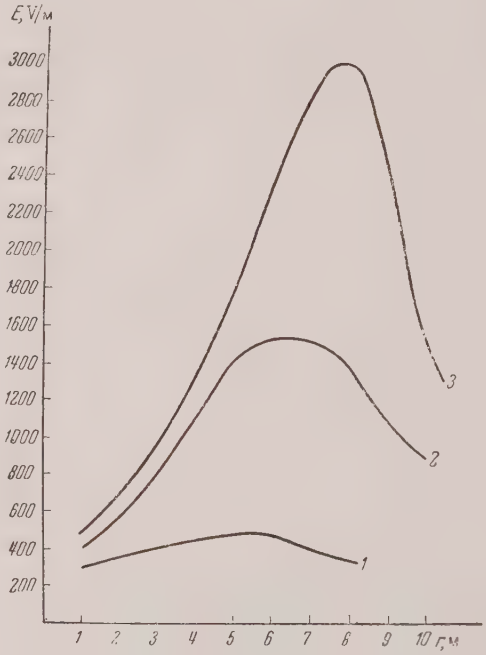

FIG. 2 Dependence of Potential gradient E of the space charge with respect to ground on the distance r from the nozzle along the axis of flow at the pressures: *1* – 1 atm. *2* – 2 atm. *3* – 6 atm.

of droplet-steam flow. At fixed distances from the nozzle, the greater the pressure of steam in the boiler before exhaust, the greater is the potential gradient which occurs. Also noteworthy is the fact that the electrification of the air takes place not only along the axis of flow, but also in a direction perpendicular to this axis, and the higher the pressure in the boiler the stronger this effect. During the exhaust of compressed air from a compressor within the limits of 1 to 6 atm no electrification at all was observed. The error in the measurement of the potential gradient in all cases did not exceed 50 V. The sign of the charge which the droplet-steam jet transmitted to the air was positive in all the measurements. The measurements were carried out in a room having the dimensions 12 x 6 x 2.75 m^3 at a height of 1 m from the surface of the stone floor. Water pipes were used for grounding. The velocity of the droplet-steam flow was measured by an anemometer at various distances from the nozzle and at different pressures, while all the measurements were carried out along the axis of symmetry of the flow. The results of measurement of the velocity of flow are presented in Fig. 3.

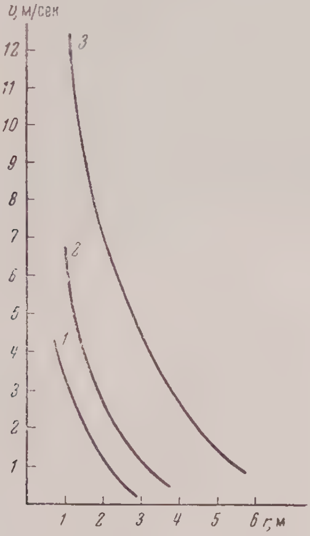

FIG. 3. Dependence of the velocity of flow v on the distance r from the nozzle along the axis of flow at steam pressures within the boiler of: *1* – 1 atm. *2* – 2 atm. *3* – 6 atm.

The electrical properties of water and ice which we investigated provide supplementary materials for the understanding of phenomena connected with the process of development of storms.

---

[1] V. I. Arabadzhi, Dokl. Akad. Nauk SSSR 60, 811 (1948).

[2] N. G. Drozdov. *Statistical Electricity in Industry*, Energoizdat, Moscow-Leningrad, 1949.

Translated by A. Certner
28

The Question of the Formation of a Cellular Structure in a Layer of Fog or Smoke

V. K. LIAPIDEVSKII
Moscow Physico-Engineering Institute

(Submitted to JETP editor September 19, 1954)
J. Exptl. Theoret. Phys. (U.S.S.R.) 30, 309-400
(February, 1956)

IN the literature, cases of the formation of a cellular structure in the layers of a liquid or a gas are described by an unsteady state, for example by heating underneath and by cooling from above.[1,2]

In addition, cases are described of the formation of a cellular structure in two-phase systems (for example in spermaceti, which contains a suspended aluminum powder,[3] in a layer of smoke, which is introduced into a chamber which is heated from below and cooled from above).[4,5] As cause of formation of a cellular layer in a two-phase system (similarly for one-phase) it is acceptable to assume a convection, determined by the difference of temperature between the lower and upper boundaries of the layer. However, as observations carried out by us show, the formation of a cellular structure in a layer of fog is possible in conditions when the gas is cooled from below and heated from above or when in general a temperature gradient is absent. The horizontally situated layer of fog of variable thickness is easily obtained in a diffusion-condensation chamber by means of a gaseous discharge. Cylindrical and rectangular chambers were employed with a bottom which is cooled and with glazed walls, differing little from the one described earlier.[6]

The chamber was filled with air or argon. A surface of ethyl alcohol gave rise to a vapor which is collected in a tube which is placed near the top. For the creation of a continuous process of diffusion near the walls at the bottom of the chamber a porous membrane was inserted which is moistened with alcohol. Under the action of the capillary force the alcohol, being at the bottom, was raised through the membrane to the top and thereupon, having evaporated, diffused downwards. Other sources of the vapor were absent in this case.

In the presence of a gaseous discharge between points which were located near the top and at the bottom of the chamber the ions, striking a sensitive layer, formed a fog, developing a heterogeneity of saturation in the space of the chamber. Such heterogeneities arise, for example, as a result of a local absence of saturation which was brought about by condensation of the charged nuclei which were created by the ionizing particles or as a result of convection currents in the volume of the chamber, subjected to the correctly chosen thermal process.

In the presence of a point discharge, a completely homogeneous layer of fog arises which, in the course of 1-2 sec., decomposes producing a cellular structure (Fig. 1) at a depth of the sensitive layer of 1.5 cm. The size of the cells is about 1 cm^2. The cellular structure, if its formation is caused by the motion of the gas in the chamber, having existed up to the formation of the fog, is obliged to be non-homogeneous. Heat transfer to the walls appears to be the cause of the convective motion of the gas in the chamber, therefore the circulation in the cells must slowly die out along the dimension of withdrawal from the walls of the chamber. Nevertheless the dependence of the size and shape of the cells upon their place of location was not ascertained.

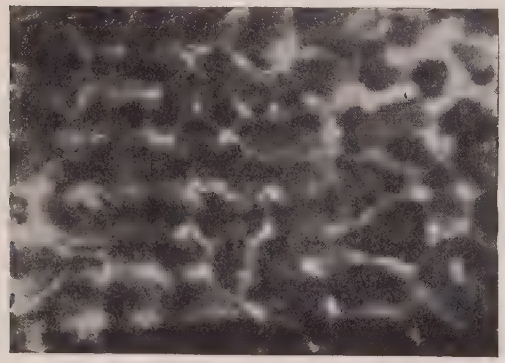

FIG. 1

If the walls of the chamber have a higher temperature than the gas then the cells are moved in a direction towards the walls. In addition to the deformation of the cells the following is observed: the depth of them is reduced, and the transverse dimensions increased (the walls are stretched laterally by the motion of the gas). The diminished depth of the cells is explained by the motion of the gas downward in the volume of the chamber compensating the upward motion of the gas at the walls. In the cooling of the walls, the convection current changes its direction. The gas is moved along the walls and the bottom to the center of the chamber. Moreover a diminishing of the lateral dimensions and an increase in the depth of the cells are observed; the cells "are shrunk", but, in the general features the cellular structure arising is not changed by the transition from one thermal condition to another.

Near the walls the circulation in the cells has one and the same direction, regardless of the direction of motion of the gas, i.e., in one case the circulation in the cell coincides with the direction of motion of the gas at the wall, and in another –opposite to it. Therefore, the formation is also decomposed drop by drop onto the ions after the passage of an ionized particle (Fig. 2), whereupon the boundary between the cells is almost always perpendicular to the direction of the track regardless of its orientation relative to the walls.

All of the empiracle data enumerated above shows that the cellular structure, being formed in the diffusion chamber, was not linked with motion of the gas, having existed until the appearance of the fog.

If the formation of the cellular structure was linked with the presence of a temperature gradient, then a dependence of the size or shape of the cells on the temperature distribution in the volume of the chamber should exist. Meanwhile, a detailed investigation showed that such a dependence does not exist.

With a view to this exclusion of the effect of condensation on the distribution of the temperature the behavior of a layer of smoke was investigated, which was introduced into the space of the chamber which was cooled, being filled with air. In all cases after the formation of a layer of smoke the latter decomposes into the cells. Further investigation showed that the cellular structure arises also in the decomposition of a layer of smoke which was produced above a plane horizontal surface, in the absence of a temperature gradient. The behavior of a layer of smoke of different origin was investigated (Nh_4 Cl, Nh_4 NO_3, tobacco smoke).

It should be noted that it is easy to obtain a homogeneous layer of smoke above the cooled surface. This, apparently, is explained by the fact that the gas near the cooled surface is found in a stable state. If however the layer of smoke is formed, its further behavior does not depend upon the temperature gradient. In all cases the layer of smoke decomposes into cells.

For a more detailed explanation of the behavior of a layer of fog, which is formed by the neutral centers of condensation, the emergence of a cellular structure is observed in a diffusion chamber with an expansion, differing negligibly in construction from the one previously described[7]. The chamber was cylindrical with glazed walls. The bottom of the chamber was cooled by dry ice. Vapor ethyl alcohol was used as a source , being poured into a pipe which was fastened to the upper lid with openings, through which the expansion took place. The operating volume of the chamber was separated from the spaces communicating with the atmosphere by a rubber diaphragm. The chamber was filled with air or argon. Supersaturation in the volume of the diffusion chamber is not constant with height. Therefore, upon rapid expansion, the fog forms itself into a layer the height of which depends on the degree of expansion, and consequently be easily varied over wide limits. The layer of fog decomposes into cells in 2 sec. The size of the cells depends on the height of the layer. The higher the layer the larger the cell size. For an increase of the layer up to a certain critical size (depending on the pressure and the properties of the gas in the chamber) the emergence of a second layer of cells is observed. The cells of the first layer, being deformed, form the cells of the second layer. The number of cells in the second layer is substantially larger than in the first.

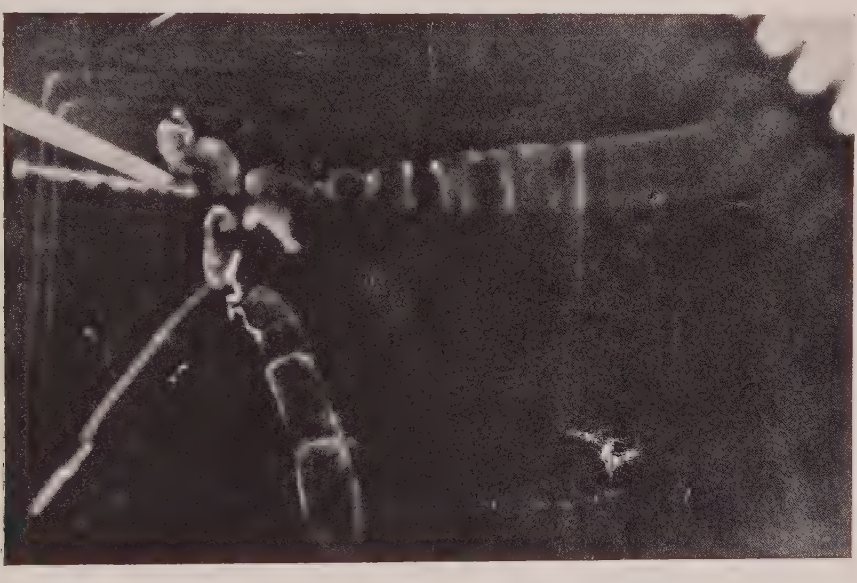

FIG. 2

For reduced pressures of the gas in the chamber the size of the cells increases and the time of formation and deformation is shortened. At a total pressure of the gas of the order of several millimeters of mercury, the cells disappear: a completely homogeneous fog settles onto the bottom in the course of 1-2 sec without the formation of a cellular structure.

The effects of the nature of the centers of condensation (charged or uncharged centers) on the phenomenon were not discovered.

The formation of a cellular structure in a layer of smoke or fog was also observed under natural conditions. Usually the formation of the cellular structure of clouds is explained by the circulation of the gas which was caused by a temperature gradient. The observations carried out by us show, however, that the formation of a cellular structure is possible under conditions when a layer of gas is found in a comparatively stable convective state. Therefore it is natural to suppose that the cellular structure of clouds in a series of cases also arises only after the formation of a homogeneous fog as a result of a precipitation of drops in the gravitational field.

The observations show that a homogeneous foggy trail, which was formed by an airplane in the upper layers of the atmosphere, in all cases produces a cellular structure. This agrees with the proposal which is expressed concerning the possibility of the formation of a cellular structure of clouds in the process of precipitation of the fog.

In conclusion I express thanks to M. S. Kozodaev and Prof. M. F. Shirokov for interest in the work and discussion.

---

[1] H. Benard, Ann. Chim. et phys. 23, 62 (1901).

[2] R. Schmidt and O. Saunders, Proc. Roy. Soc. 165, 216 (1938).

[3] S. Mal, Beitr. Z. Physik d. fr. Atm. 17, 40 (1931).

[4] D. Q. Brunt, J. Roy. Met. Soc. 63, 277 (1937).

[5] K. Chandra, Proc. Roy. Soc. (London) 164A, 231 (1938).

[6] V. K. Liapidevskii, J. Exptl. Theoret. Phys. (U.S.S.R.) 27, 103 (1954).

[7] V. K. Liapedevskii, J. Exptl. Theoret. Phys. (U.S.S.R.) 29, 263 (1955).

Translated by B. B. Cary, Jr.
67

Metal-to-Semiconductor Contact Resistance at High Contact Potential Differences

N. A. GOZHENKO AND IU. M. AMAISKII
Uzhgorod State University

(Submitted to JETP editor July 9, 1955)
J. Exptl. Theoret. Phys. (U.S.S.R.) 30, 401-402
(February, 1956)

IT is well known that at the interface between a metal and a semiconductor under certain conditions[1] there appears a layer with additional resistance R_k which is related to the contact potentail difference (*cpd*) by Davydov's equation[2]

$$R_k = (2\varkappa / \sigma)(\exp\{eV_k / kT\} - 1),$$

where R_k is the supplementary resistance, $1/\varkappa$ is the Debye screening thickness, σ is the conductivity of the semiconductor, and V_k is the *cpd* between the semiconductor and the metal. This equation is applicable for small V_k (when there is no intersection of the Fermi level and the impurity level), but it does not take into account a number of secondary phenomena: screening of the field by the space charge, tunnel effect, etc. For large V_k, when the above mentioned intersection takes place, Davydov's equation is entirely unacceptable, since a layer with reversed resistivity now appears on the surface of the semiconductor and thus dependence of R_k on V_k is different than in the case of small V_k. The degree to which the surface levels are filled with electrons must also affect the magnitude of the contact resistance

We have measured the dependence of R_k on the *cpd* V_k by the method of clamped contacts for different degrees of filling of the surface levels of samples of copper oxide[3]. The copper oxide was prepared by the standard method of heating in a high-temperature furnace followed by quenching in boiling water. The copper oxide was not separated from the copper base in order to increase the strength of the sample. Different metals were deposited on the same sheet of nickel, measuring 10 × 15 × 0.05 mm. The measurements were taken at room temperature. The contact potential difference was measured by the vibration method with an accuracy to within 0.005 v; R_k was measured by a direct current bridge with an accuracy to within 0.5%.

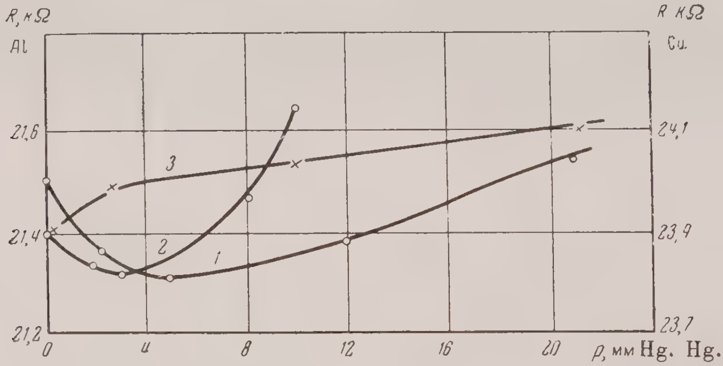

FIG. 1. Change of metal-to-semiconductor contact resistance with air pressure: *1* and *2* — copper oxide — aluminum (V_k = 1.18 v), two samples; *3* — copper oxide — copper (V_k = 0.22 v).

The filling of the surface levels was changed through adsorption on the semiconductor surface of water, alcohol, acetone and benzene vapors (as in Ref. 4). The *cpd* then changed by 0.04 – 0.06 v and the resistance changed as a function of the *cpd* and the pressure of the adsorbed vapor. For small V_k (Au, Cu, Ni) the resistance increased as the vapor pressure was raised, and decreased again as the pressure dropped. However, beginning at approximately $V_k = 0.50$ v (Ni) the behavior of the samples changed sharply: the resistance at first dropped very slightly with adsorption and began to rise only at considerable pressures. It was especially easy to observe this effect at evacuation or with slow admission of the vapors or of atmospheric air (which always contained water vapor (Fig. 1): the sample had a slightly smaller contact area with Cu than with Al). The most appreciable effect was observed with aluminum and zinc (*cpd* with samples of Cu_2O in vacuum, 1.06 and 0.88 v, respectively). With nickel ($V_k = 0.50$ v) transition effects were observed – during evacuation the resistance changed quite slowly and irregularly.

We have explained the above phenomena as follows. The normal effect, i.e., the increase of resistance with the rise of vapor pressure, can be explained by the reduction of negative surface charge due to adsorption and, consequently, to the decreased positive space charge of the semiconductor contact layer. As a result of this change the deformation of the hole semiconductor zone is increased, the potential barrier is raised and the contact resistance increases.

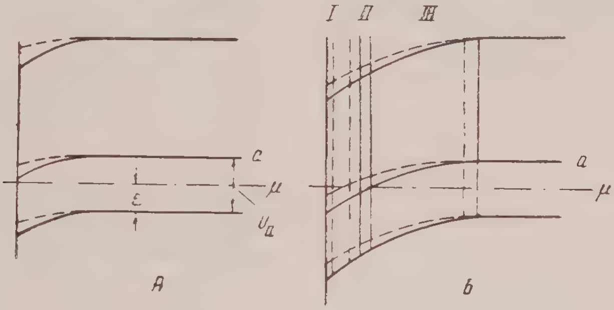

FIG. 2. Change of thickness of barrier layer of hole semiconductor with adsorption for different V_k: *A* – normal effect; *B* – anomalous effect; *a* – impurity level, *μ* – Fermi level, *I* – electron semiconductor, *II* – barrier layer, *III* – hole semiconductor; - — — — in vacuum; — — — with adsorption.

The anomalous effect, i.e., the decrease of R_k with rising pressure, is associated with the above-mentioned formation of a layer of an electron semiconductor (Fig. 2). With adsorption the resistance at first decreases, since the deformation of the zone narrows the barrier layer at the interface between the electron and hole semiconductors (region II). In addition with adsorption there is an increase of the number of current bearers in region I. However when the surface levels are largely filled the predominant increase of contact resistance is due to the curvature of the filled zone (resistance increase of region III), and there is also a decrease of *cpd* screening by the contact charge. The total resistance of the sample increases. The fact that the intersection of the chemical potential level with the impurity level takes place at $V_k = 0.50$ v, but theoretically should occur at 0.15 v (the hole activation energy is $\varepsilon = U_a 2$ and $U_a = 0.30$ v for copper oxide, as follows from the temperature dependence of the resistivity of the sample), shows that the entire *cpd* field does not penetrate into the semiconductor, but that a considerable portion of it falls in the space between the semiconductor and the metal, and also is screened by the contact charge.

Thus the above experiments show that: 1) in the study of contact resistances it is necessary to take into consideration the filling of the surface levels; 2) with clamped contacts it is easy to produce intersection of the chemical potential level with the impurity level.

When our work had been completed and was being prepared for publication there appeared a report by Kalashnijov and Iunovich[5] concerning a similar layer on the surface of germanium.

---

[1] A. V. Ioffe. J. Exptl. Theoret. Phys. (U.S.S.R.) 15, 721 (1945).

[2] B. I. Davydov, J. Exptl. Theoret. Phys. (U.S.S.R.) 9, 451 (1939).

[3] N. A. Gozhenko, Scientific Symposium of the Uzhgorod State University (in press).

[4] V. E. Lashkarev and V. I. Liashenko, Symposium in Commemoration of the 70th Birthday of A. F. Ioffe, 1950, p. 535.

[5] S. G. Kalashnikov and E. A. Iunovich, J. Tech. Phys. (U.S.S.R.) 25, 952 (1955).

Translated by I. Emin
68

Investigation of NaCl-AgCl Trapping Centers by a Metbod of Thermo-Optical Bleaching

CH. B. LUSHCHIK, F. N. ZAITOV, KH. A. MIAGI
AND K. IU. EL'KEN

Tartar State University

(Submitted to JETP editor June 18, 1955)
J. Exptl. Theoret. Phys. (U.S.S.R.) 30, 403-404
(February, 1956)

TO investigate trapping centers in a crystal, a method could be applied which is based on the measurement of the change $\Delta\varkappa$ of the absorption coefficient of the trapping centers as a function of the temperature T when the crystal is excited by heat at a constant rate β. The theory and some of its applications are explained in the following[1-3]. The dependency of $\Delta\varkappa(T)$ was investigated under conditions such that electrons released from the trapping centers by optical excitation were small compared to the thermal excitation during the measurement of $\Delta\varkappa$. Perhaps conditions can be treated such that the optical system which releases electrons from the trapping centers will be of a secondary nature. This discloses a supplementary method for investigation of trapping centers. Usually the probability of direct optical ionization of the trapping centers for the release of electrons is smaller than that of the optical release of electrons from trapping centers of thoroughly warmed crystals[4].

Let us suppose a crystal contains a single type of electron trapping center; the change of the numbers of electrons n of the thermally excited crystal would then be proportional to the condition of continuous illumination of the light flux B, and determined by the equation

$$-\frac{dn}{dT}=\beta_0^{-1}(p+\alpha Bp^*)\,n\,\frac{\sigma_p n}{\sigma_p n+\sigma_3(N-n)}. \qquad (1)$$

Here σ_r and σ_t are the effective crosssections of recombination and trapping N, the number of trapping levels, $p=p_0\exp(-E_T/kT)$ and $p^*=p_0^*\exp(-E_T^*/kT)$ — the laws of probability of thermal ionization of the trapping centers of the stable and excited states. (It would be convenient to designate the value of E_t as the thermal ionization energy of the trapping center, although this is not strictly correct. See, for example, Ref. 2. Since $\Delta\varkappa=An$, the coefficient A is slightly dependent on the temperature ($A\sim T^{-0.5}$). Equation (1) determines not only $n(T)$ but also the dependence of $\Delta\varkappa(T)$.

If $p\gg\alpha Bp^*$, which has been previously pointed out[3], the tempertaure T_k at which $n=0.5\,n_0$, is connected with the thermal ionization energy of the trapping centers by the relation

$$T_k=\frac{E_T}{k}\left\{\ln\left[\frac{p_0}{\beta_0}\,\delta_k\left(1+\frac{2\sigma_3 N}{\sigma_p n_0}-\frac{\sigma_3}{\sigma_p}\right)^{-1}\right]\right\}^{-1} \qquad (2)$$

If $p\ll\alpha Bp^*$, then most of the electrons would be liberated from the trapping centers due to optical bleaching. It is easily shown that, in this case,

$$T_k=\frac{E_T^*}{k}\left\{\ln\left[\alpha B\,\frac{p_0^*}{\beta_0}\,\delta_k\left(1+\frac{2\sigma_3 N}{\sigma_p n_0}-\frac{\sigma_3}{\sigma_p}\right)^{-1}\right]\right\}^{-1}. \qquad (3)$$

Thus, when B is small (the region of thermal bleaching) $T_k\neq T_k(B)$. When B is large (the region of optical bleaching) $T_k^{-1}=kE_T^{-1}\ln B+\text{const}$.

For measuring the bleaching curve $\Delta\varkappa(T)$ it is necessary to maintain control of the light flux for the investigation. It is possible to determine E_T from the rate of the thermal bleaching, which is dependent on $\Delta\varkappa(T)$.[2,3] From the rate of the optical bleaching, which is dependent on $\Delta\varkappa(T)$ as well as T_k for B, it is possible to determine the thermal ionization energy E_T of the excited trapping centers.

A method of thermo-optical bleaching was used by us in the investigation of trapping centers of single crystals of NaCl-AgCl. Simultaneous experiments were made of the spectral absorption of the trapping centers $\Delta\varkappa(\lambda)$ and thermal curve $I(T)$.

The quantities $\Delta\varkappa(T)$ and $\Delta\varkappa(\lambda)$ were measured on the SF-4 and SF-2M spectrophotometers. Curve $I(T)$ was recorded with the aid of an electron multiplier, amplifier, and self-recording potentiometer EPP-09. In all runs, $\beta_0=0.14$ deg./sec.

In accordance with literature[5-8], we found the $F-$ and $M-$ bands (460 and 720 mμ) in x-rayed single crystals of NaCl-AgCl 0.3 $M\%$, and additional absorption bands at 275, 315 and 345 mμ which were absent from the above mentioned source of x-rayed unactivated trapping centers.

Strong flourescence was emitted when the bands were excited (see Refs. 9-10). After initial heating to 200 °C, the bands at 276 and 345mμ started to disappear, and the band at 315 mμ remained broad. Excitation of this band produced a green flourescence of $\lambda_m = 540$ mμ, which was dependent on the transition from the excited level to the ground state. The temperature for half maximum of $\Delta\varkappa_{315}(T)$ (the band at 315 mμ) was $T_k^{\varkappa} = 530$ °K. The thermal ionization energy corresponding to this band of trapping centers can be calculated with the help of the half-life relationship obtained by Lushchik.[3] It was found that $E_T = 1.3$ ev. Liberation of the electrons from the trapping centers can be related to be dependent on the intensity of the fluorescence of the unifirmly heated crystal. The temperature at half-maximum causes a brilliant green fluorescence at $T_k^{\pm} = 505$ °K. Determination of $T_k^{\varkappa}$ and $T_k^{\pm}$ depends upon the effective thermal quenching of the trapping centers.

In the thermal bleaching curve for the phosphor NaCl-AgCl 0.3$M\%$ we observed three maxima at 345, 385 and 425°K, in agreement with the literature[2,11,12]. It was thought that the liberated electrons from the trapping level corresponding to the band at 315 mμ would appear in thermal emission with decreased sensitivity it was possible to see a sharp peak in the thermal emission at $T_m = 480°$ K. The large difference of T_m of this peak of the $T_k^{\varkappa}$ for the band at 315 mμ is probably due to strong thermal quenching of the luminescent ionic Ag^+. Thus, activating trapping centers of NaCl-AgCl and in KCl-TlCl (see Refs. 1, 12) can also appear in thermal emission.

In NaCl-AgCl 0.001 $M\%$ the temperature of half-maximum for the absorption coefficient of the F-band is $T_k^{\varkappa} = 425°$ K. At this same temperature we have observed the most intense peak of thermal emission, which corresponds to the liberation of electrons from the F-level. The energy of the thermal ionization of the F-centers, determined from the dependence of $\Delta\varkappa(T)$, $E_T = 1.02$ ev is in agreement with prior data[13].

$T_k^{\varkappa} = 395$°K for the 275 mμ band for NaCl-AgCl 0.3 $M\%$. The thermal ionization energy was calculated for the trapping centers of this band to be $E_T = 0.94$ ev.

Comparison of the complete absorption spectra of NaCl-AgCl after optical decay of the F-band at room temperature indicated that the probability of retrapping electrons liberated from the F-level to the activated trapping level measured was at least ten times smaller than the probability of their recombination with the luminescence centers.

In the temperature range where the 275 mμ bands 275 disappears, the 315 mμ band increases as a result of retrapping of electrons in the trapping level. From the comparison of the curves of $\Delta\varkappa_{275}(T)$ and $\Delta\varkappa_{315}(T)$ it follows that the probability of the retrapping A_t is five times smaller than the probability of recombination A_r. These facts confirm the previous conclusion of one of us[14] that $A_t > A_r$ in a regime of strong excitation in alkali-halide phosphors. The problem of the relation of A_t and A_r on weakly excited crystals awaits further experimentation.

In the present work, measurements of $\Delta\varkappa(T)$ were completed in the regime of thermal bleaching ($p >> \propto Bp^*$). Data on the regime of optical bleaching ($p << \propto Bp^*$) will be given in a later work.

---

*For convenience, we shall call E_T the energy of thermal ionization of the capture centers, although this is not strictly accurate (see, e.g., Ref. 2).

[1] Ch. B. Lushchik ,Trudy In. Fiz. Astron. Akad. Nauk, Estonian SSSR 1, (1955).

[2] Ch. B. Lushchik, Trudy In. Fiz. Astron. Akad. Nauk, Estonian SSSR 3, (1955).

[3] Ch. B. Lushchik, Izu. Akad. Nauk Estonian SSSR 4, 2 (1955).

[4] N. Mott and R. Gurney, *Electronic Processes in Ionic Crystals*, (1951).

[5] A. Smakula. Z. Physik 59, 603 (1930).

[6] A. C. Toparec, Dokl. Akad. Nauk SSSR 4, 25 (1935).

[7] J. Schulman, R. Ginther, C. Klick, J. Appl. Phys. 22, 1479 (1951).

[8] H. Etzel and J. Schulman, J. Chem. Phys. 22, 1549 (1954).

[9] J. Schulman, R. Ginther, L. Evens and W. Weyl, J. Electro Chem. Soc. 95, 79 (1942).

[10] M. L. Kats, Dokl. Akad. Nauk SSSR 85, 539 (1952).

[11] M. L. Kats, J. Exptl. Theoret. Phys. (U.S.S.R.) 23, 720 (1952).

[12] Ch. B. Lushchik, Izv. Akad. Nauk SSSR Ser Fiz. 18, 687 (1954).

[13] Ch. B. Lushchik, Dokl. Akad. Nauk SSSR 101, 833 (1955).

[14] Ch. B. Lushchik, Dokl. Akad. Nauk SSSR 101, 641 (1955).

Translated by M. Hacskaylo
69

The Effect of Uniform Compression on the Superconducting Properties of the ∝- and β-Modifications of Bi_2Pd

N. E. ALEKSEEVSKII AND I. I. LIFANOV
Institute of Physical Problems
Academy of Sciences, USSR

(Submitted to JETP editor November 19, 1955)
J. Exptl. Theoret. Phys. (U.S.S.R.) 30, 405-406
(February, 1956)

IT has been pointed out in a previous communication that the compound Bi_2Pd exists in two forms[1], of which the ∝-modification has a monoclinic lattice and goes over into the superconducting state at $T_c = 1.70$ °K., while the β-modification with a tetragonal lattice, becomes superconducting at $T_c = 4.25$ °K. It seemed of interest to determine the displacement of T_c under uniform compression for both forms of this compound. For this we used our previously-employed method of measuring the mutual inductance at audio frequency.[2] The pressure was developed in a beryllium bronze bomb by the change in volume of water upon freezing, following the method suggested by Lazarev[3]. The construction of the apparatus was such as to permit placement in the measuring coil, at the time of the experiment of either the specimen in the pressure bomb, or an ebonite ampule in which was placed a similar specimen not subjected to uniform compression. The amount of pressure developed in the bomb was determined from the displacement of the critical temperature for tin. To accomplish this, two completely identical samples of tin were inserted along with the Bi_2Pd samples in both the beryllium bronze bomb and the ebonite ampule; the difference in their respective transition temperatures determined the pressure in the bomb. This was generally ~ 1700 kgm/cm^2. The temperature was determined from the helium vapor pressure. In Fig. 1 are presented the transition curves for compressed and uncompressed specimens of β-Bi_2Pd and tin (along the vertical axis are given the readings in volts of a cathode voltmeter connected to the output terminals of the mutual induction measurement system[2]). A certain non-reproducibility in the transition curves for β-Bi_2Pd, observed when the pressure

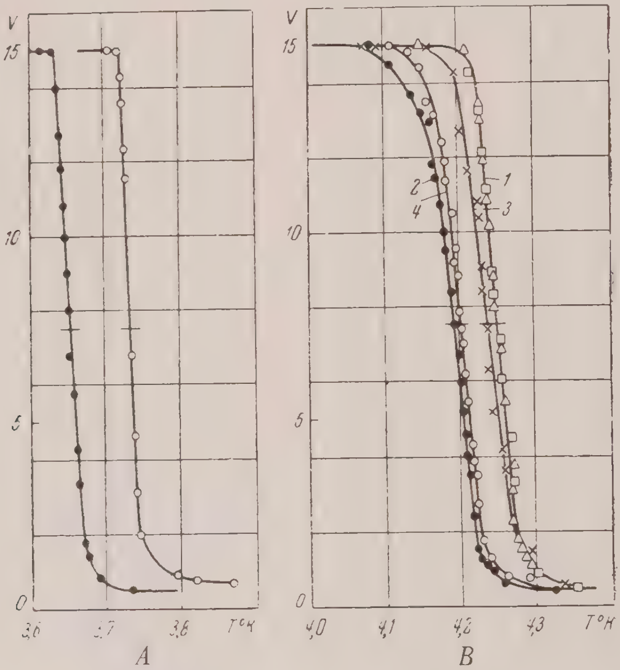

FIG. 1. Transition curves into the superconducting state: *a* — Sn in bomb with β-Bi_2Pd specimen: ○ no pressure in bomb, ● — ice pressure in bomb; *b* — β-Bi_2Pd: sample: △ — in beryllium bronze bomb, no pressure, □ — in ebonite sample, ○ — ice pressure reapplied; β-Bi_2Pd specimen in bomb with Sn sample: ice pressure in bomb, × — pressure removed.

was removed and then reapplied, can be explained as due either to a partial decomposition of the β-Bi_2Pd under compression, similar to that occurring for Au_2Bi[4], or to small residual deformations appearing in the sample. In Fig. 2 are given the transition curves for α-Bi_2Pd and for tin, the latter serving as before to determine the pressure in the bomb. In determining the displacement of the critical temperature for α-Bi_2Pd the temperature was measured with a phosphor bronze resistance thermometer which had a resistance of 11.8 ohms at $T = 4.22$ °K.

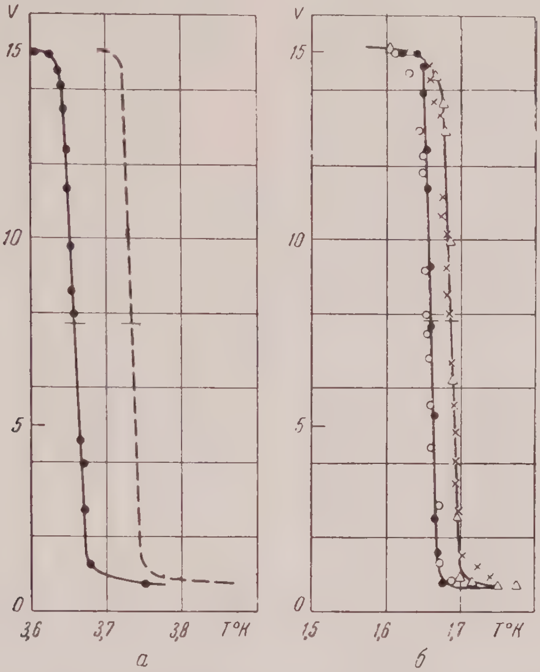

FIG. 2. Transition curves into the superconducting state: *a* – Sn, in bomb with α-Bi_2Pd specimen: ● —ice pressure in bomb; *b*: △— α-Bi_2Pd specimen in beryllium bronze bomb, no pressure in bomb; ● — α-Bi_2Pd specimen in bomb with Sn sample, ice pressure in bomb; × — pressure removed; ○ — α-Bi_2Pd specimen, ice pressure reapplied.

In contrast to β-Bi_2Pd, repeated removal and reapplication of the pressure does not lead in the case of α-Bi_2Pd to irreversible displacement of the transition curves. For both β-Bi_2Pd and α-Bi_2Pd, uniform compression leads to a reduction of the critical temperature: for α-Bi_2Pd the value is $\Delta T_c = 2.5 \times 10^{-2}$°K, while for β-Bi_2Pd $\Delta T_c = 5.5 \times 10^{-2}$°K for the first compression (the displacement being determined from curves 1 and 2 of Fig. 1) and $\Delta T_c = 3.5 \times 10^{-2}$°K when the amount of displacement is determined from curves 3 and 4. It may be remarked that the true value for the displacement of T_c is most probably 5.5×10^{-2}°K, for both the internal pressures resulting from decomposition and the small plastic deformation of the compressed specimen would serve only to reduce this quantity.

The values of $\partial T_c/\partial p$ as determined from the values for ΔT_c given above are α-Bi_2Pd, 2.5×10^{-11} °K cm²/dyne; for β-Bi_2Pd, 5.6×10^{-11}°K cm²/dyne, with $\Delta T_c = 5{,}5 \cdot 10^{-2}$ °K, or 3.6×10^{-11}°K cm²/dyne, with $\Delta T_c = 3.5 \cdot 10^{-2}$ °K.

---

[1] N. E. Alekseevskii, N. N. Zhuravlev and I. I. Lifanov, J. Exptl. Theoret. Phys. (U.S.S.R.) **27**, 125 (1954).

[2] N. E. Alekseevskii, N. B. Brandt, and T. I. Kostina, Izv. Akad. Nauk SSSR Ser Fiz. **16**, 233 (1952).

[3] B. G. Lazarev and L. S. Kan, J. Exptl. Theoret. Phys (U.S.S.R.) **14**, 470 (1954).

[4] N. E. Alekseevskii, G. S. Zhdanov and N. N. Zhuravlev, J. Exptl. Theoret. Phys. (U.S.S.R.) **25**, 123 (1953).

Translated by S. D. Elliott, Jr.
70

Concerning the Orientation of the Antenna of an Ionosphere Station

Z. Ts. Rapoport
Scientific Research Institute of Terrestrial Magnetism

(Submitted to JETP editor May 4, 1955)
J. Exptl. Theoret. Phys. (U.S.S.R.) **30**, 407-408
(February, 1956)

In a number of cases it is important to know how the orientation of an antenna system will affect the relative intensity of the magnetoionic components reflected from the ionosphere. Let us base an examination of this question on the fact that in the incidence of an electromagnetic wave upon the lower boundary of the ionosphere, two waves appear therein; the sum of their intensities yields that of the incident wave.

In magnetoionic theory,owing to the effect of the earth's magnetic field, the ionosphere is considered as anisotropic medium. In the general case, regardless of the orientation of the incident wave, the latter separates into two waves in the ionosphere; each of these waves is polarized elliptically.

In normal incidence of a plane-polarized wave upon the ionosphere, the lower boundary of which is located in the plane xy (Fig. 1) and the direction of the earth's magnetic field $H^{(0)}$ is in the plane yz, the equation defining the state of polarization of the magnetoionic components is known to be:

$$K_{1,2} = \frac{E_{y;\,1,2}}{E_{x;\,1,2}} \tag{1}$$

$$= -i\,\frac{2\sqrt{u}\,(1-v-is)\cos\alpha}{u\sin^2\alpha \mp (u^2\sin^4\alpha + 4u\,(1-v-is)^2\cos^2\alpha)^{1/2}},$$

where $K_{1,2}$ = the "polarization factors" of the extraordinary and ordinary waves

$E_{y;\,1,2}$ and $E_{x;\,1,2}$ = the components of the vector of the electric field strength for each type of wave.

$$\sqrt{u} = \omega_H/\omega = |e|\,H^{(0)}/mc\omega;$$

$$v = 4\pi e^2 N(z)/m\omega^2;$$

$$s = \nu/\omega;$$

ω_H = gyromatic frequency
ω = wave frequency
m = electron mass
e = electronic charge
c = velocity of light in vacuo
N = electron concentration
ν = effective electron collision frequency
$\alpha = \pi/2 \pm I$ = the angle between the direction of wave propagation and the vector of geomagnetic field strength $H^{(0)}$ (the plus sign corresponds to an incident wave in the northern hemisphere.)
I = the magnetic dip.

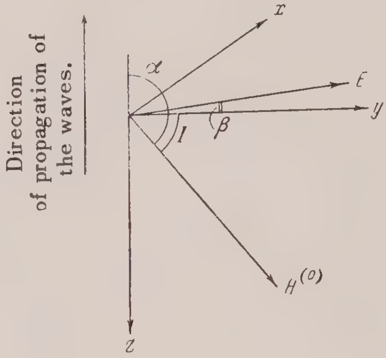

FIG. 1.

The upper sign before the radical in Eq. (1) refers to the ordinary wave, a wave of type 2; the lower sign refers to the extraordinary wave, a wave of type 1. At the lower boundary of the ionosphere we can assume $N \sim 0$; the equation for the polarization factors then reduces to the following (absorption neglected):

$$K_{1,2} = -i\,\frac{2\sqrt{u}\cos\alpha}{u\sin^2\alpha \mp (u^2\sin^4\alpha + 4u\cos^2\alpha)^{1/2}}. \tag{2}$$

From this it is seen that at the magnetic pole ($I = 90°$) the polarization of the magnetoionic components is circular and at the magnetic equator ($I = 0°$) it is plane. At any other magnetic dip the polarization of the two magnetionic components approaches the circular as a function of their separation from the gyromagnetic frequency. For example, at frequencies of 1.5 – 5.0 mc the polarization is close to plane only in the vicinity of the magnetic equator. In high and middle latitudes ($I \gtrsim 55°$) the moduli of the polarization factors differ from unity by not more than 10%. Equation (2) defines the state of polarization of the magnetoionic components corresponding to $H^{(0)}$ and I for any given place, but it fails to give an answer for the distribution of energy between the magnetoionic components. Suitable data for this can be obtained from the following calculation.

Let the wave incident upon the ionosphere have, as usual, plane polarization and let the vector of the electric field strength E of the wave form an angle β with the axis Oy, coinciding with the magnetic meridian (Fig. 1). Let us examine the field at point $z = 0$. The incident wave can be represented in the form:

$$e_x = C \sin\beta \cos(\omega t - \gamma), \quad e_y = C \cos\beta \cos(\omega t - \gamma).$$

For the ordinary wave we can write:

$$e_{x_2} = A_2 \sin(\omega t - \delta), \quad e_{y_2} = B_2 \cos(\omega t - \delta).$$

For the extraordinary wave:

$$e_{x_1} = -A_1 \sin(\omega t - \varphi), \quad e_{y_1} = B_1 \cos(\omega t - \varphi).$$

It is necessary to find the relation between the major and minor semiaxes of the ellipses of polarization of the magnetoionic components ($|B_2/A_1|$ or $|A_2/B_1|$). Solving the equation given above (using the condition of continuity of the field vectors, we find:

$$\left|\frac{B_2}{A_1}\right| = \left(\frac{|K_2|^2 + \mathrm{tg}^2\beta}{1 + |K_2|^2 \mathrm{tg}^2\beta}\right)^{1/2}. \qquad (3)$$

Now, using Eq. (3), we can compute how the energy is distributed between the magnetoionic components in the splitting of the plane-polarized wave. For this we must compare the average time values of the streams of the energies $S_{1,2}$ of the two waves:

$$S_2 = (c/4\pi)(A_2^2 + B_2^2), \quad S_1 = (c/4\pi)(A_1^2 + B_1^2).$$

In Fig . 2 we have plotted the graphs of $S_2/S_1 = f(\beta)$ for several values of $|K_2|$. From the plot it is seen that with circular polarization, $|B_2/A_1| = 1$ regardless of the angle β. The maximum dependence of the relative intensity of the components on the angle takes place with plane polarization. With $|K_2| = 1.05$, S_2/S_1 does not exceed 1.1. In other words, with $l \gtrsim 70^\circ$, at the frequencies mentioned above, the average time values of the streams of the energies of the magnetoionic components at the lower boundary of the ionosphere do not differ by more than 10%. With $\beta = 45^\circ$, which corresponds to antenna location in a NE-SW or SE-NW (magnetic direction, the ellipses of polarization and the average time values of the streams of the energies of the magnetoionic components are equal to each other.

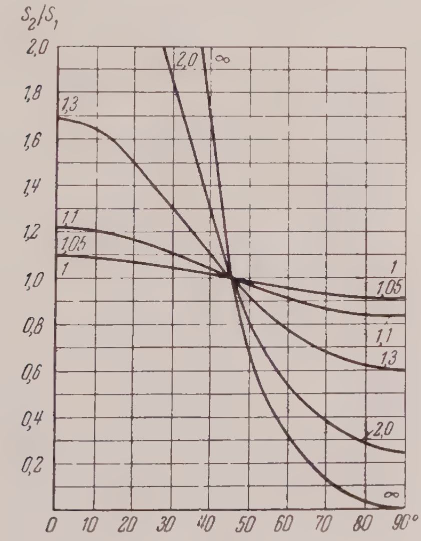

FIG. 2. Dependence of the ratios of time average values of energy flow of the magnetoionic components on the orientation of the transmitting antenna for various $|K_2|$.

The data obtained shows that if, for example, it is desired to have the magnetoionic components excited to the same degree in the ionosphere, which is sometimes important in the measurement of attenuation, the antennas should be disposed in a NW-SE or NE-SW direction. In case it is desired to "invest" the greatest possible energy in the ordinary component, the antenna should be located in a N-S direction.

Translated by G. F. Schultz
71

Comparison of Stability of Nuclear Shells and Subshells

V. A. KRAVTSOV
M. I. Kalinin Leningrad Polytechnical Institute

(Submitted to JETP editor July 5, 1955)
J. Exptl. Theoret. Phys. (U.S.S.R.) 30, 408-411
(February, 1956)

An attempt is made in the present work to compare the stability of various nuclear shells and subshells on the basis of experimental data. To this end, the values of jumps in the curves of the separation energy e_α of an α-particle in light and medium nuclei are studied.

Figure 1 a shows a typical curve, first given by Elsasser[1], of the dependence of the energy of α-decay on the number of neutrons in the nucleus, or the separation energy e_α of α-particles on the number of neutrons in nuclei with equal Z. It should be noted that, if the decay energy E_α is in the positive direction of the Y axis, the value of e_α, having the opposite sign, increases in the negative direction of the Y axis. There is a jump Δe_α of the curve $E = f(N)$, mainly in the interval from N_m to $N_m + 2$, where N_m is the number of neutrons forming a shell. As has been shown[2], the value of the jump Δe_α measured along the energy axis equals the sum of the depressions on the energy surface for the nuclei (Z, N_m) and $(Z-2, N_m)$, caused by their increased stability due to the closing of a shell or a subshell of N_m neutrons. Consequently, Δe_α is proportional to the stability of the neutron shells or subshells.

As has been shown by Sebgupt[3], the existence of a proton shell or subshell consisting of Z_m protons can be found from the curve which shows the dependence of E_α (or e_α) on the number Z of protons in nuclei with N = const, (see Fig. 1b), where the value of the shift of the curve on the Y axis, Δe_α, is also the measure of stability of proton shells and subshells.

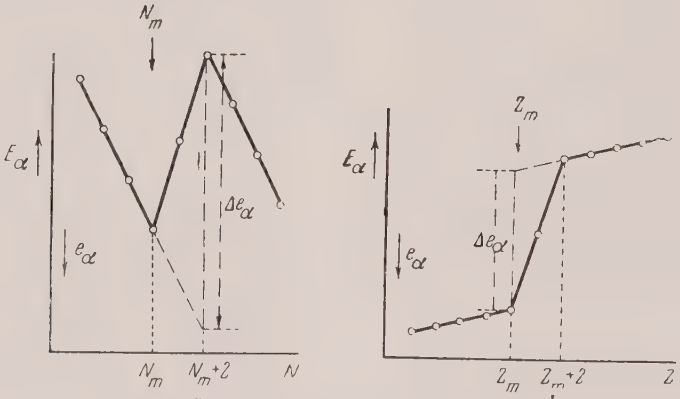

a b

FIG. 1. a — Z=const, b — N=const

In the case of α-stable nuclei, the energy $e(Z, N)$ needed for separation of an α-particle from the nucleus can be calculated from the binding energy of the nucleons. Denoting this value by $E(Z, N)$ we have:

$$e_\alpha(Z, N) = E(Z, N) - E(Z-2, N-2) - E(2,2). \qquad (1)$$

Curves showing the dependence of e_α on N (Z = const.) and of e_α on Z (N = const.), where e_α was calculated using Eq. (1), were plotted for nuclei with Z from 6 to 54 with the help of tables[4,5,6], based on experimental data.

In these curves, which are to be published separately, jumps and knees can be observed, caused by shells and subshells consisting of 8, 14, 20, 28, 32, 34, 40, 50, 58, 64 and 70 neutrons and of 8, 14, 20, 24, 28, 32, 38, 46 and 50 protons.

The values of the measure of stability Δe_α were calculated for each curve, according to the scheme of Fig. 1, for all neutron and proton shells and subshells. The curves showing the dependence of Δe_α on Z for neutron shells, and on N for proton shells, show a maximum for a certain value of Z or N (Fig. 2). This once more confirms the statement of the author[7] that the stability of a neutron shell depends on the number of protons, and the stability of a proton shell on the number of the neutrons in the nucleus.

The mean values of shell and subshell stability Δe_α and the even values of Z or N, for which Δe_α are greatest, are given in the Table (see below). Comparison of the $\bar{\Delta e}_\alpha$ in the Table shows that the most stable shells consist of 8, 50, and 82 neutrons and protons and 126 neutrons. The subshells $Z_m = 24$, $Z_m = 46$ and $N_m = 58$, the stabilities of which are relatively high, were discovered first. The confirmation of existence of the subshell $Z_m = 24$ may be seen in the slight elevation of the first excited state of Cr isotopes[8]. The same subshell is partly substantiated by Fig. 1 in Groshev's work[9], where the point corresponding to Cr lies above the curve. The existence of the subshell $N_m = 58$ is confirmed by the existence of 5 stable nuclides with 58 neutrons and by the fact, that Cd^{106} ($N = 58$) is more abundant (1,215%) than Cd^{108}(0.815%)[10]. There are as yet no additional indications for the existence of the subshell $Z_m = 46$. Since the experimental data for plotting the curves pertaining to the subshell Z_m=46 are very crude, its existence is still doubtful.

The shells and subshells are satisfactorily explained by the scheme of the nucleonic levels under

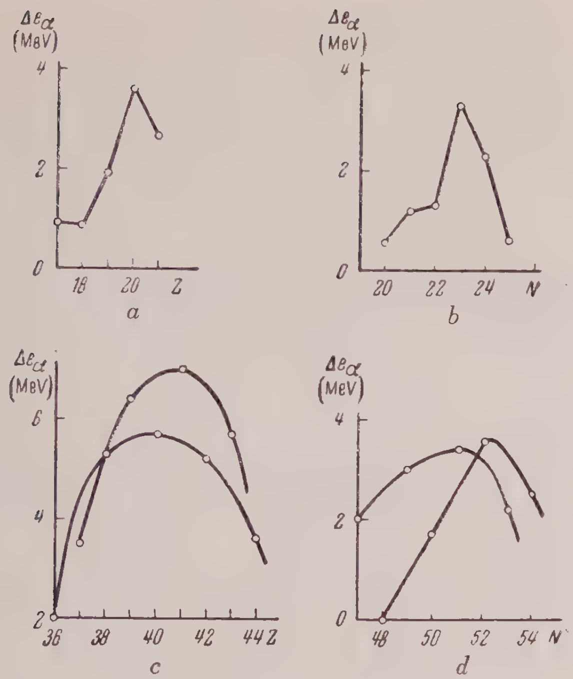

FIG. 2. $a - N_m = 20$, $b - N_m = 50$, $c - Z_m = 20$, $d - Z_m = 38$

the assumption of the spin-orbit coupling. The subshell $Z_m = 24$ is then explained as follows: the subshell $Z_m = 20$ is closed by filling the $3d_{3/2}$ level, but since the levels $3d_{3/2}$ and $4f_{7/2}$ are for protons very close to each other, the appearance of four additional protons makes it convenient, from energy considerations, to let four other protons leave the level $3d_{3/2}$ and occupy the $4f_{7/2}$ level. Additional protons fill up the $3d_{3/2}$ level once more. This is confirmed by the equal stability of subshells consisting of 20 and 24 protons. The subshell $N_m = 58$ is explained by the filling of the $5g_{7/2}$ level, coming next after the $5g_{9/2}$ level ($N_m = 50$).

The different subshells found here for neutrons and protons indicate that the sequence of level filling is different for the two types of particles. In the case of neutrons, the $4f_{7/2}$ level is followed by $3p_{3/2}$, $3p_{1/2}$, $4f_{5/2}$ and $5g_{9/2}$, while for protons the sequence is $3p_{3/2}$, $4f_{5/2}$ $3p_{1/2}$ and $5g_{9/2}$.

The previous confusion with regard to nuclides of higher stability in the region of Sr and Zr[7] can be removed here. The center of this region is formed by the nuclide Sr^{88} with double proton-neutron shell ($N_m = 50$, $Z_m = 38$).

Mean Stability of Nuclear Shells and Subshells

Neutron shells and subshells			Proton shells and subshells		
Number of neutrons N_m forming the shell or subshell	Mean Stability $\overline{\Delta e_\alpha}$ (MeV)	Even number of protons Z, for which stability is greatest	Number of protons Z_m, forming the shell or subshell	Mean Stability $\overleftrightarrow{\Delta e_\alpha}$ (MeV)	Even number of neutrons N for which stability is greatest
8	7,4±0,4	8	**8**	3,8±0,2	8
14	1,8±0,2	16	14	2,5±0,1	16
20	2,0±0.1	20	20	1,8±0,2	24
28	2,5±0,1	28	24	1,8±0,2	28
32	3,1±0,8	29	28	4,0±0,4	34
34	1,3±0.2	28	32	2,0±0,2	40
40	0,7±0,2	32	38	2,3±0,3	52
50	4,9±0,4	40	46	1,6±0,9	56?
58	1,8±0.6	48	**50**	4,2±0,7	70
64	0,6±0,4	48	—	—	—
70	1,1±0.4	>54	—	—	—
—	—	—	**82**	>4,1 ±0,4	126
—	—	—	88	0.47±0,05	136
126	>5.5 ±0,1	82	92	0.39±0,05	144
152	0.76±0,04	?	96	0,45±0,05	146

A fuller account of the results of the present work will be published separately.

Remark added during proof: A second study of the curves $e_\alpha = f(N)$ and $e_\alpha = f(Z)$ completed for $54 < Z \leq 66$ resulted in the discovery of the neutron subshells $N_m = 16$

with mean stability $\overline{\Delta e}_{\alpha} = 0.56 \pm 0.16$ mev and $N_m = 66$ with $\overline{\Delta e}_{\alpha} = 0.58 \pm 0.30$ mev and confirmed the existence of the shell $N_m = 82$ with $\overline{\Delta e}_{\alpha} = 3.42 \pm 1.50$ mev. The following proton subshells were found or confirmed: $\mathbf{Z_m = 16}$ with $\overline{\Delta e}_{\alpha} = 0.92 \pm 0.28$ mev, $Z_m = 40$ with $\overline{\Delta e}_{\alpha} = 1.54 \pm 0.6$ mev, $Z_m = 58$ with $\overline{\Delta e}_{\alpha} = 1.30 \pm 1.20$ mev and $Z_m = 64$ with $\overline{\Delta e}_{\alpha} = 0.36 \pm 0.24$ mev (newly discovered subshells are in boldface). The new subshells $N_m = Z_m = 16$ are excellently confirmed by the elevation of the first excited level of the even-even nuclei[11].

---

[1] W. J. Elsasser, J. Phys. Radium 5, 635 (1934).

[2] I. Perlman, A. Ghiorso, G. Seaborg, Uspekhi Fiz. Nauk 42, 220 (1950).

[3] S. Sengupt, Z. Physik 134, 413 (1953).

[4] B. Dzhelenov, L. Zyranova, Uspekhi Fiz. Nauk 48, 465 (1952).

[5] V. Kravtsov, ibid. 54, 3 (1954).

[6] V. Kravtsov, Izv. Akad. Nauk SSSR Ser. Fiz. 19, 377 (1955).

[7] V. Kravtsov, Izv. Akad. Nauk SSSR Ser Fiz. 18, 5 (1955).

[8] G. Scharff-Goldhaber, Phys. Rev. 90, 587 (1953).

[9] L. Groshev, Dokl. Akad. Nauk SSSR 100, 651(1955).

[10] I. Selinov, *Atomic Nuclei and Nuclear Transmutations*, 1951 (in Russian)

[11] P. Staehelin, P. Preiswerk, Helv. Phys. Acta. 24, 623 (1951).

Translated by H. Kasha
72

Estimate of the $\pi^+ - p$ Scattering Cross Section from the $\pi^- - d$ Scattering Cross Section near Resonance

Iu. A. Gol'fand

P. N. Lebedev Physical Institute

Academy of Sciences, USSR

(Submitted to JETP editor August 2, 1955)

J. Exptl. Theoret. Phys. (U.S.S.R.) 30, 413-414
(February, 1956)

A PHASE analysis of experiments on the scattering of pions by protons[1-3] reveals a strong interaction in the $p^{3/2}_{3/2}$ state (p-state with total spin $j = 3/2$ and isotopic spin $I = 3/2$. In connection with this we have undertaken a theoretical explanation of $\pi - p$ scattering based on a hypothesis regarding the resonance nature of the $\pi - p$ interaction in the $p^{3/2}_{3/2}$ state[4,5]. The thoeretical scattering curves obtained in this manner are in good agreement with experiment, so that the existence of the resonance as an important qualitative characteristic of the $\pi - p$ interaction is very probable.

We shall consider a few quantitative consequences of resonance in the $p^{3/2}_{3/2}$ state. From the phase analysis the contribution of this state to the total $\pi^+ - p$ scattering cross section is

$$\sigma^+_{3/2} = 8\pi k^{-2} \sin^2\delta, \tag{1}$$

where k is the momentum of the meson in the center of mass system and δ is the scattering phase (in the system of units in which $h = c = \mu = 1$). At resonance $\sin^2\delta = 1$, $k \approx 2.65$, which gives $\sigma^+_{3/2} = 185$ mb. Hence for the maximum of the total $\pi^+ - p$ scattering cross section we obtain the estimate

$$\sigma^+_{\max} > \sigma^+_{3/2\,\max} = 185 \text{ mb.} \tag{2}$$

The lower limit in (2) cannot be lowered essentially by increasing k^2 since this would result in a contradiction with other experimental data. Hence, if it should be definitely established by experiment that $\sigma^+_{\max} < 185$ mb this would be decisive evidence against the resonance nature of the $\pi - p$ interaction, and in particular, against the isobar theory[5].

Unfortunately the available experimental data on $\pi^+ - p$ scattering close to the cross section maximum are not exact and are at times contradictory. In this connection great interest attaches to the extremely careful measurements reported in Ref. 6 on the scattering of π^-- mesons by hydrogen and deuterium in the energy range from 140 to 400 mev. From these data, by using the relationship

$$\sigma^+ = \sigma(\pi^- d) - \sigma(\pi^- p), \tag{3}$$

indirect information can be obtained about the magnitude of σ^+, giving $\sigma^+_{\max} = 152.4 \pm 5.5$ mb, that is, a value which is below the lower limit in Eq. (2). Since this result contradicts the "resonance" hypothesis it is necessary to investigate the error in Eq. (3). As will be shown, the actual value of σ^+ is somewhat higher than the value obtained from (3).

In order to estimate the error in Eq. (3) it is, strictly speaking, necessary to solve the problem of meson scattering on the deuteron, which cannot be done for a number of reasons. It is only possible to give a rough estimate of the following factors: (1) the effect of interference of the waves scattered by the proton and neutron; (2) an allowance for the internal motion of the nucleons in the deuteron. The interference effect was examined by Brueckner[7] who showed that at scattering phases exceeding 45° interference results in a decrease of the deuteron cross section compared with the sum of the cross sections for free nucleons, with this decrease reaching 20% at $\delta = 90°$. Although this estimate is in our opinion somewhat too high there is no doubt that interference reduces σ^+.

Consideration of the internal motion of the nucleons also lowers the value of σ^+ obtained from the deuteron data by comparison with the scattering cross section for free nucleons. In order to explain this qualitatively we shall assume that the nucleon is at rest in the laboratory system and that the energy of the incident meson is such that the total energy of the meson and nucleon in the c.m. system has the resonance value. If under these conditions the nucleon is in motion in the laboratory system the energy in the c.m. system is shifted with respect to the resonance point and a smaller cross section results. As a qualitative estimate of this effect let us consider the scattering cross section of a π^--meson on the neutron of the deuteron abstracting from the $\pi^- - p$ interaction and interference. This will enable us to make a rough estimate of the effect in which we are interested since, according to Eq. (3), only the difference of the cross sections is then important.

In the impulse approximation the scattering cross section on a bound neutron is

$$\sigma_{\text{bound}} = \int \sigma_0(\varepsilon) \mid \psi_D(\mathbf{p}) \mid^2 d\mathbf{p}, \tag{4}$$

where $\varepsilon = \omega + E - M$, and ω and E are the energies of the meson and neutron in the c.m. system; p is the momentum in the system in which the deuteron as a whole is at rest. We express ϵ in terms of the momentum of the incident meson k_1 (the subscript 1 refers to quantities in the laboratory system):

$$\varepsilon = [M^2 + \mu^2 + 2(E_1\omega_1 - \mathbf{p}_1\mathbf{k}_1)]^{1/2} - M = \varepsilon_0 - \mathbf{p}_1\mathbf{k}_1/(\varepsilon_0 + M), \tag{5}$$

(ϵ_0 is the value of ϵ at $p_1 = 0$; M and μ are the nucleon and meson masses). For σ_0 we may take the value in (1) which is the main term at resonance. Removing the slowly varying function from under the integral sign we obtain $\sigma_{\text{CB}} = 8\pi k_0^{-2}\,\overline{\sin^2\delta}$ and, since at resonance $\sin^2\delta = 1$,

$$\sigma_{\text{CB}}\,\sigma_0 = \overline{\sin^2\delta} = \int \sin^2\delta \mid \psi_D(\mathbf{p}) \mid^2 d\mathbf{p}. \tag{6}$$

In the vicinity of resonance $\sin^2\delta = \Gamma^2/[(\varepsilon - \Delta)^2 + \Gamma^2]$. Substituting this quantity in (6) and taking (5) into consideration we obtain

$$\frac{\sigma_{\text{bound}}}{\sigma_0} \simeq 1 - \frac{1}{3}\left(1 + \frac{\varepsilon_0}{M}\right)^{-2}\left(\frac{k_1}{\Gamma}\right)^2 \frac{\overline{E}_{\text{kin}}}{M}, \tag{7}$$

where $\overline{E}_{\text{kin}} = \int \frac{p^2}{M} \mid \psi_D(\mathbf{p}) \mid^2 d\mathbf{p}$ — is the average kinetic energy of the deuteron.

In order to estimate (7) we use the value for Γ obtained from Ref. 5 and express all values in terms of the isobar excitation energy Δ which gives

$$\frac{\sigma_{\text{bound}}}{\sigma_0} \simeq 1 - \frac{(1 + \Delta/M)^4}{3g_1^4(\Delta/\mu^2 - 1)^2}\,\frac{\overline{E}_{\text{kin}}}{M}. \tag{8}$$

Using for our constants values which give good agreement with experiment[5] $\Delta = 2.1\ \mu$, $g_1^2 = 0.12$, and setting $E_{\text{kin}}/M = 0.02$ we obtain $\sigma_{\text{bound}}/\sigma_0 \approx 0.88$, i.e., the cross section is reduced by approximately 10%.

Both of the effects which we have considered act in the same direction and, since there is no reason for assuming that there are other effects which could change the result qualitatively, we may conclude that the data given in Ref. 6 do not contradict the hypothesis of the resonance character of pion-nucleon interaction.

---

[1] E. Fermi, N. Metropolis and E. F. Alei, Phys. Rev. **95**, 1581 (1954).

[2] F. de Hoffman, N. Metropolis, E. F. Alei and H. Bethe, Phys. Rev. 95, 1586 (1954).

[3] R. L. Martin, Phys. Rev. 95, 1606 (1954).

[4] K. A. Brueckner, Phys. Rev. 86, 106 (1952).

[5] I. E. Tamm. Iu. A. Golfand and F. Ia. Fainberg, J. Exptl. Theoret. Phys. (U.S.S.R.) 26, 649 (1954).

[6] A. E. Ignatenko, A. I. Mukhin, E. B. Ozerov and B. M. Pontecorvo, Dokl. Akad. Nauk SSSR 103, 209 (1955).

[7] K. A. Bruekner, Phys. Rev. 89, 834 (1953); 90, 715 (1953).

[8] T. A. Green, Phys. Rev. 90, 161 (1953).

Translated by I. Emin
74

Effect of Diffusion on the Kinetics of Crystallization

E. A. ARENSTEIN
Tomsk Engineering and Construction Institute

(Submitted to JETP editor August 15, 1955)
J. Exptl. Theoret. Phys. (U.S.S.R.) 30, 414-416
(February, 1956)

IN the diffusion theory of crystal growth the only factor which is considered to influence the speed of growth is the speed of diffusion of the precipitating substance to the growing face of the crystal. The influence of the physical and chemical properties of the surface is not taken into consideration, and the concentration of the solution near the growing face is taken to be equal to the saturation concentration. This theory explains a number of interesting phenomena[1-4], but its starting point is in sharp contradiction with the Curie-Woolf principle and with a number of experimental facts - for instance with the finite speed of growth during the intensive mixing of the solution[5-6].

The relative influence of diffusion and the physical and chemical properties of the surface can be clarified by the example of the growth of the plane face. We exclude convection and mixing from our consideration. The problem reduces to solving the diffusion equation.

$$\frac{\partial c}{\partial t} + D\frac{\partial^2 c}{\partial x^2} = 0 \qquad (1)$$

(where $c(x, t)$ is the concentration, and D is the coefficient of diffusion) in the region $x > 0;\ t > 0$ for the initial and limiting conditions

$$c(x, 0) = c_\infty, \quad c(\infty, t) = c_\infty \qquad (2)$$

and for the conditions on the face of the crystal determined by the physical and chemical processes of growth. Diffusion theory assumes the condition

$$c(0, t) = c_0, \qquad (3)$$

where c_0 is the concentration of the saturated solution.

The speed of growth is determined by the necessity for the coexistance of condition (3) and the condition which expresses the law of conservation of matter on the face

$$D(\partial c \cdot \partial x)_{x=0} = \delta V(t), \qquad (4)$$

where δ is the density of the crystal, and $V(t)$ is the speed of growth.

When the properties of the surface are taken into consideration condition (3) must be replaced by a condition of the type[7,8]:

$$V(t) = k\,[c^n(t, 0) - c_0^n] \qquad (5)$$

(where n is the order of the process and k the kinetic coefficient). This equation follows from the law of mass action, or from molecular and kinetic considerations. The speed of growth is determined by the necessity for the coexistence of (4) and (5). When the movement of the face is taken into consideration the problem is reduced to the former type by a substitution of variables, but in the second term of equation (1) there appears a factor $(\rho - c_\infty)/\rho^*$ of the order of unity. ρ is the density of the solution, ρ^* – the density of the clean solvent. We neglect this factor since it is unimportant.

Equation (1) with conditions (2) and (3) has the solution

$$c = c_\infty - (c_\infty - c_0)\,\mathrm{erfc}\,(x/2\sqrt{Dt}), \qquad (6)$$

where $\mathrm{erfc}\,(z) = \frac{2}{\sqrt{\pi}}\int_z^\infty e^{-u^2}du$. From (4) we determine the speed of growth

$$V(t) = \sqrt{D\pi t}\,(c_\infty - c_0)\,\delta, \qquad (7)$$

which, as usual, in diffusion theory does not depend on the properties of the face.

Let us discard condition (3). Equation (1) with conditions (2) and (4) has the solution

$$c = c_\infty - \frac{\delta}{\sqrt{\pi D}}\int_0^t V(t')\,e^{-x^2/4D(t-t')}\frac{dt'}{\sqrt{t-t'}} \qquad (8)$$

$$= c_\infty - \frac{\delta x}{D\sqrt{\pi}}\int_{x/2\sqrt{Dt}}^\infty V\left(t - \frac{x^2}{4Dz^2}\right)e^{-z^2}dz.$$

The requirement that conditions (4) and (5) hold gives the equation for the speed of growth

$$V(t) = k\left[\left(c_\infty - \frac{\delta}{\sqrt{\pi D}}\int_0^t \frac{V(t')\,dt'}{\sqrt{t-t'}}\right)^n - c_0^n\right]. \qquad (9)$$

Equation (9) can be easily solved by expanding it in powers of $\sqrt{t}$:

$$V(t) = k\,(c_\infty^n - c_0^n) \qquad (10)$$

$$- \frac{2n\delta k^2}{\sqrt{\pi D}}\,c_\infty^{n-1}\,(c_\infty^n - c_0^n)\sqrt{t} + \ldots$$

It is obvious from the above that in the initial phase of the process diffusion plays a secondary role, but asymptotically, for large values of t, the speed of growth is determined exclusively by diffusion. Actually it is seen from Eq. (9) that when $t \to \infty$ $V \approx at^{-1/2}$; a is determined by substitution into (9), and we obtain the asymptotic speed of growth, which coincides with (7).

Our conclusions, as one can easily be convinced, are preserved for a different choice of conditions on the face, for instance, for a condition of the type

$$V(t) = k\,[c(0,\,t) - c_0]^n. \tag{11}$$

Equation (9) can be easily solved for the case of a process of the first order, $n = 1$. Dividing Eq. (9) for $n = 1$ by $\sqrt{t'' - t}$, integrating with respect to t from 0 to t'', and changing the order of integration in the last term, we get the equation

$$\frac{\sqrt{\pi D}}{\delta}(c_\infty - c_0) - \frac{\sqrt{\pi D}}{k\delta} V(t) = 2k(c_\infty - c_0)\sqrt{t} - \frac{k\delta\sqrt{\pi}}{\sqrt{D}} \int\limits_0^t V(t')\,dt',$$

which has the following solution

$$V(t) = k(c_\infty - c_0)\,e^{k^2\delta^2 t/D}\operatorname{erfc}(k\delta\sqrt{t/D}). \tag{12}$$

Using the asymptotic expansion

$$\operatorname{erfc}(z) = \frac{2}{\sqrt{\pi}}\,e^{-z^2} \sum_{n=0}^{\infty} \frac{(-1)^n (2n)!}{n!\,(2z)^{2n-1}},$$

we obtain the known expression for the asymptotic behavior of the speed of growth and the criterion for the applicability of diffusion theory in the form

$$k^2\delta^2 t/D \gg 1. \tag{13}$$

From Eq. (8) one can easily determine the thickness of the depleted zone: $\Delta = 2\sqrt{Dt}$. Then criterion (13) assumes the form $k\delta\Delta/D \gg 1$. Diffusion is the dominating factor after the solution is depleted in an adequately wide zone; however, this factor is inhibiting. Mixing and convection reduce the influence of diffusion to zero, and the properties of the surface become of primary importance. The role of heat-transfer during crystallization after smelting is considered in a similar way.

---

[1] I. V. Salli, J. Exptl. Theoret. Phys. (U.S.S.R.) 25, 208 (1953).

[2] F. S. A. Sultan, Phil. Mag. 43, 1099 (1952).

[3] J. A. Barton, R. C. Prim and W. P. Slicter, J. Chem. Phys. 21, 1987, 1991 (1953).

[4] N. I. Litunovskii and O. M. Todes, J. Tech. Phys. (U.S.S.R.) 23, 1125 (1953).

[5] M. Tovbin, Zh. Fiz. Khim. 20, 1435 (1946).

[6] A. V. Beljustin, J. Exptl. Theoret. Phys. (U.S.S.R.) 28, 725 (1955).

[7] D. A. Frank-Kamenetskii, Zh. Fiz. Khim. 13, 756 (1939).
N. A.

[8] N. A. Figurovskii and T. A. Komarova, Zh. Fiz. Khim Khim. 28, 1479 (1954).

Translated by M. Polonsky
75

Relativistic Repulsion Effects in a Scalar Field and Attraction Effects in a Vector Field

IA. P. TERLETSKII
Institute of Nuclear Problems

(Submitted to JETP editor November 10, 1955)
J. Exptl. Theoret. Phys. (U.S.S.R.) 30
419-420 (February, 1956)

IN the recent times, it has been shown by a number of authors[1-6] that in the relativistic theory of a particle moving in a scalar field, the effect of relativistic repulsion takes place. For instance, in the case of a radial field with a purely attractive potential this effect produces a repulsion in the neighborhood of the center. In quantum mechanics this effect has been discovered and investigated by Kuni and Taksar[1], in the case of a Dirac particle with spin. The effect of relativistic repulsion for a classical particle has been investigated most prominently by Werle[2], Marks and Chamosi[3] and also by Infeld.[4] Werle[5] considered also the case of a spinless quantum particle, subject to the Klein-Gordon equation, in a scalar and a vector field, and showed that, in the non-relativistic approximation, some additional effective potentials appear which can be considered as repulsive potentials in the case of a scalar field, and as attractive potentials in the case of a static vector field. It is easy to show, however, that the latter deduction can be made without making a nonrelativistic approximation. Furthermore, for a spinless particle, the existence of relativistic effects--repulsive in a scalar field and attractive in a static vector field--can be deduced in a very convincing and clear manner.

The Klein-Gordon equation for a spinless particle in a scalar field with potential Φ, and simultaneously in a vector field with potential A, A_4

has the form:

$$\left[\left(\frac{\hbar}{i}\nabla - \mathbf{A}\right)^2 - \frac{1}{c^2}\left(-\frac{\hbar}{i}\frac{\partial}{\partial t} - A_4\right)^2\right]\psi = -\frac{1}{c^2}[mc^2 + \Phi]^2\psi. \quad (1)$$

In the case of a static vector potential with components A=0, $A_4 = U$, assuming for the static case, as usual, $\psi = u\exp(-iEt/h)$ we get:

$$\nabla^2 u + \hbar^{-2}c^{-2}[(E-U)^2 - (mc^2+\Phi)^2]u = 0. \quad (2)$$

The latter equation can easily be written in a form identical to the nonrelativistic stationary Schrödinger equation. Introducing the notation

$$U' = \left(\Phi + \frac{\Phi^2}{2mc^2}\right) + \left(\frac{E}{mc^2}U - \frac{U^2}{2mc^2}\right), \quad (3)$$

$$E' = (E - mc^2)\left(1 + \frac{E - mc^2}{2mc^2}\right),$$

Eq. (2) can be written in the form:

$$-(\hbar^2/2m)\nabla^2 u + [U' - E']u = 0. \quad (4)$$

In this manner, the eigenfunctions of the considered problem may be found as eigenfunctions of an equivalent nonrelativistic problem with effective potential U'. In the case of a purely scalar field, i.e., for $U=0$, Eq. (4) is identical to the usual stationary Schrödinger equation with a potential $U' = \Phi + \Phi^2/2mc^2$. In the case of a pure vector static field, i.e., for $\Phi=0$, Eq. (4) must be considered as some generalization of the Schrödinger equation, as far as the parameter E is involved in the expression of the effective potential $U' = (EU - \frac{1}{2}U^2)/mc^2$. However, for each given value of E, the function U' can be considered as an effective potential. It is with this potential, in particular, that the definite solution of Eq. (2) with $E = E_k$ is determined.

One sees from the expression (3), that, in the case of a potential monotonically decreasing towards the center, i.e., in the case of an attractive potential $\Phi(r)$, the effective potential $U'(r)$ increases towards the center, i.e., becomes repulsive for $r < r_0$, where r_0 is determined by $\Phi = (r_0) = -mc^2$. In the case of a potential, monotonically increasing towards the center, i.e., in the case of a repulsive potential $U(r)$, the effective potential $U'(r)$ becomes decreasing towards the center, i.e., becomes attractive for $r < r_m$ where r_m is determined by $U(r_m) = E$. However, for a repulsive potential $\Phi(r)$ of a scalar field, the effective potential is everywhere repulsive, and for an attractive potential $U(r)$ of a vector field, the effective potential is everywhere attractive.

The effect of relativistic repulsion in a scalar field has been satisfactory studied in the literature.[1-4] To take the simplest example of relativistic attraction effect in a repulsive vector field, let us consider the problem of the motion of a scalar particle in a static field with a potential which is a step function, high at the origin, i.e., a potential:

$$\Phi = 0, \quad U(r) = \begin{cases} U_m & \text{for } r < r_0, \\ 0 & \text{for } r > r_0, \end{cases} \quad U_m > 0. \quad (5)$$

For the function $\chi(r) = ru(r)$ in the state $l=0$, Eq. (2) takes the form

$$(d^2\chi/dr^2) + \hbar^{-2}c^{-2}[(E-U)^2 - m^2c^4]\chi = 0. \quad (6)$$

It is easy to see, that for sufficiently large values of U_m there exist solutions of (6) which are of the form

$$\chi(r) = \begin{cases} A\sin k_1 r & \text{for } r < r_0, \\ Be^{-k_2 r} & \text{for } r > r_0, \end{cases} \quad E < mc^2 \quad (7)$$

$$k_1^2 = (\hbar c)^{-2}[(E - U_m)^2 - m^2c^4], \; k_2^2 = (\hbar c)^{-2}(m^2c^4 - E^2),$$

From the continuity conditions on the function χ and on its derivatives at $r = r_0$ it follows that the coefficients k_1 and k_2 are subject to the relationship $\tan r_0 k_1 = -k_1/k_2$. The eigenvalues E are determined from this equation. It is easy to see that it has solutions with eigenvalues E lying in the interval $-mc^2 < E < mc^2$ for $U_m > E + mc^2$ (then $k_1 > 0$, $k_2 > 0$).

The easiest way to convince oneself in the truth of the last statement is to take a constant E in the interval mentioned above (for instance take $E=0$), and to vary U_m, i.e., take a constant k_2 and vary k_1.

Hence, for a purely repulsive potential (7) there are solutions of Eq. (2) for $E < mc^2$, which have the same form as the solutions of a nonrelativistic problem with an attractive step-function potential. However, in the case of a pure Coulomb repulsive potential $U = e^2/r$, the relativistic attractive effect in a vector field does not give rise to stable or metastable energy levels. Indeed, in this case, the maximum value of the effective potential is, according to (3): $U'_{\max} = E^2/2mc^2$ and the minimum possible value of E' for a particle localized in the region of "attraction" can be estimated, using the uncertainty relations, to be $(\hbar c/e^2)^2\, 3E^2/2mc^2$. Then the ratio $E'/U'_{\max} \sim 3(\hbar c/e^2)^2 = 3(137)^2$, i.e, the lowest level E' lies much higher than $U'_{\max}$.

It is clear that the relativistic attraction effect in a quasi-coulombic repulsive potential with potential g^2/r can give rise to metastable levels only if the constant g is more than 15 times larger than the elementary charge e.

The calculations shown above confirm that in the relativistic quantum theory for a spinless particle in a scalar purely attractive field, appears a repulsion effect, and in a static vector, purely repulsive field, an attractive effect takes place.

---

[1] P. E. Kunin and I. M. Taksar, Izv. Akad. Nauk SSSR 8, 137 (1952).

[2] Ia. Werle, Bull. Pol. Acad. Sci., Ser. Fiz. III 1, 281 (1953).

[3] G. Marks and G. Chamosi, Bull. Pol. Acad. Sci., Ser. Fiz. III 2, 477 (1954).

[4] L. Infeld, Uspekhi Fiz. Nauk, 56, 646 (1955).

[5] J. Werle, Nuovo Cimento 1, 536 (1955).

[6] G. Györgyi, Acta. Phys. Hung. 5, 119 (1955).

Translated by E. S. Troubetzkoy
77

The Kinetics of Paramagnetic Phenomena

V. P. Silin
P. N. Lebedev Physical Institute
Academy of Sciences, U.S.S.R.

(Submitted to JETP editor November 23, 1955)
J. Exptl. Theoret. Phys. (U.S.S.R.) 30, 421-422
(February, 1956)

In the kinetic theory of electrons in metals, it usually suffices to limit oneself to the use of the distribution function $f(\mathbf{p},\mathbf{r})$ which gives the number of electrons per cell of phase space. However, for processes related to the change of spin states of the electrons, this appears to be insufficient and one has to introduce the vector phase space magnetization density $\vec{\sigma}(\mathbf{p},\mathbf{r})$, which is a generalization of the density matrix in the mixed representation for the case of a system of particles with spin ½. One can write the following equation* for $\vec{\sigma}(\mathbf{p},\mathbf{r})$:

$$\frac{\partial\vec{\sigma}}{\partial t}+\left(\frac{\mathbf{p}\partial}{m\partial\mathbf{r}}\right)\vec{\sigma}+e\left(\mathbf{E}+\frac{[\mathbf{pH}]}{mc},\frac{\partial}{\partial\mathbf{p}}\right)\vec{\sigma} \tag{1}$$

$$+\frac{\beta}{\hbar}[\vec{\sigma}\mathbf{H}]=-\mathbf{J}_U-\mathbf{J}_\tau$$

where $\beta/2$ is the effective magnetic moment of the particle and $\mathbf{J}_\tau$ and $\mathbf{J}_U$ are integral operators, taking into account collisions without and with spin change, respectively. Usually the corresponding relaxation times τ and U satisfy the inequality $U \gg \tau$, hence the introduced separation between the integral operators does not give rise to any problems. Note that $\mathbf{J}_\tau$ and $\mathbf{J}_U$, generally speaking, depend on $\vec{\sigma}$ as well as on f. We shall not write their exact expression. We can approximate $\mathbf{J}_U$ by:

$$\mathbf{J}_U=U^{-1}(\vec{\sigma}-\vec{\sigma}_{00}), \tag{2}$$

where U is the spin relaxation time, and $\vec{\sigma}_{00}$ is the equilibrium value of the phase density of magnetization, which differs from zero in the case of a permanent magnetic field. In general, one cannot use for $\mathbf{J}_\tau$ an approximation similar to (2), because

$$\int \mathbf{J}_\tau d\mathbf{p}=0, \tag{3}$$

which is inconsistent with the equation analogous to (2). Equation (3) is an obvious consequence of the fact that a collision without spin change does not change the magnetization.

Being interested in the equation for the space magnetization density $\mathbf{M}(\mathbf{r},t)$ we assume that

$$\vec{\sigma}=\vec{\sigma}_0+\vec{\Sigma}=\mathbf{M}(\mathbf{r},t)F(p^2)+\vec{\Sigma}, \tag{4}$$

where

$$\int d\mathbf{p}F(p^2)=1,\quad \int d\mathbf{p}\vec{\Sigma}=0. \tag{5}$$

Then, from (1), we get the following system of equations:

$$\frac{\partial\mathbf{M}}{\partial t}+\int d\mathbf{p}\left(\frac{\mathbf{p}}{m}\frac{\partial}{\partial\mathbf{r}}\right)\vec{\Sigma} \tag{6}$$

$$+\frac{\beta}{\hbar}[\mathbf{M}\mathrm{x}\mathbf{H}]=-\frac{1}{U}(\mathbf{M}-\mathbf{M}_0),$$

$$F(p^2)\left(\frac{\mathbf{p}}{m}\frac{\partial}{\partial\mathbf{r}}\right)\mathbf{M}+\mathbf{M}e\left(\mathbf{E}\frac{\partial}{\partial\mathbf{p}}\right)F \tag{7}$$

$$+\frac{\partial\vec{\Sigma}}{\partial t}+\frac{\vec{\Sigma}}{U}+\left(\frac{\mathbf{p}}{m}\frac{\partial}{\partial\mathbf{r}}\right)\vec{\Sigma}$$

$$-F\int d\mathbf{p}'\left(\frac{\mathbf{p}'}{m}\frac{\partial}{\partial\mathbf{r}}\right)\vec{\Sigma}(\mathbf{p}')+e\left(\mathbf{E}+\frac{[\mathbf{p}\mathrm{x}\mathbf{H}]}{mc},\frac{\partial}{\partial\mathbf{p}}\right)\vec{\Sigma}$$

$$+\frac{\beta}{\hbar}[\vec{\Sigma}\mathrm{x}\mathbf{H}]=-\mathbf{J}_\tau(\vec{\sigma}_0+\vec{\Sigma})$$

to get the equation for $\mathbf{M}$ it is sufficient, with the help of (7) to express $\vec{\Sigma}$ in terms of M. This is not difficult to do in the case $\Sigma \ll \sigma$ i.e., when the part of the phase magnetization density, which is assymetric in p-space is small.** In first approximation equation (7) can be written in the following form:

$$F(p^2)\left(\frac{\mathbf{p}}{m}\frac{\partial}{\partial \mathbf{r}}\right)\mathbf{M} + Me\left(\mathbf{E}\frac{\partial}{\partial \mathbf{p}}\right)F = -J_\tau(\vec{\sigma}_0) - J_\tau(\vec{\Sigma}). \tag{8}$$

The form of the right hand side of (8) is possible because of the linearization of the integral J_τ. The approximations made to get (8) from (7) are in any case legitimate if $J_\tau(\vec{\Sigma})$ is much larger than all the other members containing $\vec{\Sigma}$ in the left hand side of (7). This condition is realized in the region of small deviations from homogeneity, of small frequencies and weak fields. Furthermore, it is assumed that $J_\tau(\vec{\sigma}_0) \lesssim J_\tau(\Sigma)$. The latter condition is satisfied in spite of the inequality $\sigma_0 >> \Sigma$, because $J_\tau(\vec{\sigma}_0)$ is a quantity assymetric in momentum space.

The solution of (8) can be written in the form

$$\Sigma_i = \alpha_{ikl}\frac{\partial M_k}{\partial r_l} + \beta_{ikl}M_kE_l + \gamma_{ik}M_k, \tag{9}$$

where α, β and γ are tensors depending only on the vector p. Neglecting terms of the form $E_i\,\partial M_i/\partial r_k$, we get the following equation for the space density of magnetization:

$$\frac{\partial M_i}{\partial t} - c_1\Delta M_i - c_2\frac{\partial^2 M_k}{\partial r_i \partial r_k} + \frac{\beta}{h}[\mathbf{M}\mathrm{x}\mathbf{H}]_i = -\frac{1}{U}(\mathbf{M}-\mathbf{M}_0)_i. \tag{10}$$

Note that the approximation $J_\tau(\vec{\Sigma}) = \vec{\Sigma}/\tau$ which satisfies (3) because of the relation (5), gives the following values for the coefficients c_1 and c_2:

$$c_1 = \frac{1}{3}\int d\mathbf{p}\,\frac{p^2}{m^2}\tau F, \quad c_2 = 0. \tag{11}$$

For metallic electrons in a degenerate state, F differs from zero only for momenta lying on the Fermi surface, hence:

$$c_1 = {}^1\!/_3\,(p_0/m)^2\tau(p_0) = {}^1\!/_3\,v_0\Lambda,$$

where v_0 is the electron velocity on the Fermi surface, and $\Lambda = v_0\,t$ is the mean free path. In this case Eq. (10) takes the form

$$\frac{\partial \mathbf{M}}{\partial t} - \frac{1}{3}v_0\Lambda\Delta\mathbf{M} + \frac{\beta}{\hbar}[\mathbf{M}\mathrm{x}\mathbf{H}] = -\frac{1}{U}(\mathbf{M}-\mathbf{M}_0). \tag{12}$$

Equation (12) is an equation for the magnetization density discovered by Dyson[2] in his theory of electron diffusion in metals.

To finish, let us study the limiting conditions for which one has to solve Eqs. (10) and (12). For this purpose, let us consider the limiting conditions for the phase magnetization density $\vec{\sigma}$. Let n be the normal to the surface of the body. Denote $\vec{\sigma}$ by $\vec{\sigma}^{(1)}$ for pn> 0 and by $\vec{\sigma}^{(2)}$ for pn< 0. The conservation law of the magnetic moment of the particle during the collision with the surface can then be written in the form

$$\vec{\sigma}^{(1)}(-\mathbf{pn};\,0) = \vec{\sigma}^{(2)}(\mathbf{pn};\,0). \tag{13}$$

Here, the zero value of the argument corresponds to a magnetization of the surface of the body. From condition (13) it follows that

$$\int d\mathbf{p}\,(\mathbf{pn})\,\vec{\sigma}(\mathbf{p},\,0) = 0. \tag{14}$$

In particular, for the linear approximation of $J_\tau(\vec{\Sigma})$ mentioned above, the relation (14) gives (n grad) M=0 which corresponds to the limiting condition used by Dyson[2] when he neglected the surface relaxation.

---

*For sake of simplicity, we shall assume a quadratic dependence of the kinetic energy on the momentum. Generalization to any case is evident. The derivation of equation (1) is absolutely identical to the derivation of the equation for the quantum distribution function-the density matrix in the mixed representation (see for instance Ref. 1)

** When Σ is neglected, Eq. (6) becomes the well known Bloch[3] equation for $T_1 = T_2 = U$.

[1] J. E. Moyal, Proc. Cambr. Phil. Soc. 49, 99 (1949); Iu. L. Klimontovich and V. P. Silin, J. Exptl. Theoret. Phys. (U.S.S.R.) 23, 151 (1952).

[2] F. J. Dyson, Phys. Rev. 98, 349 (1955).

[3] F. Bloch, Phys. Rev. 70, 460 (1946).

E. S. Troubetzkoy
78

The Conservation of Isotopic Spin and the Scattering of Antinucleons by Nucleons

I. IA. POMERANCHUK
Academy of Sciences, USSR

(Submitted to JETP editor, November 26, 1955)
J. Exptl. Theoret. Phys. (U.S.S.R.) 30
423, (February, 1956)

IN recent times, evidence for the conservation of isotopic spin in the interaction of nucleons with nucleons has been obtained. With the discovery of the antiproton[1], it becomes expedient to determine the consequences of the conservation of isotopic spin in the interaction of nucleons with antinucleons In particular, such calculations can enable us to check the hypothesis itself of the conservation of isotopic spin in the interaction of nucleons (neutrons n, protons p) and antinucleons (antiprotons $\bar{p}$, antineutrons $\bar{n}$). Let us consider collisions in which mesons do not occur:

1) $\bar{p}+p\to\bar{p}+p$ (elastic scattering of antiprotons by protons)

2) $\bar{p}+n\to\bar{p}+n$ (elastic scattering of antiprotons by neutrons)

3) $\bar{p}+p\to\bar{n}+n$ (conversion of a proton and antiproton into a neutron and antineutron)

4) $\bar{n}+n\to\bar{n}+n$ (elastic scattering of antineutrons by neutrons)

5) $\bar{n}+p\to\bar{n}+p$ (elastic scattering of antineutrons by protons)

6) $\bar{n}+n\to\bar{p}+p$ (conversion of an antineutron and neutron into an antiproton and proton).

From charge symmetry, if we neglect electromagnetic forces:

$$\sigma_1=\sigma_4;\ \sigma_2=\sigma_5;\ \sigma_3=\sigma_6.$$

Thus only processes 1,2 and 3 need be considered.

Keep in mind, that all the particles entering into the reactions have isotopic spin $T=\frac{1}{2}$ and the following isotopic spin projections, T_3:

p	n	$\bar{p}$	$\bar{n}$
$^1/_2$	$-^1/_2$	$-^1/_2$	$^1/_2$

The nucleon-antinucleon system has, in general, two isotopic states: $T=1$ and $T=0$. If we denote the scattering amplitudes in these states respectively by f and g, then it is easy to see that the differential cross sections of reactions 1-3 are expressed in terms of f and g as follows:

$$\sigma_1={}^1/_4\,|f+g|^2;\quad \sigma_2=|f|^2;\quad \sigma_3={}^1/_4\,|f-g|^2.$$

Note that f and g are complex functions of the initial and final momenta of the particles and their spins. Thus the three cross sections are expressed in terms of three independent quantities: the moduli of the amplitudes, $|f|$ and $|g|$, and their relative phase. It follows from this, that, in general, there are no equations linking these cross sections.

However, in the scattering of antinucleons by nucleons at high energies, one can consider that $|f-g|\ll|f|$. This has to do with the fact that σ_3 is the cross section of a peculiar inelastic process (double "overcharging"). Such an "inelastic" process must have a significantly smaller probability than that of "genuine" inelastic processes. Considering nucleons and antinucleons as "gray" bodies (in particular cases they will be black bodies) of radius $\rho\sim10^{-13}$ cm, one gets an elastic cross section (mainly of a diffraction type) of the order of the inelastic (i.e., of the order of the annihilation cross section). Therefore, from the fact that the process $\bar{p}+p\to\bar{n}+n$ embraces a small portion of all the inelastic processes, it follows that its cross section is small compared to the elastic scattering $\bar{p}+p\to\bar{p}+p$ ($\bar{p}+n\to\bar{p}+n$), but this means that the inequality $|f-g|\ll|f|$ is satisfied.

On the basis of this result, we obtain $\sigma_1=\sigma_2$, i.e., the differential cross sections of the elastic scattering of antiprotons by protons and by neutrons are equal. Applying this to the forward direction, 0°, and recalling the connection between the imaginary part of the scattering amplitude and the total cross section σ_t, we find

$$\sigma_t(\bar{p}+p)\approx\sigma_t(\bar{p}+n).$$

Together with the equality of the elastic cross sections, this means that the total annihilation cross sections for the collision of high energy antiprotons (antineutrons) with protons and with neutrons are equal.

In conclusion, I thank L. D. Landau for an interesting discussion.

Translated by M. Rosen
79

The Conservation of Isotopic Spin and the Cross Section of the Interaction of High-Energy π-Mesons and Nucleons with Nucleons

L. B. OKUN' AND I. IA. POMERANCHUK
Academy of Sciences, USSR

(Submitted to JETP editor, November 26, 1955)
J. Exptl. Theoret. Phys. (U.S.S.R.) 30
424 (February, 1956)

IN reference 1, the consequences of the conservation of isotopic spin in the scattering of antinucleons by nucleons were considered. The fact was used that the charge exchange cross section for the collision of antinucleons with nucleons is much less than the cross section for the other inelastic processes. For the scattering of π-mesons and nucleons, there are analogous results, justified at least for those energies at which inelastic reactions (creation of mesons) occur with high probability.

In the scattering of protons, the following reactions are possible:

1) $p+p\rightarrow p+p$ (elastic scattering of protons by protons)
2) $p+n\rightarrow p+n$ elastic scattering of protons by neutrons)
3) $p+n\rightarrow n+p$ (exchange scattering of protons by neutrons).

The neutron scattering reactions can be written analogously.

The differential cross sections of these reactions can be written in terms of the scattering amplitudes of the states with $T=1$ and $T=0$, as follows:

$$\sigma_1=|f|^2,\quad \sigma_2={}^1/_4\,|f+g|^2,\quad \sigma_3={}^1/_4\,|f-g|^2.$$

It is known that at low energies($\sim 10^8$ ev) $|f|\gg|g|$, which leads, in particular, to a significant exchange scattering cross section at these energies ($\sigma_2\approx\sigma_3$). At high energies ($\lesssim 10^9$ ev) exchange scattering $p+n\rightarrow n+p$ constitutes a small part of all the inelastic processes, so that, at such energies, π-meson creation reaction processes occur with high probability. In these circumstances, the total cross sections of the elastic and the inelastic processes are approximately equal; this is connected with the fact that we are dealing with scattering from "gray", "semi-transparent" bodies, where, within very wide limits of variation of opacity, elastic scattering has, in the main, a diffraction character. Therefore, the cross section σ_3 must be small as compared with σ_1 and σ_2. From this we find that $|f\text{-}g|\ll|f|$, i.e.,

$$\sigma_1\approx\sigma_2;\quad \sigma_3\approx 0.$$

Using the connection between the elastic and the total cross sections, we find that the total cross sections for the scattering of protons and neutrons from protons (neutrons) are equal to each other:

$$\sigma_t(p+n)=\sigma_t(p+p).$$

This also implies the equality of the corresponding inelastic cross sections.

In an analogous manner, one can also consider the scattering of high energy π-mesons by nucleons. The following elastic scattering and charge exchange reactions for π-mesons on protons are possible:

1) $\pi^+ + p\rightarrow\pi^+ + p;$
2) $\pi^0 + p\rightarrow\pi^0 + p;$
3) $\pi^0 + p\rightarrow\pi^+ + n;$
4) $\pi^- + p\rightarrow\pi^- + p;$
5) $\pi^- + p\rightarrow\pi^0 + n.$

The reactions with neutrons can be written analogously. All these reactions go through channels with isotopic spin $T=3/2$ or $T=1/2$. Their differential cross sections, expressed in terms of f and g, corresponding to $T=3/2$ and $T=1/2$, are:

$$\sigma_1=|f|^2;\quad \sigma_2={}^1/_9\,|2f+g|^2;$$

$$\sigma_3=\sigma_5={}^2/_9\,|f-g|^2;$$

$$\sigma_4={}^1/_9\,|f+2g|^2.$$

It is known that at low energies ($\sim 10^8$ ev) the scattering cross sections for π^-- and π^+-mesons on protons are substantially different.

At high energies ($\gtrsim 10^9$ ev) the charge exchange cross section of $\pi^- + p\rightarrow\pi^0 + n$ must be small compared to the total cross section of the inelastic processes, and, therefore, as compared with the cross section of the elastic processes. As in the scattering of nucleons, this is connected with the fact that, at these energies, inelastic processes occur intensively, and we are dealing with scattering from a very "gray" body, where elastic scattering has, in the main, a diffraction character and is equal to the inelastic in order of magnitude. From this it follows that $|f\text{-}g| << |$, i.e., $f\approx g$. Therefore:[2]

$$\sigma_1\approx\sigma_2\approx\sigma_4\approx|f|^2;\quad \sigma_3=\sigma_5\approx 0.$$

Thus, at high energies, the differential cross sections for the elastic scattering of π^+-, π^--, π^0-mesons from protons (neutrons) are equal to each other. Considering the forward direction, 0°, we obtain for the total cross section:

$$\sigma_t(\pi^+ + p)\approx\sigma_t(\pi^- + p)\approx\sigma_t(\pi^0 + p).$$

This also implies that the corresponding total inelastic cross sections are equal to each other.

---

[1] I. Ia. Pomeranchuk, J. Exptl. Theoret. Phys.(U.S.S.R.) 30, 424 (1956); Soviet Phys. 3, 305 (1956).

[2] K. M. Watson, Phys. Rev. 85, 852, (1952).

Translated by M. Rosen
80

CONTENTS — *continued*

Letters to the Editor:

Some Electrical Properties of Water and Ice . . . . V. I. Arabadzhi 285 30, 193

The Question of the Formation of a Cellular Structure in a Layer of Fog or Smoke . . . . V. K. Liapidevskii 287 30, 399

Metal-to-Semiconductor Contact Resistance at High Contact Potential Differences . . . . N. A. Gozhenko and Iu. M. Amaiskii 290 30, 401

Investigation of NaCl-AgCl Trapping Centers by a Method of Thermo-Optical Bleaching . . . . Ch. B. Lushchik, F. N. Zaitov, Kh. A. Miagi and K. Iu. El'ken 292 30, 403

The Effect of Uniform Compression on the Superconducting Properties of the α- and β- Modifications of Bi_2Pd . . . . N. E. Alekseevskii and I. I. Lifanov 294 30, 405

Concerning the Orientation of the Antenna of an Ionosphere Station . . . . Z. Ts. Rapoport 296 30, 407

Comparison of Stability of Nuclear Shells and Subshells . . . . V. A. Kravtsov 297 30, 408

Estimate of the $\pi^+ - p$ Scattering Cross Section from the $\pi^- - d$ Scattering Cross Section near Resonance . . . . Iu. A. Gol'fand 300 30, 413

Effect of Diffusion on the Kinetics of Crystallization . . . . E. A. Arenstein 302 30, 414

Relativistic Repulsion Effects in a Scalar Field and Attraction Effects in a Vector Field . . . . Ia. P. Terletskii 303 30, 419

The Kinetics of Paramagnetic Phenomena . . . . V. P. Silin 305 30, 421

The Conservation of Isotopic Spin and the Scattering of Antinucleons by Nucleons . . . . I. Ia. Pomeranchuk 306 30, 423

The Conservation of Isotopic Spin and the Cross Section of the Interaction of High-Energy π-Mesons and Nucleons with Nucleons . . . . L. B. Okun' and I. Ia. Pomeranchuk 307 30, 424

SOVIET PHYSICS JETP VOLUME 3, NUMBER 2 SEPTEMBER, 1956

CONTENTS

		Russian Reference
Investigation at Low Gas Pressure of an Intermediate Frequency Discharge Occurring Between High Frequency and Low Audio Frequency Discharges . . . N. A. Popov and N. A. Kaptsov	147	30, 68
The Structure of Superconductors. IX. Roentgenographic Determination of the Structure of α-Bi$_4$Rh . . . V. P Glagoleva and G. S. Zhdanov	155	30, 248
Effect of an Adsorbed Film of Dipole Molecules on the Electronic Work Function . . . N. D. Morgulis and V. M. Gavriliuk	159	30, 149
Contact Phenomena in a Plasma . . . L. A. Sena and N. S. Taube	168	30, 287
Paramagnetic Resonance in Synthetic Ruby . . . M. M. Zaripov and Iu.Ia. Shamonin	171	30, 291
The Inelastic Scattering of Electrons from a Copper Oxide Surface . . . N. B. Gornyi	175	30, 160
The Reaction $p + p \rightarrow \pi^0 + p + p$ in the Range 400-660 mev . . . L. M. Goroko	184	30, 296
The Possibility of a Two-Step Excitation Mechanism on Sulfide Phosphors . . . N. A. Tolstoi	190	30, 171
General Theory of Relativity or a Theory of Gravitation? . . . M. F. Shirokov	197	30, 180
The Electron Spectrum of U^{237} . . . S. A. Baranov and K. N. Shliagin	200	30, 225
Nucleomesodynamics in Strong Coupling. I. Approximate Method. Spin- Charge Motion . . . S. I. Pekar	205	30, 304
Investigation of Radioactive Decay Chains . . . V. S. Shpinel' and G. A. Kuznetsova	216	30, 231
Dependence of the Dielectric Strength of Some Alkali Halide Monocrystals on the Applied Voltage . . . G. A. Vorob'ev	225	30, 256
Investigation of the Close-Pair Effect in Cosmic-Ray Stars by Means of Moving Photographic Plates . . . I. M. Gramenitskii, M. I. Podgoretskii and Iu. F. Sharapova	230	30, 277
On the Theory of Stochastic Processes in Cosmic Radiation . . . L. Pal	233	30, 362
Matrix Aspects of Boson Theory . . . A. A. Borgardt	238	30, 334
Interrelation between the Anisotropy of the Hall Effect and the Change in Resistance of Metals in a Magnetic Field. I. Investigation of Zinc . . . E. S. Borovik	243	30, 262
Probe Studies of Rarefied Flames . . . V. I. Tverdokhlebov	252	30, 252
Paramagnetic Resonance in Anthracite and Other Carbonaceous Substances . . . N. S. Garif'ianov and B. M. Kozyrev	255	30, 272
Some Hydrodynamical Phenomena Accompanying the Passage of a Current Through Insulating Liquids . . . G. A. Ostroumov	259	30, 282
Application of the Theory of Stochastic Processes to the Investigation of Nuclear Fission . . . L. Pal	264	30, 367
Theory of Elliptic Polarization of Light Reflected from Isotropic Media . . . D. V. Sivukhin	269	30, 374
The Solution of Inhomogeneous, One-Dimensional Motion Problems in Magnetic Gasodynamics . . . S. A. Kaplan and K. P. Staniukovich	275	30, 382
The Theory of the Interaction of an Electron Gas with the Vibrations of the Crystalline Lattice . . . V. L. Bonch-Bruevich	278	30, 342

(*Contents continued on inside back cover*)